

Freie Universität



Berlin

Pyridyl-substituted Phosphinines and Pyridines:
Tuning Ligand Properties for Applications in Catalysis

Inaugural-Dissertation

to obtain the academic degree

Doctor rerum naturalium (Dr. rer. nat.)

submitted to the Department of Biology, Chemistry and Pharmacy
of Freie Universität Berlin

by

M. Sc. Antonia Loibl

from Berlin, Germany

2017

The described work was carried out within the time period of June 2013 until August 2017 under the supervision of Prof. Dr. Christian Müller at the Freie Universität Berlin

1. reviewer: Prof. Dr. Christian Müller

2. reviewer: Prof. Dr. Dieter Lentz

Disputation: 27.10.2017

Declaration

I herewith confirm that I have prepared this dissertation without the help of any impermissible resources. All citations are marked as such. The present thesis has neither been accepted in any previous doctorate degree procedure nor has it been evaluated as insufficient.

Antonia Loibl

Berlin, 22 August 2017

Acknowledgement

I thank Prof. Dr. Christian Müller for taking me into his group as a student for a research project and then supporting and encouraging me through more than five years until the end of my PhD. His door was always open for discussions and advice which was a tremendous help on my way of becoming an independent researcher.

Prof. Dr. Dieter Lentz, I thank for his continuous help with seemingly unsolvable issues in the lab: solving difficult X-Ray structures, finding replacements bulbs for really out-dated UV-light lamps and of course again and again fighting stubborn NMR machines. I am also very grateful for him reading my PhD thesis as a second reviewer.

I thank our cooperation partner Evgeny A. Pidko from Eindhoven University of Technology for the DFT calculations. And Iris de Krom, I want to thank for her contributions in form of the synthesis and characterisation of the unsubstituted tungsten complexes, her advice about cyclic voltammetry and other laboratory issues as well as for nice tea and apple breaks in the afternoons.

I am very grateful to Jelena Wiecko for her huge support, especially in the beginning when I was still very unsure of a great number of things. She was always willing to talk my problems through, to protect and to fight for me.

I also thank Manuela Weber and Jelena Wiecko for all X-ray structure determinations, Dorian Reich and Markus Peschke for the help in the lab with all things heavy and technical and Simon Steinhauer for countless hours spent at the NMR instruments learning, working but also having quite a bit of fun. AG Kulak and the NatLab Team, I want to thank for letting me use their UV-Vis and fluorescence spectrometers. And to the service personnel, I am grateful for their help.

Massimo, Annika and Cathérine, I thank for proof reading this thesis.

A huge thank you goes to Massimo, who has been my rock through the last, difficult one and a half years! Thank you for feeding me, urging me on, distracting me and hugging me. You cooked me saffron risotto for lunch! We had a great time exploring Russia and so much fun

creating hate-lists during tea breaks. And with your habit of hugging at random, you manage to spread some love when it is really needed but very hard to ask for!

Marlene, I want to thank for her friendship and support! We have such different personalities but share so many opinions and interests. I loved all the ideas developing from our talks like baking bread or ordering the Landkorb and I hope we will come up with many more in the future!

I am also very grateful to all the members of “the cooking group”: Marlene, Massimo, Fanni, Julian, Wiebke, Annet and Johan. I loved spending my lunch breaks with really good food and really good company! Also to our honorary member Annika, I am thankful for all the help and advice she provided, often in the form of Milchreis or bunny support!

My fellow group members Marija, Julian, Gregor, Steven, Martin, Friedrich, Daniel, Fanny, Erlin and Cathérine, I want to thank for all the good times we had together at various parties and barbecues, at cake sessions in the kitchen, at conferences in Kassel, Dublin, Berlin or Brisbane but also in our everyday life in the lab. It has been great to have you all with me during this adventure!

I am very grateful for the contributions of all the students in my lab. Maria, Andrea, Susanne and Anna, it was a joy to work with you. A special note goes to Wiebke, who was not only a huge help for the synthesis of ligands and complexes but also shared a lab with me for a long time and became a good friend. Thank you for all the laughter, cake and instant understanding we shared!

Meinen Eltern, Ruth und Gerhard, sowie meinen Geschwistern, Iris und Lukas, bin ich für ihre immerwährende Unterstützung sehr dankbar. Mama und Papa, euer ungebrochenes Vertrauen, dass ich alles schaffen kann, was ich mir in den Kopf setze, gibt mir so viel Selbstvertrauen und Zuversicht, und eure vielfältigen Interessen sind eine ständige Inspiration meine Gedanken und Aufmerksamkeit in die unterschiedlichsten Richtungen fliegen zu lassen und neues zu lernen! Iris und Lukas, ihr holt meinen Kopf aus dem Chemie- und Karrieredickicht und erinnert mich, was wirklich wichtig ist: familiäre Kuchentafeln, berliner Bürgerläden, Zoobesuche, Zeit zum Quatschen sowie Fischchen, Kätzchen und Häschen. Ich möchte auch meiner Großmutter Helma einen großen Dank für ihre Hilfe durch viel leckeres Obst in allen Formen sowie unglaublich großzügiger finanzieller Unterstützung

aussprechen, die einen großen Druck von mir genommen hat und mich ruhig an die stressige Schreibphase hat gehen lassen!

Ich danke meiner Patentante Uta für ihre Unterstützung und ihre nicht müde werdenden Fragen nach meinem Wohlergehen, auch wenn ich mal wieder scheinbar unerreichbar in meinem Alltagstrott verschwunden bin. Uta, ich bin dir unendlich dankbar dafür, wie du mich 30 Jahre lang Schritt für Schritt auf meinem Weg begleitet hast! Und meinem Patensohn David möchte ich danken für seine Geduld mit mir in den letzten Jahren in denen ich viel zu wenig Zeit und zu oft den Kopf nur voll mit Chemie hatte. David, jede deiner Postkarten und Nachrichten bedeutet mir sehr viel!

Auch bei meinen Freunden Silvana, Luca, Michael und Gandhi von der KSG FU Gruppe möchte ich mich ganz herzlich bedanken! Silvana, elf Jahre sind wir zusammen Schritt für Schritt durch das Studium gegangen; von der aller ersten Woche bis heute durch alle Höhen und Tiefen! Ich kann dir gar nicht sagen, wie viel mir das bedeutet. Wie auch immer unsere Wege weitergehen, lass sie uns gemeinsam weitergehen! Luca, vielen Dank für all die schönen Stunden bei Zitroneneis und Käsekuchen oder auch Thunfischsandwich und Bulgursalat im Café Cross. Du hast gewusst, was der andauernde Stress bedeutet, und hast es verstanden meinen Kopf mit ganz anderen Themen und Diskussionen zu füllen. Michael, wir haben uns oft lange nicht gesprochen und trotzdem hast du immer wieder nach mir gefragt, was stets zu spaßigen Stunden in der Küche und sehr gutem Essen geführt hat. Dafür und für unsere geteilte Leidenschaft für Apfelstrudel danke ich dir! Gandhi, du hast so viel fröhliches Lachen und sooo gutes Essen in unsere Gruppe gebracht. Danke dir für das Wissen, dass man jedes Gericht ein wenig flambieren sollte, für die besondere Geschmacksnote und besonders für den extra Spaß in der Küche!

Ich danke auch der DISS-CUS Gruppe von promovierenden Cusanuswerk-Stipendiaten in Berlin für die nette zusammen verbrachte Zeit mit tollen Themen, anregenden Diskussionen und Platz um Frust loszuwerden. Das Auftauchen in ganz andere Themenwelten war oft super um Atem zu holen für ein neues Abtauchen in meine Forschung.

Abstract

Fascinated by the versatility of 2,2'-bipyridine and its successful application in a wide range of fields such as catalysis, molecular materials or polymers, the idea of substituting one pyridine moiety with the higher homologue, a phosphinine ring, was captivating. While pyridines are known for more than 150 years, phosphinines were considered as laboratory curiosities for a long time and are significantly less-well researched. P,N hybrid ligands analogous to 2,2'-bipyridine are 2-pyridylphosphinines. A few derivatives were reported in literature but a stable 2-pyridylphosphinine with a synthetic route able to easily provide larger amounts of substance was only developed recently by the group of Müller. With 2-(2-pyridyl)-4,6-diphenylphosphinine now easily accessible, a detailed study of the properties and reactivity of 2-pyridylphosphinines especially in comparison to the respective 2,2'-bipyridine derivative became possible.

For this work, a special interest was put on the investigation of substituent effects on 2-pyridylphosphinine and 2,2'-bipyridines. With the introduction of small groups in the backbone of these molecules, the steric characteristics of a two-dimensional framework stay untouched but the electronic properties can be tuned to meet requirements for targeted applications (Figure I).

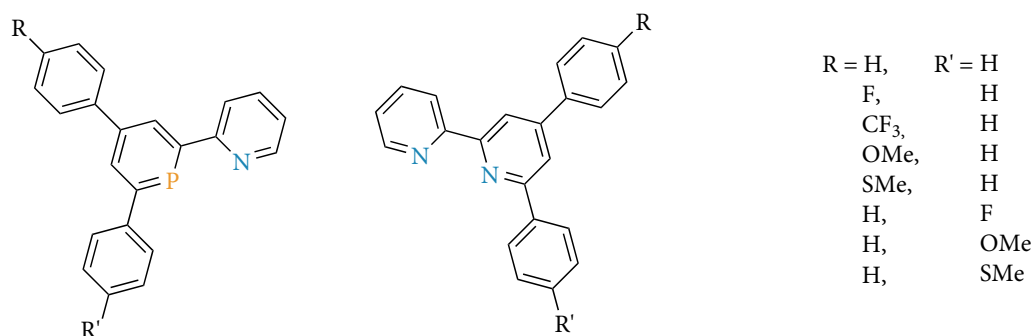


Figure I: Comparison of differently substituted 2-pyridylphosphinines and 2,2'-bipyridines.

The scope of the modular synthetic route towards 2-(2-pyridyl)-4,6-diphenylphosphinine was successfully broadened to include a range of different substituents from electron withdrawing to electron donating. For a direct, in-depth comparison the respective substituted 2,2'-bipyridines were synthesised as well. Both set of compounds were used for the coordination to tungsten(0) hexacarbonyl. The impact of the substituents on the electronic

properties was evaluated using a variety of different methods such as DFT calculations, X-ray diffraction and NMR, IR, UV-Vis and fluorescence spectroscopy. The presented results show a significant effect of these substituting groups on the experimental and theoretical characteristics of the 2-pyridylphosphinine and 2,2'-bipyridine compounds. Systematic tuning of the electronic properties was shown to be possible.

Most interestingly, the introduction of substituents able to donate electrons to the aromatic system lead to a significant destabilisation of the π -shaped HOMO in 2-pyridylphosphinines (Figure II). This gives the molecules noticeable π -donor properties which have never been taken into account in the consideration of phosphinines so far. Additionally, the shape and orientation of HOMO and LUMO makes phosphinines unique in comparison with conventional π -donor ligands with observable consequences for their ligand properties. While a similar effect has been observed for 2,2'-bipyridines, it is less pronounced.

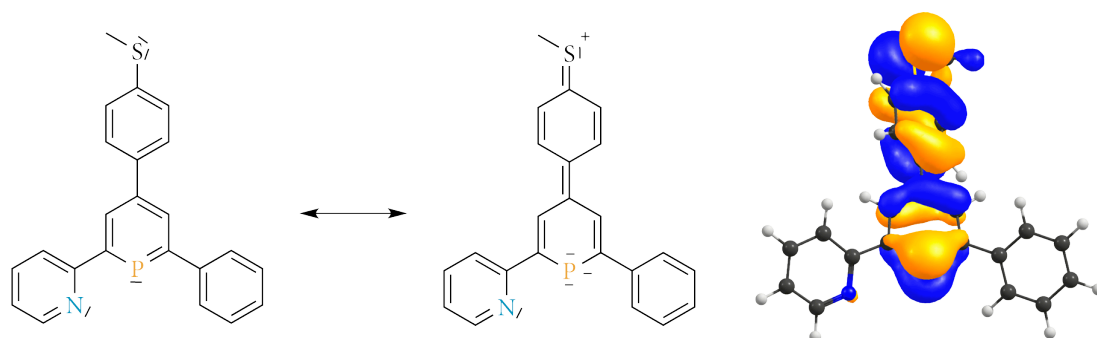
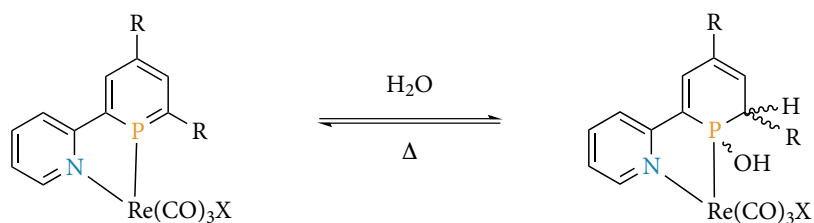


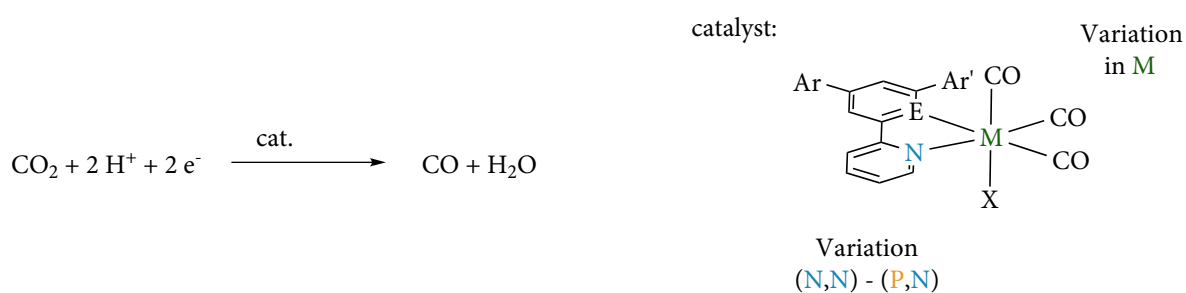
Figure II: Energetically high-lying HOMO of a SMe-substituted pyridylphosphinine giving π -donor properties.

In a second part of the presented work, the synthesised 2-pyridylphosphinines and 2,2'-bipyridines have been used to complex rhenium(I) carbonyl precursors. Derived complexes have been characterised and their reactivity has been studied. Interestingly, an unselective but reversible water addition reaction to the external P=C double bond of pyridylphosphinine rhenium(I) compounds has been observed while bipyridine-based complexes are unreactive towards nucleophiles (Scheme I).



Scheme I: Reversible water addition reaction to pyridylphosphinine rhenium(I) complexes.

First steps towards the application of synthesised 2-pyridylphosphinine- and 2,2'-bipyridine-rhenium(I) carbonyl complexes as catalysts in the photocatalytic reduction of carbon dioxide to carbon monoxide are presented (Scheme II). In cyclic voltammetry experiments P,N- and N,N-based complexes of rhenium(I) as well as tungsten(0) showed a significant current enhancement under CO₂ atmosphere which indicates a catalytic reaction taking place. For 2-pyridylphosphinine-based complexes this could not yet be translated into a running catalysis setup at laboratory scale but several possible adjustments were presented. Bipyridine-rhenium(I) compounds on the other hand were active and selective catalysts for the photocatalytic production of CO from CO₂.



Scheme II: Catalytic CO₂ reduction experiments using 2-pyridylphosphinine- and 2,2'-bipyridine-based catalysts.

Kurzbeschreibung

Beeindruckt von der Vielfältigkeit von 2,2'-Bipyridinen, die heute eine ganze Reihe von interessanten Anwendungen unter anderem in Homogenkatalyse, molekularen Materialien und Polymeren gefunden haben, schien die Idee einen der Pyridinringe gegen das schwerere Homologe, das Phosphinin, auszutauschen spannend. Während Pyridine bereits seit über 150 Jahren Teil der chemischen Forschung sind, wurden Phosphinine lange als Labor-kuriositäten angesehen und sind daher sehr viel weniger gut erforscht. Die zu 2,2'-Bipyridin analogen P,N-Hybridliganden sind die 2-Pyridylphosphinine, wovon einige wenige Exemplare in der Literatur beschrieben wurden. Ein stabiles Derivat mit einer auch in größeren Mengen gut handhabbaren Syntheseroute fehlte jedoch bis die Gruppe von Müller 2007 2-(2-Pyridyl)-4,6-diphenylphosphinin vorstellte. Erst dann war eine detaillierte Erforschung der Eigenschaften und Reaktivität von 2-Pyridylphosphininen sowie ein Vergleich mit dem entsprechenden 2,2'-Bipyridinderivat denkbar.

Für diese Arbeit wurde ein besonderer Fokus auf die Untersuchung von Substituenteneinflüssen in 2-Pyridylphosphininen im Vergleich zu 2,2'-Bipyridinen gelegt. Durch die Einführung von kleinen Gruppen in das Rückgrat dieser Moleküle sollten die elektronischen Eigenschaften gezielt modifiziert werden, während die durch die Planarität besonderen sterischen Eigenschaften unangetastet bleiben (Abb. I).

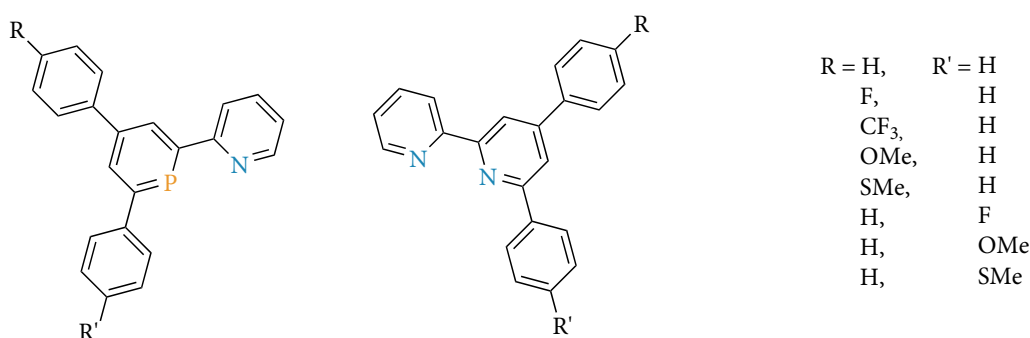


Abbildung I: Vergleich von unterschiedlich substituierten 2-Pyridylphosphininen und 2,2'-Bipyridinen.

Die modulare Syntheseroute für 2-(2-Pyridyl)-4,6-diphenylphosphinin wurde angepasst für die Einführung von verschiedenen, elektronenziehenden bis elektronenschiebenden Substituenten. Zusätzlich wurden die entsprechend substituierten 2,2'-Bipyridinderivate für einen direkten Vergleich ebenfalls synthetisiert. In einem nächsten Schritt wurden beide Reihen von Liganden mit Wolfram(0)hexacarbonyl zu Komplexverbindungen umgesetzt.

Durch den Einsatz von verschiedenen Analysemethoden wie DFT Rechnungen, Röntgenstrukturanalyse sowie NMR-, IR-, UV-Vis- und Fluoreszenzspektroskopie wurde schließlich der Einfluss der substituierenden Gruppen auf die elektronischen Eigenschaften der Moleküle untersucht. Die hier vorgestellten Ergebnisse zeigen einen klaren Substituenteneffekt der im Rückgrat eingeführten Gruppen auf die theoretischen und praktischen Eigenschaften der 2-Pyridylphosphinine und 2,2'-Bipyridine. Somit ist eine systematische Modifikation von elektronischen Charakteristika auf diesem Weg möglich.

Hervorzuheben ist die beobachtete Destabilisierung des HOMO in 2-Pyridylphosphininen durch Substituenten, die Elektronendichte in das aromatische System schieben, wodurch die Verbindungen signifikante und experimentell nachweisbare π -Donoreigenschaften erhalten (Abb. II). In den bisherigen Einschätzungen von Phosphininen sind jedoch mögliche π -Donoreigenschaften nicht berücksichtigt worden. Zusätzlich heben sich Phosphinine von herkömmlichen π -Donoren durch die sehr ähnliche Form und Orientierung von HOMO und LUMO deutlich ab, was sichtbare Konsequenzen für ihr Verhalten in Komplexverbindungen hat. Zwar wurde ein ähnliches Phänomen für die 2,2'-Bipyridine beobachtet, dieses ist jedoch deutlich weniger ausgeprägt.

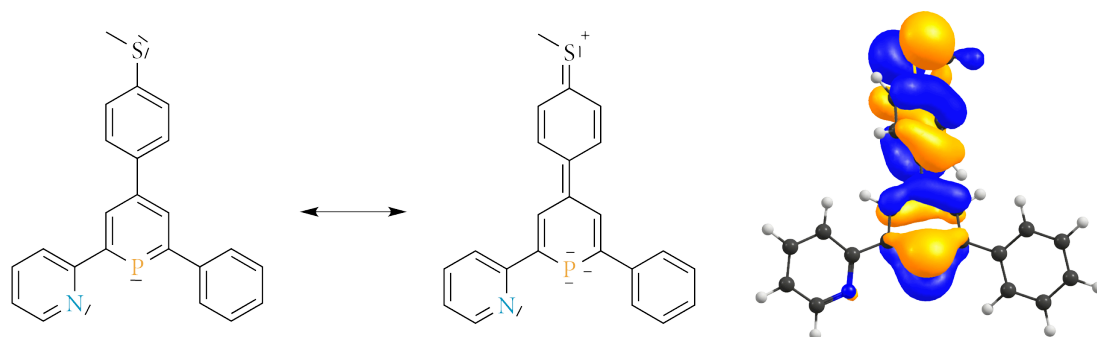
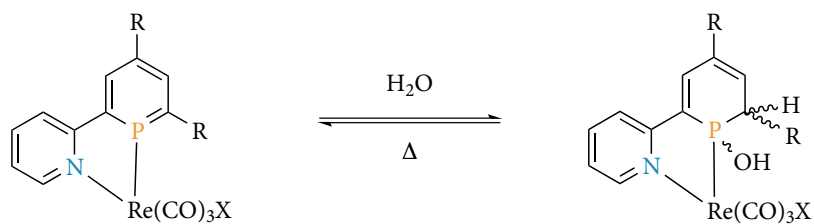


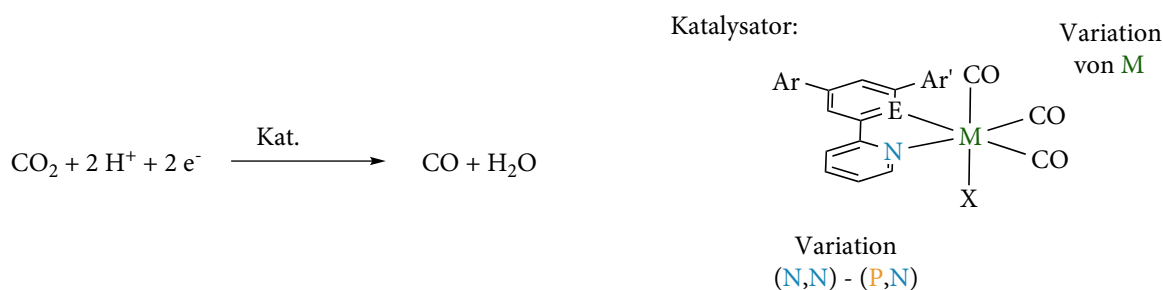
Abbildung II: π -Donoreigenschaften eines SME-substituierten 2-Pyridylphosphinines.

In einem zweiten Teil der vorliegenden Arbeit wurden dann Rhenium(I)carbonylkomplexe der 2-Pyridylphosphinine und 2,2'-Bipyridine synthetisiert, welche charakterisiert und auf ihre Reaktivität hin untersucht wurden. Interessanterweise konnte für die P,N-basierten Rheniumkomplexe eine nicht selektive aber reversible Addition von Wasser an die externe P=C-Doppelbindung beobachtet werden. Während das Gleichgewicht bei Raumtemperatur vollständig auf der rechten Seite liegt, kann es durch höhere Temperaturen zurück auf die Seite der Edukte verschoben werden (Schema I). Die entsprechenden Bipyridinkomplexe sind dagegen stabil gegenüber nukleophilem Angriff.



Schema I: Reversible Addition von Wasser an die P=C-Doppelbindung von Pyridylphosphinin-Rheniumkomplexen.

Erste Versuche zur Verwendung der synthetisierten Rhenium(I)komplexe mit auf 2-Pyridylphosphinin oder 2,2'-Bipyridin basierenden Liganden in der katalytischen Reduktion von CO₂ zu CO wurden ebenfalls durchgeführt (Schema II). Unter CO₂ Atmosphäre zeigten sowohl 2-Pyridylphosphinin- als auch 2,2'-Bipyridinkomplexe mit Rhenium- oder Wolframzentren einen Stromanstieg in Zyclovoltammetrierversuchen. Dies kann als starken Hinweis auf eine katalytische Aktivität dieser Verbindungen gegenüber CO₂ gewertet werden. Leider konnte für P,N-basierte Komplexe bisher kein funktionierender Katalysaufbau im Labormaßstab entwickelt werden, jedoch werden vielversprechende Idee für Anpassungen vorgestellt. Die hergestellten 2,2'-Bipyridinrheniumverbindungen sind jedoch aktive und selektive Katalysatoren für die Umwandlung von CO₂ in CO.



Schema II: Katalytische Reduktion von CO₂ durch 2-Pyridylphosphinin- and 2,2'-Bipyridin-enthaltende Komplexe.

List of Publications

- “Recent Developments in the Chemistry of Pyridyl-functionalized Low-coordinate Phosphorus Heterocycles”, Christian Müller, Julian A. W. Sklorz, Iris de Krom, Antonia Loibl, Marija Habicht, Marlene Bruce, Gregor Pfeifer, Jelena Wiecko, *Chem. Lett.* **2014**, 43 (9), 1390.
- “Tuning the electronic effects of aromatic phosphorus heterocycles: an unprecedented phosphinine with significant $P(\pi)$ -donor properties”, Antonia Loibl, Iris de Krom, Evgeny Pidko, Manuela Weber, Jelena Wiecko, Christian Müller, *Chem. Comm.* **2014**, 50 (64), 8842.
- “Substituent Effects in Pyridyl-Functionalized λ^3, σ^2 -Phosphinines: A Fundamental and Systematic Study”, Antonia Loibl, Wiebke Oschmann, Maria Vogler, Evgeny A. Pidko, Manuela Weber, Jelena Wiecko, Christian Müller, *to be submitted*.
- “Pyridylphosphinine- and Bipyridine-Based Rhenium(I) Complexes – Synthesis, Characterisation and Reactivity”, Antonia Loibl, Manuela Weber, Jelena Wiecko, Christian Müller, *in preparation*.

Table of Content

1 Phosphinine, the Higher Homologue of Pyridine: Synthesis and Electronic, Steric and Coordination Properties	III
1.1 $\lambda^3\sigma^2$ -Phosphinines	3
1.2 Structural Properties.....	3
1.3 Electronic Properties.....	5
1.4 Synthetic Routes.....	6
1.5 Coordination Chemistry.....	9
1.6 Applications in Catalysis	11
1.7 Pyridylphosphinines as P,N-Hybrid Ligands.....	15
2,2'-Bipyridine and 2-Pyridylphosphinine Analogues.....	15
The NIPHOS Ligand and Its Metal Complexes.....	16
2-(2-Pyridyl)-4,6-diphenylphosphinine: Synthesis, Reactivity and Metal Complexes .	19
1.8 Motivation of this Thesis	25
2 Substituent Effects in Pyridylphosphinines and Bipyridines	27
2.1 Introduction.....	29
2.2 Ligand Synthesis.....	30
2.3 Synthesis of [(P,N)W(CO) ₄] and [(N,N)W(CO) ₄] complexes.....	33
2.4 Investigation of the Substituent Effects	37
UV-Vis and Fluorescence Spectra of Pyrylium Salts	37
Molecular Structures of Pyrylium Salts.....	44

Frontier Orbitals of Pyridylphosphinines and Bipyridines.....	46
Molecular Structures of Bipyridine Ligands.....	51
IR Spectra of [(P,N)W(CO) ₄] and [(N,N)W(CO) ₄] Complexes.....	54
Molecular Structures of Tungsten Carbonyl Complexes	57
2.5 Experimental Data	64
General Remarks	64
Synthetic Procedures	65
Diketones (2.1b-h)	65
3-(4-Fluorophenyl)-1-phenyl-5-(2-pyridyl)pentane-1,5-dione (2.1b).....	66
3-(4-Trifluoromethylphenyl)-1-phenyl-5-(2-pyridyl)pentane-1,5-dione (2.1c)	66
3-(4-Methoxyphenyl)-1-phenyl-5-(2-pyridyl)pentane-1,5-dione (2.1d).....	67
3-(4-Methylthiophenyl)-1-phenyl-5-(2-pyridyl)pentane-1,5-dione (2.1e)	67
1-(4-Fluorophenyl)-3-phenyl-5-(2-pyridyl)pentane-1,5-dione (2.1f).....	68
1-(4-Methoxyphenyl)-3-phenyl-5-(2-pyridyl)pentane-1,5-dione (2.1g)	68
1-(4-Methylthiophenyl)-3-phenyl-5-(2-pyridyl)pentane-1,5-dione (2.1h).....	69
Pyrilium Salts (2.2b-d).....	69
2-(2-Pyridyl)-4-(4-fluorophenyl)-6-phenylpyrylium tetrafluoroborate (2.2b).....	70
2-(2-Pyridyl)-4-(4-trifluoromethylphenyl)-6-phenylpyrylium tetrafluoroborate (2.2c).....	70
2-(2-Pyridyl)-4-(4-methoxyphenyl)-6-phenylpyrylium tetrafluoroborate (2.2d)	71
2-(2-Pyridyl)-4-(4-methylthiophenyl)-6-phenylpyrylium tetrafluoroborate (2.2e)	71
2-(2-Pyridyl)-4-phenyl-6-(4-fluorophenyl)pyrylium tetrafluoroborate (2.2f).....	72
2-(2-Pyridyl)-4-phenyl-6-(4-methoxy)phenylpyrylium tetrafluoroborate (2.2g)	73
2-(2-Pyridyl)-4-phenyl-6-(4-methylthiophenyl)pyrylium tetrafluoroborate (2.2h)	73
Pyridylphosphinines (2.3b-h).....	74

2-(2-Pyridyl)-4-(4-fluorophenyl)-6-phenylphosphinine (2.3b).....	75
2-(2-Pyridyl)-4-(4-trifluoromethylphenyl)-6-phenylphosphinine (2.3c).....	75
2-(2-Pyridyl)-4-(4-methoxyphenyl)-6-phenylphosphinine (2.3d).....	76
2-(2-Pyridyl)-4-(4-methylthiophenyl)-6-phenylphosphinine (2.3e).....	76
2-(2-Pyridyl)-4-phenyl-6-(4-fluorophenyl)phosphinine (2.3f).....	77
2-(2-Pyridyl)-4-phenyl-6-(4-methoxyphenyl)phosphinine (2.3g).....	77
2-(2-Pyridyl)-4-phenyl-6-(4-methylthiophenyl)phosphinine (2.3h).....	78
Bipyridines (2.4b-h).....	78
2-(2-Pyridyl)-4-(4-fluorophenyl)-6-phenylpyridine (2.4b).....	78
2-(2-Pyridyl)-4-(4-trifluoromethylphenyl)-6-phenylpyridine (2.4c).....	79
2-(2-Pyridyl)-4-(4-methoxyphenyl)-6-phenylpyridine (2.4d).....	80
2-(2-Pyridyl)-4-(4-methylthiophenyl)-6-phenylpyridine (2.4e).....	80
2-(2-Pyridyl)-4-phenyl-6-(4-fluorophenyl)pyridine (2.4f).....	80
2-(2-Pyridyl)-4-phenyl-6-(4-methoxyphenyl)pyridine (2.4g).....	81
2-(2-Pyridyl)-4-phenyl-6-(4-methylthiophenyl)pyridine (2.4h).....	81
P,N-Tungsten Tetracarbonyl Complexes (2.6b-h).....	82
2-(2-Pyridyl)-4-(4-fluorophenyl)-6-phenylphosphinine-P,N-tungsten tetracarbonyl (2.6b).....	82
2-(2-Pyridyl)-4-(4-trifluoromethylphenyl)-6-phenylphosphinine-P,N-tungsten tetracarbonyl (2.6c)	83
2-(2-Pyridyl)-4-(4-methoxyphenyl)-6-phenylphosphinine-P,N-tungsten tetracarbonyl (2.6d).....	84
2-(2-Pyridyl)-4-(4-methylthiophenyl)-6-phenylphosphinine-P,N-tungsten tetracarbonyl (2.6e)....	85
2-(2-Pyridyl)-4-phenyl-6-(4-fluorophenyl)phosphinine-P,N-tungsten tetracarbonyl (2.6f).....	85
2-(2-Pyridyl)-4-phenyl-6-(4-methoxyphenyl)phosphinine-P,N-tungsten tetracarbonyl (2.6g).....	86
2-(2-Pyridyl)-4-phenyl-6-(4-methylthiophenyl)phosphinine-P,N-tungsten tetracarbonyl (2.6h)....	87
N,N-Tungsten Tetracarbonyl Complexes (2.7b-h).....	88

2-(2-Pyridyl)-4-(4-fluorophenyl)-6-phenylpyridine-N,N-tungsten tetracarbonyl (2.7b).....	88
2-(2-Pyridyl)-4-(4-trifluoromethylphenyl)-6-phenylpyridine-N,N-tungsten tetracarbonyl (2.7c)...	89
2-(2-Pyridyl)-4-(4-methoxyphenyl)-6-phenylpyridine-N,N-tungsten tetracarbonyl (2.7d).....	90
2-(2-Pyridyl)-4-(4-methylthiophenyl)-6-phenylpyridine-N,N-tungsten tetracarbonyl (2.7e)	91
2-(2-Pyridyl)-4-phenyl-6-(4-fluorophenyl)pyridine-N,N-tungsten tetracarbonyl (2.7f).....	92
2-(2-Pyridyl)-4-phenyl-6-(4-methoxyphenyl)pyridine-N,N-tungsten tetracarbonyl (2.7g)	93
2-(2-Pyridyl)-4-phenyl-6-(4-methylthiophenyl)pyridine-N,N-tungsten tetracarbonyl (2.7h)	94
3 Pyridylphosphinine- and Bipyridine-Based Rhenium(I) Complexes – Synthesis, Characterisation and Reactivity.....	97
3.1 Introduction.....	99
3.2 Results for the Synthesis of Pyridylphosphinine- and Bipyridine-Rhenium(I) Complexes.....	102
3.3 General Characterisation of Rhenium(I) Complexes	104
IR Spectroscopy	105
Molecular Structures in the Crystal	106
Rotation Barrier of the 6-Phenyl Ring.....	112
3.4 Reactivity of [(P,N)Re(CO)₃X] Complexes Towards Water	117
3.5 Experimental Data	123
General Remarks	123
Synthetic Procedures	124
P,N-Rhenium(I) Carbonyl Complexes	124
2-(2-Pyridyl)-4,6-diphenylphosphinine-P,N-rhenium(I) tricarbonyl chloride (3.4a).....	124
2-(2-Pyridyl)-4,6-diphenylphosphinine-P,N-rhenium(I) tricarbonyl bromide (3.5a)	124

2-(2-Pyridyl)-4-(4-fluorophenyl)-6-phenylphosphinine-P,N-rhenium(I) tricarbonyl chloride (3.4b)	125
2-(2-Pyridyl)-4-(4-fluorophenyl)-6-phenylphosphinine-P,N-rhenium(I) tricarbonyl bromide (3.5b)	125
2-(2-Pyridyl)-4-(4-methoxyphenyl)-6-phenylphosphinine-P,N-rhenium(I) tricarbonyl chloride (3.4d)	126
NN,-Rhenium(I) Carbonyl Complexes	126
2-(2-Pyridyl)-4,6-diphenylpyridine-N,N-rhenium(I) tricarbonyl chloride (3.6a)	126
2-(2-Pyridyl)-4,6-diphenylpyridine-N,N-rhenium(I) tricarbonyl bromide (3.7a)	127
2-(2-Pyridyl)-4-(4-fluorophenyl)-6-phenylpyridine-N,N-rhenium(I) tricarbonyl chloride (3.6b)	128
2-(2-Pyridyl)-4-(4-fluorophenyl)-6-phenylpyridine-N,N-rhenium(I) tricarbonyl bromide (3.7b)	129
2-(2-Pyridyl)-4-(4-methoxyphenyl)-6-phenylpyridine-N,N-rhenium(I) tricarbonyl chloride (3.6d)	130
2-(2-Pyridyl)-4-(4-methoxyphenyl)-6-phenylpyridine-N,N-rhenium(I) tricarbonyl bromide (3.7d)	131
2-(2-Pyridyl)-4-(4-methylthiophenyl)-6-phenylpyridine-N,N-rhenium(I) tricarbonyl chloride (3.6e)	131
2-(2-Pyridyl)-4-(4-methylthiophenyl)-6-phenylpyridine-N,N-rhenium(I) tricarbonyl bromide (3.7e)	132
2-(2-Pyridyl)-4-phenyl-6-(4-fluorophenyl)pyridine-N,N-rhenium(I) tricarbonyl (3.7f)	133
2-(2-Pyridyl)-4-phenyl-6-(4-methoxyphenyl)pyridine-N,N-rhenium(I) tricarbonyl (3.7g)	134
2-(2-Pyridyl)-4-phenyl-6-(4-methylthiophenyl)pyridine-N,N-rhenium(I) tricarbonyl (3.7h)	135
Reactivity of [(P,N)Re(CO)₃X]-type Complexes Towards Water	136
Water addition to [(P,N)Re(CO) ₃ Cl] 3.4a	136
Water addition to [(P,N)Re(CO) ₃ Br] 3.5a	136
Water addition to [(P,N)Re(CO) ₃ Br] 3.5b	136

4 Pyridylphosphinines and Bipyridines – Application as Ligands in Catalysts for the Reduction of CO₂	137
4.1 Introduction	139
4.2 Cyclic Voltammetry Experiments	142
4.3 Photocatalytic Reduction of CO₂	147
Development of a Reaction Setup	147
[(N,N)Re(CO) ₃ X]-type Complexes as Catalysts	150
[(P,N)Re(CO) ₃ X]- and [(P,N)W(CO) ₄]-type Complexes as Catalysts	152
4.4 Experimental Data	155
General Remarks	155
Cyclic Voltammetry Experiments.....	155
Catalytic CO ₂ Reduction Experiments.....	156
General procedure – lab scale.....	156
General procedure - NMR scale.....	156
Catalyst [(bipy)Re(CO) ₃ Cl] (3.1)	157
Catalyst [(N,N)Re(CO) ₃ Cl] (3.5a).....	157
Catalyst [(P,N)Re(CO) ₃ Cl] (3.4a)	158
Catalyst [(P,N)W(CO) ₄] (2.6a).....	158
Catalyst [(P,N)W(CO) ₄] (2.6a) / [(4,4'-Me ₂ bipy) ₃ Ru](PF ₆) ₂ (4.1).....	158
5 Conclusions and Outlook	159
6 Appendix	173
6.1 Frontier Orbitals of Ligands	175
6.2 Temperature Dependent NMR Experiments	178

6.3	Cyclic Voltammograms of Rhenium(I) Complexes.....	179
6.4	Photocatalytic Reduction of CO₂.....	181
6.5	Table of Abbreviations.....	183
6.6	Literature References	187

*If you will stay close to nature, to its simplicity, to
the small things hardly noticeable, those things
can unexpectedly become great and immeasurable.*

Letters to a Young Poet, Rainer Maria Rilke

1 Phosphinine, the Higher Homologue of Pyridine: Synthesis and Electronic, Steric and Coordination Properties

1.1 $\lambda^3\sigma^2$ -Phosphinines

Phosphinine, or as it used to be called phosphabenzene, is a heteroaromatic six-membered ring similar to benzene, where one CH group is substituted by an isolobal phosphorus(III) atom (Phosphorus-carbon analogy of a CH group and a P-lone pair fragment, Figure 1-1). Therefore it is the higher homologue of pyridine. The descriptor of $\lambda^3\sigma^2$ in the IUPAC name refers to the valency and number of binding partners of the phosphorus atom, namely three and two, respectively. While pyridine was already isolated in pure form by Anderson in 1851,¹ the synthesis of phosphinine only succeeded much later. Triphenylphosphinine (**1.1**) was prepared by Märkl in 1966 and Ashe III was able to present the synthetic route towards the unsubstituted parent compound (**1.2**) in 1971 (Figure 1-1).^{2,3}

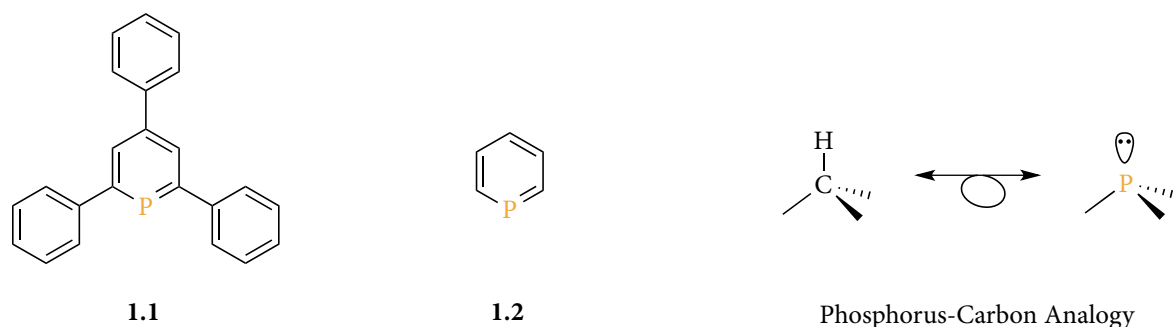


Figure 1-1: The first two $\lambda^3\sigma^2$ -phosphinines and the phosphorus-carbon analogy.

Phosphinines have been considered to be laboratory curiosities for a long time. First, they violate the double bond rule stating that elements of the third and higher period cannot form stable multiple bonds. Also, the concept of aromaticity was extended by the discovery of phosphinines to include higher main group elements.⁴

1.2 Structural Properties

The molecular structures in the crystal of several differently substituted phosphinines are known for many years now.⁵ In contrast to benzene, phosphinine does not form a perfect hexagon. The larger size of the phosphorus atom and its lower ability to hybridise results in a longer P-C bond length of 1.75 Å and a reduction of the C-P-C angle from 120° in benzene with six formally sp^2 hybridised carbon atoms to about 100° in phosphinine, which is much closer to the angle of 90° for an unhybridised phosphorus atom (Figure 1-2).⁶⁻⁸

The fact that there is no bond alternation between the four C-C bonds or the two P-C bonds indicates a delocalisation of the six electrons in the π -system. With a length of 1.75 Å the P-C bond is in between the lengths of typical P-C single bonds (triphenylphosphine: 1.83 Å)^{6,9} and P-C double bonds (diphenylmethylenephosphaalkene: 1.66 Å)⁹.

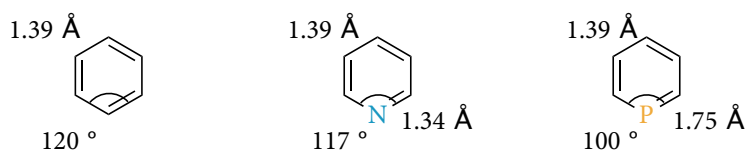


Figure 1-2: Comparison of average bond lengths and angles between benzene, pyridine and phosphinine.¹⁰⁻¹²

Additionally, phosphinines are planar cyclic systems that show a downfield shift in the ¹H and ³¹P NMR spectra attributed to the ring current and follow Hückel's rule of [4n+2] π -electrons, hence they are aromatic molecules. Calculations of bond separations and superhomodesmotic reactions gave phosphinine an aromatic stabilisation of 88-90% compared to the one of benzene whereas pyridine is as aromatic as benzene.^{13,14} Other methods to determine aromaticity are nuclear independent chemical shifts (NICS) or the absolute chemical hardness of a compound that is derived from the HOMO-LUMO gap. NICS values are reported as -11.5 for benzene, -10.6 for pyridine and -10.2 for phosphinine, where negative values denote aromaticity and positive values antiaromaticity.¹⁵ The chemical hardness on the other hand is a measurement for the stability of a compound, which is thought to be connected to aromaticity. Compounds with values above 1.28 eV are aromatic, below they are considered nonaromatic. For benzene and phosphinine, 2.27 eV and 1.66 eV have been calculated respectively.¹⁶

Due to the planarity of phosphinine the steric demand of such compounds is significantly different from other phosphorus(III) species and therefore the common method to determine steric bulk, the Tolman's cone angle, cannot be used. Instead the occupancy angles of α and β in the x- and y-plane have been introduced (Figure 1-3).

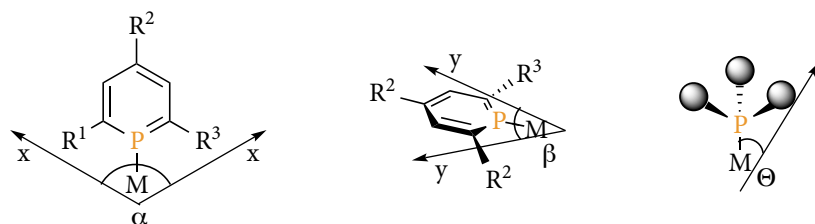


Figure 1-3: Methods to measure steric demand: occupancy angles α and β and Tolman's cone angle θ .

While phosphinines are quite bulky in the x-plane showing large α -values, they have very little steric demand in the y-plane.^{5,17} A second useful concept to determine steric bulk of phosphinines is the amount of space occupied by the ligand in a sphere with a defined radius around the metal, expressed in percentage of buried volume ($\%V_{\text{bur}}$).^{18,19} The group of Müller has calculated this value for 2,4,6-triphenylphosphinine (**1.1**), which is $\%V_{\text{bur}} = 33.1\%$ at a P-M distance of 2.28 Å.²⁰

1.3 Electronic Properties

Looking at the electronic properties it is reasonable to compare phosphinines with pyridines, the very well researched lower homologue. First, it has to be noted, that the differences in electronegativity between nitrogen, carbon and phosphorus (Pauling electronegativities: 2.19 for P, 2.55 for C, and 3.04 for N)²¹ lead to oppositely polarised bonds with a negatively charged nitrogen in pyridine but a partially positive charge at the phosphorus atom in phosphinine.

The molecular orbital (MO) scheme of both heterocycles (Figure 1-4)^{22,23} tells us that the lone pair of the phosphorus atom is represented by the HOMO-2 orbital and lies lower in energy than the nitrogen lone pair of pyridine represented by the HOMO. The phosphinine lone pair is also more diffuse and less directed than its pyridine analogue, which, like the distortion of the six-membered ring, can again be attributed to the low ability of the phosphorus atom to hybridise. While the nitrogen is almost perfectly sp^2 -hybridised with a s-character of the lone pair of 29.1%, the calculations resulted in 63.8% s-character for the lone pair of the phosphorus atom in phosphinine.¹⁵ Consequently, phosphinines show a very low basicity in aqueous solutions with a $pK_a(\text{C}_5\text{H}_6\text{P}^+) = 16.1 \pm 1.0$ ($pK_a(\text{C}_5\text{H}_6\text{N}^+) = 5.23$).^{21,24} In coordination chemistry phosphinines can be classified as weak σ -donors due to the energetically low lying, diffuse lone pair of the phosphorus atom.

Apart from the lone pair also the aromatic system can be used for coordination to metal centres. While pyridine only shows η^6 -coordination when the nitrogen atom is sterically blocked, the π -system of phosphinine is higher in energy and therefore available for reactions with appropriate metal precursors.²⁵ According to the shape of the orbitals the HOMO and HOMO-1 of the phosphinine can contribute to a metal-phosphorus bond *via*

π -donation. The equivalent orbitals on the pyridine are the HOMO-1 and HOMO-2 that are significantly lower in energy, resulting in a much lower reactivity towards metals.

Comparing the LUMOs the phosphinine shows a π -shaped orbital low in energy with a high coefficient on the phosphorus atom, explaining the good π -accepting properties. In contrast, the LUMO of pyridine is high in energy with a low coefficient on the nitrogen atom.

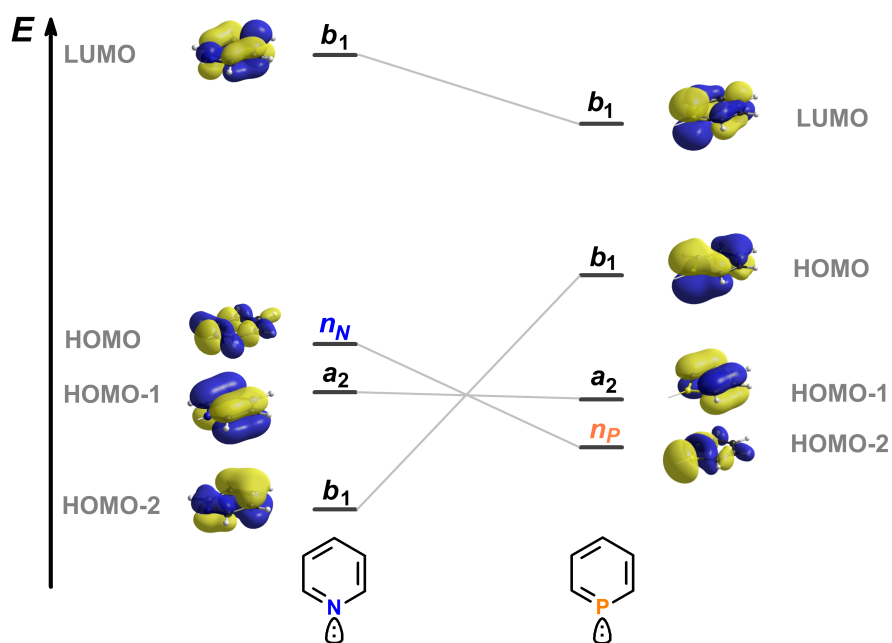


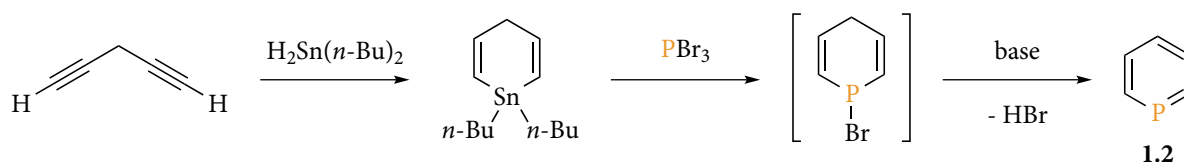
Figure 1-4: Molecular orbital scheme of pyridine and phosphinine.²⁶

In summary, phosphinines are weaker σ -donor and stronger π -acceptor ligands than pyridines which explains their preference for coordination to late transition metals in low oxidation states.¹²

1.4 Synthetic Routes

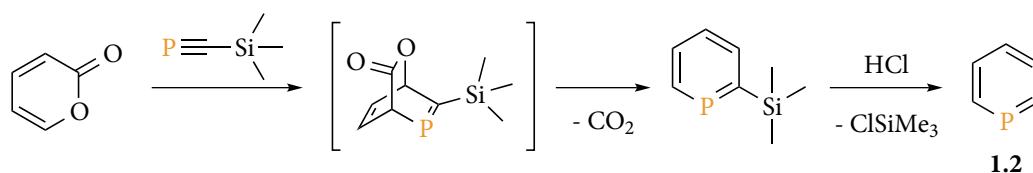
Nowadays, quite a few synthetic pathways towards phosphinines are known and have been summarised in a number of reviews so only the most common ones shall be described here.²⁷

The unsubstituted parent phosphinine **1.2** can be synthesised *via* the tin route (Scheme 1-1), which was published by Ashe III in 1971.³ In a first step 1,4-dihydro-1,1-dibutylstannacyclohexadiene, a useful precursor for several heteroaromatic six-membered rings,²⁵ is made by hydrostannation of 1,4-pentadiyne. Reaction with phosphorus tribromide and elimination of hydrogen bromide gives **1.2** as a colourless liquid.



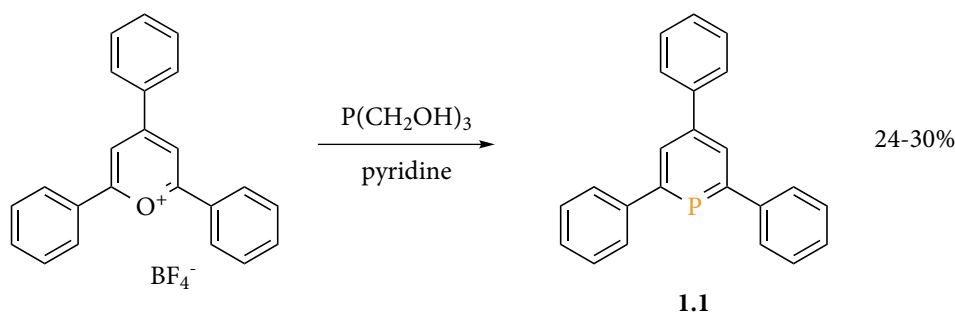
Scheme 1-1: Synthesis of phosphinine from 1,4-pentadiyne.

A second pathway to low-substituted phosphinines is the [4+2]-cycloaddition reaction with phosphalkynes. First published by Regitz in 1986 for the reaction of *t*-butylphosphalkyne with cyclic 1,3-dienes, it has since been adapted to other available phosphalkynes and differently substituted dienes, mainly pyrones (Scheme 1-2).²⁸⁻³¹ While the low stability of phosphalkynes limits the number of possible substituents in 2-position of the phosphinine, this route affords similar yields as the reaction mentioned above and is therefore still useful to avoid toxic tin compounds and as a way to synthesise low-substituted, functionalised phosphinines.^{30,32}



Scheme 1-2: [4+2]-cycloaddition of a phosphalkyne to a pyrone.

The oldest route is the still often used pyrylium salt route; an O⁺/P exchange from a pyrylium salt to a phosphinine, which was introduced by Märkl for the synthesis of 2,4,6-triphenylphosphinine as the first known derivative. Refluxing 2,4,6-triphenylpyrylium tetrafluoroborate with tris(hydroxymethyl)phosphane in pyridine gave the air and moisture stable **1.1** in 24-30% yield (Scheme 1-3).²

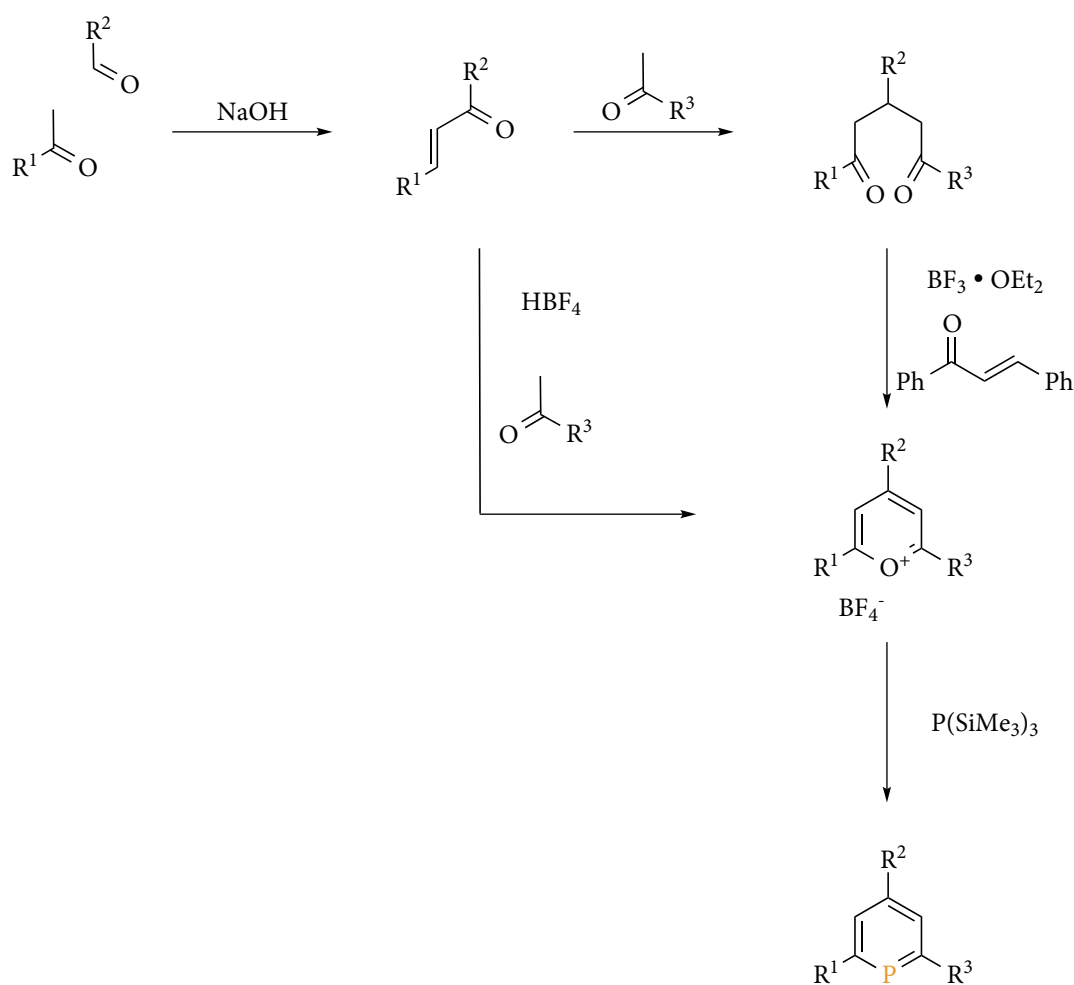


Scheme 1-3: Synthesis of 2,4,6-triphenylphosphinine by Märkl in 1966.²

By adjusting the reaction conditions and using tris(trimethylsilyl)phosphane or its lithium salt Li[P(SiMe₃)₂] as phosphorus source, the yield has been improved to up to 77%.^{33,34} The

use of PH_3 leads to even higher yields but is often avoided due to its hazardous nature.³⁵ Further improvement of the reaction can be reached by switching to other polar, aprotic solvents like acetonitrile, tetrahydrofuran or dichloroethane and changing the counterion of the pyrylium salt to iodide to form the favoured Me_3SiI instead of Me_3SiBF_4 .^{12,36}

The reason why this old synthetic route is still used is its modular approach, allowing a range of different groups and functionalities to be introduced into the framework of the phosphinine and starting materials are generally cheap and easily available. While pyridines and arenes can be functionalised by electrophilic substitution, reagents for this type of reactions usually attack the phosphorus atom instead of the backbone in case of phosphinines. Therefore the pyrylium salt route is often used to introduce various donor functionalities, chirality or certain steric or electronic properties.³⁷⁻⁴⁰ The pyrylium ring is formed stepwise with up to three different substituents in 2-, 4- and 6-position from functionalised benzaldehydes and acetophenones (Scheme 1-4).



Scheme 1-4: The pyrylium salt route: a modular approach to 2,4,6-substituted phosphinines.

In a classical aldol condensation a chalcone is formed from a benzaldehyde and an acetophenone. It is possible to convert the chalcone directly to the pyrylium salt by the addition of half an equivalent of acetophenone and tetrafluoroboric acid, respectively. For functional groups that are not compatible with Brønsted acidic conditions like pyridine, a diketone can be formed first through nucleophilic addition of an acetophenone to the chalcone under basic conditions. Diketones react then with borontrifluoride etherate and chalcone to the pyrylium salt. In this reaction as well as the former mentioned one with tetrafluoroboric acid, the additional equivalent of chalcone is used as a hydrogen acceptor ensuring completion of the reaction to the aromatic ring system.⁴¹

1.5 Coordination Chemistry

The differences in electronic properties of phosphinines compared to pyridines are responsible for their more versatile coordination chemistry (Figure 1-5). A multitude of different phosphinine-based complexes has been presented in the literature until today so only a few examples should be reviewed here in order to show the broad scope of this ligand class.

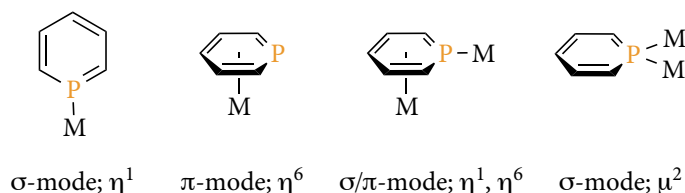


Figure 1-5: Possible coordination modes for phosphinines.

As discussed in chapter 1.3 phosphinines can coordinate in a σ -fashion to metal centres *via* the lone pair of the phosphorus (HOMO-2) along with π -backbonding *via* the LUMO. The energetically high lying aromatic system (HOMO and HOMO-1) can bind metal centres in a π -mode. The exact coordination mode depends on the metal, the type of precursor used and the steric properties of the phosphinine.

Due to the weak σ -donor and strong π -acceptor properties of the phosphinine and the resulting preference for electron-rich metal centres, a big part of the known coordination compounds are η^1 -type complexes with late transition metals in low oxidation states (Figure 1-6).¹² One example being the homoleptic tetra(η^1 -phosphinine)nickel(0) complex **1.3**

published by Elschenbroich *et al.* in 1992. Nickel(0) complexes have to be stabilised with chelating or strongly π -accepting ligands, crystals of phosphinine complex **1.3** proved to be air stable up to $T = 180\text{ }^\circ\text{C}$.⁴²

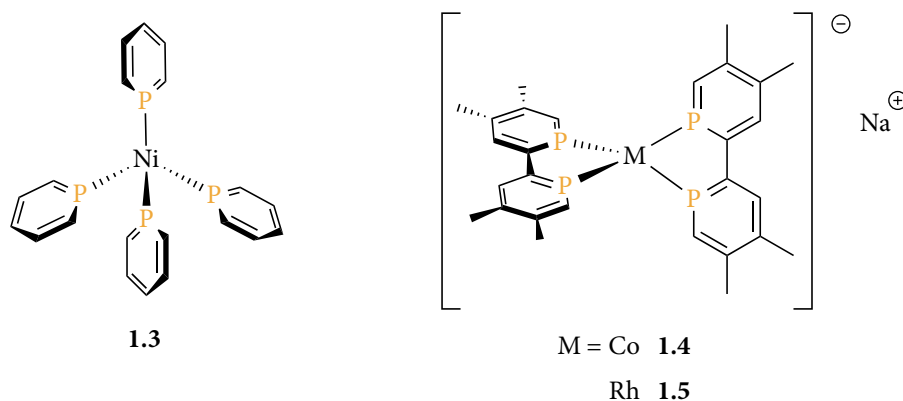


Figure 1-6: Examples for phosphinine complexes with σ -mode coordination.

Combining the π -accepting abilities with the chelate effect and using a biphosphinine as ligand, Le Floch *et al.* were able to isolate cobalt (**1.4**) and rhodium (**1.5**) complexes with the formal oxidation state of $-I$. In a two-step procedure, the biphosphinine was first reduced with lithium or sodium to the dianion and then the complexes were formed upon addition of $[\text{M}(\text{acac})_3]$ ($\text{M} = \text{Co}, \text{Rh}$).⁴³

However, phosphinines are also able to stabilise electron deficient metals through a η^6 -coordination mode *via* the aromatic system (Figure 1-7).

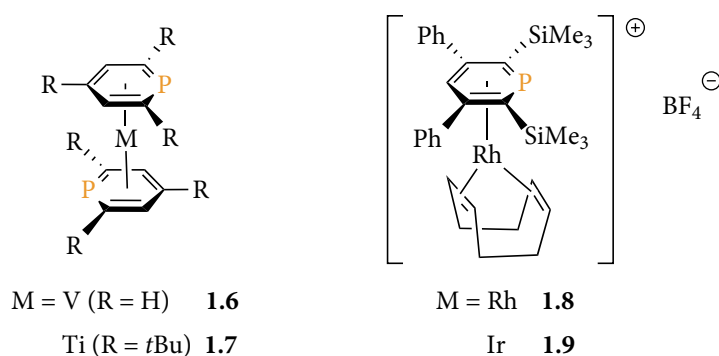


Figure 1-7: Examples for π -coordinated phosphinines.

Early transition metals such as vanadium(0) or titanium(0) form sandwich-type complexes with phosphinines (**1.6** and **1.7**, Figure 1-7).^{44,45} η^6 -Coordination can also be enforced for other metals by shielding the phosphorus lone pair with bulky groups.⁴⁶ With trimethylsilyl groups in 2- and 6-position rhodium(I) or iridium(I) cannot bind directly to the phosphorus

anymore giving π -complexes **1.8** and **1.9** (Figure 1-7) instead as presented for the first time by Mézailles and Le Floch *et al.*⁴⁷

For transition metals in the middle of the d-block both binding modes are similarly favourable which can result in bimetallic complexes with mixed η^1/η^6 -coordination. Mathey *et al.* report on a manganese precursor, that forms with phosphinines σ -type complexes at room temperature and sandwich complexes under irradiation. With a stepwise combination of both, they were able to show the formation of bimetallic complex **1.9** (Figure 1-8).⁴⁸

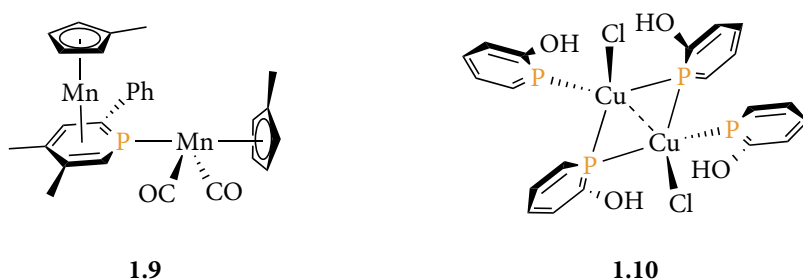


Figure 1-8: Examples of one phosphinine coordinating two metal centres.

The ability of phosphinines to bridge two metal centres can be attributed to the strong s-character of the phosphorus's lone pair, which was discussed already in chapter 1.3. Since the orbital is diffuse and not very directed, it can build three-centre two-electron bonds.⁴⁶ Mathey *et al.* isolated such compounds with a hydroxy-substituted phosphinine coordinated to copper(I) (**1.10**, Figure 1-8) and also Müller and coworkers presented a dimeric copper complex with bridging phosphinine ligands.^{20,49}

1.6 Applications in Catalysis

Investigation of phosphinines as ligands in homogeneous catalysis only started in the late 1990's. Until today there is a very limited number of publications covering few reactions catalysed by transition metal complexes based on phosphinines. A vast amount of further basic research is needed to scope out the true potential of phosphinines, the higher homologues of the well researched and widely and successfully used pyridines, in catalytic processes.

In a first example, cyclotrimerisation and cyclodimerisation reactions facilitated by η^6 -phosphinine-iron complexes **1.13** and **1.14** (Figure 1-10) have been reported by Zenneck *et al.* in

the late 1990s.^{50,51} Both processes suffer, however, from very low chemoselectivity and low turnover numbers (TON).

So far, the maybe most promising use of phosphinines in homogeneous catalysis is in the hydroformylation of alkenes studied in detail by Breit and coworkers. 2,4,6-Substituted phosphinines proved to be highly active and very regioselective towards the branched product in the Rh-catalysed hydroformylation of styrene whereas α -unsubstituted phosphinines are inactive.⁵² Substituents in 2- and 6-position on the phosphinine are thought to prevent coordination of more than one ligand to the rhodium centre which inhibits the catalytic activity. The strong π -accepting properties of phosphinines favour the dissociation of a carbonyl ligand from the rhodium complex creating an active site for the hydroformylation process (1.11, Figure 1-9). Due to both factors, phosphinines can compete with known phosphine and phosphite systems concerning regioselectivity and even exceed them with higher activity at milder conditions.⁵³

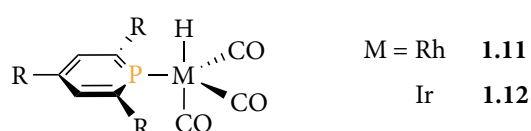


Figure 1-9: Proposed resting state in hydroformylation with phosphinine complexes.³⁵

Further research showed good catalytic activities also for more difficult substrates like higher substituted or internal alkenes. Even tandem isomerisation-hydroformylation reactions were successful. A screening of differently substituted phosphinines was also done and a very high stability of the phosphinine-based catalysts under common hydroformylation conditions was shown by NMR experiments.³⁵ Only the application of chiral bidentate phosphinine ligands to achieve enantiomeric excess did not lead to promising results so far.^{40,52,54} However, overall phosphinines show great potential in Rh-catalysed hydroformylation reactions.

In the cycloisomerisation of dieneynes with a catalyst system based on 2,4,6-triphenylphosphinine (1.1) and Ni(COD)₂ again the π -accepting properties of phosphinines are exploited, in this case to stabilize the increase of electron density on the metal centre during the reaction cycle.⁵⁵

For the asymmetric hydrogenation catalysed by Rh- or Ir-complexes several examples are mentioned in literature. Reetz *et al.* extended the idea of combinatorial homogeneous

catalysis to mixtures of chiral and achiral monodentate phosphorus ligands in transition metal catalysis by using chiral phosphonite **1.15** and achiral phosphinine **1.16** (Figure 1-10) as ligands together with $\text{Rh}(\text{COD})_2\text{BF}_4$ in the hydrogenation of acetamidoacrylate. Interestingly enough, the heterocombination led to an inversion of the enantioselectivity compared to the homocombination of **1.15**. The homocombination of the phosphinine **1.16** on the other hand was inactive.⁵⁶ Müller *et al.* studied the synthesis and reactivity of phosphinines with a chiral phosphite moiety. In the Rh-catalysed hydrogenation of dimethyl itaconate and 2-(N-acetylamino)cinnamate moderate enantiomeric excesses were achieved and kinetic data were determined.⁵⁷ Oxazoline substituted phosphinines were applied in the Ir-catalysed hydrogenation of alkenes and imines as well as in the transfer hydrogenation of acetophenone with potassium methoxide with high to moderate enantiomeric excesses by Neumann und Pfaltz.⁵⁸ However, the phosphinine might not stay intact during the reaction since alcohols or amines are known to add to the $\text{P}=\text{C}$ double bond of phosphinine transition metal complexes.⁵⁹

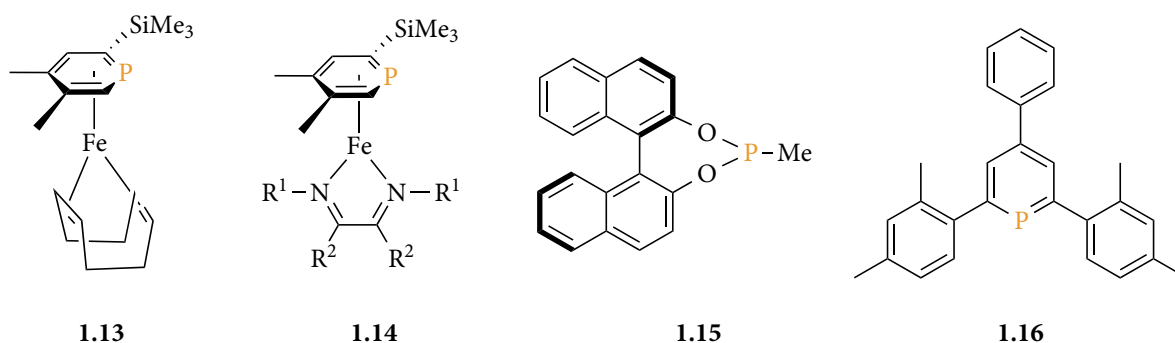
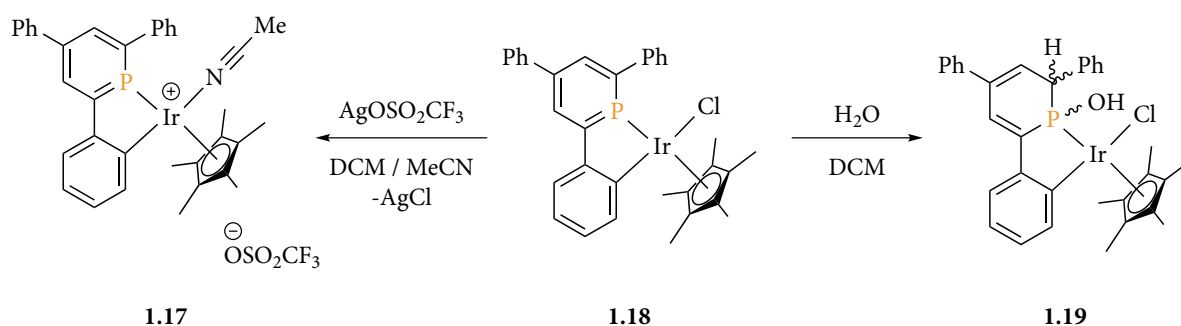


Figure 1-10: Catalysts for cyclotri- and cyclodimerisation (**1.14**, **1.15**) and ligands (**1.16**, **1.17**) used for hydrogenation reactions.

Iyoda *et al.* showed in 2006 the hydrosilylation of alkynes with phosphinine-iridium catalysts. In the absence of phosphinine the reaction led to β -(*Z*)-vinylsilanes. With the addition of 4,4'-5,5'-tetramethylbiphosphinine inversion of selectivity took place and β -(*E*)-vinylsilanes were produced in moderate to high yields. The change in regioselectivity was attributed to the electron withdrawing properties of the phosphinine ligand.⁶⁰ In 2009 Garner *et al.* applied an asymmetric phosphinine in palladium catalysed hydrosilylation of styrene achieving a quantitative reaction with an *ee* of 27%. The low stereoselectivity was explained to be due to the ligand not reaching far enough into the coordination sphere of the metal centre thereby having not enough influence on the hydrosilylation reaction.⁶¹

A combination of $[\text{Rh}(\text{NBD})_2]\text{BF}_4$ and phosphinine **1.16** (Figure 1-10) proved to be a fairly good catalytic system for the isomerisation of allylic alcohols into saturated carbonyl compounds as reported by Reetz *et al.* in 2006.⁶²

Cyclometalated phosphinine-iridium(III) complex **1.17** was used in cerium ammonium nitrate driven water oxidation by Müller *et al.* in 2015. Measured turnover frequencies (TOF) were comparable to other non-phosphorus containing catalysts. Additionally, the reactivity of the catalysing iridium complex towards water was studied and a reversible water addition to the P=C double bond of the phosphinine ring was found thus possibly indicating a ligand/metal cooperation (Scheme 1-5).^{63,64}



Scheme 1-5: Cyclometalated iridium(III) precursor for catalytic water oxidation.

The newest application of phosphinines in homogeneous catalysis was again reported by Müller *et al.* in 2017. A comparative study of 2,4,6-triaryl substituted phosphinines and mesoionic carbenes in gold(I) catalysed cycloisomerisation reactions gave similar results for those structurally related ligands when using standard substrates. With more challenging substrates the stronger π -accepting properties of phosphinines were advantageous and led to a more active catalytic species.⁶⁵

With only these eight examples, the investigation of phosphinines in homogeneous catalysis is still at the very beginning. Much more research is needed to reveal the full potential of these ligands. However, it seems to be clear that the interesting electronic properties of phosphinines, especially their strong π -accepting abilities, can be efficiently employed in catalysis.

systems. Substituting one of the pyridine rings of 2,2'-bipyridines with a phosphinine leads to 2-pyridylphosphinines and opens a new class of intriguing P,N-hybrid ligands.

Until today the unsubstituted 2-pyridylphosphinine (**1.21**) remains unpublished. It is considered to be very reactive and therefore difficult to isolate. To get an idea about the properties of this ligand, the frontier orbitals were visualised by means of DFT calculations (Figure 1-12).

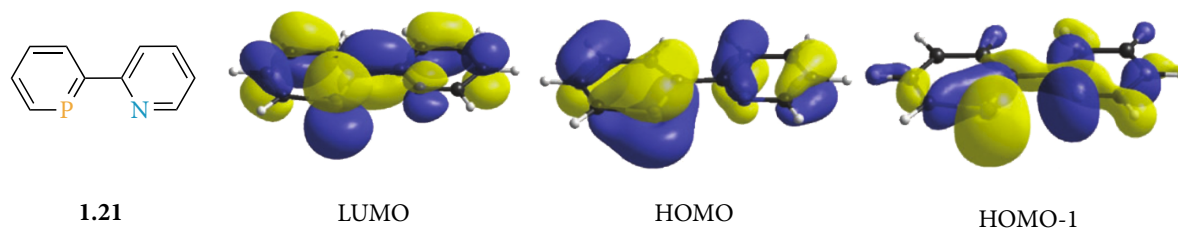
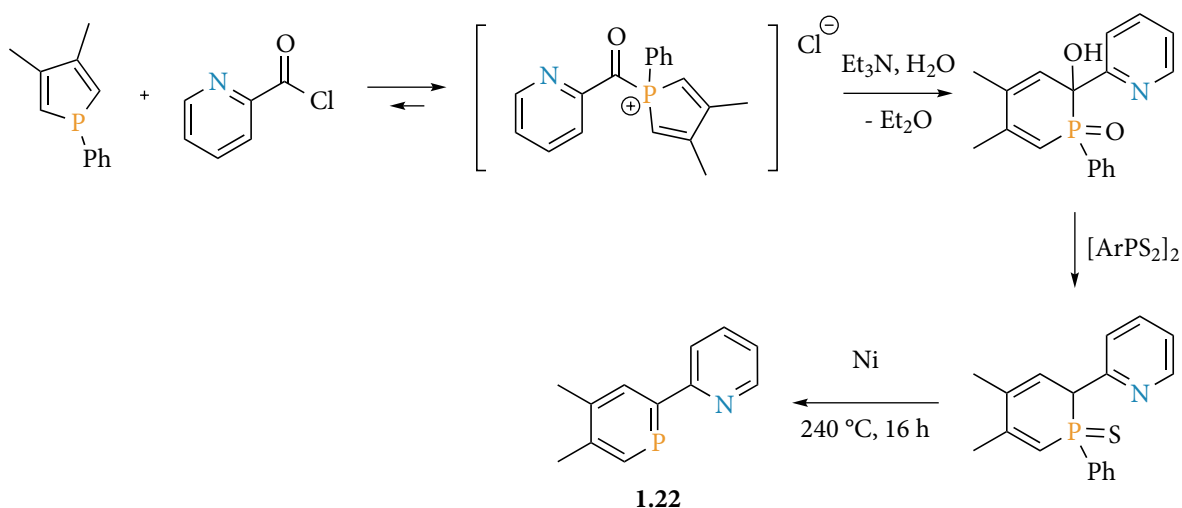


Figure 1-12: Molecular orbitals of 2-pyridylphosphinine (**1.21**)⁸⁰

The lone pairs of both, the phosphinine as well as the pyridine, are represented by the HOMO-1. As can be expected from the electronic properties of phosphinines and pyridines described in chapter 1.3, the HOMO-1 shows a spherical shape with a large coefficient for the phosphorus lone pair compared to the more directed lone pair of the pyridine moiety. The HOMO has π -symmetry and is predominantly localised on the phosphinine ring with very little contribution of the nitrogen. Similarly, also the π -shaped LUMO is centred on the phosphinine reflecting its much stronger π -accepting character. The large coefficients on the phosphorus atom in all three frontier orbital should result in a sizable influence of the phosphinine ring on the reactivity of this compound. Interestingly enough, the order of HOMO and HOMO-1 are reversed in 2,2'-bipyridine (**1.20**) which indicates its better σ -donor properties as a ligand as well as the low reactivity of the π -electron system.⁸⁰

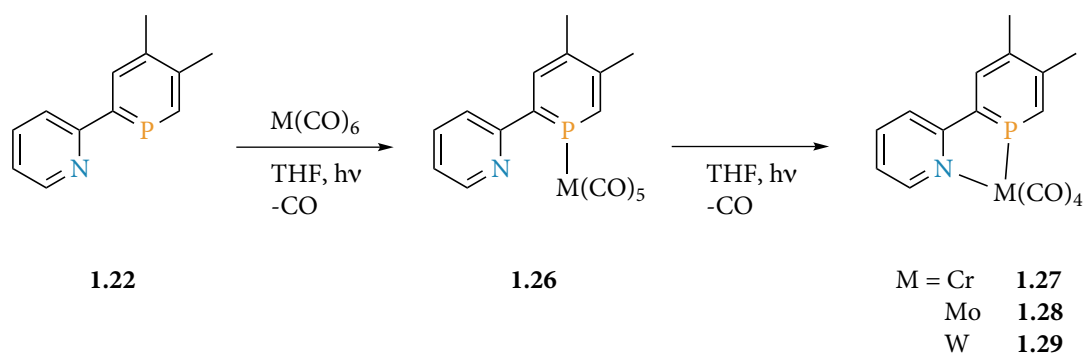
The NIPHOS Ligand and Its Metal Complexes

While the parent compound **1.21** is still unknown, Mathey *et al.* presented a 4,5-dimethyl substituted derivative, the so-called NIPHOS ligand **1.22** in 1982. Starting from 1-phenyl-3,4-dimethylphosphole and 2-pyridinecarbonyl chloride, **1.22** is synthesised *via* ring expansion, transformation into the phosphorus sulfide and lastly pyrolysis with nickel powder (Scheme 1-6).⁸¹



Scheme 1-6: Synthetic pathway to the NIPHOS ligand **1.22**.

Even though the preparation is difficult and not suitable for larger scale synthesis, some coordination chemistry has been done with this ligand. With the zero-valent group-6-metals Cr, Mo and W, complexes of the type $[(\mathbf{1.22})\text{M}(\text{CO})_4]$ (**1.27** – **1.29**) could be synthesised and, in the case of chromium, crystallised. When following the reaction by means of ^{31}P NMR spectroscopy, a two-step mechanism can be seen. The preliminary monocoordinated species **1.26** with the ligand only binding *via* the phosphorus were observed but due to spontaneous loss of carbon monoxide under formation of $[(\text{P},\text{N})\text{M}(\text{CO})_4]$ -complexes, they could not be isolated (Scheme 1-7).⁸²



Scheme 1-7: Complexation of group six precursors $[\text{M}(\text{CO})_6]$ with NIPHOS **1.22**.

Starting from Ir(I) and Rh(I) dimers $[\text{M}_2\text{Cl}_2(\text{L})_2]$ (L = NBD, COD), coordination with NIPHOS (**1.22**) gave unusual dimeric structures of the form $[\text{M}_2\text{L}_2(\mathbf{1.22})_2]^{2+}$ with the phosphinine bridging two metal centres (**1.30**, Figure 1-13). Intriguingly, NIPHOS seems to be the better ligand for Ir(I) and Rh(I) since 2,2'-bipyridine (**1.20**) is replaced by NIPHOS in complexes of the type $[\text{M}_2\text{L}_2(\mathbf{1.20})_2]\text{X}_2$.⁸³

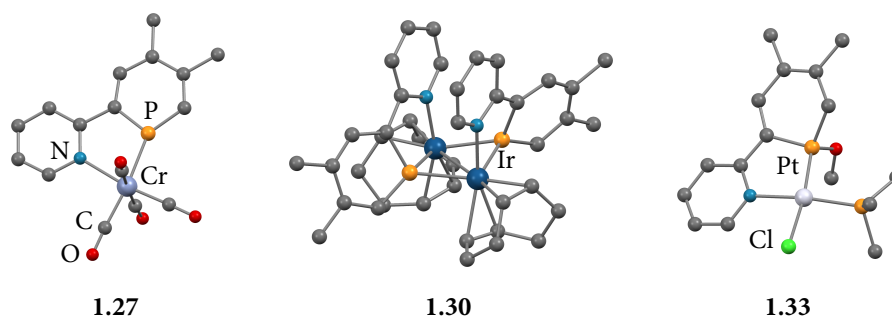
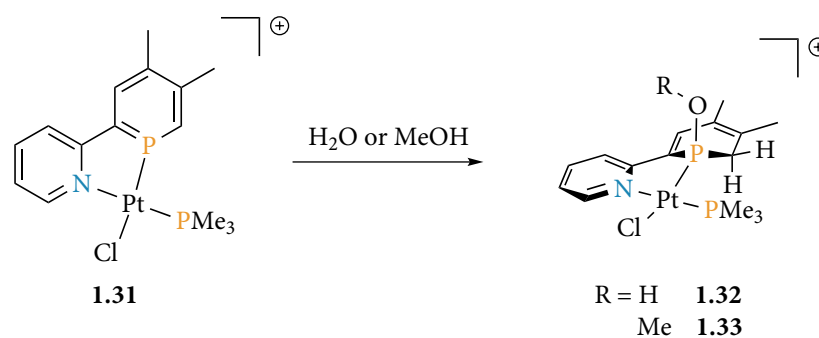


Figure 1-13: NIPHOS complexes [(**1.22**)Cr(CO)₄] (**1.27**), [Ir₂(COD)₂(**1.22**)₂]²⁺ (**1.30**) and [Pt(**1.22**H-OMe)(PMe₃)Cl]⁺ (**1.33**).⁸²⁻⁸⁴

Further increase of the oxidation state of the metal centre proved to be difficult. Only [M₂Cl₄L₂] (M = Pd(II), Pt(II); L = tertiary phosphane) precursors resulted in the successful formation of complexes. These [MCl(**1.22**)L][MCl₃L] type salts (**1.31**, Scheme 1-8) were highly sensitive towards nucleophilic attack and decomposed during drying. Therefore any characterisation was limited to ¹H and ³¹P NMR spectroscopy.⁸⁴ The reason is considered to be the disruption of aromaticity in the phosphinine through coordination to metals in higher oxidation states. As a result the phosphinine behaves more like a cyclophosphahexatriene with a highly reactive P=C double bond.^{85,86} The reactivity towards water and alcohols was studied in more detail and an immediate addition exclusively to the external P=C-double bond was observed (Scheme 1-8). The product with methanol could be crystallised (**1.33**, Figure 1-13). Differentiation between a concerted reaction mechanism or a two-step process was not possible with this molecular structure due to the α-carbon only bearing a proton and therefore *syn* and *anti* addition resulting in the same product. The latter, however, was considered to be more likely.⁸⁴ Interestingly, also bipyridine transition metal complexes react with water in a similar fashion. Caused by the opposite polarity of the P-C bond, the OH-group adds, however, to the carbon atom.⁸⁷

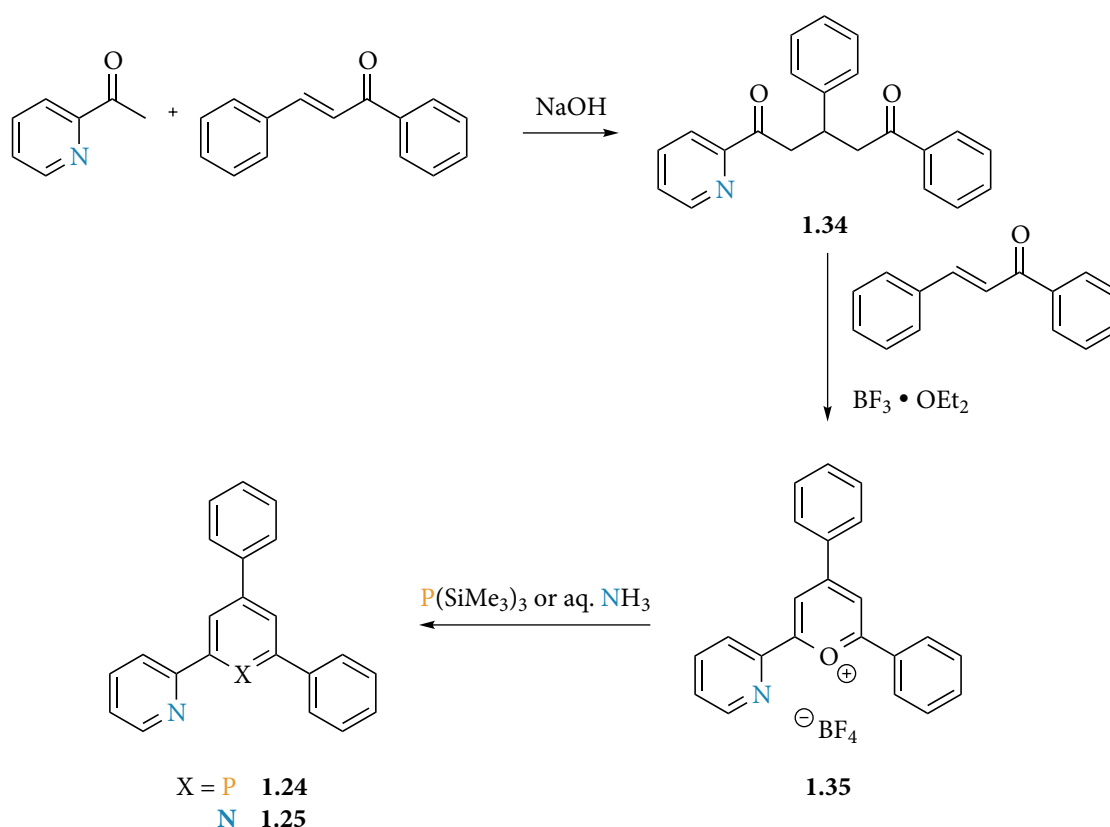


Scheme 1-8: Reaction of NIPHOS-Pt(II) complex **1.31** with water/alcohol.

With these first intriguing results on coordination properties and reactivity of resulting complexes in hand, interest in pyridylphosphanes as new type of P,N-hybrid ligands was awakened. The multi-step synthesis of NIPHOS, however, was not conducive for further research. Therefore, the same group around Mathey tried a new synthetic approach with Pd(0)-catalysed cross-coupling reactions of bromophosphanes. 2-Pyridyl-3-methyl-4,6-dibromophosphine (**1.23**, Figure 1-11) was derived in rather low yield of 40% and described as unstable in solution.⁸⁸

2-(2-Pyridyl)-4,6-diphenylphosphinine: Synthesis, Reactivity and Metal Complexes

A breakthrough was the development of 2-(2-pyridyl)-4,6-diphenylphosphinine (**1.24**, Figure 1-11) by Müller *et al.* in 2007, using the advantages of the modular pyrylium salt route (Scheme 1-4).



Scheme 1-9: Synthesis of 2-pyridyl-4,6-diphenylphosphinine (**1.24**).

From cheap and readily available starting materials 2-acetylpyridine and *trans*-chalcone, diketone **1.34** is formed in a Michael addition. Upon oxidation with *trans*-chalcone in the presence of borontrifluorid etherate, pyrylium salt **1.35** is produced, which can be converted

into the desired pyridylphosphinine **1.24** with $\text{P}(\text{SiMe}_3)_3$. Besides the possibility for larger scale synthesis and a rather stable P,N-hybrid ligand, this synthetic route also allows the formation of the analogous bipyridine compound **1.25** (Figure 1-11) from the pyrylium salt by using aqueous ammonia instead; facts that make comparative studies of both ligand types very accessible.^{37,80}

Up to now, the properties and reactivity of 2-pyridylphosphinine **1.24** has been well investigated in several directions (Figure 1-14).

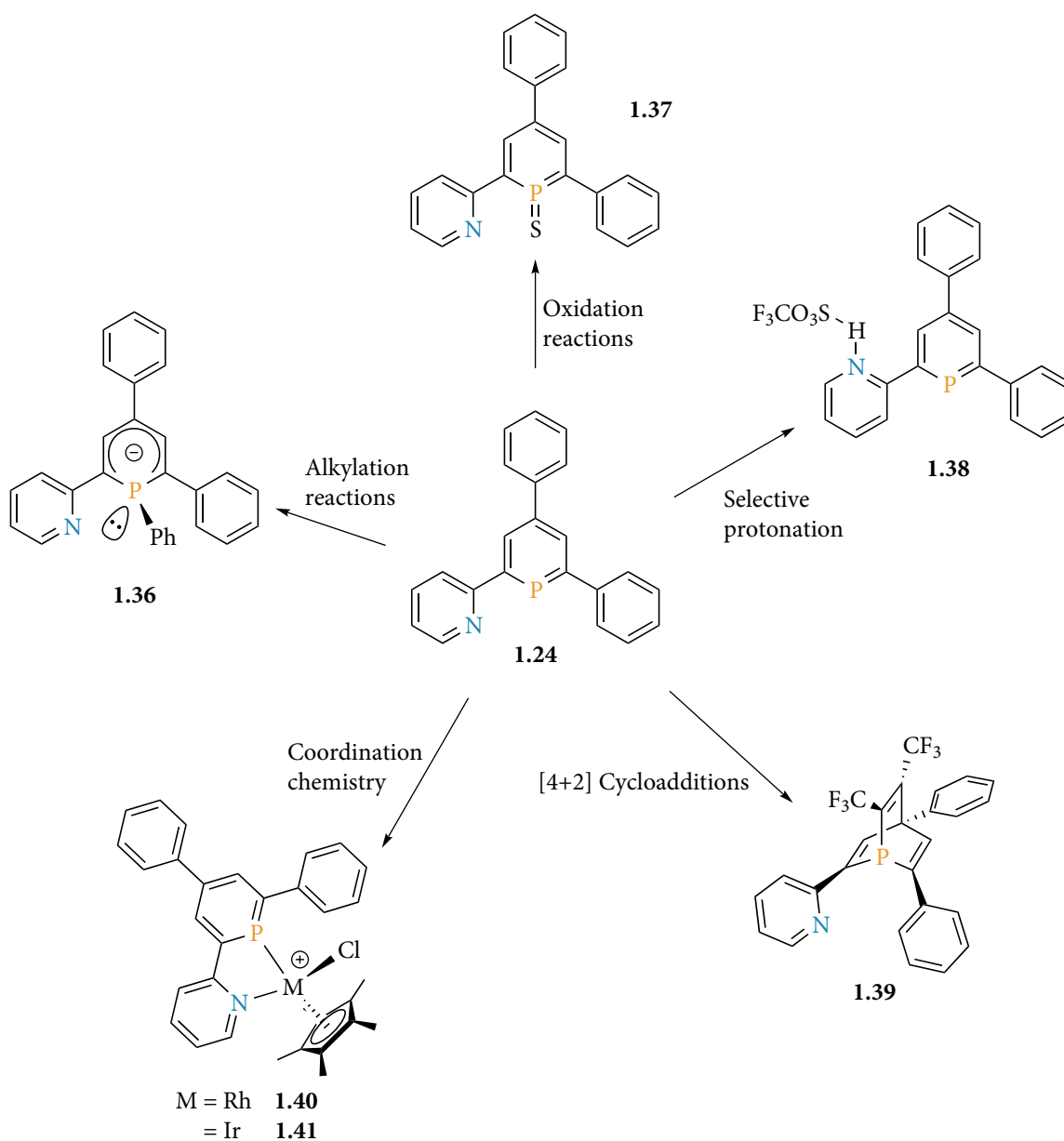


Figure 1-14: Overview of reactivity studies of 2-pyridyl-4,6-diphenylphosphinine (**1.24**) with exemplary products.

The opposite charge distribution in the phosphinine and pyridine rings leads to very different behaviour. While pyridines undergo substitution in 2-position with strong nucleophiles like organolithium compounds or Grignard reagents, phosphinines are alkylated or arylated to form $\lambda^4\sigma^3$ -phosphinine anions.^{25,89} **1.24** has been reacted with methyl, phenyl and ferrocenyl lithium and the $\lambda^4\sigma^3$ -phosphinine-structure has been proven by X-ray crystallography. The reaction creates a stereogenic phosphorus centre so it is interesting to note that even at low temperatures only one sharp signal is observed in the $^{31}\text{P}\{^1\text{H}\}$ NMR spectra although the barrier for inversion on the phosphorus should be high. Not surprisingly, phosphinine anions are extremely sensitive towards nucleophiles, hence the regio- and stereoselectivity of the reaction with water was studied in detail. In coordination experiments with rhodium precursors the pyridyl substituent was shown to enforce complexation *via* the phosphorus lone pair in a chelating fashion whereas other $\lambda^4\sigma^3$ -phosphinine anions usually form η^5 -complexes.^{20,90}

Triaryl-substituted phosphinines are known to be rather stable to air. Deliberate oxidation, however, can be achieved in several ways. 2,4,6-Triphenylphosphinine oxide has been detected but could never be isolated due to its highly reactive nature. With hydrogen peroxide the phosphinine oxide hydrate is formed first, which then decomposes to the 2-hydrophosphinic acid.⁹¹ Oxidation with sulphur, however, leads to comparatively stable phosphinine sulfides and can be achieved under harsh conditions with very long reaction times.⁹² Interestingly, the process can be considerably accelerated with the addition of pyridine to the reaction mixture, which can be attributed to the nucleophilic character of pyridine facilitating the ring opening of S_8 . Incorporation of the pyridine into the phosphinine molecule increases the effect even more so that **1.24** can be converted into 2-pyridylphosphinine sulfide **1.37** at $T = 90\text{ }^\circ\text{C}$ in toluene with over 90% yield within 18 hours.⁹³

As can be expected from the substantial difference in basicity of phosphinines and pyridines mentioned above (Chapter 1.3), the reaction of 2-pyridylphosphinine **1.24** with triflic acid leads to exclusive protonation of the nitrogen atom in the pyridine ring as was confirmed crystallographically for **1.38**.⁹³

Through [4+2] cycloaddition reactions of phosphinines with dienophiles a new ligand class, the so-called phosphabarrelenes, become accessible. Even though phosphabarrelenes are known since 1968 and several transition metal complexes have been reported in literature and employed in homogeneous catalysis, no P,N-hybrid phosphabarrelene has been made until recently.^{33,94–97} Müller *et al.* showed that **1.24** does form phosphabarrelene **1.39** with the highly reactive dienophile hexafluorobutyne, while reaction with benzyne leads to decomposition. A few complexes of **1.39** with transition metals like rhodium, tungsten and gold have been synthesised and their reactivity towards UV light radiation has been explored; discovering a pathway to yet another class of P,N-hybrid ligands, the pyridyl-substituted 5-phospha-semibullvalenes.²⁰

The coordination chemistry of 2-pyridyl-4,6-diphenylphosphinine (**1.24**) towards a wide variety of transition metals in different oxidation states has been studied and compared to the bipyridine analogue **1.25** by the group of Müller *et al.* for several years now and was presented in six publications and two PhD theses.^{20,80,98–103} Therefore only a few examples can be showcased here. As expected for phosphinine ligands, **1.24** readily reacts with metals in low oxidation states. Different coordination modes were observed (Figure 1-15). The chelating nature of 2-pyridylphosphinine, however, reliably prohibits η^6 -coordination *via* the π -system of the phosphinine.

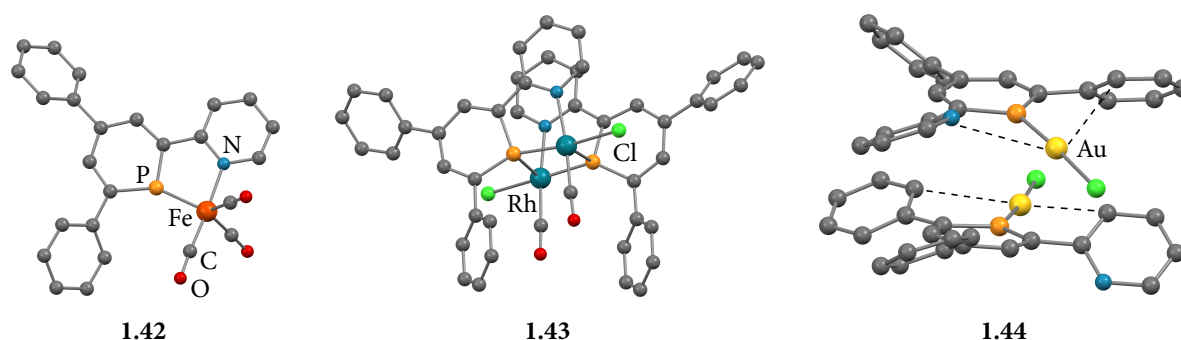


Figure 1-15: Examples of transition metal complexes with **1.24** in low oxidation states.²⁰

Contrary to 2,2'-bipyridines which show unpredictable behaviour and often form complex product mixtures with iron carbonyl precursors, the reaction of P,N-ligand **1.24** with $[\text{Fe}_3(\text{CO})_{12}]$ is straightforward and yields the pentacoordinated iron(0) complex **1.42** where the 2-pyridylphosphinine displays the classical chelating coordination mode.²⁰

In the dimeric rhodium(I) complex **1.43** the 2-pyridylphosphinine ligand **1.24** shows coordination to the metal centre in a μ^2 -P- η^1 -N fashion. The diamond-shaped structure of two rhodium centres and two bridging phosphinine ligands is instantly produced when dissolving **1.25** and $[\text{RhCl}(\text{CO})_2]_2$ in dichloromethane.²⁰

Upon addition of gold(I) precursor $[\text{AuCl}(\text{SMe}_2)]$, P,N-hybrid ligand **1.24** immediately forms κ^1 -P complex **1.44** as can be predicted from the preference for linear complexes with soft donors of gold(I) metal centres. Interesting to note, however, is the presence of Au-C_{arene} interactions in the reaction products (Figure 1-15).²⁰ They can be as strong as aurophilic gold-gold interactions and have recently been recognised to play a role in gold catalysis.^{104,105}

Due to the good accessibility, relative stability and chelating nature of 2-pyridyl-4,6-diphenylphosphinine (**1.24**), it was possible to investigate the coordination chemistry of phosphinines to metals in higher oxidation states in more detail. While no product could be isolated from a reaction mixture of PtCl_2 or PdCl_2 and the NIPHOS ligand **1.22**, **1.24** forms complexes with $[\text{MCl}_2(\text{COD})]$ ($\text{M} = \text{Pd}, \text{Pt}$) in good yields.^{84,103} The resulting planar coordination compounds could be crystallised and represent the first known molecular structures of phosphinine-Pd(II) and -Pt(II) complexes (**1.45**, Figure 1-16).

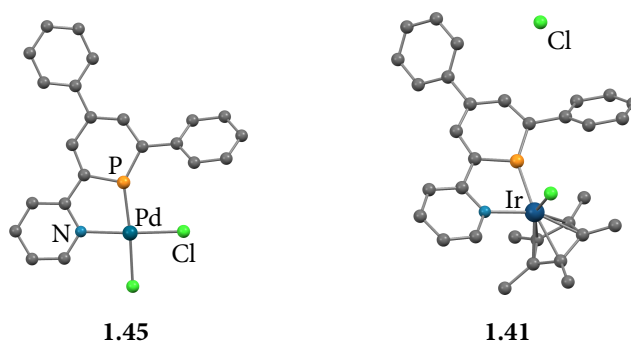
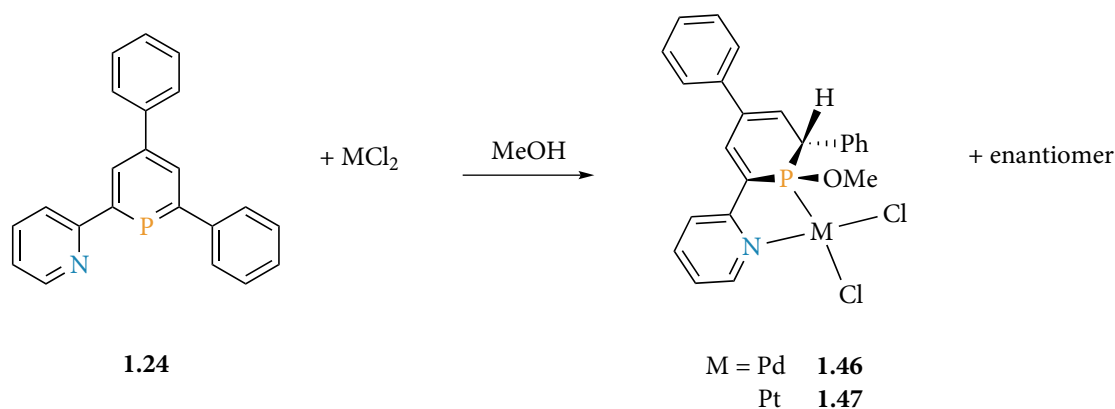


Figure 1-16: Examples of metal complexes with **1.24** in higher oxidation states.^{101,103}

The bidentate P,N-hybrid ligand **1.24** also allowed for the first time the synthesis of phosphinine complexes with rhodium and iridium in a formal oxidation state of +III. With $[\text{MCl}_2(\text{Cp}^*)]_2$ ($\text{M} = \text{Rh}, \text{Ir}$) and **1.24** an instantaneous reaction takes place, leading to mononuclear complexes of the type $[\text{MCl}(\text{Cp}^*)(\mathbf{1.24})]\text{Cl}$ ($\text{M} = \text{Rh}$ (**1.40**), Ir (**1.41**)) (Figure 1-16). Interestingly enough, the bipyridine analogue **1.25** behaves differently and bimetallic ion pairs $[\text{MCl}(\text{Cp}^*)(\mathbf{1.25})]^+[\text{MCl}_3(\text{Cp}^*)]^-$ are produced.⁹⁸

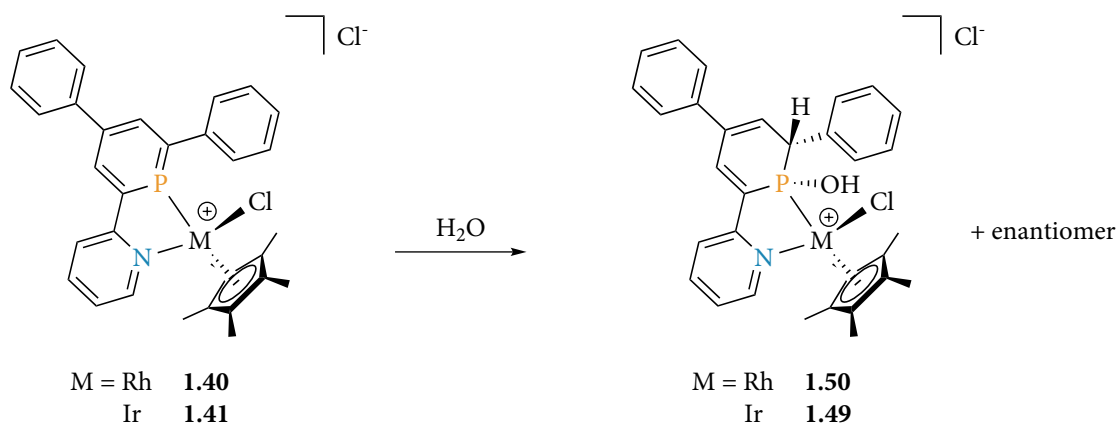
Similar to the NIPHOS complexes of the type $[MCl(\mathbf{1.22})L]^+$ ($M = Pd(II), Pt(II)$; $L =$ tertiary phosphane) (Scheme 1-8), complexes of 2-pyridyl-4,6-diphenylphosphinine ($\mathbf{1.24}$) with transition metals in higher oxidation states were observed to be highly sensitive towards nucleophiles like water and alcohol. Contrary to the NIPHOS ligand $\mathbf{1.22}$, $\mathbf{1.24}$ bears a substituent on the reactive α -carbon that allows insight into the reaction mechanism of the water/alcohol addition to the $P=C$ double bond (Scheme 1-10).



Scheme 1-10: Reactivity study of $[M(\mathbf{1.25})Cl_2]$ ($M = Pd, Pt$) complexes with methanol.

When reacting P,N ligand $\mathbf{1.25}$ with MCl_2 ($M = Pd(II), Pt(II)$) in a 1:1 mixture of methanol and DCM, only one signal was observed by $^{31}P\{^1H\}$ NMR spectroscopy. Therefore, the reaction is regio- as well as diastereoselective, forming only the two enantiomers of either a *syn* or an *anti* addition of methanol to the $P=C$ double bond of the phosphinine ring. Crystals suitable for X-ray diffraction could be obtained from planar $Pd(II)$ complex $\mathbf{1.46}$ and the resulting molecular structure unambiguously proves selective *syn* addition, which conclusively implies a concerted reaction mechanism with a four-membered transition state.¹⁰³

Interestingly, investigation of the water addition reaction to tetrahedral $Rh(III)$ and $Ir(III)$ complexes $\mathbf{1.40}$ and $\mathbf{1.41}$ lead to opposite results (Scheme 1-11). Again the mechanism is regio- and diastereoselective, as shown by only one product signal in $^{31}P\{^1H\}$ NMR spectra, the molecular structure in the crystal of $\mathbf{1.48}$ and $\mathbf{1.49}$, nevertheless, revealed *anti* addition of water to the external $P=C$ double bond.¹⁰¹



Scheme 1-11: Water addition reaction to a Rh(III)/Ir(III) complex of **1.24**.

The reasons for different reaction mechanisms and therefore altered diastereoselectivity in these two systems remain so far unknown. The regioselectivity of the reaction, however, was attributed to the slightly higher electron withdrawing character of the pyridine moiety compared to the phenyl group and the resulting higher nucleophilicity of the external P=C double bond.¹⁰¹

1.8 Motivation of this Thesis

As described above, 2-pyridyl-4,6-diphenylphosphinine (**1.24**) is a well studied compound in the group of Müller *et al.* Its reactivity was investigated in detail and its behaviour towards a multitude of transition metal centres as well as in the derived complexes was explored. With all this basic knowledge in hand, the next logical step was to work towards possible interesting applications of **1.24** and its metal complexes. Since the development of useful processes often requires the exact adjustment of a molecule and its properties to the wanted reaction conditions or outcome, the first aim of this work was to investigate in detail the influence of small substituents in the ligand framework on the properties of P,N-hybrid ligand **1.24** (A, Figure 1-17). In the best case, the addition of electron-donating or -withdrawing groups to the backbone of the molecule would allow a fine tuning of the bonding situation in metal complexes, thereby changing the reactivity in applications of these complexes while leaving the steric characteristics untouched. With bipyridines being well established and often used in various applications, results should be compared with the analogous bipyridine system (B, Figure 1-17).

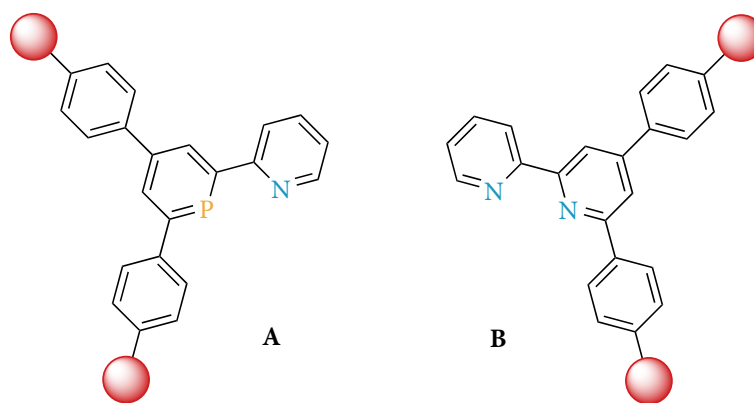
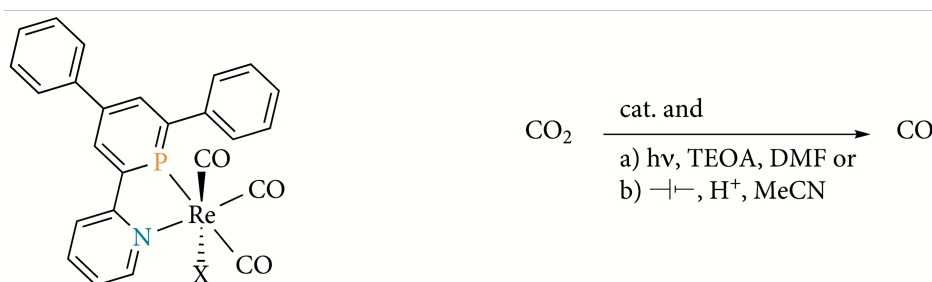


Figure 1-17: Targeted P,N and N,N ligands bearing substituents on the *para*- or *ortho*-phenyl rings.

In a second step, with newly gained understanding about the details of their properties in hand, ligands of type **A** should be applied in homogeneous catalysis. For this purpose the catalytic reduction of carbon dioxide by rhenium(I) carbonyl complexes was chosen as this particular reaction has not been reported for phosphinine-based coordination compounds so far. Opening up a sustainable pathway of producing C_1 -building blocks from the overly abundant CO_2 , the development of a functioning process has been under investigation for several decades. With bipyridine-rhenium(I) complexes as well established catalysts and the proposed idea of π -acceptor ligand properties enhancing catalyst performance, trying the application of pyridylphosphinines in CO_2 reduction processes seemed to be a valuable next step.^{106,107}



Scheme 1-12: P,N-rhenium complex to be synthesised and employed in catalytic CO_2 reduction.

Since no photo- or electrocatalysis has been done in the Müller group at FU Berlin so far, an experimental setup as well as appropriate analytical tools for these reactions needed to be developed and tested first. Secondly, pyridylphosphinine-rhenium complexes were to be synthesised and characterised, then to be employed in the catalytic reduction of CO_2 and compared to the corresponding bipyridine-based systems.

2 Substituent Effects in Pyridylphosphinines and Bipyridines

2.1 Introduction

With 2,2'-bipyridine being a broadly used ligand for complexing a large variety of metal centres, the effects of substituents in the backbone have been studied for decades now. The introduction of substituents is a common way for the adjustment of physical properties and chemical reactivity of resulting complexes to the specific needs of targeted applications. From the tuning of spectroscopic and electrochemical characteristics to the enhancement of catalytic activity in reactions as diverse as transfer hydrogenation, C-H borylation or water oxidation, many examples are known in literature.¹⁰⁸⁻¹¹³ For phosphinines on the other hand, no systematic evaluation of substituent effects has been done so far. The substitution pattern has been determined by the synthetic pathway and the goal of high yields and stability of the products. However, the recent development of a modular synthetic approach to pyridyl-phosphinines allows the introduction of specific substituents in the designated position and the subsequent study of their impact on coordination properties for the first time.³⁷

The electronic situation of a ligand-metal bond in transition metal complexes is often described using ligand field theory (LFT) in conjunction with the Dewar-Chatt-Duncanson model.¹¹⁴ Combining the electrostatic model of crystal field theory with molecular orbital (MO) theory, LFT focuses on the interaction of the frontier orbitals of the ligand with the valence d-orbitals of the metal.¹¹⁵ Dewar, Chatt and Duncanson's approach of splitting the ligand-metal interaction into L->M σ - and π -donation and M->L π -back-donation was originally developed to analyse alkene-transition metal complexes but has since been generalised to different types of ligands.¹¹⁶⁻¹¹⁹

Various methods have been established for the experimental exploration of electron donating and accepting abilities of ligand systems over the years. For Tolman's electronic parameter (TEP), the CO stretching frequencies of A_1 symmetry in the infrared (IR) spectra of $[(L)Ni(CO)_3]$ -complexes are used.^{17,120,121} Due to the toxicity of nickel(0) tetracarbonyl, the concept of exploiting CO stretching bands in IR spectra as electronic probes for the net donating properties of ligands has been extended to a variety of different carbonyl complexes. The Crabtree scale for example uses an average of the two CO stretching frequencies of *cis*- $[(L)M(CO)_2Cl]$ -complexes ($M = Rh, Ir$).¹²² Alternatively, group six metal

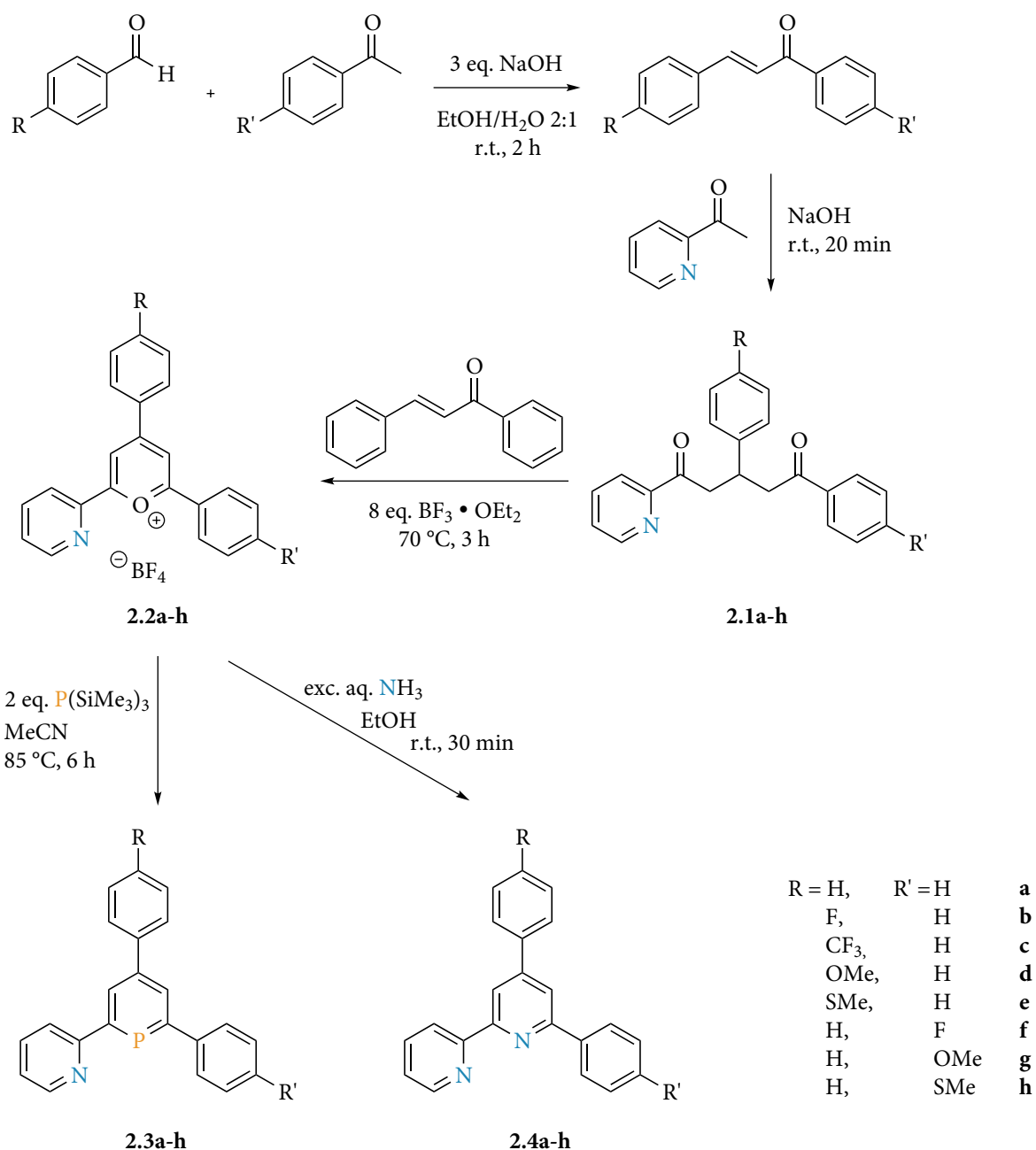
carbonyl complexes are established as common reference system.^{123,124} Also the ¹³C and ³¹P NMR shift or ³¹P-⁷⁷Se coupling constant values have been used to evaluate electronic ligand properties.¹²⁵⁻¹²⁸ Other experimental methods to learn about the electronic properties of ligands include the use of redox potentials, UV-Vis spectroscopy or calorimetry.¹²⁹⁻¹³¹

Nearly every experimental approach to examine the electronic situation in a ligand-metal bond, however, leads to the overall net donation from the ligand. Separation between L->M σ - and π -donation and M->L π -back-donation is difficult. Even though attempts to find an experimental indicator such as the correlation of ³¹P-⁷⁷Se NMR coupling constants to σ -donor properties or ³¹P NMR shift values of phosphinidene-carbene adducts with the π -accepting abilities of the carbene ligand have been made,¹²⁶ theoretical methods are heavily relied on for an insight into the bonding situation of complexes nowadays. MO schemes derived from DFT calculations with the visualisation of the frontier orbitals of the ligands as well as their energy values are commonly provided and relied on to estimate donor and acceptor properties.

Steric demand of ligands can be expressed through occupancy angles or percentage of buried volume as was discussed in chapter 1.2. However, evaluating here the influence of substituents in the backbone of the ligand system, differences in the steric properties of the derivatives are minimal and can be considered negligible.

2.2 Ligand Synthesis

The synthesis of 2-pyridyl-4,6-diphenylphosphinine (**2.3a**, Scheme 2-1) has been developed by Müller *et al.* in 2007 and was described in chapter 1.7.³⁷ Since its synthetic pathway follows the modular approach of the pyrylium salt route by Märkl (Scheme 1-4), it could easily be modified to allow the introduction of substituents into the backbone of the phosphinine. To get a spectrum from electron-withdrawing to electron-donating effects, F-, CF₃-, OMe- and SMe-groups were introduced in 4-position of the *ortho*- or *para*-phenyl rings of **2.3a** (**2.3b-h**, Scheme 2-1). For comparison with the well-studied bipyridine system, the nitrogen equivalents **2.4b-h** were prepared as well, which is easily accomplished by the pyrylium salt route. Pyridylphosphinines **2.3f** and **g** as well as Bipyridines **2.4b**, **e**, **f** and **g** were synthesised before in the group of Müller.^{132,133}



Scheme 2-1: Synthesis of substituted pyridylphosphinines (**2.3a-h**) and bipyridines (**2.4a-h**).

Many substituted benzaldehydes and acetophenones are commercially available or can easily be synthesised *via* literature known Friedel-Crafts reactions,^{134,135} which makes them ideal starting materials for ligand synthesis. In a first step, these benzaldehydes and acetophenones undergo base catalysed aldol condensation to form chalcones. This reaction is reported for a multitude of different substituents including the ones discussed in this work, so the desired products could be obtained in very high yields (generally >97%) *via* a modified procedure from literature.^{136–138}

In a solvent-free Michael addition of 2-acetylpyridine to the chalcones, diketones **2.1b-h** can be derived as colourless to slightly yellow (SMe-derivatives **e** and **h**) solids. Even though isolated yields are normally between 68-80%, thin-layer chromatography of the reaction mixtures shows several by-products explaining the tendency of diketones to form viscous oils during recrystallisation. However, this problem can be overcome by repeated recrystallisation, increase of the amount of solvent or variations in temperature, so **2.1b-h** were all obtained in pure form and fully characterised. Success of the reaction can easily be determined by ¹H NMR spectroscopy where the five alkylic protons show very distinctive resonances between $\delta = 3.30$ to 4.20 ppm, one quintet for the aliphatic C-H group and four doublet of doublets for the two diastereotopic CH₂ groups.

Diketones **2.1b-h** are then converted into the respective pyrylium salts **2.2b-h** in a solvent-free procedure with an excess of borontrifluoride and one equivalent of *trans*-chalcone as hydrogen acceptor. Clean products can be isolated after first washing the reaction mixture with diethyl ether and then recrystallizing it from hot methanol. Only with **2.2d** and **e**, a second washing step with chloroform is necessary before recrystallisation is possible. Alternative workup methods such as recrystallizing from either acetonitrile or ethanol/water mixtures, column chromatography over silica with either acetone or methanol as eluents were tried but led to very similar results. For the substituted derivatives yields are with 9-45% considerably lower than the 60% reported for **2.2a**.³⁷ Problems here are likely caused by the sequence of three reversible reaction steps in the synthetic pathway. With three different aromatic rings and *trans*-chalcone in the mixture a number of recombinations towards other pyrylium salts or different side-products is imaginable.⁴¹ Experimentally, this can be seen in the ³¹P NMR spectra when monitoring the phosphinine synthesis where several small resonances around $\delta = 180$ ppm are often observed and indicate the presence of differently substituted phosphinines besides the main product.

The desired pyridylphosphinines **2.3b-h** can then be derived through O⁺/P exchange from the pyrylium salts **2.2b-h** in refluxing acetonitrile with two equivalents of tris(trimethylsilyl)-phosphane as phosphorus source. Inert column chromatography over silica gives the phosphinines as crude products. Starting with pure petroleum ether as eluent flushes out silicon by-products before isolation of the phosphinine fraction with petroleum ether/ethyl acetate mixtures. Finally, the clean phosphinines **2.3b, d-h** are obtained as pale yellow solids

through recrystallisation from hot acetonitrile. Yields are generally low with 8 – 22%, comparing to the reported yield of 31% for **2.3a**.³⁷ Reasons are again the possible recombination of aromatic rings to different phosphinines, the difficult separation of the desired product from several similar side products as well as the challenging inert column chromatography. Pyridylphosphinine **2.3c** bearing a CF₃-group on the 4-phenyl ring could not be isolated in pure form. During repeated recrystallisation attempts after column chromatography, **2.3c** formed a red oil which turned into a red solid upon drying still showing impurities in NMR spectra. Washing with pentane did not help either, so this ligand was characterised as well as possible and then used as such for coordination experiments. It should, however, be mentioned that the pyridylphosphinines are usually obtained in a rather pure form after column chromatography despite the observed low yields.

Since pyridines are easily accessible from pyrylium salts *via* O⁺/N exchange, the substituted bipyridine derivatives **2.4b-h** have been synthesised and characterised to be used as a reference system. Upon addition of aqueous ammonia to a suspension of pyrylium salt in ethanol, bipyridines **2.4b-h** are formed as colourless solids precipitating from the reaction mixture. After filtration and washing with ethanol/water, no further workup is needed. With up to 98%, yields are generally very good. Filtration being the only workup, yields are largely influenced by the amount of solvent used in the reaction and can be maximised by keeping the ratio of ethanol to pyrylium salt rather small. Bipyridine ligands **2.4b** and **d-g** were reported in literature with different synthetic pathways before. Fluorine and methoxy containing derivatives **2.4b** and **d** were obtained from reaction of enones with pyridinium salts.¹³⁹ Amino allenes were reacted first with aldehydes and then with aryl iodides under palladium catalysis to give bipyridines **2.4f** and **g**.¹⁴⁰ Methylthio-substituted ligand **2.4e** was derived from acetophenone, benzaldehyde and ammonium, similar to what is described in this work. However, none of the products involved in the precedent steps, chalcone, diketone and pyrylium salt, were isolated.¹⁴¹

2.3 Synthesis of [(P,N)W(CO)₄] and [(N,N)W(CO)₄] complexes

The synthesis of tungsten(0) carbonyl complexes with a pyridylphosphinine ligand has been reported for NIPHOS by Mathey and coworkers in 1984 as shown in chapter 1.7.⁸² After

activation of $[W(CO)_6]$ in THF under UV irradiation, the derived $[W(CO)_5(THF)]$ reacts with NIPHOS in a step-wise mechanism first to a monocoordinated species and finally to the $[(P,N)W(CO)_4]$ -complex (Scheme 1-7).

Since phosphinines **2.3a-h** proofed to be stable under UV radiation under these conditions, no separate activation step was needed. In a J. Young NMR tube, $[W(CO)_6]$ was added to a solution of the ligand in THF and placed under UV irradiation. Alternatively, benzene or acetonitrile are suitable solvents as well, especially when trying to get single crystals directly out of the reaction mixture since solubility of the product is lower than in THF. For a faster reaction, regular release of CO overpressure from the reaction vessel by a quick opening to air is helpful especially when using NMR tubes with a small gas volume above the liquid phase. The reaction process can be monitored *via* ^{31}P NMR spectroscopy. Since the general observations are similar for all pyridylphosphinines **2.3a-h**, $^{31}P\{^1H\}$ NMR spectra are shown exemplarily for the reaction of **2.3b** with $[W(CO)_6]$ (Figure 2-1).

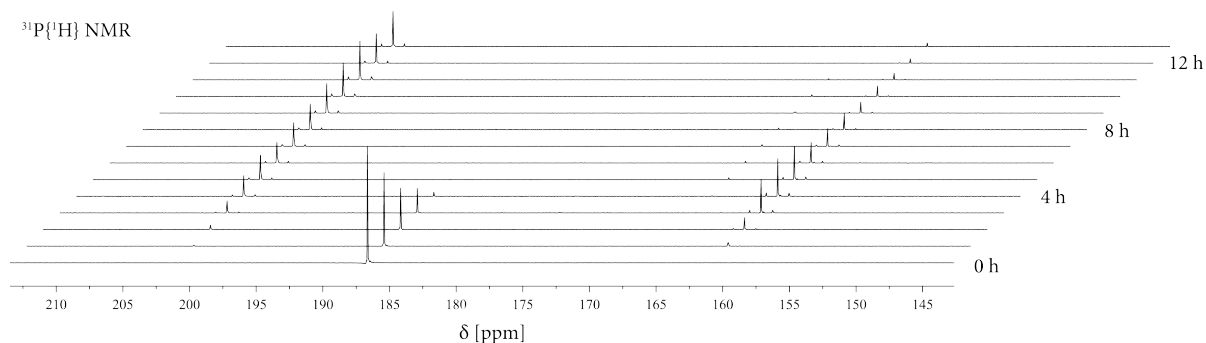
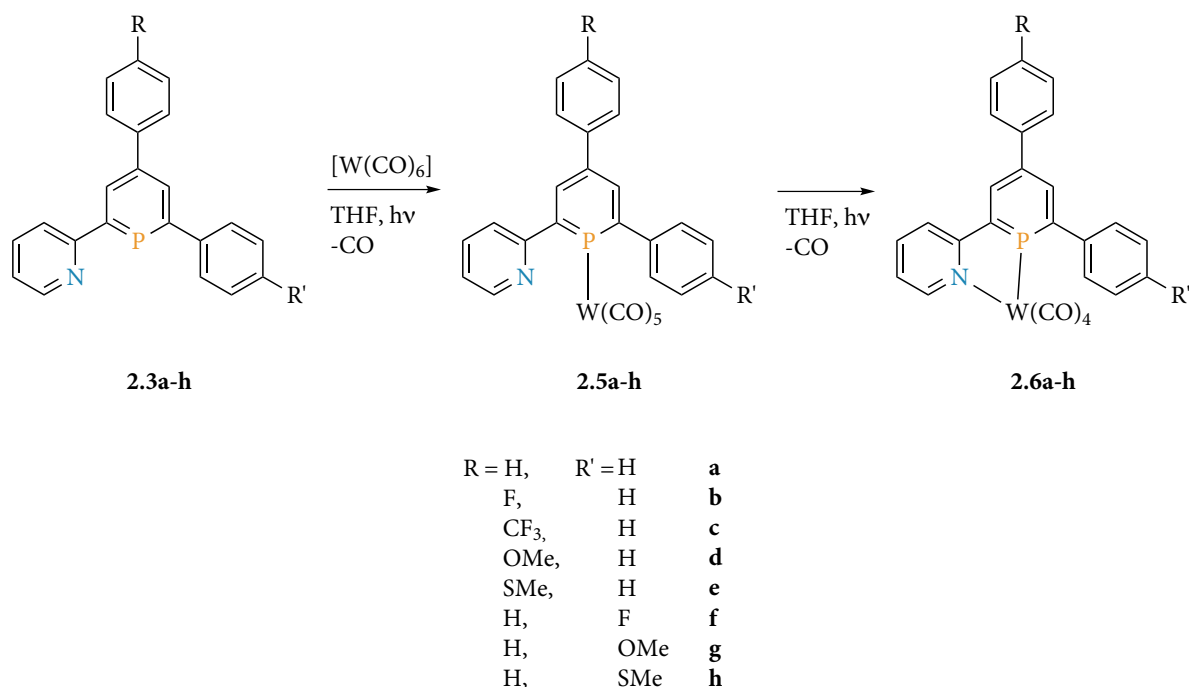


Figure 2-1: Monitoring of the reaction process of **2.3b** with $[W(CO)_6]$ in THF under UV irradiation at room temperature *via* $^{31}P\{^1H\}$ NMR spectroscopy.

The free ligand, giving a resonance at $\delta = 186.7$ ppm, is consumed completely within five hours and two new species appear; one at $\delta = 160.9$ ppm that shows tungsten satellites with a coupling constant of $^1J_{P-W} = 276$ Hz and one at $\delta = 165.8$ ppm which never rises above a ratio of 1:50 compared to the first one. The final product gives a resonance at $\delta = 201.0$ ppm with a tungsten coupling of $^1J_{P-W} = 278$ Hz. Considering the phosphorus-tungsten coupling constant barely changes from the intermediate at $\delta = 160.9$ ppm to the final product and the chemical shift values are very similar to the reported ones for the reaction with NIPHOS, a step-wise mechanism of the complexation with a $[(\kappa-P,N)W(CO)_5]$ -intermediate (**2.5a-h**) as was suggested by Mathey *et al.* is assumed to predominate (Scheme 2-2).⁸² Possibly, the

very small resonance at $\delta = 165.8$ ppm belongs to the second possible intermediate, a $[(\kappa\text{-N,P})\text{W}(\text{CO})_5]$ -type complex.

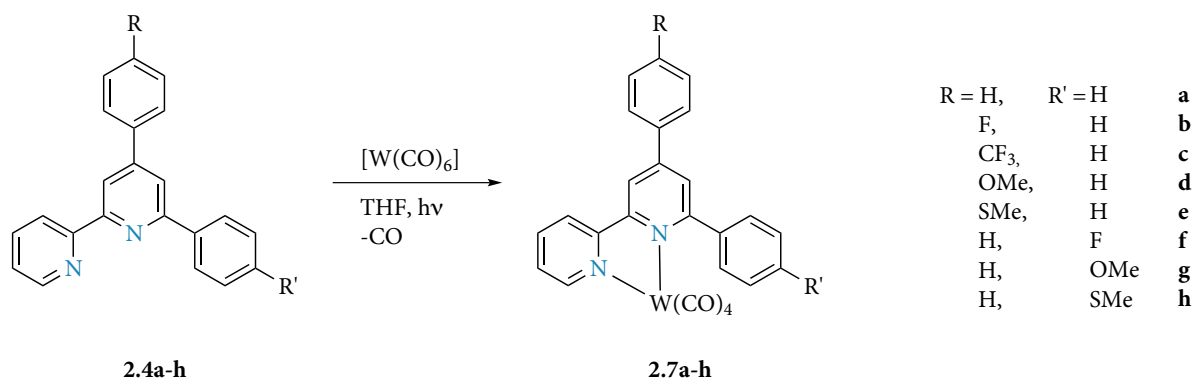


Scheme 2-2: Synthesis of $[(\text{P,N})\text{W}(\text{CO})_4]$ -complexes with pyridylphosphinines **2.3a-h**.

As reported for the NIPHOS derivative, the monocoordinated phosphinine-tungsten complexes **2.5a-h** could not be isolated from the reaction mixture but form the final products **2.6a-h** under spontaneous loss of CO upon workup.⁸² After completion of the reaction in approximately 15 h, $[(\text{P,N})\text{W}(\text{CO})_4]$ -complexes **2.6a-h** are derived as dark red solids through recrystallisation from acetonitrile. According to ³¹P NMR spectroscopy, the reaction is quantitative.

Equivalent to the described complexation with pyridylphosphinines **2.3a-h**, the respective bipyridine-tungsten complexes **2.7a-h** can be synthesised as well (Scheme 2-3). In a Young-NMR-tube $[\text{W}(\text{CO})_6]$ is suspended in a solution of bipyridine in THF, or alternatively acetonitrile or benzene, and set under UV irradiation. Compared to the synthesis of phosphinine complexes **2.6a-h**, the reaction towards $[(\text{N,N})\text{W}(\text{CO})_4]$ -complexes **2.7a-h** is significantly slower and more difficult to push to completion with reaction times of 1-2 days. As can also be seen in the step-wise complexation of pyridylphosphinine ligands, the $[\text{W}(\text{CO})_6]$ -precursor seems to prefer the soft phosphorus-donor over pyridine ligands. Furthermore, ligand exchange experiments showed that pyridylphosphinine **2.3a** replaces

bipyridine **2.4a** almost quantitatively from its tungsten carbonyl complex **2.7a** within a few hours.⁹⁹



Scheme 2-3: Complexation of bipyridines **2.4a-h** with $[W(CO)_6]$ towards $[(N,N)W(CO)_4]$ -type compounds.

With bipyridine ligands, progress of the reaction can only be monitored *via* 1H NMR spectroscopy. Success of the complexation can easily be determined from the significant shift of H_{10} , the proton α to the nitrogen on the outer pyridine moiety (For details on the numbering of atoms see Figure 2-23 in chapter 2.5). Taking the CF_3 -substituted derivative as example, H_{10} shows a resonance of $\delta = 8.71$ ppm in the free ligand **2.4c** which shifts upon coordination to $\delta = 9.33$ ppm in the final complex **2.7c** (Figure 2-2).

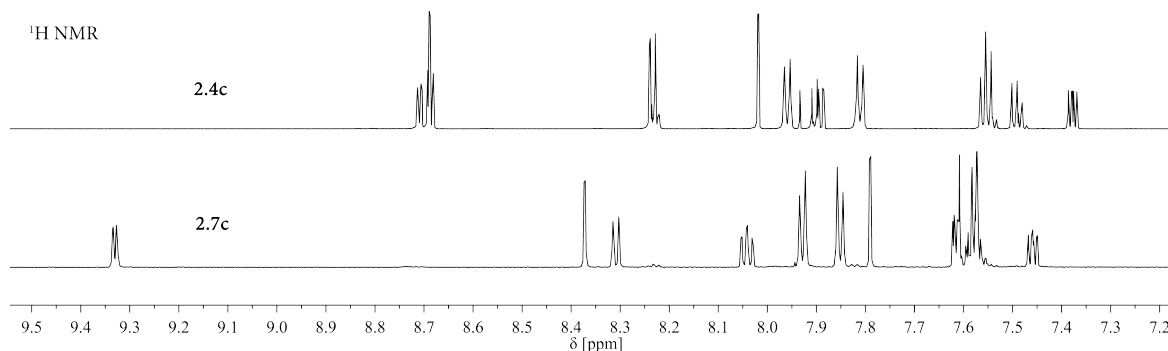


Figure 2-2: 1H NMR spectra of the free ligand **2.4c** and the $[(N,N)W(CO)_4]$ -complex **2.7c** in $DCM-d_2$.

1H NMR spectra measured from the mixture before completion of the reaction are complicated with a multitude of broader resonances. Contrary to the clear mechanism with pyridylphosphinines, the complexation of $[W(CO)_6]$ with bipyridine derivatives **2.4a-h** does not have one defined intermediate. Supposedly, there is no preference for which of the two pyridine moieties coordinates first, explaining broadness and number of resonances in spectra with the presence of two intermediates.

Complexes **2.6a** and **2.7a** with the unsubstituted ligands were synthesised and characterised parallel to this work.^{99,100}

2.4 Investigation of the Substituent Effects

Influences of the different substituents in two positions have been investigated on three synthetic stages from the pyrylium salt to the pyridylphosphinine and bipyridine ligands and the resulting tungsten(0) carbonyl complex using a variety of experimental and theoretical methods. Since pyrylium salts are strongly coloured substances that are often also fluorescent, UV-Vis and fluorescence spectra were measured of **2.2a-h**. DFT calculations afforded shape and energy levels of the frontier orbitals of pyridylphosphinines **2.3a-h** and bipyridines **2.4a-h**. For tungsten complexes **2.6a-h** and **2.7a-h** stretching frequencies of the carbonyl ligands in the IR spectra were used as a source of information about the electronic situation in the complexes and changes through substituents. In addition pyrylium salts (**2.2b, d, e, h**), bipyridine ligands (**2.4c, h**) and tungsten carbonyl complexes (**2.6b, f, g** and **2.7b-h**) were characterised crystallographically as well.

UV-Vis and Fluorescence Spectra of Pyrylium Salts

Over the years numerous applications for pyrylium salts were found. Besides the use as precursors for other hetero- and carbocycles through the attack by nucleophile–ring opening–ring closure sequence also valid for the synthesis of phosphinines,¹⁴² many of them exploit the special photophysical properties of the aromatic pyrylium cations. With intense colours and often strongly fluorescent behaviour, pyrylium salts are, for example, used as photosensitizers in electron-transfer reactions or photocatalysis, as laser dyes, fluorescent probes and polymerisation initiators but also as food additives since 2-phenyl-1-benzopyrylium derivatives are naturally occurring pigments in fruits, flowers and leaves.^{142–148} The influence of substituents on the properties of pyrylium salts has been tested before and was, for example, successfully used for colour tuning the fluorescence emission.^{149–151}

The effect of substituents **a-h** on the pyridylpyrylium salts **2.2** is already visible when the substances are isolated after synthesis. While **2.2a** and fluorine containing derivatives **2.2b,c** and **f** are bright yellow, crystalline solids, methoxy substituted compounds **2.2d** and **g** are

orange. With a methylthio group the colour darkens further to red for **2.2h** and even dark red to violet for **2.2e**. Those observations are confirmed when UV-Vis spectra are measured of **2.2a-h** dissolved in acetonitrile (Figure 2-3 for **2.2a-e**, Figure 2-4 for **2.2a,f-h**).

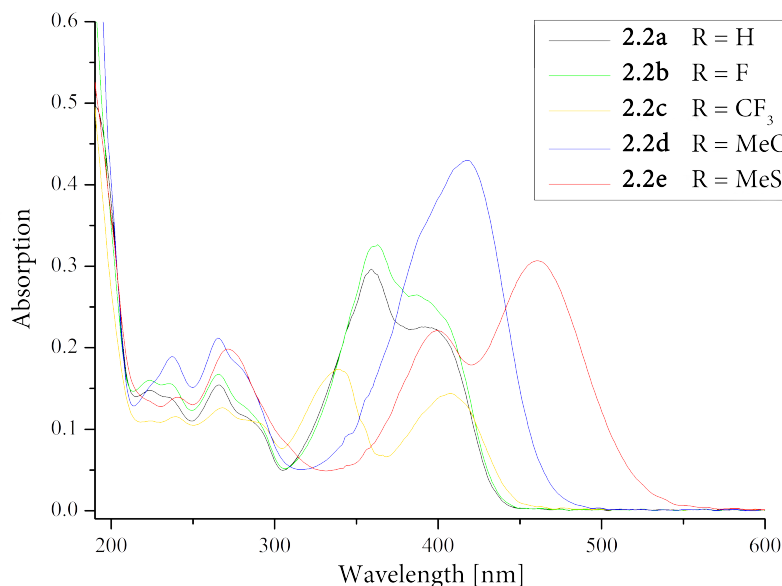


Figure 2-3: UV-Vis spectra of pyrylium salts **2.2a-e** $1 \cdot 10^{-5}$ M in acetonitrile at room temperature.

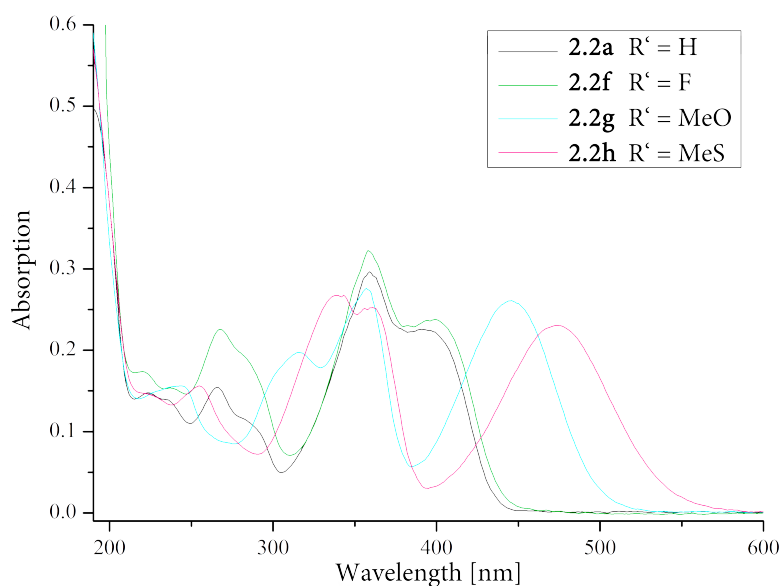


Figure 2-4: UV-Vis spectra of pyrylium salts **2.2a** and **f-h** $1 \cdot 10^{-5}$ M in acetonitrile at room temperature.

Pyrylium salt **2.2a** shows an absorption maximum at $\lambda_2 = 359$ nm with a strong shoulder at $\lambda_1 = 392$ nm. This pattern of two absorption bands in the area of visible light can be noticed for all pyrylium salts **2.2a-h** (Table 2-1). Apart from a slight increase in intensity, fluorine substituted compounds **2.2b** and **f** (**2.2b**: $\lambda = 389$ and 361 nm; **2.2f**: $\lambda = 398$ and 358 nm) give

very similar spectra than **2.2a**. The CF₃-group of **2.2c** causes the absorption to separate into two distinct bands of lower intensity at $\lambda = 406$ and 338 nm.

As expected from the colours in the solid state, a clear bathochromic shift of the longest-wavelength absorption band (λ_1) is observed for the substituents with +M-effect, namely methoxy and methylthio groups. Contrary to all other compounds, the longest wavelength band is also the absorption maximum for pyrylium salts substituted on the *para*-phenyl ring and can be seen at $\lambda_1 = 417$ and 461 nm for **2.2d** and **e**, respectively. Methoxy and methylthio groups on the *ortho*-phenyl ring of the pyrylium salt have an even stronger effect with a shift to $\lambda_1 = 445$ nm for **2.2g** and $\lambda_1 = 473$ nm for **2.2h**. The intensity of the band decreases slightly, however.

	2.2a R = H	2.2b R = F	2.2c R = CF ₃	2.2d R = OMe	2.2e R = SMe	2.2f R' = F	2.2g R' = SMe	2.2h R' = OMe
λ_1 [nm]	392	389	404	417	461	398	445	473
λ_2 [nm]	359	361	338	392 (sh)	400	358	357	360
A ₁ /A ₂	0.76	0.81	0.84	1.20	1.38	0.74	0.94	0.92

Table 2-1: Absorption spectra data of pyrylium salts **2.2a-h** 1·10⁻⁵ M in acetonitrile at room temperature; λ_1 : maximum of the longest-wavelength absorption band, λ_2 : maximum of the second longest-wavelength absorption band, A₁/A₂: ratio of the absorbance at λ_1 and λ_2 , sh: shoulder.

Before attempting to find reasons for these observations, it should be mentioned that pyrylium salts are able to form dimers, aggregates, liquid crystals and films which potentially complicates explaining their properties and behaviour.¹⁵²⁻¹⁵⁴

However, the effect of substituents capable of donating electrons into the π -system of the pyrylium salt onto the absorption spectrum of the compound has been known and used for several decades. Reynolds *et al.* reported in 1973 on the spectroscopy of pyrylium salts taking into account different alkyl, aryl and more complicated substitution patterns. As an example, when comparing 2,4,6-triphenylpyrylium with 2,6-diphenyl-4-(4-dimethylaminophenyl)-pyrylium the longest wavelength absorption band shifts from $\lambda = 405$ nm to $\lambda = 535$ nm.¹⁵⁵ Alternatively, a bathochromic shift can also be reached by the addition of more aromatic rings to the backbone of pyrylium salts.^{150,155}

A comprehensive study on the absorption and fluorescence of pyrylium salts published in 1992 by Czerney *et al.* considers 2,4,6-triarylpyrylium salts as two-dimensional chromophore systems analogous to a model used for triphenylmethane dyes, allowing them to explain the

photophysical properties of a broad variety of differently substituted pyrylium salts. The pyrylium ring together with the *ortho*-substituents build the x-chromophore with a transition dipole moment approximately through the 2- and 6-positions. The y-chromophore is made up of the pyrylium ring and the 4-aryl group (Figure 2-5). Accordingly, the two absorption bands in the visible area of light are called x- and y-bands with the longest-wavelength absorption corresponding to the x-chromophore for pyrylium salts bearing three identical substituents. The y-band is usually of higher intensity than the x-band. Since the pyrylium ring is a strong electron acceptor, a bathochromic shift of each band can be reached by increasing the donor strength of the substituents on the respective chromophore.¹⁵⁶

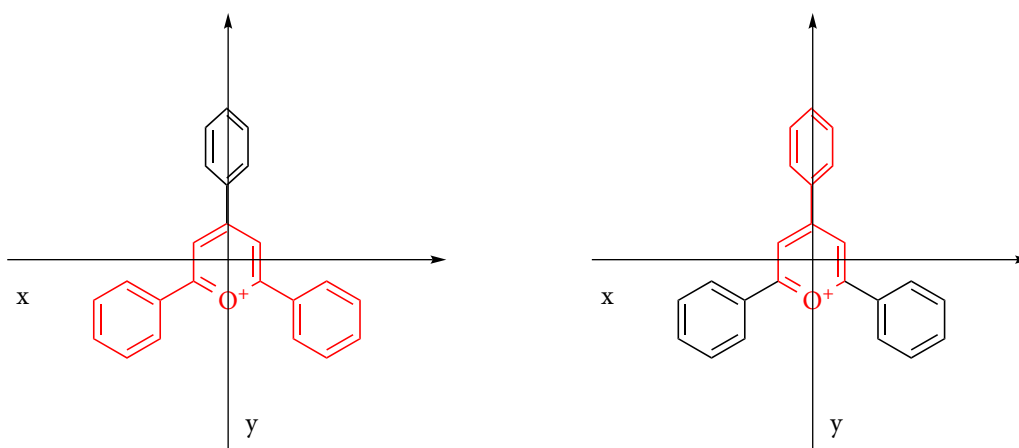


Figure 2-5: 2,4,6-Triarylpyrylium salt with a co-planar x-chromophore (marked left) and a twisted y-chromophore (marked right).

Transferring this concept to here described results, the longest-wavelength absorption of **2.2a** can be classified as x-band ($\lambda_1 = 392$ nm) and the second absorption of higher intensity as y-band ($\lambda_2 = 359$ nm). When introducing substituents into the x-chromophore on the phenyl ring in 6-position, no changes are observed for the y-band ($\lambda_2 = 358$ (**2.2f**), 357 (**2.2g**), 360 nm (**2.2h**)). The x-band, however, exhibits the expected bathochromic shift for electron donating substituents ($\lambda_1 = 398$ (**2.2f**), 445 (**2.2g**), 473 nm (**2.2h**)). The same is true for substituents in the y-chromophore, even though the change in position of x- and y-band makes it harder to recognise. Always being the absorption of lower intensity, the x-band appears roughly between $\lambda = 390$ -400 nm ($\lambda_1 = 392$ (**2.2a**), 389 (**2.2b**), 404 nm (**2.2c**); $\lambda_2 = 392$ (**2.2d**), 400 nm (**2.2e**)) while the y-band shifts towards longer wavelengths with electron donating substituents ($\lambda_2 = 359$ (**2.2a**), 361 (**2.2b**), 338 nm (**2.2c**); $\lambda_1 = 417$ (**2.2d**), 461 nm

(**2.2e**)). The switch in positions of x- and y-band for compounds **2.2d** and **e** can also be seen in the ratio of the intensities (A_1/A_2 ; Table 2-1).

The strong fluorescence of pyrylium salts can often already be seen when handling their solutions in daylight. Differences in colour and intensity of the emitted light depending on the substitution pattern become visible after placing them under UV light. However, the direct connection of the properties of a substituent with changes seen in fluorescence does not always seem to be straightforward (Figure 2-6).

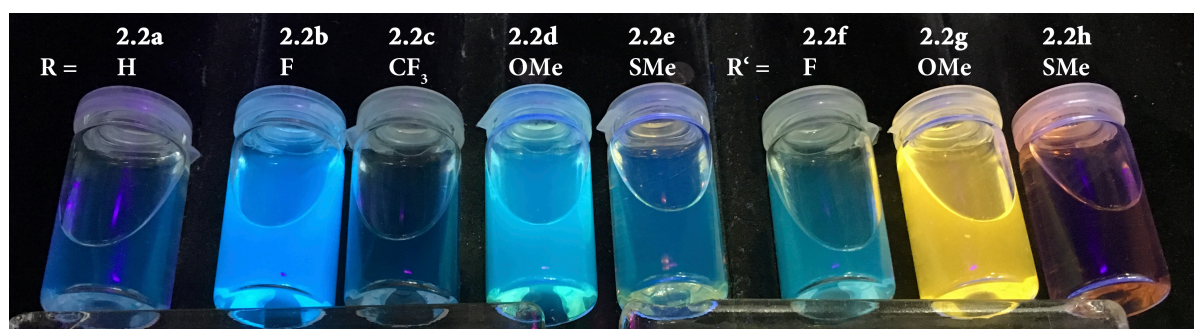


Figure 2-6: Pyrylium salts **2.2a-h** $1 \cdot 10^{-4}$ M in methanol under UV light ($\lambda = 365$ nm).

While compounds **2.2b** and **d** with a fluorine and methoxy group, respectively, in the *para*-phenyl ring exhibit a strong blue fluorescence, the corresponding derivatives with substituents on the *ortho*-phenyl ring emit much weaker in case of **2.2f** ($R' = F$) or show strong yellow emission in case of **2.2g** ($R' = OMe$). The impression of the picture is confirmed when fluorescence emission spectra are measured (Figure 2-7).

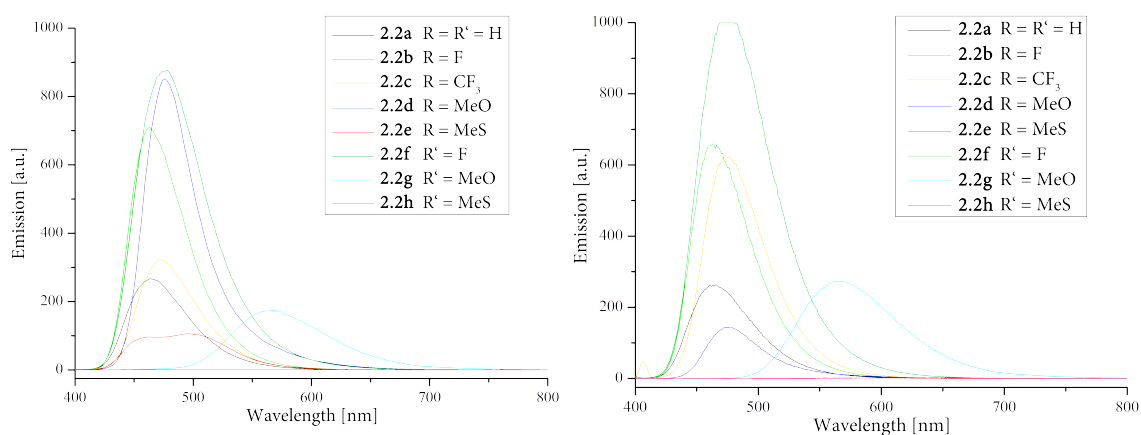


Figure 2-7: Fluorescence emission spectra of pyrylium salts **2.2a-h** $1 \cdot 10^{-4}$ M in methanol with a) excitation at $\lambda = 360$ nm (left), b) excitation at λ_1 (right).

As was expected from the colours of pyrylium salt solutions under UV light (Figure 2-6), the wavelength of emission barely changes for compounds **2.2a-f**. The exact wavelengths of all

bands are listed in Table 2-2. With an excitation wavelength of $\lambda = 360$ nm the intensity of the observed fluorescence is high for **2.2b,d** and **f** (R = F, OMe and R' = F) and decreases substantially for **2.2a,c** and **e** (R = H, CF₃, SMe). Substituents donating electrons to the π -system on the *ortho*-phenyl ring seem to cause a bathochromic shift. The emission of methoxy substituted derivative **2.2g** is seen as yellow light with a band relatively low in intensity at $\lambda = 566$ nm. Methylthio derivative **2.2h** displays a very weak red fluorescence as shown in Figure 2-6. However, the band at $\lambda = 637$ nm is extremely low in intensity and therefore not visible in the reported spectra (Figure 2-7 left).

When switching the excitation wavelength to the maximum absorption wavelength λ_1 for each compound, **2.2c** and **g** become stronger emitters while the emission intensity for **2.2d** and **e** decreases. (Figure 2-7 right)

	2.2a R = H	2.2b R = F	2.2c R = CF ₃	2.2d R = OMe	2.2e R = SMe	2.2f R' = F	2.2g R' = OMe	2.2h R' = SMe
Wavelength [nm]	464	462	473	476	464, 476	476	566	637

Table 2-2: Emission wavelenths in fluorescence spectra of **2.2a-h** 1·10⁻⁴ M in methanol with excitation at $\lambda = 360$ nm.

Similar to these results, electron-accepting substituents such as -F, -CF₃ or -Br that mainly influence the system *via* a (-I)-effect have been reported to be relatively inefficient in changing the fluorescence wavelength of pyrylium salts before.¹⁵⁰ More successful is the variation of the π -electron system through the addition of further aromatic rings into the structure or the incorporation of substituents donating electrons into the π -system.^{150,157} 2,4,6-Triphenylpyrylium tetrafluoroborate in acetonitrile exhibits a fluorescence band at $\lambda = 470$ nm. The addition of methoxy groups shifts this band to $\lambda = 558$ nm for 2,6-di(4-methoxyphenyl)-4-phenylpyrylium tetrafluoroborate, a change very similar to what is seen here for **2.2a** and **g** (R = H and R' = OMe).¹⁵⁸ However, analogous to what was observed in this work for the stronger donating methylthio substituents that substantially weakens or completely quenches the fluorescence, 2,6-diphenyl-4-(4-dimethylaminophenyl)pyrylium tetrafluoroborate did not show any photoluminescence properties.¹⁵⁸

Coming back to the model of 2,4,6-triarylpyrylium salts as two-dimensional chromophore systems by Czerney *et al.*, the photoluminescence results for compounds **2.2a-h** can be rationalised. Looking at light emission properties now, the possible formation of a non-

radiative twisted intramolecular charge transfer (TICT) state has to be taken into account for both, the x- and y-chromophore. Rotation of an aryl ring out of the central pyrylium plane causes a charge separation and therefore decreases or extinguishes the fluorescence. Such a TICT state is promoted by high polarity and low viscosity of the solvent as well as by an increase in acceptor strength of the pyrylium ring. Since the pyrylium centre is stronger accepting for substituents in 4-position, the y-chromophore is more likely to twist. An effect that is further enhanced by strong donating groups on the substituent in *para*-position. In general a high intensity of the emission occurs when the fluorescence transition is due to the x-chromophore.^{153,156}

Considering that the fluorescence was measured in methanol, a very polar solvent of low viscosity, twisting of the y-chromophore especially is very likely. For all compounds except for **2.2d** and **e** the longest wavelength absorption and therefore the fluorescence emission is due to the x-chromophore. The Stokes-shift is with $\Delta\lambda = 70\text{-}80$ nm very similar for pyrylium salts without substituent in the x-chromophore. An increase in donor strength in the x-chromophore leads to an increasing Stokes-shift. ($\Delta\lambda = 78$ (**2.2f**), 121 (**2.2g**), 164 nm (**2.2h**)). The highest fluorescence intensity is reached for **2.2f**; possibly due to its weakly π -donating fluorine substituent in the x-chromophore. For the stronger donating methoxy group (**2.2g**) the emission intensity weakens considerably and the methylthio derivative (**2.2h**) does not show any mentionable emission. Obviously, the formation of a TICT state in the x-chromophore gains importance from **2.2a** and **e** to **2.2g** and **h**. For pyrylium salts **2.2d** and **e** the longest wavelength absorption transfers to the y-chromophore. When exciting at λ_1 **2.2d** only shows weak emission, **2.2e** none at all. Again this can be attributed to twisting in the responsible y-chromophore. However, the emission of both compounds can be greatly increased with excitation of shorter wavelength as can also be seen in the photograph of pyrylium salt solutions under UV light (Figure 2-6) but also from fluorescence spectra (Figure 2-7 right). From these results and the absence of a bathochromic shift of the emission wavelength due to the π -donating methoxy and methylthio groups, a twisting of the y-chromophore also in compounds **2.2d** and **e** and consequently the light emission being due to the x-chromophore is very likely.

Should the fluorescence properties of these pyridylpyrylium salts be used for an application, enhancement of light emission might be achievable through combinations of substituents in

4- and 6-position. As was shown here, the colour of emission can be tuned with variation in the x-chromophore from blue (**2.2f**) to yellow (**2.2g**) to red (**2.2h**). With the addition of a second donating substituent on the 4-phenyl ring in **2.2g** and **h**, the acceptor strength of the pyrylium moiety decreases for the donating groups on the 6-phenyl ring, making the formation of a TICT state in the x-chromophore less likely.¹⁵⁶ This could be an interesting strategy to reach pyrylium salts with tuneable light emission of good intensity.

Molecular Structures of Pyrylium Salts

Crystals suitable for X-ray structure determination could be obtained of fluorine substituted pyrylium salt **2.2b** and both methylthio derivatives, **2.2e** and **h**. The molecular structure of **2.2e** was already presented in earlier work but since it can only be put into context now it will be shown and discussed in detail.¹³³ The compounds crystallised with one molecule in the asymmetric unit in the space group $P2_1/c$ in case of **2.2b** and **h** through slow evaporation of an acetone solution and in the space group $P\bar{1}$ from hot methanol for **2.2h**. X-ray crystal structure data of the methoxy substituted pyrylium salt **2.2d** proves only the connectivity as the data were of too poor quality for a reliable discussion of bond length and angles (Figure 2-8). For more crystallographic information see section 2.5 Experimental Data.

Looking at bond length and angles in these pyrylium salts, similar observations can be made for all three structures (Table 2-3). The central heterocycle only shows minimal widening of the C1-O1-C6 angle to 121°. Due to the slightly smaller size of an oxygen atom which is further enhanced by the positive charge and the higher electronegativity, the two C-O bonds are with approximately 1.35 Å the shortest in the pyrylium ring and bonds get longer towards the opposite side of the ring. Connecting bonds between the four aromatic rings are considerably shorter (≈ 1.47 Å) than standard C-C single bonds (1.53 Å) indicating conjugation of π -electrons over the whole structure.²¹ In case of derivatives **2.2e** and **h**, the methylthio group is in plane with the attached phenyl ring allowing overlap of the π -electron system with one lone pair of the sulphur and thereby confirming the expected +M-effect of this substituent. The same observation can be made for the methoxy substituted pyrylium salt **2.2d**.

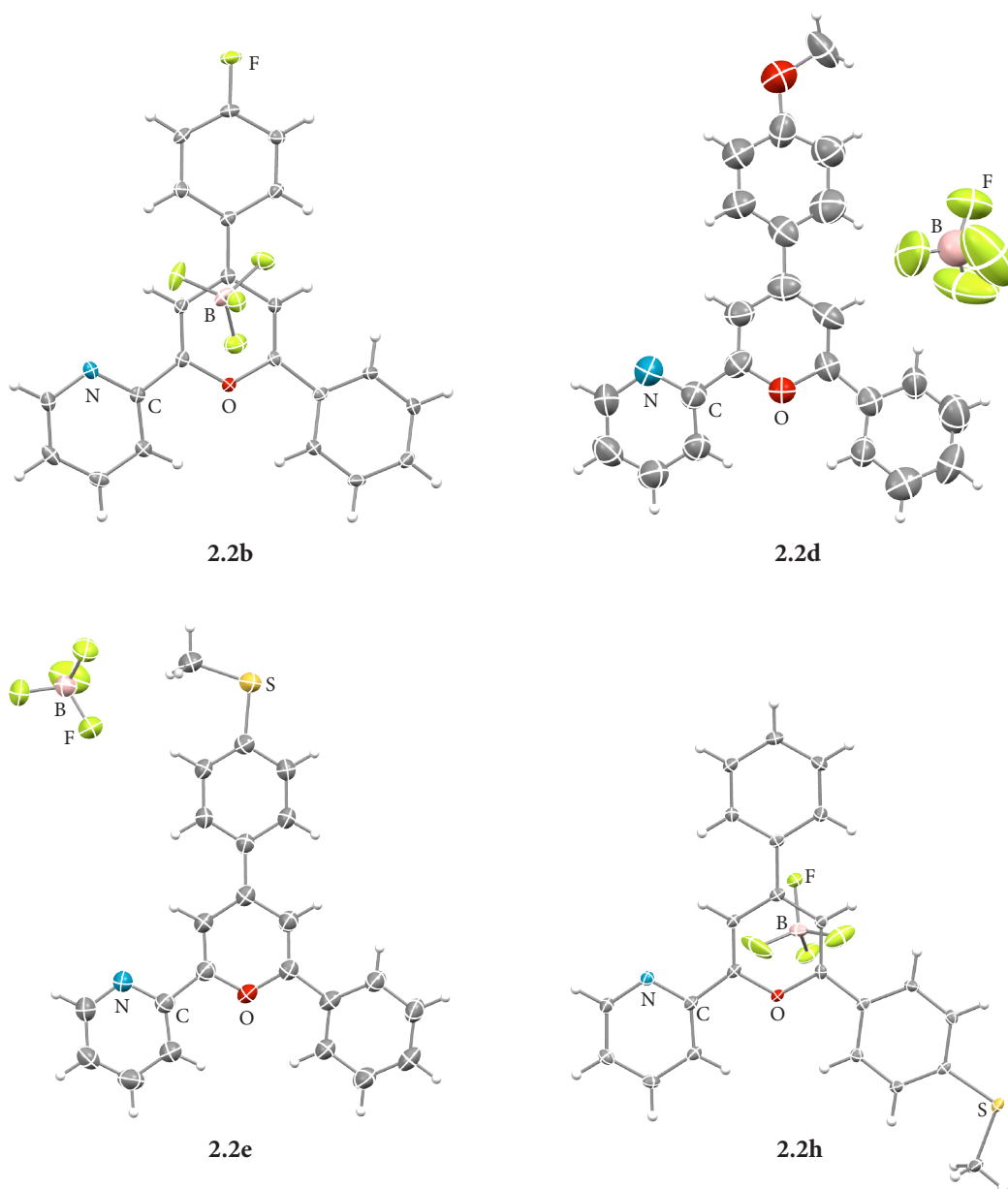


Figure 2-8: Molecular structures in the crystal of pyrylium salts **2.2b**, **d**, **e** and **h**. Displacement ellipsoids are shown at the 50% probability level. The structure of compound **2.2d** is not suited for publication or discussion of bond lengths and angles. The BF_4^- -anion is disordered in the structure of **2.2b**.

Torsion angles of 12.8° maximum between the rings in 2-, 4- and 6-position and the central pyrylium moiety show an almost perfectly co-planar arrangement of the four rings in the solid state. In the crystal, the pyrylium salt molecules build flat layers with distances of around 3.1 \AA (**2.2b**), 3.4 \AA (**2.2e**) and 3.1 \AA (**2.2h**) which is slightly shorter than the sum of van der Waals radii for carbon (3.54 \AA) thereby indicating π - π stacking interactions.¹⁵⁹ Between the layers the aromatic rings are staggered and each cationic pyrylium ring is paired with a BF_4^- -anion of the next layer (Figure 2-9).

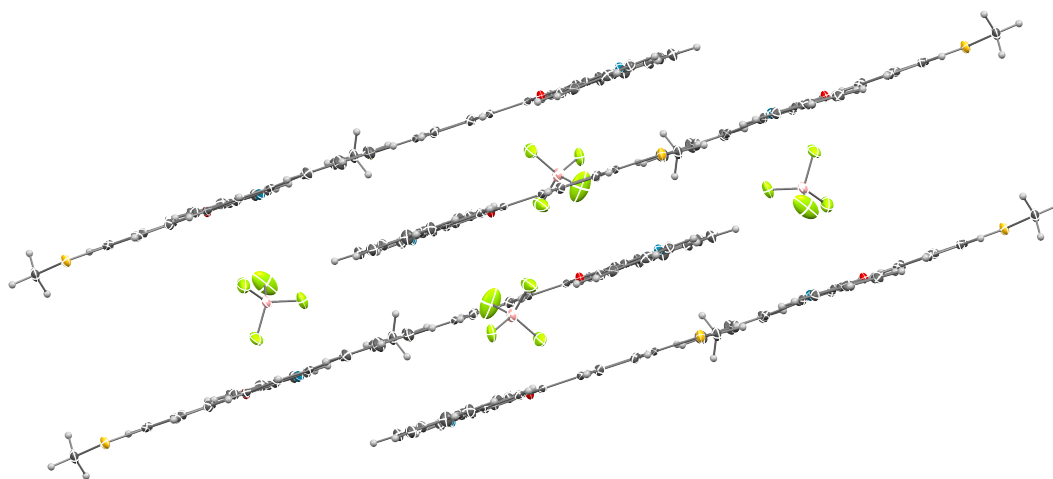


Figure 2-9: Packing of pyrylium salts in the crystal, exemplarily shown for methylthio substituted derivative **2.2h**.

Bond length (Å), angle (°) or torsion angle (°)	2.2b R = F	2.2e R = SMe	2.2h R' = SMe
O1-C1	1.351(2)	1.348(3)	1.350(4)
O1-C5	1.348(2)	1.346(3)	1.355(3)
C1-C2	1.361(2)	1.365(3)	1.366(4)
C2-C3	1.398(3)	1.460(3)	1.401(4)
C3-C4	1.413(3)	1.407(4)	1.405(4)
C4-C5	1.355(3)	1.362(3)	1.357(4)
C1-C11	1.462(2)	1.460(3)	1.456(4)
C3-C17	1.467(3)	1.467(3)	1.474(4)
C5-C6	1.475(3)	1.470(4)	1.461(4)
C1-O1-C5	121.0(1)	121.3(2)	121.3(2)
C20-S1-C23 / C14-S1-C23		103.9(1)	103.9(2)
O1-C1-C11-C12	10.5(2)	6.5(3)	-2.0(4)
C2-C3-C17-C22	0.3(3)	12.8(4)	2.7(4)
O1-C5-C6-C7	4.0(2)	-1.4(3)	3.7(4)
C19-C20-S1-C23 / C13-C14-S1-C23		-4.9(3)	3.9(3)

Table 2-3: Selected bond length (Å), angles (°) and torsion angles (°) of pyrylium salts **2.2b**, **e** and **h**. Numbering of atoms is consistent throughout this work and explained in **Figure 2-23**.

Frontier Orbitals of Pyridylphosphinines and Bipyridines

For more insight into the electronic properties of substituted pyridylphosphinines **2.3a-h** and bipyridines **2.4a-h**, the frontier orbitals were calculated at the B3LYP/6-311+G(d,p) level of DFT theory.²⁶ When comparing shape and energy levels of the frontier orbitals of pyridylphosphinine **2.2a** (Figure 2-10) with the parent phosphinine (**1.2**, Figure 1-4), the dominant influence of the phosphinine moiety becomes obvious. The low-lying LUMO is of π -symmetry with a large coefficient on the phosphorus atom and only a small contribution

by the pyridine. As expected from the parent compound, the lone pair of the phosphorus atom is of high s-character, low in energy and represented by the HOMO-2, which also contains the lone pair of the nitrogen. The visualisation of the HOMO shows the conjugated π -electron system of the phosphinine moiety and the 4-phenyl ring with a large contribution of the phosphorus atom.

Comparison with the respective bipyridine derivative **2.4a** (Figure 2-10) reveals two lone pairs very close in energy to the ones of the phosphinine compound **2.3a** which are represented by the HOMO-2 and HOMO-3. However, they are smaller, more directed and less diffuse, making the compounds slightly better σ -donors. The shapes of the LUMOs are very similar. As expected, the LUMO of **2.4a** is higher in energy with a smaller coefficient on the nitrogen of the central pyridine moiety, leading to decreased π -acceptor properties in comparison to the pyridylphosphinine **2.3a**. Contrary to **2.3a**, no relevant π -donating abilities can be expected from the bipyridine since the two nitrogen atoms barely contribute to the HOMO, while the HOMO-1 is considerably lower in energy.

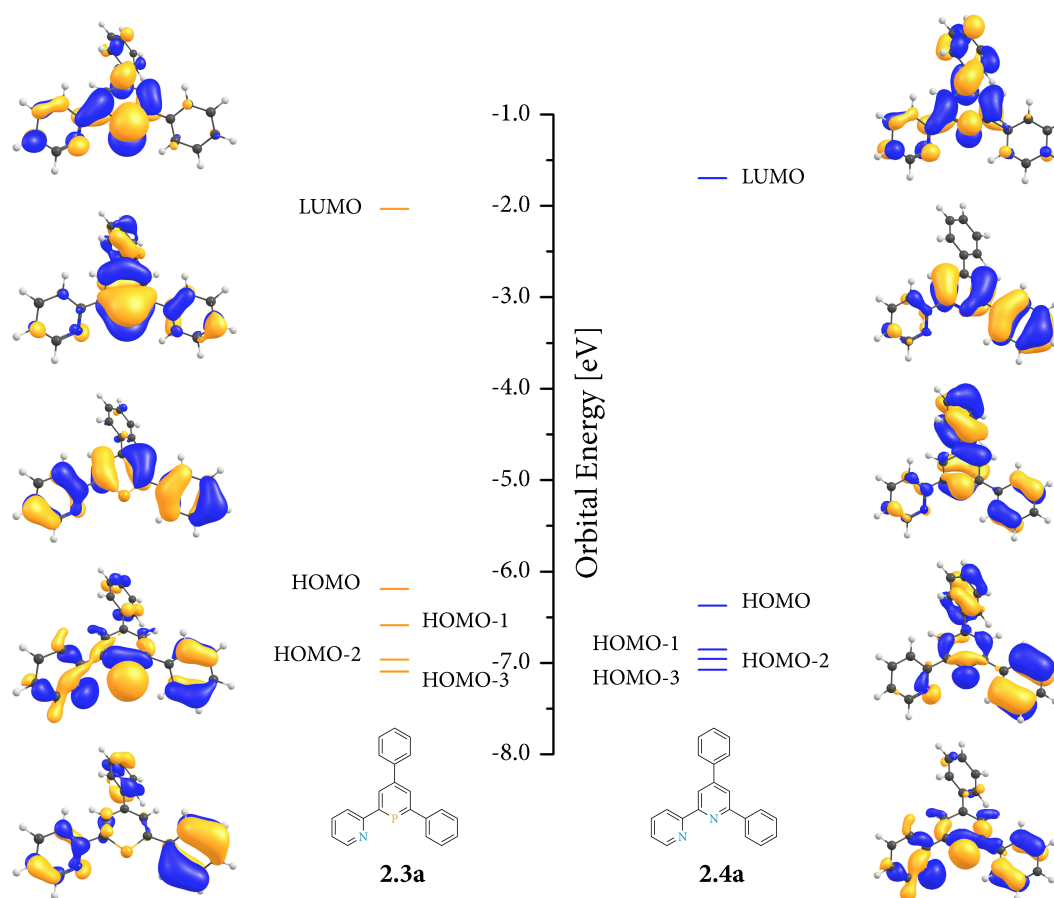


Figure 2-10: Frontier orbitals of the unsubstituted ligands **2.3a** and **2.4a**.

The introduction of fluorine substituents **b**, **c** and **f** does not change the general sequence of orbitals merely the energy levels (Figure 2-12, Figure 2-12; Visualisation of the frontier orbitals of all compounds can be found in the appendix. (Figure 6-1 - Figure 6-6).

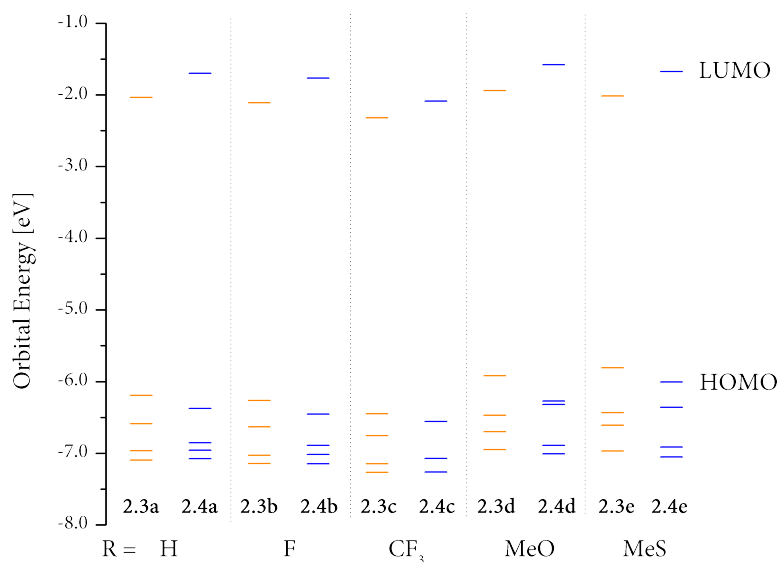


Figure 2-11: Energy levels of frontier orbitals LUMO to HOMO-3 for pyridylphosphinines **2.3a-e** (orange) and bipyridines **2.4a-e** (blue) with substituents in *para*-position of the 4-phenyl ring.

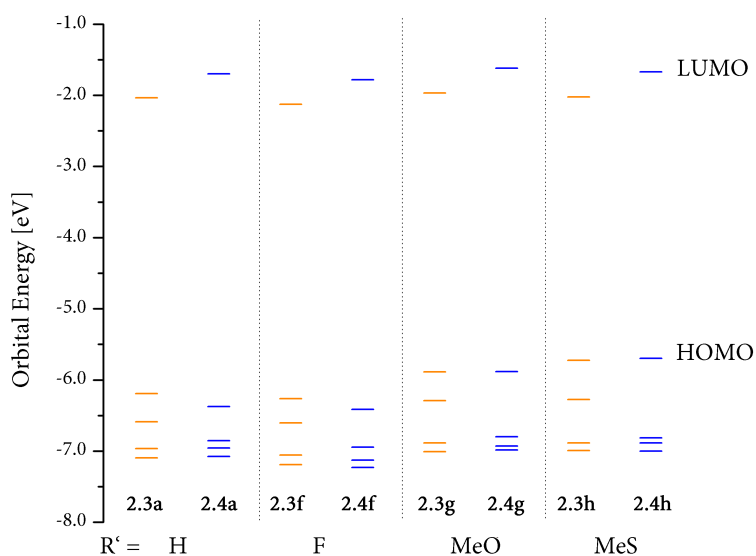


Figure 2-12: Energy levels of frontier orbitals LUMO to HOMO-3 for pyridylphosphinines **2.3a,f-h** (orange) and bipyridines **2.4a,f-h** (blue) with substituents in *para*-position of the 6-phenyl ring.

Electron withdrawing abilities cause all frontier orbitals to decrease in energy for both, pyridylphosphinines (**2.3b**, **c**, **f**) as well as bipyridines (**2.4b**, **c**, **f**). An effect that is more pronounced for the CF₃-derivatives (**2.3c** and **2.4c**). In line with basic chemical intuition these substituents make the compounds weaker σ - and π -donors and stronger π -acceptors. Interestingly, the CF₃-substituted bipyridine **2.4c** exhibits a LUMO at approximately the

same energy as phosphinine **2.3a** and should therefore possess similar π -acceptor strength, once coordinated to a metal.

The influence of +M-substituents OMe and SMe in the 4- or 6-phenyl ring on the frontier orbitals can be determined from compounds **2.3d**, **e**, **g** and **h** as well as **2.4d**, **e**, **g** and **h** (Figure 2-11, Figure 2-12). All eight derivatives show a slight increase in energy for the LUMO suggesting weaker π -acceptor properties for the methoxy and the methylthio substituted compounds. The lone pairs are represented by the HOMO-2 and HOMO-3. Only for **2.4h** the HOMO-2 is of π -symmetry while the lone pairs are solely located in the HOMO-3 (Figure 2-14). Considering the energy levels, there is no difference in σ -donation abilities between reference compound **2.4a** and bipyridines bearing a methoxy or methylthio group (**2.4d**, **e**, **g**, **h**). Also phosphinines substituted on the 6-phenyl ring (**2.3g**, **h**) do not show changes in energy of the lone pair. However, **2.3d** and **e** exhibit elevated energy levels for their lone pairs and can therefore be considered better σ -donors compared to pyridylphosphinine **2.3a**.

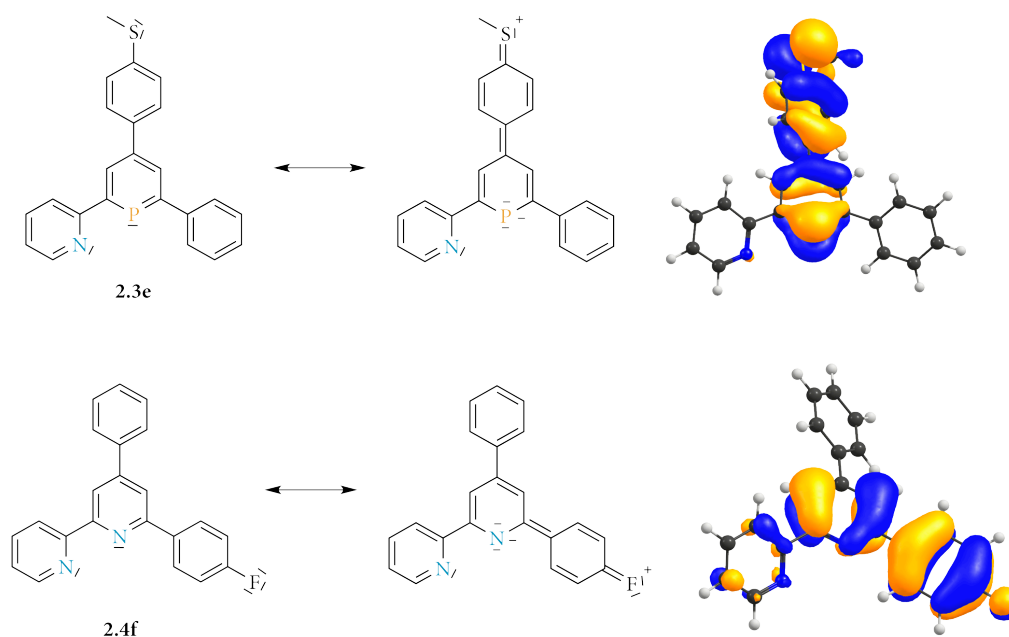


Figure 2-13: Comparison between mesomeric structures and the respective HOMO of compounds bearing a substituent with +M-effect, exemplarily shown for pyridylphosphinine **2.3e** and bipyridine **2.4f**.

Simple resonance structures of substituted pyridylphosphinine and bipyridine ligands already give an idea of the effects of groups able to donate electrons to their π -system. Through the conjugated phenyl rings methoxy and methylthio groups but to a lesser degree

also the fluorine atom are able to push electron density onto the central phosphorus or nitrogen atom which is reflected in the visualisation of the respective HOMO (Figure 2-13).

Going back to the MO scheme, the impact of substituents with +M-effect can be seen on filled orbitals of π -symmetry, namely HOMO (**2.3d, e, g, h**) and HOMO-1 (**2.3e, g, h**) of phosphinines. Those are considerably higher in energy compared to the respective orbitals of **2.3a** and consequently give distinct π -donor properties. The situation is less clear for bipyridine derivatives **2.4 d, e, g** and **h** whose HOMOs and HOMO-1s are of π -symmetry but with only small contributions of the nitrogen in the central pyridine moiety. In conclusion, π -donation abilities should be much less pronounced or not observable when comparing to reference compound **2.4a**. Exemplarily, only the visualisation of the frontier orbitals of **2.3h** is shown here (Figure 2-14), further molecular orbital schemes can be found in the appendix.

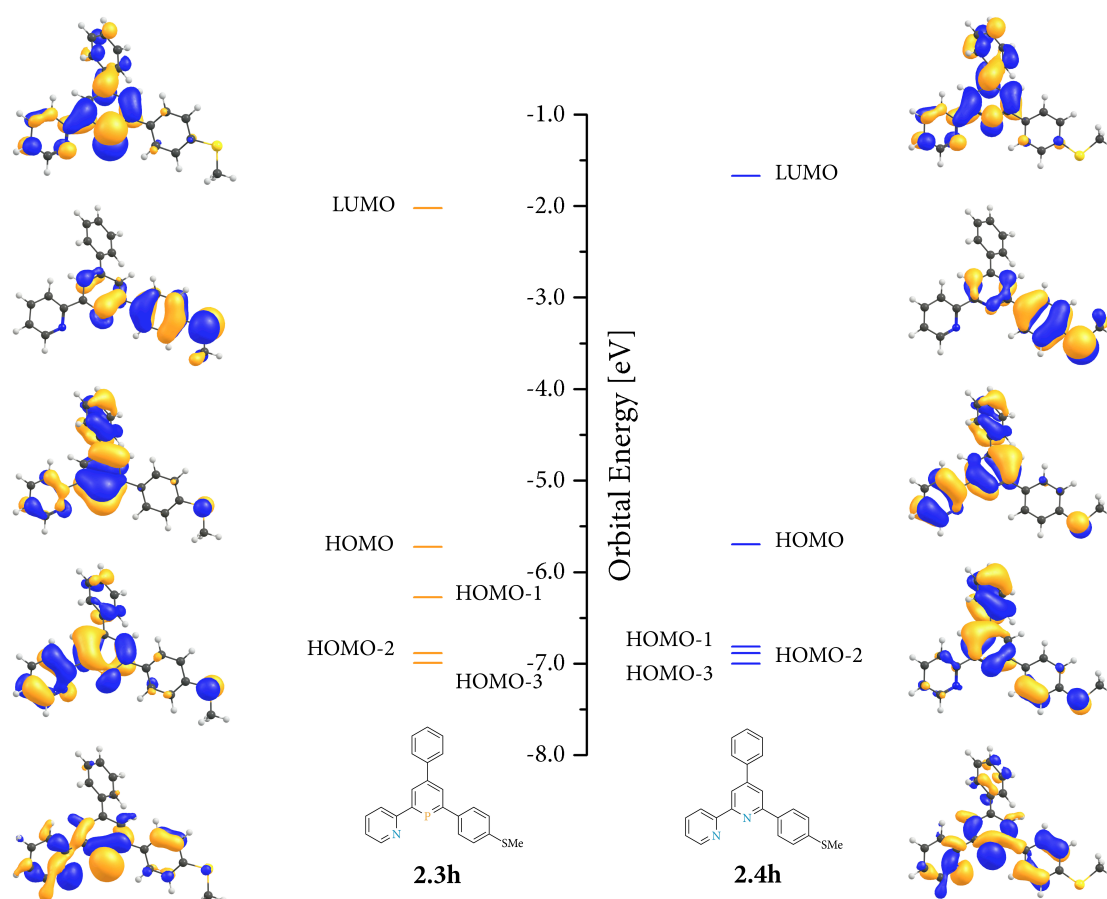


Figure 2-14: Frontier orbitals of the methylthio substituted ligands **2.3h** and **2.4h**.

Molecular Structures of Bipyridine Ligands

Molecular structures of the two literature unknown bipyridines **2.4c** and **h** were obtained by means of X-ray diffraction (Figure 2-15). Both compounds crystallised with one molecule in the asymmetric unit in the space group $P2_1/c$. More crystallographic data can be found in section 2.5 Experimental Data. All bipyridines **2.4a-h** crystallise easily from hot ethanol solutions. For the methylthio substituted compound **2.4e**, the molecular structure is reported in literature and shown here for comparison reasons (Figure 2-15).¹⁴¹

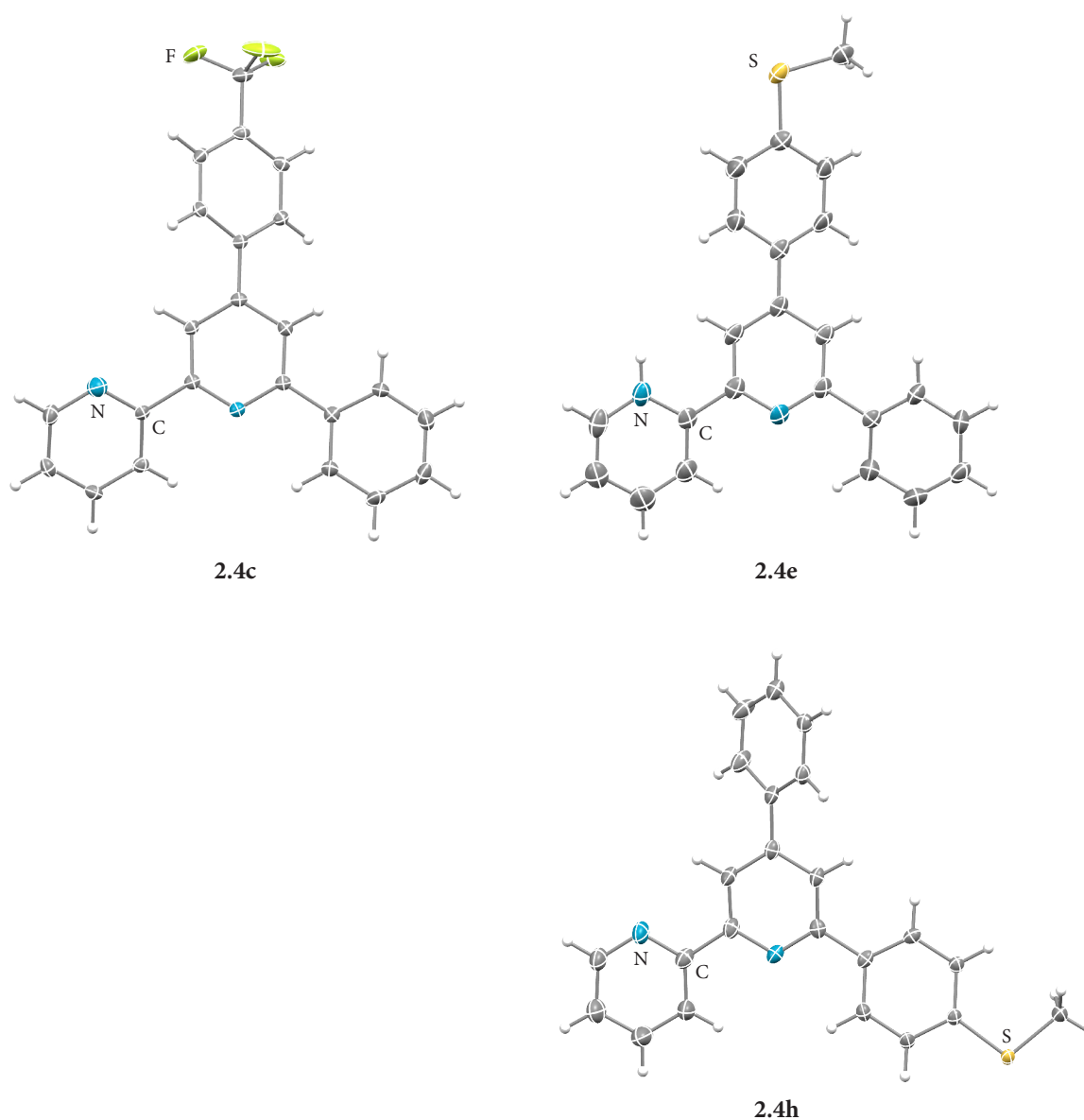


Figure 2-15: Molecular structures in the crystal of bipyridine type ligands. Displacement ellipsoids are shown at the 50% probability level. The structure of compound **2.4e** is taken from literature for comparison.¹⁴¹

As expected, all three structures show the nitrogen atoms of the two pyridine moieties facing away from each other in order to minimise any repulsion between hydrogen atoms. The C-N bonds are slightly shortened with around 1.35 Å and with 118° the C-N-C angle is just below the 120° found for benzene (Table 2-4); both fitting well with literature reported numbers.¹¹ Parallel to the observations made for the pyrylium salts, the methylthio group of bipyridines **2.4e** and **h**, is arranged in a way to let one of the sulfur lone pairs overlap with the aromatic π -electron system; a phenomenon that was also observed in the results of DFT calculations (Figure 2-14).

Contrary to the solid state structures of the pyrylium salts, the aromatic rings in the bipyridines are not completely co-planar. For both, **2.4c** and **h**, the 4-phenyl ring is twisted with a torsion angle of 35.1° and -36.7°, respectively. In case of **2.4c** also the 2-pyridyl moiety is rotated out of the central pyridine plane by 26.1° (Table 2-4). Looking at the positively charged pyrylium ring as a much stronger acceptor unit than pyridine, the co-planar arrangement with perfect conjugation of the π -electron system is likely less favoured for these bipyridines and other factors such as steric repulsion between protons or interactions in the crystal become relevant.

Bond length (Å), angle (°) or torsion angle (°)	2.4c R = CF ₃	2.4h R' = SMe
N1-C1	1.348(2)	1.341(4)
N1-C5	1.345(2)	1.354(4)
C1-C2	1.394(2)	1.387(5)
C2-C3	1.391(3)	1.394(4)
C3-C4	1.390(3)	1.389(5)
C4-C5	1.393(3)	1.384(5)
C1-C11	1.487(3)	1.493(4)
C3-C17	1.484(2)	1.478(5)
C5-C6	1.489(2)	1.488(5)
C1-N1-C5	118.0(1)	117.6(3)
C14-S1-C23		103.4(2)
N1-C1-C11-C12	1.8(3)	-12.1(4)
C2-C3-C17-C18 / C2-C3-C17-C22	35.1(2)	-36.7(5)
N1-C5-C6-C7	-26.1(2)	3.3(5)
C15-C14-S1-C23		-9.2(3)

Table 2-4: Selected bond length (Å), angles (°) and torsion angles (°) of bipyridine-type ligands **2.4c** and **h**. Numbering of atoms is consistent throughout this work and explained in **Figure 2-23**.

Similar to what was observed for pyrylium salts, bipyridine **2.2c** crystallises in layers (Figure 2-16). The distance between the layers, however, is with around 3.7 Å above the sum of the van der Waals radii of carbon (3.54 Å) and no short contacts are found between them.

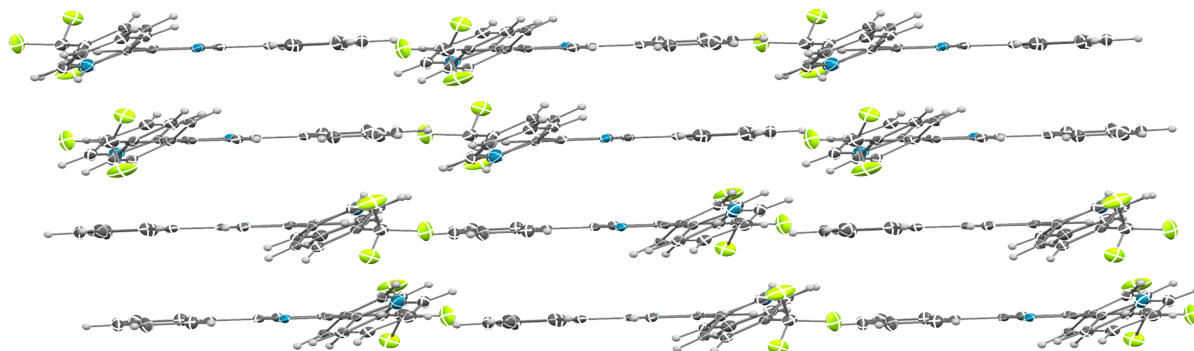


Figure 2-16: Packing in the crystal of CF₃-substituted bipyridine **2.4c**.

The methylthio substituted Ligand **2.4h** on the other hand builds zigzag layers 3.8 Å apart where each molecule is perpendicular to the next one and T-shaped C-H- π interactions can be found connecting the molecules in one layer (Figure 2-17).

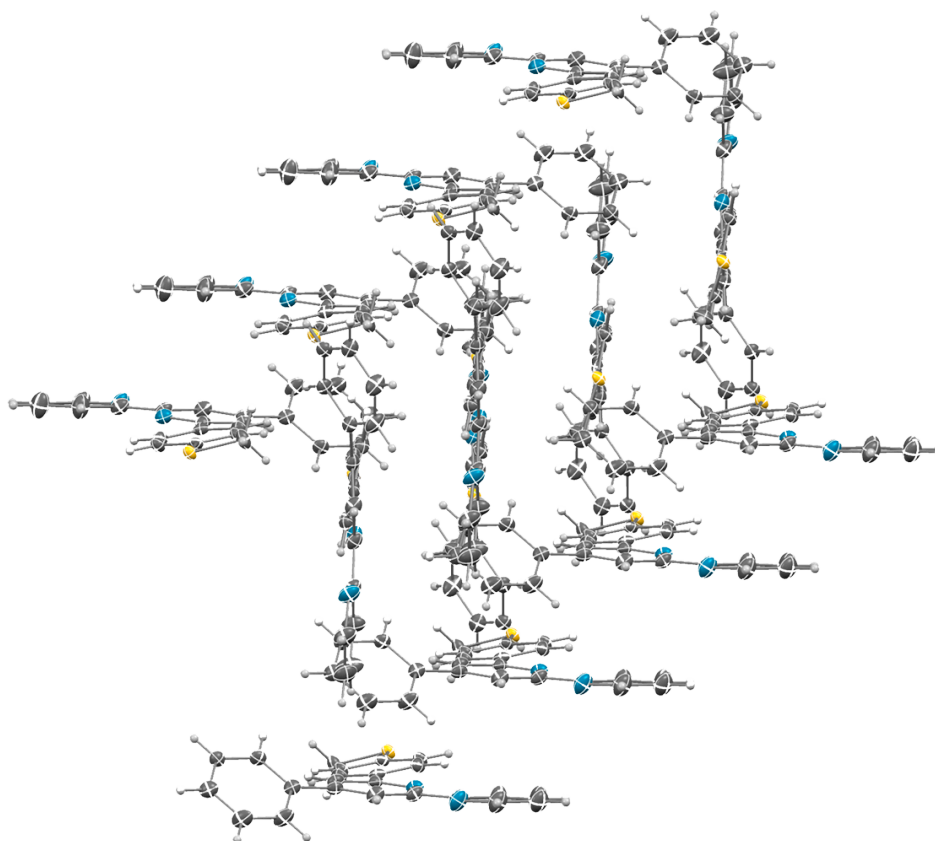


Figure 2-17: Packing in the crystal of SMe-substituted bipyridine derivative **2.4h**.

IR Spectra of [(P,N)W(CO)₄] and [(N,N)W(CO)₄] Complexes

Since tungsten carbonyl complexes were synthesised for both sets of ligands **2.3a-h** and **2.4a-h** (Chapter 2.3), the stretching bands of the carbonyl units in IR spectra were used as indicators for the electronic situation in the complexes. Electron rich metals push more electron density into the antibonding π^* -orbital of the carbonyl moiety leading to a weakening of its bond which can be observed through a shift of the CO stretching bands towards lower wavenumbers and *vice versa*.¹⁶⁰ The IR bands are indicative of the net donation from the ligand to the metal and do not allow separation of σ -donation, π -donation and π -acceptance.¹²⁶ In agreement with related compounds, all complexes show characteristic bands in the area of $\tilde{\nu} = 2000\text{-}1800\text{ cm}^{-1}$ (**2.6a-h**: Table 2-5, **2.7a-h**: Table 2-6).^{82,161}

Generally, carbonyl stretching bands of pyridylphosphinine complexes appear at higher wavenumbers ($10\text{-}20\text{ cm}^{-1}$) than the respective bipyridine compounds. Since σ -donating abilities proved to be quite similar for both ligand types in the results of DFT calculations, this can be attributed to the considerably higher π -acceptor strength of phosphinines, which is again in line with DFT calculations discussed above (Figure 2-11).

	2.6a ¹⁰⁰ R = H	2.6b R = F	2.6c R = CF ₃	2.6d R = OMe	2.6e R = SMe	2.6f R' = F	2.6g R' = OMe	2.6h R' = SMe
$\tilde{\nu}(\text{CO}) [\text{cm}^{-1}]$	2008	2012		2015	2014	2009	2007	2016
	1893	1893	2014	1973	1971	1902	1882	1975
	1870	1877	1920	1891	1889	1870	1854	1893
	1836	1840	1857	1857	1859	1840	1827 (sh)	1859

Table 2-5: Carbonyl stretching bands in solid state FT-IR spectra of [(P,N)W(CO)₄]-type complexes **2.6a-h**.

	2.7a ¹⁰⁰ R = H	2.7b R = F	2.7c R = CF ₃	2.7d R = OMe	2.7e R = SMe	2.7f R' = F	2.7g R' = OMe	2.7h R' = SMe
$\tilde{\nu}(\text{CO}) [\text{cm}^{-1}]$	1999	2000	2002, 1997	1996			1989	
	1872	1872	1887, 1877	1873	1999	2002	1867	1991
	1846	1853	1867	1846	1934	1882	1853	1873
	1813	1802	1859, 1848	1806	1865	1851	1817	1850
		1783	1817, 1805	1777 (sh)	1823	1819	1810	1816

Table 2-6: Carbonyl stretching bands in solid state FT-IR spectra of [(N,N)W(CO)₄]-type complexes **2.7a-h**.

The two sets of values observed for **2.7c** can be explained through two independent molecules found in the asymmetric unit in X-ray crystal structure determination.

Electron withdrawing substituents should shift the CO stretching bands to higher wavenumbers through a strengthening of the carbonyl bond. The expected effect is visible for pyridylphosphinine and bipyridine compounds bearing fluorine and trifluoromethyl

groups in their backbone (**2.6b, c, f** and **2.7b, c, f**). For the fluorine atom the impact is minimal due to the $-I$ -effect being counteracted by a small $+M$ -effect. Since the mesomeric effect of fluorine atoms does not play a role in the impact of the CF_3 -group, the shift is more pronounced for complexes **2.6c** and **2.7c**. Interpretation of the IR spectrum of CF_3 -substituted bipyridine complex **2.7c** is, however, complicated due to the large number of bands observed in the area of carbonyl stretching bands. X-ray crystal structure determination revealed two independent molecules of **2.7c** in the asymmetric unit, leading to the assumption of two observable sets of CO bands in IR spectra measured from crystals.

Following the above mentioned theory of electron rich metal centres transferring electron density into a π^* -orbital of the carbonyls, electron donating substituents in the ligand should strengthen the C-O bond and lead to decreased wavenumbers for the stretching bands of those carbonyls. In contrast to these expectations the CO stretching bands of pyridylphosphinine complexes bearing a methylthio (**2.6e, h**) or methoxy (**2.6d**) group shifted to higher wavenumbers. A change that is much more pronounced than what was observed for the electron withdrawing substituent CF_3 (**2.6c**). For an explanation of this phenomenon, the results of DFT calculations have to be consulted again. Introduction of either a methoxy or methylthio group into pyridylphosphinines (**2.3d, e, g, h**) leads to a severe destabilisation of the HOMO which shows π -symmetry and a large coefficient on the phosphorus atom. Contrary to conventional π -donor ligands such as sulphide, thiocyanate or halides, the HOMO of phosphinines has the same shape and points in the same direction as the LUMO responsible for their strong π -acceptor abilities. While electron-rich metal centres usually favour binding to phosphinines due to the low-lying LUMO, the rise in energy of the π -shaped HOMO causes a repulsion with a filled d-orbital of the tungsten atom (Figure 2-18).

The repulsion between the energetically high lying HOMO of the phosphinine and the filled d-orbital of the tungsten leads to a weakening of the metal-ligand bond which results in less electron density on the metal centre and a strengthening of the carbonyl bond. Therefore the counterintuitive shift towards higher wavenumbers for the methoxy and methylthio substituted pyridylphosphinine complexes **2.6d, e** and **h** can thus be attributed to the HOMO. However, while the methoxy substituted ligand **2.3g** does have a HOMO similarly

high in energy, the respective tungsten complex **2.6g** does not show the same shift of the carbonyl bands in the IR spectra. A fact that cannot be explained with present results.

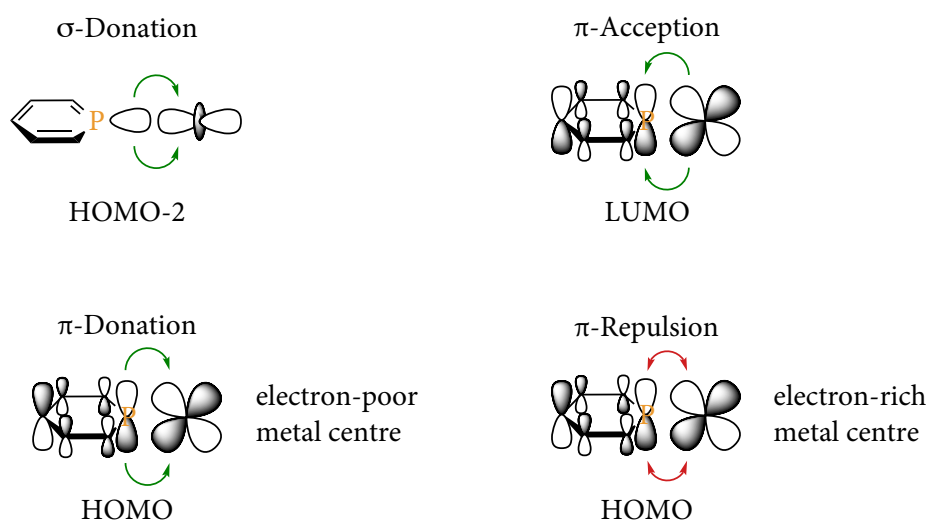


Figure 2-18: Simplified visualisation of the interaction of phosphinine ligand and metal d-orbital.

Recapitulating the effects of methoxy and methylthio groups on the frontier orbitals of bipyridine ligands, it can be said that substitution on the 6-phenyl ring leads to severe destabilisation of the HOMO (**2.4g, h**), while the impact is slightly less pronounced for the methylthio group and insignificant for the methoxy group on the 4-phenyl ring (**2.4d, e**). Further, the coefficients on the central nitrogen atoms are relatively small. Consistent with the results of DFT calculations, repulsion between the HOMO of the ligand and the tungsten atom is reflected in the IR values of methylthio substituted complex **2.7e** but not of methoxy derivative **2.7d**. However, also coordination compounds **2.7g** and **h** should exhibit a shift of the carbonyl bands in IR spectra due to repulsion. A possible reason why they do not, can be found in the molecular structure in the crystal. The calculated minimum structures of the ligands display rather small torsion angles of 19.5° (**2.4g**) and 19.4° (**2.4h**) for the substituted phenyl ring in 6-position (Figure 2-19). In the corresponding tungsten carbonyl complex, however, this phenyl ring is pushed much further out of the pyridine plane by one of the CO ligands resulting in torsion angles of $-61.4(4)^\circ$ (**2.7g**) and $-88(2)^\circ$ (**2.7h**) and thereby effectively interrupting the conjugative effect of the +M-substituents (Also see Figure 2-22, Table 2-8).

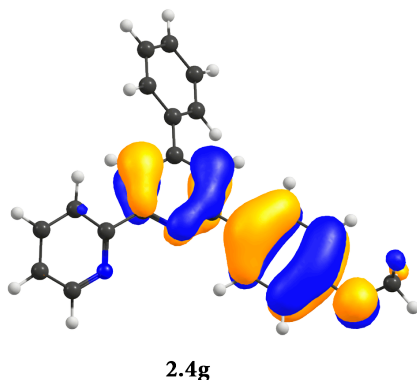


Figure 2-19: Calculated minimum structure and HOMO of bipyridine ligand **2.4g** with a torsion angle of 19.5° between the 6-phenyl ring and the central pyridine moiety.

Molecular Structures of Tungsten Carbonyl Complexes

Crystals suitable for X-ray structure determination were obtained of pyridylphosphinine tungsten carbonyl complexes **2.6b**, **f** and **g** (Figure 2-20) as well as bipyridine-based compounds **2.7b-h** (Figure 2-21 and Figure 2-22). Crystallographic details can be found under 2.5 Experimental Data.

In agreement with known values for phosphinines, the P-C bond is 1.72-1.77 Å long and C-C bonds of the aromatic ring show values of 1.35-1.40 Å.¹² Connecting bonds between the four rings are shorter (1.48-1.50 Å) than a standard C-C single bond (1.54 Å)²¹ indicating delocalisation of the aromatic system over the whole molecule. The effect is less pronounced than observed for pyrylium salts which can be attributed to their electron acceptor strength but also to their almost perfectly co-planar arrangement. The C-P-C angle of 104.0-104.8° is widened compared to standard values of around 100° for uncomplexed phosphinines (Table 2-7).¹² An increase in the C-P-C angle upon coordination of the phosphinine is common and attributed to the lone pair having to gain p-character for successful binding to a metal centre, which in turn leads to disruption of the aromatic system.⁹⁹ Therefore the C-P-C angle can be used as an indicator for the electron accepting qualities of the metal fragment as well as for the stability of the coordination compound towards water and alcohols. In fact, phosphinine complexes with C-P-C angles below 106° are usually quite stable towards water or alcohols which is in line with observations for tungsten complexes **2.6a-h**.²⁰

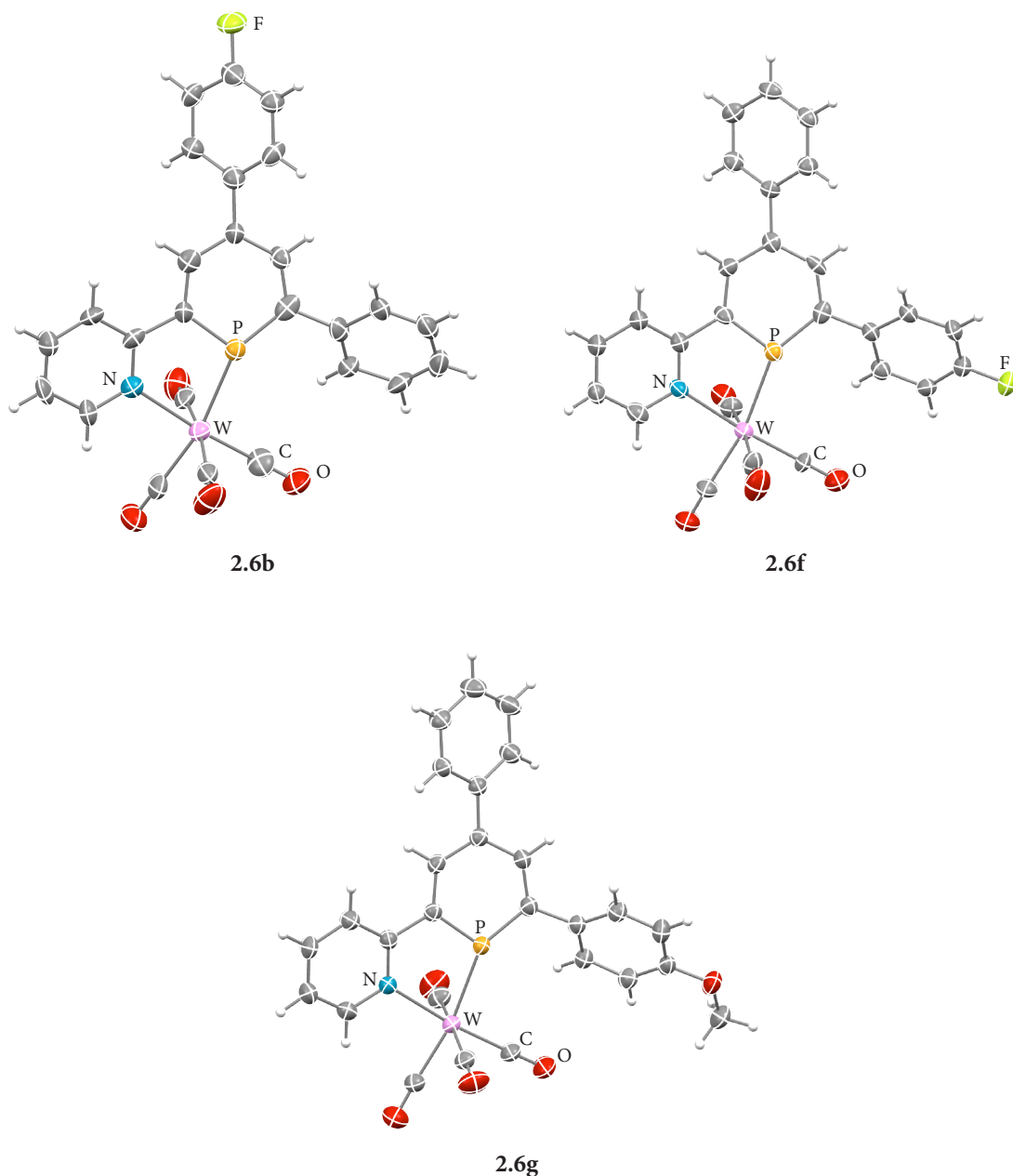


Figure 2-20: Molecular structures in the crystal of pyridylphosphinine tungsten carbonyl complexes **2.6b**, **f** and **g**. Displacement ellipsoids are shown at the 50% probability level.

The tungsten centres have a distorted octahedral coordination environment. As can already be seen in Figure 2-20, the metal is located perfectly in the axis of the pyridine lone pair but slightly shifted from its ideal position on the axis of the phosphorus. A situation that has been seen before for various pyridylphosphinine complexes.^{20,99,100} Obviously, this is necessary for coordination with the rigid chelating ligand and easier facilitated by the larger, more diffuse and less directional lone pair of the phosphorus atom compared to the one of the nitrogen. Ligand-metal bond lengths are very similar among the differently substituted complexes with P-W bonds of 2.45-2.46 Å and N-W bonds of 2.30-2.31 Å (Table 2-7). Axial

carbonyl ligands show longer C-W bonds with 2.02-2.06 Å than equatorial CO groups (1.96-1.99 Å) that experience the influence of a stronger donating phosphinine or pyridine ligand in *trans*-position. No difference in C-O bond length is observed either between axial (1.13-1.17 Å) and equatorial (1.14-1.15 Å) carbonyls or between carbonyls opposite a pyridine (1.14-1.15 Å) or a phosphinine (1.14 Å) moiety.

Bond length (Å), angle (°) or torsion angle (°)	2.6b R = F	2.6f R' = F	2.6g R' = OMe
P1-W1	2.464(4)	2.450(3)	2.447(1)
N2-W1	2.31(2)	2.30(1)	2.296(3)
P1-C1	1.77(2)	1.76(1)	1.730(4)
P1-C5	1.72(2)	1.77(1)	1.726(3)
C1-C2	1.36(2)	1.35(1)	1.393(6)
C2-C3	1.39(2)	1.43(1)	1.402(7)
C3-C4	1.39(2)	1.40(1)	1.396(5)
C4-C5	1.40(2)	1.36(2)	1.388(5)
C1-C11	1.49(2)	1.48(1)	1.481(7)
C3-C17	1.50(2)	1.50(1)	1.486(6)
C5-C6	1.49(2)	1.48(2)	1.475(5)
W1-C24 (ax.)	2.02(3)	2.04(1)	2.029(5)
W1-C25	1.97(2)	1.988(9)	1.993(5)
W1-C26 (ax.)	2.02(2)	2.04(1)	2.056(5)
W1-C27	1.96(2)	1.99(1)	1.983(5)
C24-O1 (ax.)	1.16(3)	1.14(1)	1.137(7)
C25-O2	1.15(2)	1.14(1)	1.148(6)
C26-O3 (ax.)	1.17(3)	1.15(2)	1.129(6)
C27-O4	1.14(3)	1.14(1)	1.140(4)
C1-P1-C5	104.1(8)	104.0(5)	104.8(2)
C6-N2-C10	118(1)	117(1)	116.7(4)
P1-W1-N2	74.1(4)	73.8(3)	73.78(9)
P1-C1-C11-C12	39(2)	36(1)	40.3(6)
C2-C3-C17-C18	-37(2)	-35(1)	26.8(6)
P1-C5-C6-N2	12(2)	-12(1)	-10.3(5)

Table 2-7: Selected bond length (Å), angles (°) and torsion angles (°) for pyridylphosphinine tungsten carbonyl complexes. Numbering of atoms is consistent throughout this work and explained in **Figure 2-23**.

Looking at the orientation of the four rings towards each other, some degree of twisting in all three connecting bonds becomes noticeable. The phenyl ring in 6-position exhibits torsion angles of 36-40° probably due to steric hindrance through one equatorial carbonyl ligand. However, these values are relatively consistent with the minimum structure derived from DFT calculations where the P1-C1-C11-C12 torsion angles are 44.971° (**2.3b**), 44.705° (**2.3f**) and 42.978° (**2.4g**), respectively. Therefore, orbital interaction similar to the results of the DFT calculation seem reasonable for the pyridylphosphinine ligands. Interestingly, also the

pyridine ring is rotated out of the phosphinine plane by 10-12° which likely is again to minimise steric hindrance between the 6-phenyl ring and a carbonyl ligand.⁹⁹

Molecular structures of bipyridine complexes are very well known and countless examples are described in literature thus derived structure of complexes **2.7b-h** (Figure 2-21, Figure 2-22) will be mainly discussed in comparison to phosphinine tungsten compounds.

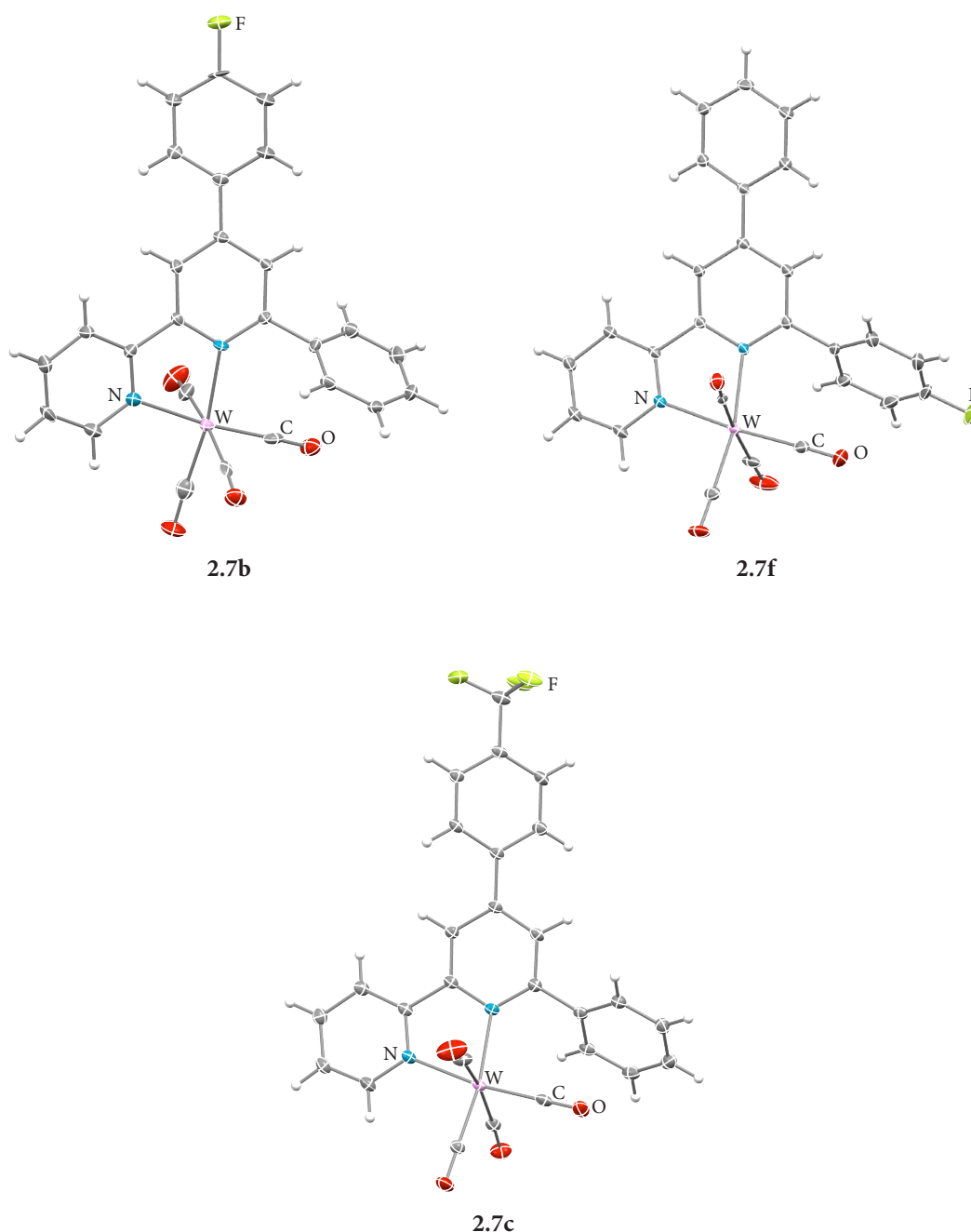


Figure 2-21: Molecular structures in the crystal of bipyridine tungsten carbonyl complexes **2.7b-h**. Displacement ellipsoids are shown at the 50% probability level. Compound **2.7c** contains two molecules in the asymmetric unit, of which only one is shown. Compound **2.7h** has a disordered methylthiophenyl ring which cannot be displays as ellipsoids.

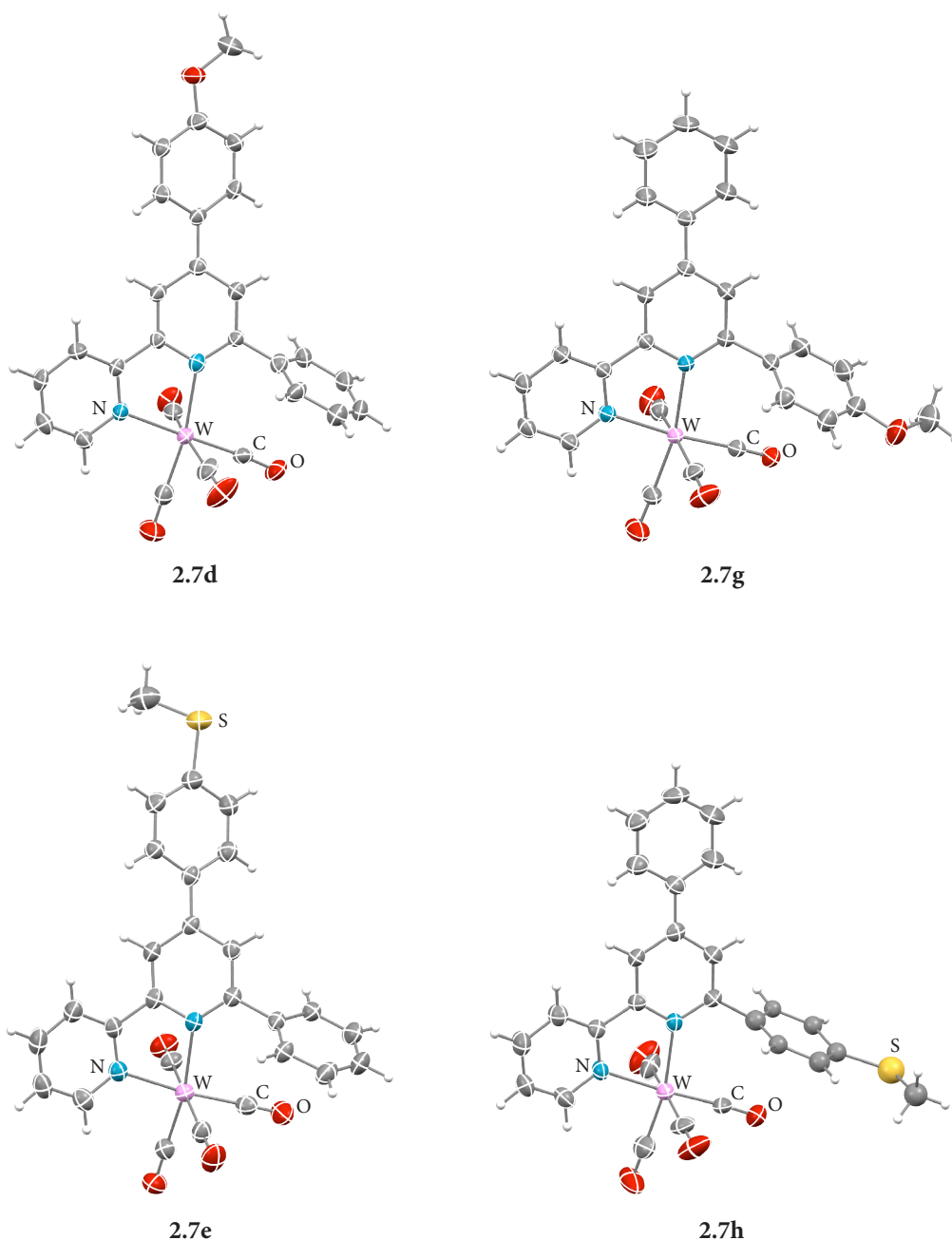


Figure 2-22: Molecular structures in the crystal of bipyridine tungsten carbonyl complexes **2.7d**, **e**, **g** and **h**. Displacement ellipsoids are shown at the 50% probability level. Compound **2.7h** has a disordered methylthio-phenyl ring.

Not surprisingly, the ligand-metal bond is shorter for pyridine than for phosphinine (Table 2-8); a fact that could already be noticed in the pyridylphosphinine complexes. Nonetheless, the N1-W bond (2.28-2.29 Å) of the central pyridine moiety is slightly longer than the N2-W bond (2.22-2.25 Å) which can most likely again be attributed to steric hindrance between the 6-phenyl ring and a carbonyl. Compared to the pyridylphosphinine complexes with their considerably longer P-W bond, this hindrance is even more pronounced for bipyridine

compounds. This also becomes visible in a greater twisting of the 6-phenyl ring in relation to the central pyridine plane. Measured torsion angles in the solid state are 52-88° while the DFT calculated values for the minimum structures of the bipyridine ligands are 19-23°. From these results, delocalisation of π -electrons between those two rings can be considered as disrupted in the complex in solid state, explaining why no substituent effect is observed for complexes **2.6g** and **h** in the IR spectra.

Bond length (Å), angle (°) or torsion angle (°)	2.7b R = F	2.7c R = CF ₃	2.7d R = OMe	2.7e R = SMe	2.7f R' = F	2.6g R' = OMe	2.6h R' = SMe
N1-W1	2.291(6)	2.286(2) / 2.287	2.287(7)	2.281(3)	2.276(1)	2.284(2)	2.277(5)
N2-W1	2.252(6)	2.224(2) / 2.222(2)	2.233(7)	2.229(3)	2.229(2)	2.221(3)	2.222(5)
N1-C1	1.345(8)	1.359(2) / 1.360(2)	1.35(1)	1.356(5)	1.359(2)	1.356(4)	1.379(9)
N1-C5	1.353(9)	1.369(2) / 1.366(3)	1.39(1)	1.366(5)	1.357(3)	1.364(4)	1.342(8)
C1-C2	1.392(9)	1.391(3) / 1.391(3)	1.39(1)	1.390(7)	1.391(3)	1.393(4)	1.37(1)
C2-C3	1.399(9)	1.395(3) / 1.397(3)	1.39(1)	1.394(5)	1.392(3)	1.390(5)	1.392(9)
C3-C4	1.39(1)	1.395(4) / 1.397(3)	1.40(1)	1.398(6)	1.398(3)	1.391(4)	1.41(1)
C4-C5	1.399(8)	1.392(3) / 1.389(3)	1.37(1)	1.382(6)	1.386(3)	1.392(4)	1.40(1)
C1-C11	1.504(8)	1.483(3) / 1.490(3)	1.48(1)	1.482(5)	1.482(3)	1.487(4)	1.58(3)
C3-C17	1.499(9)	1.478(3) / 1.487(3)	1.47(1)	1.472(5)	1.480(2)	1.488(4)	1.48(1)
C5-C6	1.488(9)	1.475(3) / 1.478(3)	1.47(1)	1.476(5)	1.481(3)	1.471(4)	1.477(9)
W1-C24 (ax.)	2.023(9)	2.032(2) / 2.018(2)	2.01(1)	2.034(5)	2.039(3)	2.022(4)	2.023(9)
W1-C25	1.936(7)	1.975(2) / 1.953(2)	1.92(1)	1.952(5)	1.955(2)	1.961(4)	1.925(8)
W1-C26 (ax.)	2.018(7)	2.023(2) / 2.052(2)	2.03(1)	2.030(5)	2.014(2)	2.030(4)	2.010(8)
W1-C27	1.972(7)	1.958(2) / 1.978(2)	1.95(1)	1.981(4)	1.981(3)	1.986(3)	1.957(7)
C24-O1 (ax.)	1.15(1)	1.153(2) / 1.160(3)	1.15(1)	1.134(6)	1.150(3)	1.143(5)	1.14(1)
C25-O2	1.186(9)	1.172(3) / 1.169(2)	1.21(1)	1.164(6)	1.167(2)	1.156(5)	1.18(1)
C26-O3 (ax.)	1.162(9)	1.150(3) / 1.136(3)	1.16(1)	1.138(6)	1.145(4)	1.153(5)	1.15(1)
C27-O4	1.162(9)	1.161(3) / 1.163(3)	1.17(1)	1.146(5)	1.157(3)	1.146(4)	1.164(8)
C1-N1-C5	116.7(6)	117.3(2) / 117.2(2)	116.7(7)	117.1(3)	117.3(2)	116.8(3)	116.5(6)
C6-N2-C10	118.5(6)	118.4(2) / 117.6(2)	116.7(7)	118.4(4)	118.1(2)	118.0(3)	117.7(6)
N1-W1-N2	72.4(2)	71.92(6) / 72.47(6)	72.4(2)	72.3(1)	72.11(6)	72.63(9)	72.1(2)
N1-C1-C11-C12	-55.5(8)	-59.0(2) / 52.2(3)	-68(1)	-53.9(6)	55.8(3)	-61.4(4)	-88(2)
C2-C3-C17-C18	-17(19)	-31.8(3) / 19.5(3)	19(1)	23.8(6)	-21.8(3)	3.0(5)	6(1)
N1-C5-C6-N2	-12.3(9)	-6.9(2) / 8.6(2)	-10(1)	-15.9(5)	13.8(3)	-4.9(4)	-7.0(9)

Table 2-8: Selected bond length (Å), angles (°) and torsion angles (°) for bipyridine tungsten carbonyl complexes. Numbering of atoms is consistent throughout this work and explained in **Figure 2-23**.

W-C bonds and C-O bonds of the carbonyl ligands in bipyridine-based compounds **2.7b-h** give exactly the same results as was analysed for the pyridylphosphinine compounds above. Axially bound CO ligands have slightly longer bonds than equatorial ones (2.01-2.05 Å vs. 1.92-1.99 Å) and no difference in C-O bond length (1.12-1.19 Å) can be observed for them. Interestingly, there is also no difference in the W-C or C-O bond length of the carbonyls

between bipyridine and pyridylphosphinine compounds proving that X-ray structure analysis is much less sensitive than IR spectroscopy in this type of study. Therefore it is not surprising that no influences of the rather small substituent groups in the backbone of the ligands can be found in their molecular structures in the crystal.

2.5 Experimental Data

General Remarks

Experiments performed under an inert argon atmosphere were carried out using modified Schlenk techniques or in a MBraun dry box. All common chemicals were commercially available and purchased from Aldrich Chemical Co., ABCR, Alfa Aesar, Acros as well as Eurisol and were used as received. 1-phenyl-3-(4-fluorophenyl)prop-2-en-1-one, 1-phenyl-3-(4-trifluoromethyl-phenyl)prop-2-en-1-one, 1-phenyl-3-(4-methoxyphenyl)prop-2-en-1-one, 1-phenyl-3-(4-methylthiophenyl)prop-2-en-1-one, 1-(4-fluorophenyl)-3-phenylprop-2-en-1-one, 1-(4-methoxyphenyl)-3-phenylprop-2-en-1-one, 1-(4-methylthiophenyl)-3-phenylprop-2-en-1-one (Chalcones)¹³⁶ and Tris(trimethylsilyl)phosphane¹⁶² were prepared according to the literature. For reactions under UV radiation a Philips HPK 125W high-pressure mercury vapor lamp was used.

Dry or deoxygenated solvents were prepared using standard techniques or used from a MBraun MB SBS-800 solvent purification system. Tetrahydrofuran and diethyl ether were distilled under argon over potassium/benzophenone and sodium/benzophenone respectively. For column chromatography silica 60M by Macherey-Nagel was used as stationary phase.

The ¹H, ¹³C{¹H}, ¹⁹F and ³¹P{¹H} NMR spectra were recorded on a JEOL EXZ400 (400 MHz), a JEOL ECX400 (400 MHz), a JEOL ECP500 (500 MHz), a Bruker AVANCE III 500 (500 MHz) or a Bruker AVANCE III 700 (700 MHz) FT spectrometer and chemical shifts are reported relative to the residual resonance of the deuterated solvents. The mass characterizations have been performed on an Agilent 6210 ESI-TOF instrument by Agilent Technologies with standard settings of 5 L/min, 4 kV and 15 psi for ESI-TOF and on a MAT 711 by Varian MAT with an electron energy of 0.8 mA for EI-MS. All other parameters have been optimized for each substance. IR spectra were measured on a Nicolet iS10 FTIR-ATR spectrometer by Thermo Scientific, UV-Vis spectra on a Cary 300 UV-Vis and fluorescence spectra on a Cary Eclipse spectrometer both by Agilent Technologies. Elemental analyses were performed with a vario MACRO cube by Elementar.

The numbering of atoms is continuous in NMR spectra and molecular structures in the crystal as well as through the complete synthetic pathway (Figure 2-23). Hydrogen atoms bear the same number as the carbon they are attached to.

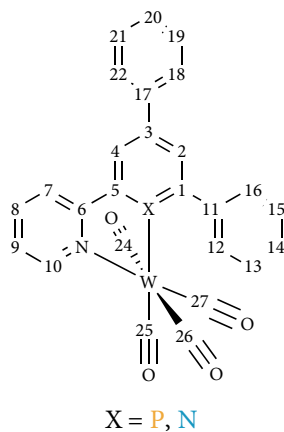


Figure 2-23: Numbering of atoms.

Density Functional Theory (DFT) calculations were carried out at the B3LYP/6-311+G(d,p) level of theory with the Gaussian 09 program.¹⁶³ Full geometry optimization without any symmetry constraints was performed prior to the analysis of the electronic structure of the different phosphinine ligands. The nature of the stationary points was evaluated from the analytically computed harmonic modes. No imaginary frequencies were found for the optimized structures confirming that these correspond to local minima on the potential energy surface. Data files can be found in the attachment.

Synthetic Procedures

Diketones (2.1b-h)

The respective chalcone (1 eq.), 2-acetylpyridine (1 eq.) and NaOH (1 eq.) were mixed with mortar and pestle until after around 10 min a sticky mixture was formed. The product was then recrystallized from water/ethanol 1:2.

3-(4-Fluorophenyl)-1-phenyl-5-(2-pyridyl)pentane-1,5-dione (2.1b)

1-Phenyl-3-(4-fluorophenyl)prop-2-en-1-one (8.6 g, 38 mmol), 2-acetylpyridine (4.3 mL, 4.6 g, 38 mmol) and NaOH (1.6 g, 40 mmol) gave the product (9.7 g, 28 mmol, 73%) as a colourless solid.

^1H NMR (500 MHz, CDCl_3): δ = 3.33 (dd, J = 16.7, 7.1 Hz, 1 H, H_2), 3.45 (dd, J = 16.7, 7.1 Hz, 1 H, H_2), 3.61 (dd, J = 17.6, 7.1 Hz, 1 H, H_4), 3.75 (dd, J = 17.6, 7.1 Hz, 1 H, H_4), 4.12 (quin, J = 7.1 Hz, 1 H, H_3), 6.93 (m_s, 2 H, $\text{H}_{19/21}$), 7.27 – 7.32 (m, 2 H, $\text{H}_{18/22}$), 7.40 – 7.45 (m, 3 H, H_9 , $\text{H}_{13/15}$), 7.50 – 7.55 (m, 1 H, H_{14}), 7.78 (ddd, J = 7.8, 7.8, 1.7 Hz, 1 H, H_7), 7.89 – 7.93 (m, 2 H, $\text{H}_{12/16}$), 7.95 – 7.97 (m, 1 H, H_7), 8.63 (ddd, J = 4.8, 1.6, 0.9 Hz, 1 H, H_{10}) ppm;

$^{13}\text{C}\{^1\text{H}\}$ NMR (101 MHz, CDCl_3): δ = 36.0 (C_3), 44.1 (C_4), 45.3 (C_2), 115.3 (d, $^2J_{\text{C-F}}$ = 21.1 Hz, $\text{C}_{19/21}$), 121.9 (C_7), 127.3 (C_9), 128.2 ($\text{C}_{12/16}$), 128.7 ($\text{C}_{13/15}$), 129.2 (d, $^3J_{\text{C-F}}$ = 7.8 Hz, $\text{C}_{18/22}$), 133.2 (C_{14}), 137.0 (C_{11}), 137.0 (C_8), 140.0 (d, $^4J_{\text{C-F}}$ = 3.3 Hz, C_{17}), 149.0 (C_{10}), 153.3 (C_6), 161.5 (d, $^1J_{\text{C-F}}$ = 244.2 Hz, C_{20}), 198.4 (C_1), 199.9 (C_5) ppm;

^{19}F NMR (376 MHz, CDCl_3): δ = -116.5 – -116.6 (m) ppm;

ESI-TOF (m/z): 370.1232 g/mol (calc.: 370.1214 g/mol) $[\text{M} + \text{Na}]^+$;

Elemental analysis calc (%) for $\text{C}_{22}\text{H}_{18}\text{FNO}_2$ (347.38 g/mol): C 76.06, H 5.22, N 4.03; found: C 76.00, H 4.92, N 3.94.

3-(4-Trifluoromethylphenyl)-1-phenyl-5-(2-pyridyl)pentane-1,5-dione (2.1c)

1-Phenyl-3-(4-trifluoromethylphenyl)prop-2-en-1-one (10.4 g, 38 mmol), 2-acetylpyridine (4.2 mL, 4.5 g, 37 mmol) and NaOH (1.5 g, 38 mmol) gave the product (10.1 g, 25 mmol, 68%) as a colourless solid.

^1H NMR (400 MHz, CDCl_3): δ = 3.39 (dd, J = 17.1, 7.6 Hz, 1 H), 3.50 (dd, J = 17.1, 6.6 Hz, 1 H), 3.65 (dd, J = 17.8, 6.6 Hz, 1 H), 3.80 (dd, J = 17.8, 7.6 Hz, 1 H), 4.20 (quin, J = 7.1 Hz, 1 H), 7.41 – 7.58 (m, 8 H), 7.81 (ddd, J = 7.7, 7.7, 1.7 Hz, 1 H), 7.90 – 7.94 (m, 2 H), 7.98 (ddd, J = 7.8, 1.1, 1.1 Hz, 1 H), 8.65 (ddd, J = 4.7, 1.7, 0.9 Hz, 1 H) ppm;

$^{13}\text{C}\{^1\text{H}\}$ NMR (101 MHz, CDCl_3): δ = 36.4, 43.8, 44.9, 122.0, 124.3 (q, $J_{\text{C-F}}$ = 271.9 Hz), 125.6 (q, $J_{\text{C-F}}$ = 3.8 Hz), 127.5, 128.2, 128.2, 128.8, 128.9 (q, $J_{\text{C-F}}$ = 32.4 Hz) 133.3, 136.9, 137.1, 148.6 (q, $J_{\text{C-F}}$ = 1.4 Hz), 149.1, 153.3, 198.0, 199.7 ppm;

^{19}F NMR (376 MHz, CDCl_3): δ = -62.3 (s) ppm;

ESI-TOF (m/z): 398.1360 g/mol (calc.: 398.1368 g/mol) $[\text{M} + \text{H}]^+$;

Elemental analysis calc (%) for C₂₂H₁₈F₃NO₂ (397.39 g/mol): C 69.52, H 4.57, N 3.52; found: C 69.66, H 4.61, N 3.23.

3-(4-Methoxyphenyl)-1-phenyl-5-(2-pyridyl)pentane-1,5-dione (2.1d)

1-Phenyl-3-(4-methoxyphenyl)prop-2-en-1-one (6.0 g, 25 mmol), 2-acetylpyridine (2.9 mL, 3.1 g, 25 mmol) and NaOH (1.0 g, 25 mmol) gave the product (8.0 g, 22 mmol, 88%) as a colourless solid.

¹H NMR (400 MHz, CDCl₃): δ = 3.32 (dd, *J* = 16.5, 7.5 Hz, 1 H, H₂), 3.43 (dd, *J* = 16.5, 6.8 Hz, 1 H, H₂'), 3.60 (dd, *J* = 17.5, 6.8 Hz, 1 H, H₄), 3.74 (dd, *J* = 17.5, 7.5 Hz, 1 H, H₄'), 3.74 (s, 3 H, OMe), 4.08 (quin, *J* = 7.1 Hz, 1 H, H₃), 6.80 (m_s, 2 H, H_{19/21}), 7.22 – 7.27 (m, 2 H, H_{18/22}), 7.40 – 7.46 (m, 3 H, H₉, H_{13/15}), 7.50 – 7.56 (m, 1 H, H₁₄), 7.79 (ddd, *J* = 7.8, 7.7, 1.7 Hz, 1 H, H₈), 7.90 – 7.94 (m, 2 H, H_{12/16}), 7.97 (ddd, *J* = 7.9, 1.1, 1.1 Hz, 1 H, H₇), 8.64 (ddd, *J* = 4.7, 1.7, 0.9 Hz, 1 H, H₁₀) ppm;

¹³C{¹H} NMR (101 MHz, CDCl₃): δ = 36.0 (C₃), 44.2 (C₄), 45.6 (C₂), 55.3 (OMe), 114.0 (C_{19/21}), 121.9 (C₇), 127.2 (C₉), 128.2 (C_{12/16}), 128.6 (C_{13/15} or C_{18/22}), 128.6 (C_{13/15} or C_{18/22}), 133.1 (C₁₄), 136.4 (C₁₇), 137.0 (C₈), 137.1 (C₁₁), 149.0 (C₁₀), 153.5 (C₆), 158.2 (C₂₀), 198.0 (C₁), 200.2 (C₅) ppm;

ESI-TOF (m/z): 382.1442 g/mol (calc.: 382.1414 g/mol) [M + Na]⁺;

Elemental analysis calc (%) for C₂₃H₂₁NO₃ (359.42 g/mol): C 76.86, H 5.89, N 3.90; found: C 76.60, H 5.87, N 3.62.

3-(4-Methylthiophenyl)-1-phenyl-5-(2-pyridyl)pentane-1,5-dione (2.1e)

1-Phenyl-3-(4-fluorophenyl)prop-2-en-1-one (10.0 g, 39 mmol), 2-acetylpyridine (4.4 mL, 4.8 g, 39 mmol) and NaOH (1.6 g, 39 mmol) gave the product (11.5 g, 31 mmol, 78%) as a pale yellow solid.

¹H NMR (400 MHz, CDCl₃): δ = 2.43 (s, 3 H, Me), 3.34 (dd, *J* = 16.7, 7.4 Hz, 1 H, H₂), 3.45 (dd, *J* = 16.8, 6.8 Hz, 1 H, H₂'), 3.61 (dd, *J* = 17.6, 6.6 Hz, 1 H, H₄), 3.75 (dd, *J* = 17.7, 7.6 Hz, 1 H, H₄'), 4.09 (quin, *J* = 7.0 Hz, 1 H, H₃), 7.14 – 7.18 (m, 2 H, H_{19/21}), 7.24 – 7.28 (m, 2 H, H_{18/22}), 7.41 – 7.47 (m, 3 H, H₉, H_{13/15}), 7.51 – 7.57 (m, 1 H, H₁₄), 7.80 (ddd, *J* = 7.7, 7.7, 1.7 Hz, 1 H, H₈), 7.90 – 7.94 (m, 2 H, H_{12/16}), 7.97 (ddd, *J* = 7.8, 1.1, 1.1 Hz, 1 H, H₇), 8.64 (ddd, *J* = 4.7, 1.7, 0.9 Hz, 1 H, H₁₀) ppm;

¹³C{¹H} NMR (101 MHz, CDCl₃): δ = 16.2 (Me), 36.1 (C₃), 44.0 (C₄), 45.3 (C₂), 122.0 (C₇), 127.1 (C_{19/21}), 127.3 (C₉), 128.2 (C_{12/16} or C_{18/22}), 128.3 (C_{12/16} or C_{18/22}), 128.7 (C_{13/15}), 133.2

(C₁₄), 136.2 (C₂₀), 137.0 (C₈), 137.1 (C₁₁), 141.4 (C₁₇), 149.0 (C₁₀), 153.4 (C₆), 198.5 (C₁), 200.0 (C₅) ppm;

ESI-TOF (m/z): 398.1221 g/mol (calc.: 398.1185 g/mol) [M + Na]⁺;

Elemental analysis calc (%) for C₂₃H₂₁NO₂S (375.48 g/mol): C 73.57, H 5.64, N 3.73, S 8.54; found: C 73.44, H 5.55, N 3.58, S 8.45.

1-(4-Fluorophenyl)-3-phenyl-5-(2-pyridyl)pentane-1,5-dione (2.1f)

1-(4-Fluorophenyl)-3-phenylprop-2-en-1-one (5.0 g, 22 mmol), 2-acetylpyridine (2.5 mL, 2.7 g, 22 mmol) and NaOH (0.9 g, 22 mmol) gave the product (3.4 g, 10 mmol, 44%) as a colourless solid.

¹H NMR (500 MHz, CDCl₃): δ = 3.32 (dd, *J* = 16.5, 7.5 Hz, 1 H, H₂), 3.44 (dd, *J* = 16.5, 6.8 Hz, 1 H, H₂'), 3.65 (dd, *J* = 17.7, 7.0 Hz, 1 H, H₄), 3.76 (dd, *J* = 17.7, 7.1 Hz, 1 H, H₄'), 4.10 (quin, *J* = 7.1 Hz, 1 H, H₃), 7.09 (m_s, 2 H, H_{13/15}), 7.13 – 7.18 (m, 1 H, H₂₀), 7.23 – 7.28 (m, 2 H, H_{19/21}), 7.30 – 7.35 (m, 2 H, H_{18/22}), 7.43 (ddd, *J* = 7.6, 4.8, 1.3 Hz, 1 H, H₉), 7.78 (ddd, *J* = 7.7, 7.7, 1.7 Hz, 1 H, H₈), 7.92 – 7.99 (m, 3 H, H₇, H_{12/16}), 8.64 (ddd, *J* = 4.8, 1.8, 0.9 Hz, 1 H, H₁₀) ppm;

¹³C{¹H} NMR (101 MHz, CDCl₃): δ = 36.8 (C₃), 44.0 (C₄), 45.2 (C₂), 115.7 (d, ²*J*_{C-F} = 21.8 Hz, C_{13/15}), 121.9 (C₇), 126.7 (C₂₀), 127.3 (C₉), 127.6 (C_{18/22}), 128.6 (C_{19/21}), 130.8 (d, ³*J*_{C-F} = 9.4 Hz, C_{12/16}), 133.5 (d, ⁴*J*_{C-F} = 2.9 Hz, C₁₁), 137.0 (C₈), 144.2 (C₁₇), 148.9 (C₁₀), 153.3 (C₆), 165.7 (d, ¹*J*_{C-F} = 254.5 Hz, C₁₄), 197.1 (C₁), 200.0 (C₅) ppm;

¹⁹F NMR (376 MHz, CDCl₃): δ = -105.4 (m_s) ppm;

ESI-TOF (m/z): 348.1396 g/mol (calc.: 348.1400 g/mol) [M + H]⁺, 370.1256 g/mol (calc.: 370.1219 g/mol) [M + Na]⁺;

Elemental analysis calc (%) for C₂₂H₁₈FNO₂ (347.38 g/mol): C 76.06, H 5.22, N 4.03; found: C 75.99, H 5.28, N 3.74.

1-(4-Methoxyphenyl)-3-phenyl-5-(2-pyridyl)pentane-1,5-dione (2.1g)

1-(4-Methoxyphenyl)-3-phenylprop-2-en-1-one (6.5 g, 27 mmol), 2-acetylpyridine (3.1 mL, 3.2 g, 27 mmol) and NaOH (1.1 g, 27 mmol) gave the product (7.4 g, 21 mmol, 76%) as a colourless solid.

¹H NMR (400 MHz, CDCl₃): δ = 3.30 (dd, *J* = 16.4, 7.2 Hz, 1 H, H₂), 3.41 (dd, *J* = 16.4, 7.1 Hz, 1 H, H₂'), 3.63 (dd, *J* = 17.7, 6.7 Hz, 1 H, H₄), 3.77 (dd, *J* = 17.7, 7.5 Hz, 1 H, H₄'), 3.85 (s, 3 H, OMe), 4.11 (quin, *J* = 7.1 Hz, 1 H, H₃), 6.90 (m_s, 2 H, H_{13/15}), 7.12 – 7.18 (m, 1 H, H₂₀),

7.23 – 7.28 (m, 2 H, H_{19/21}), 7.31 – 7.35 (m, 2 H, H_{18/22}), 7.44 (ddd, $J = 7.6, 4.8, 1.3$ Hz, 1 H, H₉), 7.79 (ddd, $J = 7.7, 7.7, 1.7$ Hz, 1 H, H₈), 7.87 – 7.94 (m, 2 H, H_{12/16}), 7.97 (ddd, $J = 7.9, 1.1, 1.1$ Hz, 1 H, H₇), 7.64 (ddd, $J = 4.7, 1.7, 0.9$ Hz, 1 H, H₁₀) ppm;

¹³C{¹H} NMR (101 MHz, CDCl₃): $\delta = 36.8$ (C₃), 44.0 (C₄), 45.0 (C₂), 55.5 (OMe), 113.7 (C_{13/15}), 121.9 (C₇), 126.5 (C₂₀), 127.2 (C₉), 127.7 (C_{18/22}), 128.6 (C_{19/21}), 130.2 (C₁₁), 130.5 (C_{12/16}), 137.0 (C₈), 144.5 (C₁₇), 148.9 (C₁₀), 153.4 (C₆), 163.4 (C₁₄), 197.2 (C₁), 200.1 (C₅) ppm;

ESI-TOF (m/z): 382.1418 g/mol (calc.: 382.1414 g/mol) [M + Na]⁺;

Elemental analysis calc (%) for C₂₃H₂₁NO₃ (359.42 g/mol): C 76.86, H 5.89, N 3.90; found: C 76.93, H 5.93, N 3.77.

1-(4-Methylthiophenyl)-3-phenyl-5-(2-pyridyl)pentane-1,5-dione (2.1h)

1-(4-Methylthiophenyl)-3-phenylprop-2-en-1-one (7.0 g, 28 mmol), 2-acetylpyridine (3.2 mL, 3.5 g, 29 mmol) and NaOH (1.1 g, 28 mmol) gave the product (8.3 g, 22 mmol, 80%) as a pale yellow solid.

¹H NMR (400 MHz, CDCl₃): $\delta = 2.51$ (s, 3 H, SMe), 3.30 (dd, $J = 16.4, 7.3$ Hz, 1 H, H₂), 3.42 (dd, $J = 16.4, 7.0$ Hz, 1 H, H_{2'}), 3.63 (dd, $J = 17.7, 6.8$ Hz, 1 H, H₄), 3.76 (dd, $J = 17.7, 7.3$ Hz, 1 H, H_{4'}), 4.10 (quin, $J = 7.0$ Hz, 1 H, H₃), 7.13 – 7.18 (m, 1 H, H₂₀), 7.21 – 7.28 (m, 4 H, H_{13/15}, H_{19/21}), 7.30 – 7.35 (m, 2 H, H_{18/22}), 7.44 (ddd, $J = 7.5, 4.7, 1.3$ Hz, 1 H, H₉), 7.79 (ddd, $J = 7.7, 7.7, 1.7$ Hz, 1 H, H₈), 7.82 – 7.86 (m_s, 2 H, H_{12/16}), 7.97 (ddd, $J = 7.9, 1.1, 1.1$ Hz, 1 H, H₇), 8.64 (ddd, $J = 4.8, 1.8, 0.9$ Hz, 1 H, H₁₀) ppm;

¹³C{¹H} NMR (101 MHz, CDCl₃): $\delta = 14.9$ (SMe), 36.8 (C₃), 44.0 (C₄), 45.1 (C₂), 121.9 (C₇), 125.0 (C_{13/15}), 126.6 (C₂₀), 127.2 (C₉), 127.7 (C_{18/22}), 128.6 (C_{19/21} or C_{12/16}), 128.7 (C_{19/21} or C_{12/16}), 133.4 (C₁₁), 137.0 (C₈), 144.3 (C₁₇), 145.8 (C₁₄), 149.0 (C₁₀), 153.4 (C₆), 197.7 (C₁), 200.1 (C₅) ppm;

ESI-TOF (m/z): 398.1222 g/mol (calc.: 398.1185 g/mol) [M + Na]⁺;

Elemental analysis calc (%) for C₂₃H₂₁NO₂S (375.48 g/mol): C 73.57, H 5.64, N 3.73, S 8.54; found: C 76.18, H 5.54, N 3.34, S 8.71.

Pyrylium Salts (2.2b-d)

Under Argon the respective diketone (1 eq.) was mixed with 1,3-diphenylprop-2-en-1-one (1 eq.) and boron trifluoride diethyl etherate (8 eq.) was added. The mixture was heated to 70 °C for 3 h and then dropped into 400 mL diethyl ether. The precipitate was filtered off, dried, and recrystallized from methanol.

2-(2-Pyridyl)-4-(4-fluorophenyl)-6-phenylpyrylium tetrafluoroborate (2.2b)

Diketone **2.1b** (4.7 g, 14 mmol), 1,3-diphenylprop-2-en-1-one (2.8 g, 14 mmol) and BF₃ etherate (13.5 mL, 15.5 g, 109 mmol) gave the product (2.284 g, 6 mmol, 43%) as yellow crystals. Crystals suitable for X-ray diffraction were obtained from slow evaporation of a acetone solution.

¹H NMR (400 MHz, (CD₃)₂CO): δ = 7.60 (m_s, 2 H, H_{19/21}), 7.80 – 7.95 (m, 4 H, H_{13/15}, H₉, H₁₄), 8.31 (ddd, *J* = 7.9, 7.8, 1.7 Hz, 1 H, H₈), 8.69 – 8.74 (m, 4 H, H_{12/16}, H_{18/22}), 8.82 (ddd, *J* = 8.0, 1.0, 1.0 Hz, 1 H, H₇), 9.02 (ddd, *J* = 4.7, 1.7, 0.9 Hz, 1 H, H₁₀), 9.31 – 9.34 (m, 2 H, H₂, H₄) ppm;

¹³C{¹H} NMR (101 MHz, (CD₃)₂SO): δ = 114.7 (C₂ or C₄), 115.9 (C₂ or C₄), 116.9 (d, ²*J*_{C-F} = 22.0 Hz, C_{19/21}), 124.1 (C₇), 128.1 (C₉), 128.4 (d, ⁴*J*_{C-F} = 2.8 Hz, C₁₇), 128.5 (C₁₁), 128.6 (C_{12/16}), 129.5 (C_{13/15}), 132.9 (d, ³*J*_{C-F} = 10.1 Hz, C_{18/22}), 135.0 (C₁₄), 138.1 (C₈), 145.9 (C₆), 150.5 (C₁₀), 163.9 (C₃), 166.1 (d, ¹*J*_{C-F} = 256.8 Hz, C₂₀), 167.4 (C₁ or C₅), 170.1 (C₁ or C₅) ppm;

¹⁹F NMR (376 MHz, (CD₃)₂CO): δ = -102.8 (m_s), -151.3 (s, ¹⁰BF₄⁻), -151.4 (s, ¹¹BF₄⁻) ppm;

ESI-TOF (m/z): 328.1166 g/mol (calc.: 328.1132 g/mol) [M]⁺;

Elemental analysis calc (%) for C₂₂H₁₅BF₅NO (415,16 g/mol): C 63.80, H 3.75, N 3.02; found: C 63.65, H 3.64, N 3.37.

Crystallographic data: C₂₂H₁₅NOF x BF₄, *Fw* = 415.16, 0.22×0.20×0.06 mm³, yellow platelet, monoclinic, *P*2₁/*c*, *a* = 7.2677(2), *b* = 14.2809(3) *c* = 17.5498 (5) Å, β = 97.5668(9)°, *V* = 1805.62(8) Å³, *Z* = 4, *D_x* = 1.527 gcm⁻³, μ = 0.128 mm⁻¹. 28487 reflections were measured by using a D8 Venture, Bruker Photon CMOS Detector (MoKα radiation, λ = 0.71073 Å) up to a resolution of (sinθ/λ)_{max} = 0.60 Å⁻¹ at a temperature of 100 K.¹⁶⁴ 2532 reflections were unique (*R*_{int} = 0.061). The structures were solved with SHELXS-2014¹⁶⁵ by using direct methods and refined with SHELXL-2014¹⁶⁵ on *F*² for all reflections. Non-hydrogen atoms were refined by using anisotropic displacement parameters. The positions of the hydrogen atoms were calculated for idealized positions. 290 parameter were refined without restraints. *R*₁ = 0.040 for 2532 reflections with *I* > 2σ(*I*) and *wR*₂ = 0.100 for 3204 reflections, *S* = 1.048, residual electron density was between -0.23 and 0.22 eÅ⁻³. Geometry calculations and checks for higher symmetry were performed with the PLATON program.¹⁶⁶ A .cif data file can be found in the attachments.

2-(2-Pyridyl)-4-(4-trifluoromethylphenyl)-6-phenylpyrylium tetrafluoroborate (2.2c)

Diketone **2.1c** (4.6 g, 12 mmol), 1,3-diphenylprop-2-en-1-one (2.4 g, 12 mmol) and BF₃ etherate (11 mL, 12.7 g, 89 mmol) were heated to *T* = 80 °C for 3 h and gave the product (1.921 g, 4 mmol, 34%) as yellow crystals.

^1H NMR (400 MHz, $(\text{CD}_3)_2\text{CO}$): $\delta = 7.82 - 7.97$ (m, 4 H, $\text{H}_{13/15}$, H_9 , H_{14}), $8.12 - 8.16$ (m, 2 H, $\text{H}_{19/21}$), 8.32 (ddd, $J = 7.9, 7.8, 1.7$ Hz, 1 H, H_8), $8.72 - 8.78$ (m, 4 H, $\text{H}_{12/16}$, $\text{H}_{18/22}$), 8.86 (ddd, $J = 7.9, 1.0, 1.0$ Hz, 1 H, H_7), 9.03 (ddd, $J = 4.6, 1.7, 0.9$ Hz, 1 H, H_{10}), 9.41 (d, $J = 1.8$ Hz, 1 H, H_4), 9.43 (d, $J = 1.8$ Hz, 1 H, H_2) ppm;

$^{13}\text{C}\{^1\text{H}\}$ NMR (176 MHz, $(\text{CD}_3)_2\text{CO}$): $\delta = 117.6$ (C_4), 119.0 (C_2), 124.7 (q, $^1J_{\text{C-F}} = 272.3$ Hz, CF_3), 125.6 (C_7), 127.7 (q, $^3J_{\text{C-F}} = 3.7$ Hz, $\text{C}_{19/21}$), 129.9 (C_9), 130.3 ($\text{C}_{12/16}$), 131.1 ($\text{C}_{13/15}$), 131.5 ($\text{C}_{18/22}$), 135.7 (q, $^2J_{\text{C-F}} = 32.8$ Hz, C_{20}), 136.5 (C_{11}), 136.9 (C_{14}), 137.8 (C_{17}), 139.5 (C_8), 147.3 (C_6), 152.2 (C_{10}), 166.8 (C_3), 170.5 (C_5), 173.4 (C_1) ppm;

^{19}F NMR (376 MHz, $(\text{CD}_3)_2\text{CO}$): $\delta = -63.6$ (s), -151.3 (s, $^{10}\text{BF}_4^-$), -151.4 (s, $^{11}\text{BF}_4^-$) ppm;

ESI-TOF (m/z): 378.1106 g/mol (calc.: 356.1100 g/mol) $[\text{M}]^+$;

Elemental analysis calc (%) for $\text{C}_{22}\text{H}_{18}\text{FNO}_2$ (465,17 g/mol): C 59.39, H 3.25, N 3.01; found: C 59.59, H 3.31, N 2.67.

2-(2-Pyridyl)-4-(4-methoxyphenyl)-6-phenylpyrylium tetrafluoroborate (2.2d)

Diketone **2.1d** (4.0 g, 11 mmol), 1,3-diphenylprop-2-en-1-one (2.3 g, 11 mmol) and BF_3 etherate (11.0 mL, 12.7 g, 89 mmol) gave the product (0.450 g, 1 mmol, 9%) as orange crystals after washing with chloroform and recrystallizing from acetonitril.

^1H NMR (400 MHz, $(\text{CD}_3)_2\text{CO}$): $\delta = 4.04$ (s, 3 H, OMe), 7.32 (m_s, 2 H, $\text{H}_{19/21}$), $7.75 - 7.92$ (m, 4 H, $\text{H}_{13/15}$, H_9 , H_{14}), 8.27 (ddd, $J = 7.8, 7.8, 1.7$ Hz, 1 H, H_8), $8.61 - 8.67$ (m, 4 H, $\text{H}_{12/16}$, $\text{H}_{18/22}$), 8.73 (ddd, $J = 8.0, 1.0, 1.0$ Hz, 1 H, H_7), $8.99 - 8.98$ (ddd, $J = 4.7, 1.8, 1.0$ Hz, 1 H, H_{10}), 9.14 (d, $J = 1.9$ Hz, 1 H, H_4), 9.18 (d, $J = 1.9$ Hz, 1 H, H_2) ppm;

$^{13}\text{C}\{^1\text{H}\}$ NMR (101 MHz, $(\text{CD}_3)_2\text{CO}/(\text{CD}_3)_2\text{SO}$): $\delta = 56.7$ (OMe), 114.1 (C_4), 115.1 (C_2), 116.6 ($\text{C}_{19/21}$), 124.7 (C_7), 125.1 (C_{17}), 129.0 (C_9), 129.5 ($\text{C}_{12/16}$), 129.9 (C_{11}), 130.5 ($\text{C}_{13/15}$), 133.9 ($\text{C}_{18/22}$), 135.7 (C_{14}), 139.1 (C_8), 147.3 (C_6), 151.6 (C_{10}), 165.3 (C_3), 167.4 (C_{20}), 167.8 (C_5), 170.5 (C_1) ppm;

^{19}F NMR (376 MHz, $(\text{CD}_3)_2\text{CO}$): $\delta = -151.3$ (s, $^{10}\text{BF}_4^-$), -151.4 (s, $^{11}\text{BF}_4^-$) ppm;

ESI-TOF (m/z): 340.1337 g/mol (calc.: 340.1332 g/mol) $[\text{M}]^+$;

Elemental analysis calc (%) for $\text{C}_{23}\text{H}_{18}\text{BF}_4\text{NO}_2$ (443,26 g/mol): C 64.66, H 4.25, N 3.28; found: C 64.77, H 4.24, N 3.00.

2-(2-Pyridyl)-4-(4-methylthiophenyl)-6-phenylpyrylium tetrafluoroborate (2.2e)

Diketone **2.1e** (7.1 g, 19 mmol), 1,3-diphenylprop-2-en-1-one (4.1 g, 20 mmol) and BF_3 etherate (20 mL, 23.0 g, 162 mmol) were heated to $T = 80$ °C for 6 h. The mixture was

dropped into diethyl ether (400 mL). The precipitate was filtered off, dried and washed with chloroform (50 mL). Afterwards recrystallization of the solid from ethanol/methanol 2:1 gave the product (3.070 g, 7 mmol, 37%) as dark red crystals. Crystals suitable for X-ray diffraction were obtained by from a hot methanol solution.

^1H NMR (400 MHz, $(\text{CD}_3)_2\text{CO}$): δ = 2.70 (s, 3 H, SMe), 7.64 – 7.69 (m, 2 H, $\text{H}_{19/21}$), 7.80 – 7.94 (m, 4 H, $\text{H}_{13/15}$, H_9 , H_{14}), 8.29 (ddd, J = 4.7, 1.7, 0.9 Hz, 1 H, H_8), 8.55 – 8.60 (m, 2 H, $\text{H}_{18/22}$), 8.65 – 8.69 (m, 2 Hz, $\text{H}_{12/16}$) 8.78 (ddd, J = 7.9, 1.0, 1.0 Hz, 1 H, H_7), 9.01 (ddd, J = 4.7, 1.7, 0.9 Hz, 1 H, H_{10}), 9.26 (d, J = 1.9 Hz, 1 H, H_4), 9.29 (d, J = 1.9 Hz, 1 H, H_2) ppm;

$^{13}\text{C}\{^1\text{H}\}$ NMR (101 MHz, $(\text{CD}_3)_2\text{SO}$): δ = 13.9 (SMe), 113.9 (C_4), 114.9 (C_2), 124.3 (C_7), 125.9 ($\text{C}_{19/21}$), 127.7 (C_{17}), 128.4 (C_9), 128.9 ($\text{C}_{12/16}$), 129.1 (C_{11}), 129.9 ($\text{C}_{13/15}$), 131.5 ($\text{C}_{18/22}$), 135.2 (C_{14}), 138.6 (C_8), 146.6 (C_6), 150.9 (C_{10}), 151.0 (C_{20}), 164.1 (C_3), 167.1 (C_5), 169.8 (C_1) ppm;

^{19}F NMR (376 MHz, $(\text{CD}_3)_2\text{SO}$): δ = -148.1 (s, $^{10}\text{BF}_4^-$), -148.1 (s, $^{11}\text{BF}_4^-$) ppm;

ESI-TOF (m/z): 356.1139 g/mol (calc.: 356.1104 g/mol) $[\text{M}]^+$;

Elemental analysis calc (%) for $\text{C}_{23}\text{H}_{18}\text{BF}_4\text{NOS}$ (443,26 g/mol): C 62.32, H 4.09, N 3.16, S 7.23; found: C 62.32, H 4.23, N 2.63, S 6.93.

Crystallographic data: $\text{C}_{23}\text{H}_{18}\text{NOS}$, BF_4 , F_w = 443.26, $0.21 \times 0.13 \times 0.09$ mm³, orange needle, triclinic, $P\bar{1}$, a = 8.1048(16), b = 11.553(2), c = 12.473(3) Å, α = 64.34(3)°, β = 81.29(3)°, γ = 77.44(3)°, V = 1025.4(5) Å³, Z = 2, D_x = 1.436 gcm⁻³, μ = 0.21 mm⁻¹. 11647 reflections were measured by using a Stoe IPDS 2T diffractometer with a rotating anode (MoK α radiation, λ = 0.71073 Å) up to a resolution of $(\sin\theta/\lambda)_{\text{max}}$ = 0.60 Å⁻¹ at a temperature of 200 K.¹⁶⁴ 2875 reflections were unique (R_{int} = 0.055). The structures were solved with SHELXS-97¹⁶⁵ by using direct methods and refined with SHELXL-97 on F^2 for all reflections. Non-hydrogen atoms were refined by using anisotropic displacement parameters. The positions of the hydrogen atoms were calculated for idealized positions. 280 parameters were refined without restraints. R_1 = 0.056 for 2875 reflections with $I > 2\sigma(I)$ and wR_2 = 0.143 for 5484 reflections, S = 0.922, residual electron density was between -0.28 and 0.36 eÅ⁻³. Geometry calculations and checks for higher symmetry were performed with the PLATON program.¹⁶⁶ A .cif data file can be found in the attachments.

2-(2-Pyridyl)-4-phenyl-6-(4-fluorophenyl)pyrylium tetrafluoroborate (2.2f)

Diketone **2.1f** (3.4 g, 10 mmol), 1,3-diphenylprop-2-en-1-one (2.0 g, 10 mmol) and BF_3 etherate (9.5 mL, 11.0 g, 77 mmol) gave the product (0.886 g, 2 mmol, 22%) as yellow crystals.

^1H NMR (400 MHz, $(\text{CD}_3)_2\text{CO}$): δ = 7.61 (m_s, 2 H, H_{13/15}), 7.79 – 7.94 (m, 4 H, H_{19/21}, H₉, H₂₀), 8.30 (ddd, J = 7.9, 7.8, 1.7 Hz, 1 H, H₈), 8.55 – 8.59 (m, 2 H, H_{18/22}), 8.81 – 8.86 (m, 3 H, H_{12/16}, H₇), 9.02 (ddd, J = 4.7, 1.7, 0.9 Hz, 1 H, H₁₀), 9.32 (d, J = 1.8 Hz, 1 H, H₂ or H₄), 9.32 (d, J = 1.8 Hz, 1 H, H₂ or H₄) ppm;

$^{13}\text{C}\{^1\text{H}\}$ NMR (101 MHz, $(\text{CD}_3)_2\text{CO}$): δ = 116.4 (C₂ or C₄), 117.7 (C₂ or C₄), 118.3 (d, $^2J_{\text{C-F}}$ = 22.7 Hz, C_{13/15}), 125.3 (C₇), 126.7 (d, $^4J_{\text{C-F}}$ = 3.0 Hz, C₁₁), 129.6 (C₉), 130.8 (C_{18/22}), 131.1 (C_{19/21}), 133.3 (d, $^3J_{\text{C-F}}$ = 10.1 Hz, C_{12/16}), 133.8 (C₁₇), 136.5 (C₂₀), 139.5 (C₈), 147.4 (C₆), 152.0 (C₁₀), 167.9 (C₃), 168.0 (d, $^1J_{\text{C-F}}$ = 259.6 Hz, C₁₄), 169.7 (C₁ or C₅), 171.6 (C₁ or C₅) ppm;

^{19}F NMR (376 MHz, $(\text{CD}_3)_2\text{CO}$): δ = -102.2 (m_s), -151.3 (s, $^{10}\text{BF}_4^-$), -151.4 (s, $^{11}\text{BF}_4^-$) ppm;

ESI-TOF (m/z): 328.1159 g/mol (calc.: 328.1132 g/mol) [M]⁺;

Elemental analysis calc (%) for C₂₂H₁₅BF₅NO (415,16 g/mol): C 63.65, H 3.64, N 3.37; found: C 63.61, H 3.72, N 3.21.

2-(2-Pyridyl)-4-phenyl-6-(4-methoxy)phenylpyrylium tetrafluoroborate (2.2g)

Diketone **2.1g** (5.3 g, 15 mmol), 1,3-diphenylprop-2-en-1-one (3.1 g, 15 mmol) and BF₃ etherate (17.0 mL, 19.6 g, 138 mmol) gave the product (2.812 g, 7 mmol, 45%) as orange crystals.

^1H NMR (400 MHz, $(\text{CD}_3)_2\text{CO}$): δ = 4.05 (s, 3 H, OMe), 7.36 (m_s, 2 H, H_{13/15}), 7.77 – 7.92 (m, 4 H, H_{19/21}, H₉, H₂₀), 8.28 (ddd, J = 7.8, 7.8, 1.7 Hz, 1 H, H₈), 8.49 – 8.53 (m, 2 H, H_{18/22}), 8.71 – 8.78 (m, 3 H, H_{12/16}, H₇), 9.00 (ddd, J = 4.7, 1.6, 0.9 Hz, 1 H, H₁₀), 9.16 (d, J = 1.8 Hz, 1 H, H₄), 9.18 (d, J = 1.8 Hz, 1 H, H₂) ppm;

$^{13}\text{C}\{^1\text{H}\}$ NMR (101 MHz, $(\text{CD}_3)_2\text{CO}$): δ = 56.7 (OMe), 115.2 (C₄), 116.7 (C₂), 116.7 (C_{13/15}), 122.2 (C₁₁), 124.8 (C₇), 129.3 (C₉), 130.5 (C_{18/22}), 131.0 (C_{19/21}), 132.9 (C_{12/16}), 134.0 (C₁₇), 136.0 (C₂₀), 139.3 (C₈), 147.6 (C₆), 152.0 (C₁₀), 166.5 (C₃), 167.4 (C₁₄), 168.3 (C₅), 172.7 (C₁) ppm;

^{19}F NMR (376 MHz, $(\text{CD}_3)_2\text{CO}$): δ = -151.5 (s, $^{10}\text{BF}_4^-$), -151.6 (s, $^{11}\text{BF}_4^-$) ppm;

ESI-TOF (m/z): 340.1360 g/mol (calc.: 340.1332 g/mol) [M]⁺;

Elemental analysis calc (%) for C₂₃H₁₈BF₄NO₂ (427,20 g/mol): C 64.66, H 4.25, N 3.28; found: C 64.21, H 4.30, N 2.91.

2-(2-Pyridyl)-4-phenyl-6-(4-methylthiophenyl)pyrylium tetrafluoroborate (2.2h)

Diketone **2.1h** (3.2 g, 9 mmol), 1,3-diphenylprop-2-en-1-one (2.0 g, 10 mmol) and BF₃ etherate (9.6 mL, 11.0 g, 78 mmol) gave the product (1.451 g, 3 mmol, 38%) as dark red

crystals. Crystals suitable for X-ray diffraction were obtained from slow evaporation of an acetone solution.

^1H NMR (400 MHz, $(\text{CD}_3)_2\text{CO}$): δ = 2.69 (s, 3 H, SMe), 7.65 (m_s, 2 H, H_{13/15}), 7.78 – 7.93 (m, 4 H, H_{19/21}, H₉, H₂₀), 8.29 (ddd, J = 7.8, 7.8, 1.7 Hz, 1 H, H₈), 8.50 – 8.55 (m, 2 H, H_{18/22}), 8.63 (m_s, 2 H, H_{12/16}), 8.77 (ddd, J = 7.9, 1.0, 1.0 Hz, 1 H, H₇), 9.01 (ddd, J = 4.7, 1.7, 0.9 Hz, 1 H, H₁₀), 9.21 (d, J = 1.8 Hz, 1 H, H₄), 9.24 (d, J = 1.8 Hz, 1 H, H₂) ppm;

$^{13}\text{C}\{^1\text{H}\}$ NMR (101 MHz, $(\text{CD}_3)_2\text{CO}/(\text{CD}_3)_2\text{SO}$): δ = 14.3 (SMe), 115.3 (C₄), 116.8 (C₂), 124.9 (C₇), 125.3 (C₁₁), 126.5 (C_{13/15}), 129.1 (C₉), 130.2 (C_{12/16}), 130.5 (C_{18/22}), 130.7 (C_{19/21}), 133.5 (C₁₇), 135.9 (C₂₀), 139.2 (C₈), 147.3 (C₆), 151.7 (C₁₀ or C₁₄), 151.7 (C₁₀ or C₁₄), 166.1 (C₃), 168.1 (C₅), 171.8 (C₁) ppm;

^{19}F NMR (376 MHz, $(\text{CD}_3)_2\text{CO}$): δ = -151.5 (s, $^{10}\text{BF}_4^-$), -151.5 (s, $^{11}\text{BF}_4^-$) ppm;

ESI-TOF (m/z): 356.1139 g/mol (calc.: 356.1104 g/mol) [M]⁺;

Elemental analysis calc (%) for C₂₃H₁₈BF₄NOS (443.26 g/mol): C 62.32, H 4.09, N 3.16, S 7.23; found: C 62.29, H 4.10, N 3.07, S 7.35.

Crystallographic data: C₂₃H₁₈NOS, BF₄, F_w = 443.25, 0.43×0.09×0.07 mm³, red needle, monoclinic, $P2_1/c$, a = 10.0880(3), b = 26.1395(7), c = 7.7459(2) Å, β = 104.137(1)°, V = 1980.70(9) Å³, Z = 4, D_x = 1.468 gcm⁻³, μ = 0.217 mm⁻¹. 17873 reflections were measured by using a D8 Venture, Bruker Photon CMOS Detector (MoK α radiation, λ = 0.71073 Å) up to a resolution of $(\sin\theta/\lambda)_{\text{max}}$ = 0.60 Å⁻¹ at a temperature of 100 K.¹⁶⁷ 2888 reflections were unique (R_{int} = 0.059). The structures were solved with SHELXS-2014¹⁶⁵ by using direct methods and refined with SHELXL-2014² on F^2 for all reflections. Non-hydrogen atoms were refined by using anisotropic displacement parameters. The positions of the hydrogen atoms were calculated for idealized positions. 281 parameter were refined without restraints. R_1 = 0.053 for 2888 reflections with $I > 2\sigma(I)$ and wR_2 = 0.125 for 3494 reflections, S = 1.054, residual electron density was between -0.70 and 1.09 eÅ⁻³. Geometry calculations and checks for higher symmetry were performed with the PLATON program.¹⁶⁶ A .cif data file can be found in the attachments.

Pyridylphosphinines (2.3b-h)

The respective pyrylium salt was stirred under argon in dry acetonitrile. Tris(trimethylsilyl)-phosphane was added dropwise. The solution was then heated to T = 85 °C for 6 h. After evaporation of the solvent the product was purified first by column chromatography (silica, 800 mL petroleum ether then petroleum ether/ethyl acetate = 20:1 to 5:1, degassed solvents) and subsequently by recrystallization from acetonitrile.

2-(2-Pyridyl)-4-(4-fluorophenyl)-6-phenylphosphinine (2.3b)

Pyrylium salt **2.3b** (6.4 g, 15 mmol) and tris(trimethylsilyl)phosphane (8.1 g, 32 mmol) in acetonitrile (37 mL) gave the product (0.529 g, 1.5 mmol, 10%) as a slightly yellow-orange solid.

^1H NMR (400 MHz, THF- d_8): δ = 7.26 (m, 2 H, H_{19/21}), 7.29 – 7.34 (m, 1 H, H₉), 7.39 – 7.43 (m, 1 H, H₁₄), 7.45 – 7.51 (m, 2 H, H_{13/15}), 7.76 – 7.86 (m, 5 H, H_{12/16}, H_{18/22}, H₈), 8.12 – 8.16 (m, 1 H, H₇), 8.26 (dd, J = 6.0, 1.2 Hz, 1 H, H₂), 8.69 (ddd, J = 4.8, 1.8, 0.9 Hz, 1 H, H₁₀), 8.89 (dd, J = 5.7 Hz, 1.2 Hz, 1 H, H₄) ppm;

$^{13}\text{C}\{^1\text{H}\}$ NMR (101 MHz, THF- d_8): δ = 116.6 (d, $^2J_{\text{C-F}}$ = 21.6 Hz, C_{19/21}), 121.8 (d, $^3J_{\text{C-P}}$ = 16.5 Hz, C₇), 123.8 (d, $^5J_{\text{C-P}}$ = 2.0 Hz, C₉), 128.5 (d, $^3J_{\text{C-P}}$ = 13.0 Hz, C_{12/16}), 128.8 (d, $^5J_{\text{C-P}}$ = 1.9 Hz, C₁₄), 129.8 (C_{13/15}), 130.5 (dd, $^3J_{\text{C-F}}$ = 8.2 Hz, $^5J_{\text{C-P}}$ = 1.7 Hz, C_{18/22}), 132.2 (d, $^2J_{\text{C-P}}$ = 13.0 Hz, C₄), 133.4 (d, $^2J_{\text{C-P}}$ = 12.0 Hz, C₂), 137.7 (C₈), 139.4 (dd, $^4J_{\text{C-F}}$ = 3.2 Hz, $^4J_{\text{C-P}}$ = 3.2 Hz, C₁₇), 144.0 (d, $^3J_{\text{C-P}}$ = 13.8 Hz, C₃), 144.5 (d, $^2J_{\text{C-P}}$ = 24.8 Hz, C₁₁), 150.8 (C₁₀), 159.8 (d, $^2J_{\text{C-P}}$ = 25.6 Hz, C₆), 163.93 (dd, $^1J_{\text{C-F}}$ = 246.8 Hz, $^7J_{\text{C-P}}$ = 0.9 Hz, C₂₀), 170.6 (d, $^1J_{\text{C-P}}$ = 50.7 Hz, C₅), 172.6 (d, $^1J_{\text{C-P}}$ = 50.9 Hz, C₁) ppm;

^{19}F NMR (376 MHz, THF- d_8): δ = -115.6 (m_s) ppm;

$^{31}\text{P}\{^1\text{H}\}$ NMR (162 MHz, THF- d_8) δ = 186.7 ppm;

ESI-TOF (m/z): 344.1027 g/mol (calc.: 344.0999 g/mol) [M + H]⁺.

2-(2-Pyridyl)-4-(4-trifluoromethylphenyl)-6-phenylphosphinine (2.3c)

Pyrylium salt **2.3c** (5.1 g, 11 mmol) and Tris(trimethylsilyl)phosphane (5.5 g, 22 mmol) in acetonitrile (24 mL) gave the product (0.214 g, 0.5 mmol, 5%) as a slightly red solid. The NMR spectra still show impurities. However, the mass spectrum confirms the successful synthesis of **3c**.

^1H NMR (400 MHz, THF- d_8): δ = 7.25 – 7.29 (m, 1 H), 7.43 – 7.48 (m, 2 H), 7.75 – 7.82 (m, 6 H), 7.95 (d, J = Hz, 2 H), 8.11 (d, J = 8.2 Hz, 1 H), 8.26 – 8.29 (m, 1 H), 8.67 – 8.70 (m, 1 H), 8.90 – 8.93 (m, 1 H) ppm;

^{19}F NMR (376 MHz, THF- d_8): δ = -62.9 (s) ppm;

$^{31}\text{P}\{^1\text{H}\}$ NMR (162 MHz, THF- d_8): δ = 192.2 ppm;

ESI-TOF (m/z): 394.0991 g/mol (calc.: 394.0967 g/mol) [M + H]⁺.

2-(2-Pyridyl)-4-(4-methoxyphenyl)-6-phenylphosphinine (2.3d)

Pyrylium salt **2.3d** (3.5 g, 8 mmol) and tris(trimethylsilyl)phosphane (4.1 g, 16 mmol) in acetonitrile (20 mL) gave the product (0.560 g, 1.5 mmol, 19%) as a slightly yellow-orange solid.

^1H NMR (500 MHz, DCM- d_2): δ = 3.87 (s, 3 H, OMe), 7.05 (m_s, 2 H, H_{19/21}), 7.32 (dd, J = 7.4 Hz, 4.8 Hz, 1 H, H₉), 7.42 – 7.46 (m, 1 H, H₁₄), 7.48 – 7.53 (m, 2 H, H_{13/15}), 7.71 (m_s, 2 H, H_{18/22}), 7.75 – 7.79 (m, 2 H, H_{12/16}), 7.82 (ddd, J = 7.7 Hz, 7.7 Hz, 1.9 Hz, 1 H, H₈), 8.02 (dd, J = 8.0 Hz, 1.1 Hz, 1 H, H₇), 8.23 (dd, J = 5.9 Hz, 1.3 Hz, 1 H, H₂), 8.69 (dd, J = 5.7 Hz, 1.3 Hz, 1 H, H₄), 8.73 (ddd, J = 4.7 Hz, 1.9 Hz, 0.9 Hz, 1 H, H₁₀) ppm;

$^{13}\text{C}\{^1\text{H}\}$ NMR (126 MHz, DCM- d_2): δ = 55.9 (OMe), 115.0 (d, $^6J_{\text{C-P}}$ = 2.8 Hz, C_{19/21}), 121.7 (d, $^3J_{\text{C-P}}$ = 14.0 Hz, C₇), 123.4 (C₉), 128.2 (d, $^3J_{\text{C-P}}$ = 12.8 Hz, C_{12/16}), 128.5 (C₁₄), 129.4 (C_{18/22}), 129.5 (C_{13/15}), 131.8 (d, $^2J_{\text{C-P}}$ = 13.5 Hz, C₄), 133.0 (d, $^2J_{\text{C-P}}$ = 11.7 Hz, C₂), 134.9 (d, $^4J_{\text{C-P}}$ = 3.1 Hz, C₁₇), 137.5 (C₈), 144.2 (d, $^2J_{\text{C-P}}$ = 24.6 Hz, C₁₁), 144.3 (d, $^3J_{\text{C-P}}$ = 13.4 Hz, C₃), 150.4 (C₁₀), 159.8 (d, $^2J_{\text{C-P}}$ = 24.6 Hz, C₆), 160.5 (C₂₀), 169.9 (d, $^1J_{\text{C-P}}$ = 49.7 Hz, C₁ or C₅), 172.1 (d, $^1J_{\text{C-P}}$ = 50.2 Hz, C₁ or C₅) ppm;

$^{31}\text{P}\{^1\text{H}\}$ NMR (162 MHz, DCM- d_2) δ = 183.9 ppm; $^{31}\text{P}\{^1\text{H}\}$ NMR (162 MHz, C₆D₆) δ = 184.2 ppm;

ESI-TOF (m/z): 356.1236 g/mol (calc.: 356.1199 g/mol) [M + H]⁺.

2-(2-Pyridyl)-4-(4-methylthiophenyl)-6-phenylphosphinine (2.3e)

Pyrylium salt **2.3e** (4.3 g, 10 mmol) and Tris(trimethylsilyl)phosphane (5.5 g, 22 mmol) in acetonitrile (24 mL) gave the product (0.286 g, 0.8 mmol, 8%) as a slightly yellow-orange solid.

^1H NMR (400 MHz, THF- d_8): δ = 2.52 (s, 3 H), 7.30 (m_s, 1 H), 7.37 – 7.42 (m, 3 H), 7.45 – 7.50 (m, 2 H), 7.72 – 7.84 (m, 5 H), 8.11 – 8.15 (m, 1 H), 8.28 (dd, J = 6.0 Hz, 1.3 Hz, 1 H), 8.70 (ddd, J = 4.8 Hz, 1.9 Hz, 1.0 Hz, 1 H), 8.91 (dd, J = 5.7 Hz, 1.3 Hz, 1 H) ppm;

$^{13}\text{C}\{^1\text{H}\}$ NMR (101 MHz, THF- d_8): δ = 15.4, 121.8 (d, $J_{\text{C-P}}$ = 16.5 Hz), 123.7 (d, $J_{\text{C-P}}$ = 2.0 Hz), 127.5, 128.5 (d, $J_{\text{C-P}}$ = 13.0 Hz), 128.8 (d, $J_{\text{C-P}}$ = 1.9 Hz), 128.9 (d, $J_{\text{C-P}}$ = 1.7 Hz), 129.7, 132.0 (d, $J_{\text{C-P}}$ = 13.1 Hz), 133.1 (d, $J_{\text{C-P}}$ = 11.9 Hz), 137.7, 139.4 (d, $J_{\text{C-P}}$ = 3.4 Hz), 140.3 (d, $J_{\text{C-P}}$ = 1.0 Hz), 144.5, 144.6 (d, $J_{\text{C-P}}$ = 38.4 Hz), 150.7, 159.9 (d, $J_{\text{C-P}}$ = 25.7 Hz), 170.5 (d, $J_{\text{C-P}}$ = 50.5 Hz), 172.5 (d, $J_{\text{C-P}}$ = 50.8 Hz) ppm;

$^{31}\text{P}\{^1\text{H}\}$ NMR (162 MHz, THF- d_8) δ = 185.8 ppm;

ESI-TOF (m/z): 372.0974 g/mol (calc.: 372.0970 g/mol) [M + H]⁺.

2-(2-Pyridyl)-4-phenyl-6-(4-fluorophenyl)phosphinine (2.3f)

Pyrylium salt **2.3f** (3.4 g, 10 mmol) and tris(trimethylsilyl)phosphane (5.1 g, 21 mmol) in acetonitrile (24 mL) gave the product (0.515 g, 1.5 mmol, 18%) as a slightly yellow-orange solid.

^1H NMR (400 MHz, THF-*d*₈): δ = 7.20 – 7.27 (m, 2 H, H_{13/15}), 7.29 – 7.34 (m, 1 H, H₉), 7.38 – 7.43 (m, 1 H, H₂₀), 7.47 – 7.53 (m, 2 H, H_{19/21}), 7.77 – 7.85 (m, 5 H, H_{18/22}, H_{12/16}, H₈), 8.11 – 8.15 (m, 1 H, H₇), 8.27 (dd, *J* = 5.9, 1.2 Hz, 1 H, H₂), 8.69 (ddd, *J* = 4.8, 1.9, 1.0 Hz, 1 H, H₁₀), 8.90 (dd, *J* = 5.8, 1.3 Hz, 1 H, H₄) ppm;

$^{13}\text{C}\{^1\text{H}\}$ NMR (101 MHz, THF-*d*₈): δ = 115.5 (d, $^2J_{\text{C-F}}$ = 21.7 Hz, C_{13/15}), 120.8 (d, $^3J_{\text{C-P}}$ = 16.0 Hz, C₇), 122.8 (C₉), 127.6 (C_{18/22}), 127.9 (C₂₀), 128.8 (C_{19/21}), 129.3 (dd, $^3J_{\text{C-F}}$ = 8.2 Hz, $^3J_{\text{C-P}}$ = 12.9 Hz, C_{12/16}), 131.4 (d, $^2J_{\text{C-P}}$ = 13.0 Hz, C₄), 132.5 (d, $^2J_{\text{C-P}}$ = 11.7 Hz, C₂), 136.6 (C₈), 140.0 (d, $^2J_{\text{C-P}}$ = 25.6 Hz, C₁₁), 142.1 (d, $^4J_{\text{C-P}}$ = 3.3 Hz, C₁₇), 144.3 (d, $^2J_{\text{C-P}}$ = 13.7 Hz, C₆), 149.8 (C₁₀), 158.8 (d, $^3J_{\text{C-P}}$ = 25.5 Hz, C₃), 163.2 (d, $^1J_{\text{C-F}}$ = 248.9 Hz, C₁₄), 169.5 (d, $^1J_{\text{C-P}}$ = 50.5 Hz, C₁ or C₅), 170.3 (d, $^1J_{\text{C-P}}$ = 51.1 Hz, C₁ or C₅) ppm;

^{19}F NMR (377 MHz, THF-*d*₈): δ = -116.3 (m_s) ppm;

$^{31}\text{P}\{^1\text{H}\}$ NMR (162 MHz, THF-*d*₈) δ = 186.3 (d, $^6J_{\text{P-F}}$ = 2.6 Hz) ppm;

ESI-TOF (m/z): 344.1003 g/mol (calc.: 344.0999 g/mol) [M + H]⁺.

2-(2-Pyridyl)-4-phenyl-6-(4-methoxyphenyl)phosphinine (2.3g)

Pyrylium salt **2.3g** (4.4 g, 10 mmol) and tris(trimethylsilyl)phosphane (5.5 g, 22 mmol) in acetonitrile (30 mL) gave the product (0.282 g, 0.8 mmol, 8%) as a slightly yellow-orange solid.

^1H NMR (400 MHz, THF-*d*₈): δ = 3.84 (s, 3 H, OMe), 7.01 – 7.06 (m, 2 H, H_{13/15}), 7.28 – 7.32 (m, 1 H, H₉), 7.37 – 7.43 (m, 1 H, H₂₀), 7.46 – 7.52 (m, 2 H, H_{19/21}), 7.72 – 7.84 (m, 5 H, H_{12/16}, H_{18/22}, H₈), 8.11 – 8.16 (m, 1 H, H₇), 8.23 – 8.27 (m, 1 H, H₂), 8.67 – 8.70 (m, 1 H, H₁₀), 8.85 – 8.88 (m, 1 H, H₄) ppm;

$^{13}\text{C}\{^1\text{H}\}$ NMR (101 MHz, THF-*d*₈): δ = 55.6 (OMe), 115.2 (C_{13/15}), 121.8 (d, $^3J_{\text{C-P}}$ = 16.6 Hz, C₇), 123.7 (d, $^5J_{\text{C-P}}$ = 2.0 Hz, C₉), 128.6 (d, $^5J_{\text{C-P}}$ = 1.7 Hz, C_{18/22}), 128.7 (C₂₀), 129.4 (d, $^3J_{\text{C-P}}$ = 13.4 Hz, C_{12/16}), 129.8 (C_{19/21}), 131.9 (d, $^2J_{\text{C-P}}$ = 13.1 Hz, C₄), 132.9 (d, $^2J_{\text{C-P}}$ = 11.6 Hz, C₂), 137.0 (d, $^2J_{\text{C-P}}$ = 25.2 Hz, C₁₁), 137.6 (C₈), 143.3 (d, $^4J_{\text{C-P}}$ = 3.3 Hz, C₁₇), 145.1 (d, $^3J_{\text{C-P}}$ = 13.7 Hz, C₃), 150.7 (C₁₀), 160.0 (d, $^2J_{\text{C-P}}$ = 25.7 Hz, C₆), 161.3 (d, $^5J_{\text{C-P}}$ = 2.1 Hz, C₁₄), 170.4 (d, $^1J_{\text{C-P}}$ = 50.6 Hz, C₅), 172.2 (d, $^1J_{\text{C-P}}$ = 50.8 Hz, C₁) ppm;

$^{31}\text{P}\{^1\text{H}\}$ NMR (162 MHz, THF-*d*₈) δ = 185.8 ppm;

ESI-TOF (m/z): 356.1236 g/mol (calc.: 356.1199 g/mol) [M + H]⁺.

2-(2-Pyridyl)-4-phenyl-6-(4-methylthiophenyl)phosphinine (2.3h)

Pyrylium salt **2.3h** (5.0 g, 11 mmol) and tris(trimethylsilyl)phosphane (5.8 g, 23 mmol) in acetonitrile (30 mL) gave the product (0.897 g, 2.5 mmol, 22%) as a slightly yellow-orange solid.

¹H NMR (401 MHz, THF-*d*₈): δ = 2.52 (s, 3 H, SMe), 7.28 – 7.33 (m, 1 H, H₉), 7.36 – 7.43 (m, 3 H, H_{13/15}, H₂₀), 7.47 – 7.52 (m, 2 H, H_{19/21}), 7.72 – 7.76 (m, 2 H, H_{12/16}), 7.77 – 7.84 (m, 3 H, H_{18/22}, H₈), 8.11 – 8.15 (m, 1 H, H₇), 8.27 (dd, *J* = 5.8 Hz, 1.3 Hz, 1 H, H₂), 8.69 (ddd, *J* = 4.8 Hz, 1.9 Hz, 1.0 Hz, 1 H, H₁₀), 8.89 (dd, *J* = 5.8 Hz, 1.3 Hz, 1 H, H₄) ppm;

¹³C{¹H} NMR (101 MHz, C₆D₆): δ = 15.5 (SMe), 121.8 (d, *J*_{C-P} = 16.2 Hz, C₇), 123.7 (d, *J*_{C-P} = 2.0 Hz, C₉), 127.6 (C_{13/15}), 128.6 (d, *J*_{C-P} = 1.7 Hz, C_{18/22}), 128.6 (C₂₀), 128.8 (C_{12/16}), 129.8 (C_{19/21}), 132.3 (d, *J*_{C-P} = 13.1 Hz, C₄), 133.1 (d, *J*_{C-P} = 11.8 Hz, C₂), 137.7 (C₈), 140.3 (d, *J*_{C-P} = 2.3 Hz, C₁₄), 141.1 (d, *J*_{C-P} = 25.1 Hz, C₁₁), 143.2 (d, *J*_{C-P} = 3.2 Hz, C₁₇), 145.2 (d, *J*_{C-P} = 13.7 Hz, C₃), 150.7 (C₁₀), 159.9 (d, *J*_{C-P} = 25.7 Hz, C₆), 170.5 (d, *J*_{C-P} = 50.5 Hz, C₅), 171.8 (d, *J*_{C-P} = 51.0 Hz, C₁) ppm;

³¹P{¹H} NMR (162 MHz, THF-*d*₈) δ = 186.0 ppm;

ESI-TOF (m/z): 372.1000 g/mol (calc.: 372.0970 g/mol) [M + H]⁺.

Bipyridines (2.4b-h)

To pyrylium salt stirred in ethanol ammonia (24% in water) was added. After a colour change to a red solution, a white solid precipitates after 10-30 min. The reaction is allowed to proceed for two hours. Then the solid product is filtered off, washed with ethanol/water and dried under vacuum.

2-(2-Pyridyl)-4-(4-fluorophenyl)-6-phenylpyridine (2.4b)

Pyrylium salt **2.2b** (0.199 g, 0.48 mmol) with ammonia (2.0 mL, 24% in water, 25 mmol) in ethanol (3 mL) gave the product (0.152 g, 0.47 mmol, 97%) as a colourless solid. **2.4b** has been synthesised before *via* a different synthetic pathway.¹³⁹

¹H NMR (400 MHz, CDCl₃): δ = 7.20 (m_s, 2 H), 7.34 (ddd, *J* = 7.4 Hz, 4.8 Hz, 1.3 Hz, 1 H), 7.44 – 7.56 (m, 3 H), 7.79 (m_s, 2 H), 7.87 (ddd, *J* = 7.7 Hz, 7.7 Hz, 1.9 Hz, 1 H), 7.92 (d, *J* = 1.6 Hz, 1 H), 8.18 – 8.23 (m, 2 H), 8.61 (d, *J* = 1.6 Hz, 1 H), 8.67 – 8.74 (m, 2 H) ppm;

$^{13}\text{C}\{^1\text{H}\}$ NMR (101 MHz, CDCl_3): $\delta = 116.1$ (d, $J_{\text{C-F}} = 21.6$ Hz), 117.4, 118.4, 121.7, 124.0, 127.2, 128.9, 129.1 (d, $J_{\text{C-F}} = 8.2$ Hz), 129.3, 134.9 (d, $J_{\text{C-F}} = 3.3$ Hz), 137.1, 139.4, 149.1, 149.3, 156.3, 156.3, 157.3, 163.5 (d, $J_{\text{C-F}} = 248.9$ Hz) ppm;

^{19}F NMR (376 MHz, CDCl_3): $\delta = -112.6$ (m_s) ppm;

ESI-TOF (m/z): 327.1304 g/mol (calc.: 327.1298 g/mol) $[\text{M} + \text{H}]^+$.

2-(2-Pyridyl)-4-(4-trifluoromethylphenyl)-6-phenylpyridine (2.4c)

Pyrylium salt **2.2c** (0.199 g, 0.57 mmol) with ammonia (3.0 mL, 24% in water, 25 mmol) in ethanol (10 mL) gave the product (0.069 g, 0.18 mmol, 33%) as a white solid. Crystals suitable for X-ray diffraction were obtained from a hot ethanol solution.

^1H NMR (700 MHz, DCM-d_2): $\delta = 7.38$ (ddd, $J = 7.4$ Hz, 4.7 Hz, 1.2 Hz, 1 H), 7.47 – 7.51 (m, 1 H), 7.54 – 7.57 (m, 2 H), 7.80 – 7.82 (m, 2 H), 7.90 (ddd, $J = 7.9$ Hz, 7.4 Hz, 1.8 Hz, 1 H), 7.95 – 7.97 (m, 2 H), 8.02 (d, $J = 1.6$ Hz, 1 H), 8.22 – 8.25 (m, 2 H), 8.69 (ddd, $J = 8.0$ Hz, 1.1 Hz, 1.1 Hz, 1 H), 8.69 (d, $J = 1.6$ Hz, 1 H), 8.71 (ddd, $J = 4.7$ Hz, 1.8 Hz, 0.9 Hz, 1 H) ppm;

$^{13}\text{C}\{^1\text{H}\}$ NMR (176 MHz, DCM-d_2): $\delta = 118.0$, 119.0, 121.8, 124.6, 124.8 (q, $J_{\text{C-F}} = 271.9$ Hz), 126.5 (q, $J_{\text{C-F}} = 3.9$ Hz), 127.6, 128.3, 129.3, 129.9, 131.25 (q, $J_{\text{C-F}} = 32.6$ Hz), 137.5, 139.7, 143.1, 149.3, 149.7, 156.5, 157.2, 157.8 ppm;

^{19}F NMR (376 MHz, DCM-d_2): $\delta = -62.8$ ppm;

ESI-TOF (m/z): 399.1086 g/mol (calc.: 399.1084 g/mol) $[\text{M} + \text{Na}]^+$.

Crystallographic data: $\text{C}_{23}\text{H}_{15}\text{F}_3\text{N}_2$, $F_w = 376.37$, $0.65 \times 0.06 \times 0.05$ mm³, colourless needle, monoclinic, $P2_1/c$, $a = 10.6860(3)$, $b = 21.8463(5)$, $c = 7.4437(1)$ Å, $\beta = 92.658(1)^\circ$, $V = 1735.86(7)$ Å³, $Z = 4$, $D_x = 1.440$ gcm⁻³, $\mu = 0.11$ mm⁻¹. 16134 reflections were measured by using a D8 Venture, Bruker Photon CMOS Detector (MoK α radiation, $\lambda = 0.71073$ Å) up to a resolution of $(\sin\theta/\lambda)_{\text{max}} = 0.60$ Å⁻¹ at a temperature of 100 K.¹⁶⁷ 2510 reflections were unique ($R_{\text{int}} = 0.045$). The structures were solved with SHELXS-2013¹⁶⁵ by using direct methods and refined with SHELXL-2013¹⁶⁵ on F_2 for all reflections. Non-hydrogen atoms were refined by using anisotropic displacement parameters. The positions of the hydrogen atoms were calculated for idealized positions. 253 parameter were refined without restraints. $R_1 = 0.043$ for 2510 reflections with $I > 2\sigma(I)$ and $wR_2 = 0.108$ for 3069 reflections, $S = 1.035$, residual electron density was between -0.32 and 0.49 eÅ⁻³. Geometry calculations and checks for higher symmetry were performed with the PLATON program.¹⁶⁶ A .cif data file can be found in the attachments.

2-(2-Pyridyl)-4-(4-methoxyphenyl)-6-phenylpyridine (2.4d)

Pyrylium salt **2.2d** (0.445 g, 1.04 mmol) with ammonia (2.5 mL, 24% in water, 32 mmol) in ethanol (10 mL) gave the product (0.466 g, 1.38 mmol, 98%) as a colourless solid. **2.4d** has been synthesised before *via* a different synthetic pathway.¹³⁹

¹H NMR (400 MHz, DCM-*d*₂): δ = 3.88 (s, 3 H), 7.07 (m_s, 2 H), 7.36 (ddd, *J* = 7.5 Hz, 4.8 Hz, 1.2 Hz, 1 H), 7.44 – 7.50 (m, 1 H), 7.51 – 7.57 (m, 2 H), 7.82 (m_s, 2 H), 7.88 (ddd, *J* = 8.0 Hz, 7.5 Hz, 1.8 Hz, 1 H), 8.00 (d, *J* = 1.6 Hz, 1 H), 8.20 – 8.23 (m, 2 H), 8.64 (d, *J* = 1.6 Hz, 1 H), 8.68 (ddd, *J* = 8.0 Hz, 1.1 Hz, 1.1 Hz, 1 H), 8.71 (ddd, *J* = 4.8 Hz, 1.8 Hz, 0.9 Hz, 1 H) ppm;

¹³C{¹H} NMR (101 MHz, DCM-*d*₂): δ = 56.0, 115.0, 117.3, 118.3, 121.7, 124.4, 127.5, 128.9, 129.2, 129.6, 131.4, 137.4, 140.1, 149.6, 150.2, 156.8, 156.9, 157.5, 161.2 ppm;

ESI-TOF (m/z): 339.1510 g/mol (calc.: 339.1497 g/mol) [M + H]⁺, 361.1331 g/mol (calc.: 361.1317 g/mol) [M + Na]⁺.

2-(2-Pyridyl)-4-(4-methylthiophenyl)-6-phenylpyridine (2.4e)

Pyrylium salt **2.2e** (0.315 g, 0.71 mmol) with ammonia (2.0 mL, 24% in water, 25 mmol) in ethanol (3 mL) gave the product (0.236 g, 0.67 mmol, 94%) as a colourless solid. **2.4e** has been synthesised before *via* a different synthetic pathway.¹⁴¹

¹H NMR (400 MHz, CDCl₃): δ = 2.56 (s, 3 H, SMe), 7.33 – 7.40 (m, 3 H, H₉, H_{19/21}), 7.44 – 7.56 (m, 3 H, H₁₄, H_{13/15}), 7.75 – 7.79 (m, 2 H, H_{18/22}), 7.84 – 7.90 (m, 1 H, H₈), 7.96 (d, *J* = 1.4 Hz, 1 H, H₂), 8.18 – 8.22 (m, 2 H, H_{12/16}), 8.63 (d, *J* = 1.4 Hz, 1 H, H₄), 8.67 – 8.71 (m, 1 H, H₇), 8.72 (ddd, *J* = 4.7 Hz, 1.8 Hz, 0.8 Hz, 1 H, H₁₀) ppm;

¹³C{¹H} NMR (101 MHz, CDCl₃): δ = 15.6 (SMe), 117.11 (C₄), 118.3 (C₂), 121.7 (C₇), 124.0 (C₉), 126.7 (C_{19/21}), 127.2 (C_{12/16}), 127.6 (C_{18/22}), 128.9 (C_{13/15}), 129.2 (C₁₄), 135.3 (C₁₇), 137.0 (C₈), 139.6 (C₁₁), 140.2 (C₂₀), 149.2 (C₁₀), 149.6 (C₃), 156.4 (C₅ or C₆), 156.4 (C₅ or C₆), 157.3 (C₁) ppm;

ESI-TOF (m/z): 355.1278 g/mol (calc.: 355.1269 g/mol) [M + H]⁺, 377.1089 g/mol (calc.: 377.1088 g/mol) [M + Na]⁺.

2-(2-Pyridyl)-4-phenyl-6-(4-fluorophenyl)pyridine (2.4f)

Pyrylium salt **2.2f** (0.144 g, 0.35 mmol) with ammonia (1.0 mL, 24% in water, 13 mmol) in ethanol (2 mL) gave the product (0.088 g, 0.27 mmol, 78%) as a colourless solid. **2.4f** has been synthesised before *via* a different synthetic pathway.¹⁴⁰

^1H NMR (400 MHz, CDCl_3): $\delta = 7.18 - 7.24$ (m, 2 H), 7.33 (ddd, $J = 7.4$ Hz, 4.8 Hz, 1.2 Hz, 1 H), 7.44 – 7.54 (m, 3 H), 7.79 – 7.83 (m, 2 H), 7.85 (ddd, $J = 7.7$ Hz, 7.7 Hz, 1.8 Hz, 1 H), 7.91 (d, $J = 1.6$ Hz, 1 H), 8.16 – 8.22 (m, 2 H), 8.63 – 8.67 (m, 2 H), 8.71 – 8.74 (m, 1 H) ppm;

$^{13}\text{C}\{^1\text{H}\}$ NMR (101 MHz, CDCl_3): $\delta = 115.7$ (d, $J_{\text{C-F}} = 21.5$ Hz), 117.6, 118.2, 121.5, 124.0, 127.3, 128.9 (d, $J_{\text{C-F}} = 8.2$ Hz), 129.1, 129.2, 135.7 (d, $J_{\text{C-F}} = 3.1$ Hz), 137.0, 138.7, 149.1, 150.4, 156.1, 156.3, 156.3, 163.7 (d, $J_{\text{C-F}} = 248.5$ Hz) ppm;

^{19}F NMR (376 MHz, CDCl_3): $\delta = -112.8 - -112.7$ (m) ppm;

ESI-TOF (m/z): 327.1308 g/mol (calc.: 327.1298 g/mol) $[\text{M} + \text{H}]^+$, 349.1127 g/mol (calc.: 349.1117 g/mol) $[\text{M} + \text{Na}]^+$.

2-(2-Pyridyl)-4-phenyl-6-(4-methoxyphenyl)pyridine (2.4g)

Pyrylium salt **2.4g** (0.600 g, 1.40 mmol) with ammonia (2.5 mL, 24% in water, 32 mmol) in ethanol (3 mL) gave the product (0.152 g, 0.47 mmol, 97%) as a colourless solid. **2.4g** has been synthesised before *via* a different synthetic pathway.¹⁴⁰

^1H NMR (400 MHz, CDCl_3): $\delta = 3.90$ (s, 3 H), 7.06 (m_s, 2 H), 7.34 (ddd, $J = 7.5$ Hz, 4.8 Hz, 1.2 Hz, 1 H), 7.44 – 7.55 (m, 3 H), 7.81 – 7.84 (m, 2 H), 7.87 (ddd, $J = 8.0$ Hz, 7.5 Hz, 1.8 Hz, 1 H), 7.93 (d, $J = 1.6$ Hz, 1 H), 8.18 (m_s, 2 H), 8.59 (d, $J = 1.5$ Hz, 1 H), 8.68 (ddd, $J = 8.0$ Hz, 1.1 Hz, 1.1 Hz, 1 H), 8.72 (ddd, $J = 4.8$ Hz, 1.8 Hz, 0.9 Hz, 1 H) ppm;

$^{13}\text{C}\{^1\text{H}\}$ NMR (101 MHz, CDCl_3): $\delta = 55.5$, 114.2, 117.0, 117.9, 121.6, 123.9, 127.4, 128.5, 129.1, 129.1, 132.3, 137.0, 139.1, 149.2, 150.3, 156.2, 156.6, 156.9, 160.7 ppm;

ESI-TOF (m/z): 339.1503 g/mol (calc.: 339.1497 g/mol) $[\text{M} + \text{H}]^+$, 361.1318 g/mol (calc.: 361.1317 g/mol) $[\text{M} + \text{Na}]^+$.

2-(2-Pyridyl)-4-phenyl-6-(4-methylthiophenyl)pyridine (2.4h)

Pyrylium salt **2.2h** (0.150 g, 0.34 mmol) with ammonia (2.5 mL, 24% in water, 32 mmol) in ethanol (10 mL) gave the product (0.095 g, 0.27 mmol, 79%) as a colourless solid. Crystals suitable for X-ray diffraction were obtained from a hot ethanol solution.

^1H NMR (400 MHz, CDCl_3): $\delta = 3.90$ (s, 3 H, SMe), 7.35 (ddd, $J = 7.5$ Hz, 4.8 Hz, 1.2 Hz, 1 H, H₉), 7.40 (m_s, 2 H, H_{13/15}), 7.44 – 7.55 (m, 3 H, H₂₀, H_{19/21}), 7.80 – 7.84 (m, 2 H, H_{18/22}), 7.87 (ddd, $J = 8.0$ Hz, 7.4 Hz, 1.8 Hz, 1 H, H₈), 7.96 (d, $J = 1.6$ Hz, 1 H, H₂), 8.13 – 8.17 (m, 2 H, H_{12/16}), 8.62 (d, $J = 1.5$ Hz, 1 H, H₄), 8.67 (ddd, $J = 8.0$ Hz, 1.1 Hz, 1.1 Hz, 1 H, H₇), 8.72 (ddd, $J = 4.8$ Hz, 1.8 Hz, 0.9 Hz, 1 H, H₁₀) ppm;

$^{13}\text{C}\{^1\text{H}\}$ NMR (101 MHz, CDCl_3): $\delta = 15.7$ (SMe), 117.5 (C_4), 118.1 (C_2), 121.6 (C_7), 123.9 (C_9), 126.5 ($\text{C}_{13/15}$), 127.4 ($\text{C}_{18/22}$), 127.5 ($\text{C}_{12/16}$), 129.1 (C_{20}), 129.1 ($\text{C}_{19/21}$), 136.3 (C_{11}), 137.0 (C_8), 138.9 (C_{17}), 140.0 (C_{14}), 149.2 (C_{10}), 150.4 (C_3), 156.3 (C_1 or C_5 or C_6), 156.4 (C_1 or C_5 or C_6), 156.6 (C_1 or C_5 or C_6) ppm;

ESI-TOF (m/z): 355.1291 g/mol (calc.: 355.1264 g/mol) $[\text{M} + \text{H}]^+$, 377.1113 g/mol (calc.: 377.1083 g/mol) $[\text{M} + \text{Na}]^+$;

Elemental analysis calc (%) for $\text{C}_{23}\text{H}_{18}\text{N}_2\text{S}$ (354.47 g/mol): C 77.93, H 5.12, N 7.90, S 9.02; found: C 77.83, H 5.08, N 7.75, S 9.23.

Crystallographic data: $\text{C}_{23}\text{H}_{18}\text{N}_2\text{S}$, $F_w = 354.45$, $0.56 \times 0.10 \times 0.05 \text{ mm}^3$, colourless needle, monoclinic, $P2_1/c$, $a = 19.3924(2)$, $b = 5.14157(5)$, $c = 18.1289(2) \text{ \AA}$, $\beta = 99.9167(7)^\circ$, $V = 1780.58(3) \text{ \AA}^3$, $Z = 4$, $D_x = 1.322 \text{ g cm}^{-3}$, $\mu = 1.661 \text{ mm}^{-1}$. 10917 reflections were measured by using a D8 Venture, Bruker Photon CMOS Detector (CuK α radiation, $\lambda = 1.54178 \text{ \AA}$) up to a resolution of $(\sin\theta/\lambda)_{\text{max}} = 0.60 \text{ \AA}^{-1}$ at a temperature of 100 K.¹⁶⁷ 2518 reflections were unique ($R_{\text{int}} = 0.068$). The structures were solved with SHELXS-2014¹⁶⁵ by using direct methods and refined with SHELXL-2014¹⁶⁵ on F^2 for all reflections. Non-hydrogen atoms were refined by using anisotropic displacement parameters. The positions of the hydrogen atoms were calculated for idealized positions. 236 parameter were refined without restraints. $R_1 = 0.062$ for 2518 reflections with $I > 2\sigma(I)$ and $wR_2 = 0.166$ for 3146 reflections, $S = 1.026$, residual electron density was between -0.57 and 0.40 e \AA^{-3} . Geometry calculations and checks for higher symmetry were performed with the PLATON program.¹⁶⁶ A .cif data file can be found in the attachments.

P,N-Tungsten Tetracarbonyl Complexes (2.6b-h)

In an Young-NMR-tube phosphinine (**2.3b-h**, 0.1 mmol) was dissolved in THF- d_8 (0.6 mL) and tungsten hexacarbonyl (0.1 mmol) was added. The tube placed under UV irradiation until $^{31}\text{P}\{^1\text{H}\}$ NMR showed complete conversion (15 - 20 h). Quick opening of the tube to release CO pressure helped to let the reaction proceed faster. After evaporation of all volatiles the product was recrystallized from acetonitrile (**5b-d**) or THF/pentane (**5a**).

2-(2-Pyridyl)-4-(4-fluorophenyl)-6-phenylphosphinine-P,N-tungsten tetracarbonyl (2.6b)

Crystals suitable for X-ray diffraction were obtained from a hot acetonitrile solution.

^1H NMR (400 MHz, THF- d_8): $\delta = 7.28$ (m_s, 2 H, $\text{H}_{19/21}$), 7.34 – 7.39 (m, 1 H, H_9), 7.44 – 7.49 (m, 1 H, H_{14}), 7.52 – 7.57 (m, 2 H, $\text{H}_{13/15}$), 7.84 (m_s, 2 H, $\text{H}_{18/22}$), 7.96 – 8.00 (m, 2 H, $\text{H}_{12/16}$),

8.05 – 8.11 (m, 1 H, H₈), 8.47 (d, $J = 17.8$ Hz, 1 H, H₂), 8.63 (d, $J = 8.2$ Hz, 1 H, H₇), 8.83 (d, $J = 14.3$ Hz, 1 H, H₄), 9.42 (m_s, 1 H, H₁₀) ppm;

¹³C{¹H} NMR (101 MHz, THF-*d*₈): $\delta = 116.7$ (d, $^2J_{C-F} = 21.7$ Hz, C_{19/21}), 121.8 (d, $^3J_{C-P} = 11.6$ Hz, C₇), 125.7 (d, $^5J_{C-P} = 3.8$ Hz, C₉), 129.0 (d, $^3J_{C-P} = 11.2$ Hz, C_{12/16}), 129.5 (d, $^5J_{C-P} = 2.2$ Hz, C₁₄), 130.1 (C_{13/15}), 130.5 (dd, $^3J_{C-F} = 8.3$, $^5J_{C-P} = 2.6$ Hz, C_{18/22}), 132.5 (d, $^2J_{C-P} = 13.5$ Hz, C₄), 138.3 (d, $^2J_{C-P} = 10.8$ Hz, C₂), 139.1 (dd, $^4J_{C-P} = 4.6$ Hz, $^4J_{C-F} = 3.3$ Hz, C₁₇), 139.4 (C₈), 139.9 (d, $^3J_{C-P} = 21.1$ Hz, C₃), 140.5 (d, $^2J_{C-P} = 15.9$ Hz, C₁₁), 158.5 (d, $^4J_{C-P} = 4.5$ Hz, C₁₀), 160.1 (d, $^1J_{C-P} = 13.9$ Hz, C₅), 160.7 (d, $^1J_{C-P} = 17.3$ Hz, C₁), 162.0 (d, $^2J_{C-P} = 17.5$ Hz, C₆), 163.9 (dd, $^1J_{C-F} = 246.8$ Hz, $^7J_{C-P} = 1.0$ Hz), 198.9 (d, $^2J_{C-P} = 11.0$ Hz, CO_{axial}), 209.2 (d, $^2J_{C-P} = 5.0$ Hz, CO_{equatorial}), 212.0 (d, $^2J_{C-P} = 41.8$ Hz, CO_{equatorial}) ppm;

¹⁹F NMR (376 MHz, THF-*d*₈): $\delta = -155.6$ (m_s) ppm;

³¹P{¹H} NMR (162 MHz, THF-*d*₈): $\delta = 201.0$ (s, $^1J_{P-W} = 278$ Hz) ppm;

FT-IR (solid ATR): $\tilde{\nu}(\text{CO})$ 2012, 1893, 1877, 1840 cm⁻¹.

Crystallographic data: C₂₆H₁₅FNO₄PW, $F_w = 639.20$, $0.17 \times 0.12 \times 0.06$ mm³, red platelet, orthorhombic, *Pna*2₁, $a = 15.8144(16)$, $b = 19.0204(17)$, $c = 7.3213(9)$ Å, $V = 2202.2(4)$ Å³, $Z = 4$, $D_x = 1.928$ gcm⁻³, $\mu = 5.36$ mm⁻¹. 9573 reflections were measured by using a Stoe IPDS 2T diffractometer with a rotating anode (MoK α radiation, $\lambda = 0.71073$ Å) up to a resolution of $(\sin\theta/\lambda)_{\text{max}} = 0.69$ Å⁻¹ at a temperature of 210 K. The reflections were corrected for absorption and scaled on the basis of multiple measured reflections by using the X-Red program (0.48–0.74 correction range).¹⁶⁴ 2997 reflections were unique ($R_{\text{int}} = 0.098$). The structures were solved with SHELXS-97¹⁶⁵ by using direct methods and refined with SHELXL-97¹⁶⁵ on F^2 for all reflections. Non-hydrogen atoms were refined by using anisotropic displacement parameters. The positions of the hydrogen atoms were calculated for idealized positions. 308 parameters were refined with one restraint. $R_1 = 0.055$ for 2997 reflections with $I > 2\sigma(I)$ and $wR_2 = 0.127$ for 5136 reflections, $S = 0.944$, residual electron density was between -1.29 and 0.96 eÅ⁻³. Geometry calculations and checks for higher symmetry were performed with the PLATON program.¹⁶⁶ (Flack x parameter = 0.12(3)).¹⁶⁸ A .cif data file can be found in the attachments.

2-(2-Pyridyl)-4-(4-trifluoromethylphenyl)-6-phenylphosphinine-P,N-tungsten tetracarbonyl (2.6c)

Phosphinine **2.3c** (not pure, 40 mg), benzene-*d*₆ (0.6 mL) and tungsten hexacarbonyl (20 mg, 0.06 mmol) were filled into a Young-NMR-tube. After irradiation with UV light until completion of the reaction recrystallization from acetonitrile gave the product (12 mg, 0.02 mmol) as a dark red solid.

^1H NMR (400 MHz, THF- d_8): δ = 7.35 – 7.40 (m, 1 H, H₉), 7.45 – 7.50 (m, 1 H, H₁₄), 7.53 – 7.59 (m, 2 H, H_{13/15}), 7.85 (d, J = 8.2 Hz, 2 H, H_{118/22}), 7.97 – 8.05 (m, 4 H, H_{12/16, 19/21}), 8.06 – 8.12 (m, 1 H, H₈), 8.53 (dd, J = 17.7 Hz, 1.3 Hz, 1 H, H₄), 8.64 (d, J = 8.3 Hz, 1 H, H₇), 8.88 (dd, J = 14.3 Hz, 1.0 Hz, 1 H, H₂), 9.43 (m, 1 H, H₁₀) ppm;

$^{13}\text{C}\{^1\text{H}\}$ NMR (101 MHz, THF- d_8): δ = 121.7 (d, J_{C-P} = 11.5 Hz), 125.5 (q, J_{C-F} = 272.5 Hz), 125.8 (d, J_{C-P} = 3.4 Hz), 126.8 (q, J_{C-F} = 3.7 Hz), 129.0 (d, J_{C-P} = 11.1 Hz), 129.2 (d, J_{C-P} = 1.9 Hz), 129.6, 130.1, 130.5, 132.5 (d, J_{C-P} = 12.2 Hz), 138.3 (d, J_{C-P} = 10.7 Hz), 139.1 (d, J_{C-P} = 20.9 Hz), 139.5, 140.4 (d, J_{C-P} = 15.9 Hz), 146.6 (d, J_{C-P} = 3.0 Hz), 158.5 (d, J_{C-P} = 4.3 Hz), 160.1 (d, J_{C-P} = 13.8 Hz), 160.6 (d, J_{C-P} = 16.8 Hz), 161.9 (d, J_{C-P} = 17.2 Hz), 198.7 (d, J_{C-P} = 10.0 Hz), 209.0 (d, J_{C-P} = 5.0 Hz), 211.5 (d, J_{C-P} = 42.0 Hz) ppm;

^{19}F NMR (376 MHz, THF- d_8): δ = -63.1 (s) ppm;

$^{31}\text{P}\{^1\text{H}\}$ NMR (162 MHz, THF- d_8): δ = 206.3 (s, $^1J_{P-W}$ = 278 Hz) ppm;

EI-MS (170 °C, m/z): 394.0991 g/mol (calc.: 689.0181 g/mol) [M]⁺;

FT-IR (solid ATR): $\tilde{\nu}(\text{CO})$ 2014, 1920, 1857 cm^{-1} .

2-(2-Pyridyl)-4-(4-methoxyphenyl)-6-phenylphosphinine-P,N-tungsten tetracarbonyl (2.6d)

Phosphinine **2.3d** (27 mg, 0.08 mmol), THF- d_8 (0.6 mL) and tungsten hexacarbonyl (27 mg, 0.08 mmol) were filled into a Young-NMR-tube. After irradiation with UV light until completion of the reaction recrystallization by slow diffusion of diethyl ether into THF gave the product (45 mg, 0.07 mmol, 91%) as a dark red solid.

^1H NMR (500 MHz, THF- d_8): δ = 3.85 (s, 3 H, OMe), 7.08 (m_s, 2 H, H_{19/21}), 7.32 – 7.36 (m, 1 H, H₉), 7.43 – 7.48 (m, 1 H, H₁₄), 7.52 – 7.57 (m, 2 H, H_{13/15}), 7.75 (m_s, 2H, H_{18/22}), 7.96 – 7.99 (m, 2 H, H_{12/16}), 8.04 – 8.09 (m, 1 H, H₈), 8.47 (dd, J = 17.9, 1.5 Hz, 1 H, H₂), 8.61 (d, J = 8.1 Hz, 1 H, H₇), 8.82 (dd, J = 14.3, 1.5 Hz, 1 H, H₄), 9.42 (ddd, J = 5.7, 1.7, 0.8 Hz, 1 H, H₁₀) ppm;

$^{13}\text{C}\{^1\text{H}\}$ NMR (126 MHz, THF- d_8): δ = 55.7 (OMe), 115.4 (C_{19/21}), 121.8 (d, J_{C-P} = 11.5 Hz, C₇), 125.6 (d, J_{C-P} = 3.8 Hz, C₉), 129.0 (d, $^3J_{C-P}$ = 11.1 Hz, C_{12/16}), 129.4 (d, $^5J_{C-P}$ = 2.0 Hz, C₁₄), 129.6 (d, $^5J_{C-P}$ = 2.4 Hz, C_{18/22}), 130.1 (C_{13/15}), 132.3 (d, $^2J_{C-P}$ = 12.5 Hz, C₄), 134.9 (d, $^4J_{C-P}$ = 4.6 Hz, C₁₇), 138.1 (d, $^2J_{C-P}$ = 11.2 Hz, C₂), 139.4 (C₈), 140.6 (d, $^2J_{C-P}$ = 16.0 Hz, C₁₁), 141.0 (d, $^3J_{C-P}$ = 21.2 Hz, C₃), 158.4 (d, $^4J_{C-P}$ = 4.5 Hz, C₁₀), 160.0 (d, $^1J_{C-P}$ = 14.3 Hz, C₅), 160.7 (d, $^1J_{C-P}$ = 17.4 Hz, C₁), 161.1 (d, $^7J_{C-P}$ = 0.8 Hz, C₂₀), 162.1 (d, $^2J_{C-P}$ = 17.5 Hz, C₆), 199.0 (d, J_{C-P} = 11.0 Hz, CO_{axial}), 209.4 (d, J_{C-P} = 5.1 Hz, CO_{equatorial}), 212.0 (d, J_{C-P} = 41.7 Hz, CO_{equatorial}) ppm;

$^{31}\text{P}\{^1\text{H}\}$ NMR (162 MHz, THF- d_8) $\delta = 196.6$ (s, $^1J_{\text{P-W}} = 274$ Hz) ppm;

FT-IR (solid ATR): $\tilde{\nu}(\text{CO})$ 2015, 1973, 1891, 1857 cm^{-1} .

2-(2-Pyridyl)-4-(4-methylthiophenyl)-6-phenylphosphinine-P,N-tungsten tetracarbonyl (2.6e)

Phosphinine **2.3e** (280 mg, 0.75 mmol), THF- d_8 (0.6 mL) and tungsten hexacarbonyl (265 mg, 0.75 mmol) were filled into a Young-NMR-tube. After irradiation with UV light until completion of the reaction recrystallization from acetonitrile gave the product (196 mg, 0.29 mmol, 39%) as a dark red solid.

^1H NMR (400 MHz, THF- d_8): $\delta = 2.52$ (s, 3 H, SMe), 7.31 – 7.36 (m, 1 H, H₉), 7.39 – 7.49 (m, 3 H, H_{19/21}, H₁₄), 7.52 – 7.58 (m, 2 H, H_{13/15}), 7.72 – 7.77 (m, 2 H, H_{18/22}), 7.95 – 8.01 (m, 2 H, H_{12/16}), 8.02 – 8.09 (m, 1 H, H₈), 8.47 (d, $J = 17.9$ Hz, 1 H, H₂), 8.60 (d, $J = 8.2$ Hz, 1 H, H₇), 8.81 (d, $J = 14.3$ Hz, 1 H, H₄), 9.42 (d, $J = 5.6$ Hz, 1 H, H₁₀) ppm;

$^{13}\text{C}\{^1\text{H}\}$ NMR (101 MHz, THF- d_8): $\delta = 15.4$ (SMe), 121.7 (d, $^3J_{\text{C-P}} = 11.6$ Hz, C₇), 125.6 (d, $^5J_{\text{C-P}} = 3.8$ Hz, C₉), 127.6 (C_{19/21}), 128.7 (d, $^5J_{\text{C-P}} = 2.5$ Hz, C_{18/22}), 129.0 (d, $^3J_{\text{C-P}} = 11.2$ Hz, C_{12/16}), 129.5 (d, $^5J_{\text{C-P}} = 2.1$ Hz, C₁₄), 130.1 (C_{13/15}), 132.2 (d, $^2J_{\text{C-P}} = 12.3$ Hz, C₄), 138.0 (d, $^2J_{\text{C-P}} = 11.1$ Hz, C₂), 139.0 (d, $^4J_{\text{C-P}} = 4.7$ Hz, C₁₇), 139.4 (C₈), 140.4 (d, $^3J_{\text{C-P}} = 21.1$ Hz, C₃), 140.5 (C₂₀), 140.5 (d, $^2J_{\text{C-P}} = 14.8$ Hz, C₁₁), 158.4 (d, $^4J_{\text{C-P}} = 4.5$ Hz, C₁₀), 160.0 (d, $^1J_{\text{C-P}} = 14.2$ Hz, C₅), 160.6 (d, $^1J_{\text{C-P}} = 17.3$ Hz, C₁), 162.0 (d, $^2J_{\text{C-P}} = 17.4$ Hz, C₆), 198.9 (d, $^2J_{\text{C-P}} = 11.0$ Hz, CO_{axial}), 209.3 (d, $^2J_{\text{C-P}} = 5.0$ Hz, CO_{equatorial}), 212.0 (d, $^2J_{\text{C-P}} = 41.8$ Hz, CO_{equatorial}) ppm;

$^{31}\text{P}\{^1\text{H}\}$ NMR (162 MHz, THF- d_8) $\delta = 199.7$ (s, $^1J_{\text{P-W}} = 276$ Hz) ppm;

FT-IR (solid ATR): $\tilde{\nu}(\text{CO})$ 2014, 1971, 1889, 1859 cm^{-1} .

2-(2-Pyridyl)-4-phenyl-6-(4-fluorophenyl)phosphinine-P,N-tungsten tetracarbonyl (2.6f)

Phosphinine **2.3f** (21 mg, 0.06 mmol), THF- d_8 (0.6 mL) and tungsten hexacarbonyl (22 mg, 0.06 mmol) were filled into a Young-NMR-tube. After irradiation with UV light until completion of the reaction recrystallization from acetonitrile gave the product (27 mg, 0.04 mmol, 69%) as a dark red solid. Crystals suitable for X-ray diffraction were obtained from a hot tetrahydrofuran solution.

^1H NMR (700 MHz, THF- d_8): $\delta = 7.30$ (m_s, 2 H, H_{13/15}), 7.35 – 7.38 (m, 1 H, H₉), 7.42 – 7.45 (m, 1 H, H₂₀), 7.50 – 7.54 (m, 2 H, H_{19/21}), 7.78 – 7.81 (m, 2 H, H_{18/22}), 8.00 (ddd, $J = 8.9, 5.1, 1.6$ Hz, 2 H, H_{12/16}), 8.06 – 8.10 (m, 1 H, H₈), 8.47 (dd, $^3J_{\text{H-P}} = 17.7, ^4J_{\text{H-H}} = 1.4$ Hz, 1 H, H₂),

8.63 (d, $J = 8.2$ Hz, 1 H, H₇), 8.85 (dd, $J = 14.4$ Hz, $J = 1.3$ Hz, 1 H, H₄), 9.42 (ddd, $J = 5.6, 1.6, 0.7$ Hz, 1 H, H₁₀) ppm;

¹³C{¹H} NMR (176 MHz, THF-*d*₈): $\delta = 117.0$ (d, $^2J_{C-F} = 22.0$ Hz, C_{13/15}), 121.8 (d, $^3J_{C-P} = 11.6$ Hz, C₇), 125.7 (d, $^5J_{C-P} = 3.5$ Hz, C₉), 128.5 (d, $^5J_{C-P} = 2.0$ Hz, C_{18/22}), 128.9 (C₂₀), 129.9 (C_{19/21}), 131.0 (dd, $^3J_{C-F} = 8.4, ^3J_{C-P} = 10.9$ Hz, C_{12/16}), 132.6 (d, $^2J_{C-P} = 12.4$ Hz, C₄), 136.8 (dd, $^2J_{C-P} = 16.5$ Hz, $^4J_{C-F} = 3.0$ Hz, C₁₁), 138.4 (d, $^2J_{C-P} = 10.9$ Hz, C₂), 139.5 (C₈), 141.1 (d, $^3J_{C-P} = 21.2$ Hz, C₃), 142.7 (d, $^4J_{C-P} = 4.3$ Hz, C₁₇), 158.5 (d, $^4J_{C-P} = 4.4$ Hz, C₁₀), 159.4 (d, $^1J_{C-P} = 17.7$ Hz, C₁), 160.0 (d, $^1J_{C-P} = 14.5$ Hz, C₅), 162.0 (d, $^2J_{C-P} = 17.3$ Hz, C₆), 164.4 (dd, $^1J_{C-F} = 247.9$ Hz, $^5J_{C-P} = 1.9$ Hz, C₁₄), 198.8 (d, $^2J_{C-P} = 10.9$ Hz, CO_{axial}), 209.4 (d, $^2J_{C-P} = 4.9$ Hz, CO_{equatorial}), 211.8 (d, $^2J_{C-P} = 41.8$ Hz, CO_{equatorial}) ppm;

¹⁹F NMR (376 MHz, THF-*d*₈): $\delta = -114.7$ (m_s) ppm;

³¹P{¹H} NMR (162 MHz, THF-*d*₈): $\delta = 201.0$ (d, $^1J_{P-W} = 278$ Hz) ppm;

FT-IR (solid ATR): $\tilde{\nu}(\text{CO})$ 2009, 1902, 1870, 1840 cm⁻¹.

Crystallographic data: C₂₆H₁₅FNO₄PW, $F_w = 639.20$, $0.38 \times 0.04 \times 0.04$ mm³, orange needle, orthorhombic, $Pna2_1$, $a = 16.3244(17)$, $b = 18.5970(12)$, $c = 7.2964(5)$ Å, $V = 2215.1(3)$ Å³, $Z = 4$, $D_x = 1.917$ gcm⁻³, $\mu = 5.33$ mm⁻¹. 10058 reflections were measured by using a Stoe IPDS 2T diffractometer with a rotating anode (MoK_α radiation, $\lambda = 0.71073$ Å) up to a resolution of $(\sin\theta/\lambda)_{\max} = 0.69$ Å⁻¹ at a temperature of 200 K. The reflections were corrected for absorption and scaled on the basis of multiple measured reflections by using the X-Red program (0.41–0.84 correction range).¹⁶⁴ 3832 reflections were unique ($R_{\text{int}} = 0.042$). The structures were solved with SHELXS-97¹⁶⁵ by using direct methods and refined with SHELXL-97 on F^2 for all reflections. Non-hydrogen atoms were refined by using anisotropic displacement parameters. The positions of the hydrogen atoms were calculated for idealized positions. 309 parameters were refined with one restraint. $R_1 = 0.041$ for 3832 reflections with $I > 2\sigma(I)$ and $wR_2 = 0.102$ for 5235 reflections, $S = 0.949$, residual electron density was between -1.18 and 1.15 eÅ⁻³. Geometry calculations and checks for higher symmetry were performed with the PLATON program.¹⁶⁶ (Flack x parameter = $-0.01(2)$).¹⁶⁸ A .cif data file can be found in the attachments.

2-(2-Pyridyl)-4-phenyl-6-(4-methoxyphenyl)phosphinine-P,N-tungsten tetracarbonyl (2.6g)

Phosphinine **2.3g** (15 mg, 0.04 mmol), THF-*d*₈ (0.6 mL) and tungsten hexacarbonyl (15 mg, 0.04 mmol) were filled into a Young-NMR-tube. After irradiation with UV light until completion of the reaction recrystallization from acetonitrile gave the product (21 mg, 0.03 mmol, 76%) as a dark red solid. Crystals suitable for X-ray diffraction were obtained from a hot acetonitrile solution.

^1H NMR (400 MHz, THF- d_8): δ = 3.85 (s, 3 H, OMe), 7.08 – 7.13 (m, 2 H, H_{13/15}), 7.32 – 7.37 (m, 1 H, H₉), 7.40 – 7.45 (m, 1 H, H₂₀), 7.49 – 7.55 (m, 2 H, H_{19/21}), 7.77 – 7.81 (m, 2H, H_{18/22}), 7.91 – 7.96 (m, 2 H, H_{12/16}), 8.03 – 8.09 (m, 1 H, H₈), 8.44 (dd, J = 17.9, 1.2 Hz, 1 H, H₂), 8.61 (d, J = 8.5 Hz, 1 H, H₇), 8.80 (d, J = 14.3 Hz, 1 H, H₄), 9.40 – 9.44 (m, 1 H, H₁₀) ppm;

$^{13}\text{C}\{^1\text{H}\}$ NMR (101 MHz, THF- d_8): δ = 55.7 (OMe), 115.6 (C_{13/15}), 121.8 (d, $^3J_{C-P}$ = 11.6 Hz, C₇), 125.6 (d, $^5J_{C-P}$ = 3.7 Hz, C₉), 128.5 (d, $^5J_{C-P}$ = 2.5 Hz, C_{18/22}), 128.8 (C₂₀), 129.9 (C_{19/21}), 130.1 (d, $^3J_{C-P}$ = 11.3 Hz, C_{12/16}), 132.1 (d, $^2J_{C-P}$ = 12.5 Hz, C₄), 132.8 (d, $^2J_{C-P}$ = 16.1 Hz, C₁₁), 137.7 (d, $^2J_{C-P}$ = 10.6 Hz, C₂), 139.4 (C₈), 141.2 (d, $^3J_{C-P}$ = 21.0 Hz, C₃), 142.9 (d, $^4J_{C-P}$ = 4.5 Hz, C₁₇), 158.4 (d, $^4J_{C-P}$ = 4.5 Hz, C₁₀), 160.0 (d, $^1J_{C-P}$ = 14.1 Hz, C₅), 160.6 (d, $^1J_{C-P}$ = 17.0 Hz, C₁), 161.7 (d, $^5J_{C-P}$ = 2.1 Hz, C₁₄), 162.1 (d, $^2J_{C-P}$ = 17.3 Hz, C₆), 198.9 (d, $^2J_{C-P}$ = 10.9 Hz, $^1J_{C-W}$ = 126.8 Hz, CO_{axial}), 209.5 (d, $^2J_{C-P}$ = 5.0 Hz, CO_{equatorial}), 212.1 (d, $^2J_{C-P}$ = 41.7 Hz, CO_{equatorial}) ppm;

$^{31}\text{P}\{^1\text{H}\}$ NMR (162 MHz, THF- d_8) δ = 197.9 (s, $^1J_{P-W}$ = 274 Hz) ppm;

FT-IR (solid ATR): $\tilde{\nu}(\text{CO})$ 2006, 1883, 1852, 1827 (shoulder), 1810 cm^{-1} .

Crystallographic data: C₂₇H₁₈NO₅PW, Fw = 651.23, 0.46×0.27×0.07 mm³, red rhombus, monoclinic, $P2_1/n$, a = 8.2075(16), b = 18.297(4), c = 16.182(3) Å, β = 98.63(3)°, V = 2402.6(9) Å³, Z = 4, D_x = 1.800 gcm⁻³, μ = 4.91 mm⁻¹. 18474 reflections were measured by using a Stoe IPDS 2T diffractometer with a rotating anode (MoK α radiation, λ = 0.71073 Å) up to a resolution of $(\sin\theta/\lambda)_{\text{max}}$ = 0.69 Å⁻¹ at a temperature of 220 K. The reflections were corrected for absorption and scaled on the basis of multiple measured reflections by using the X-Red program (0.32–0.65 correction range).¹⁶⁴ 4729 reflections were unique (R_{int} = 0.038). The structures were solved with SHELXS-97¹⁶⁵ by using direct methods and refined with SHELXL-97 on F^2 for all reflections. Non-hydrogen atoms were refined by using anisotropic displacement parameters. The positions of the hydrogen atoms were calculated for idealized positions. 317 parameters were refined without restraints. R_1 = 0.033 for 4729 reflections with $I > 2\sigma(I)$ and wR_2 = 0.078 for 6473 reflections, S = 0.908, residual electron density was between -1.34 and 1.29 eÅ⁻³. Geometry calculations and checks for higher symmetry were performed with the PLATON program.¹⁶⁶ A .cif data file can be found in the attachments.

2-(2-Pyridyl)-4-phenyl-6-(4-methylthiophenyl)phosphinine-P,N-tungsten tetracarbonyl (2.6h)

Phosphinine **2.5h** (43 mg, 0.12 mmol), THF- d_8 (0.6 mL) and tungsten hexacarbonyl (41 mg, 0.12 mmol) were filled into a Young-NMR-tube. After irradiation with UV light until completion of the reaction recrystallization from acetonitrile gave the product (13 mg, 0.02 mmol, 17%) as a dark red solid.

^1H NMR (400 MHz, DCM- d_2): δ = 2.55 (s, 3 H, SMe), 7.24 (m_s, 1 H, H₉), 7.41 – 7.46 (m, 2 H, H_{13/15}), 7.46 – 7.9 (m, 1 H, H₂₀), 7.52 – 7.58 (m, 2 H, H_{19/21}), 7.68 – 7.73 (m, 2 H, H_{18/22}), 7.87 (m_s, 2 H, H_{16/22}), 7.97 (dddd, J = 8.3, 7.4, 1.7, 1.0 Hz, 1 H, H₈), 8.27 – 8.32 (m, 1 H, H₂), 8.37 (dd, J = 17.7, 1.3 Hz, 1 H, H₇), 8.58 (dd, J = 14.2, 1.4 Hz, 1 H, H₄), 9.38 (ddd, J = 5.7, 1.7, 0.8 Hz, 1 H, H₁₀) ppm;

$^{13}\text{C}\{^1\text{H}\}$ NMR (101 MHz, THF- d_8): δ = 15.3 (SMe), 121.8 (d, $^3J_{\text{C-P}}$ = 11.7 Hz, C₇), 125.7 (d, $^5J_{\text{C-P}}$ = 3.9 Hz, C₉), 127.5 (C_{13/15}), 128.5 (d, $^5J_{\text{C-P}}$ = 2.5 Hz, C_{18/22}), 128.9 (C₂₀), 129.2 (d, $^3J_{\text{C-P}}$ = 11.4 Hz, C_{12/16}), 129.9 (C_{19/21}), 132.5 (d, $^2J_{\text{C-P}}$ = 12.8 Hz, C₄), 136.9 (d, $^2J_{\text{C-P}}$ = 16.2 Hz, C₁₁), 137.9 (d, $^2J_{\text{C-P}}$ = 10.9 Hz, C₂), 139.4 (C₈), 141.2 (d, $^3J_{\text{C-P}}$ = 20.8 Hz, C₃), 141.4 (d, $^5J_{\text{C-P}}$ = 2.4 Hz, C₁₄), 142.8 (d, $^4J_{\text{C-P}}$ = 4.5 Hz, C₁₇), 158.4 (d, $^4J_{\text{C-P}}$ = 3.4 Hz, C₁₀), 160.1 (d, $^1J_{\text{C-P}}$ = 17.4 Hz, C₁ or C₅), 160.1 (d, $^1J_{\text{C-P}}$ = 14.1 Hz, C₁ or C₅), 162.0 (d, $^2J_{\text{C-P}}$ = 17.7 Hz, C₆), 198.9 (d, $J_{\text{C-P}}$ = 11.1 Hz, CO_{axial}), 209.5 (d, $J_{\text{C-P}}$ = 5.5 Hz, CO_{equatorial}), 212.0 (d, $J_{\text{C-P}}$ = 41.8 Hz, CO_{equatorial}) ppm;

$^{31}\text{P}\{^1\text{H}\}$ NMR (162 MHz, THF- d_8) δ = 199.2 (s, $^1J_{\text{P-W}}$ = 278 Hz) ppm;

FT-IR (solid ATR): $\tilde{\nu}(\text{CO})$ 2016, 1975, 1893, 1859 cm^{-1} .

N,N-Tungsten Tetracarbonyl Complexes (2.7b-h)

2-(2-Pyridyl)-4-(4-fluorophenyl)-6-phenylpyridine-N,N-tungsten tetracarbonyl (2.7b)

Bipyridine **2.4b** (40 mg, 0.12 mmol), MeCN- d_3 (0.6 mL) and tungsten hexacarbonyl (38 mg, 0.11 mmol) were filled into a Young-NMR-tube. After irradiation with UV light until completion of the reaction the product (47 mg, 0.08 mmol, 70%) was separated from the reaction mixture as dark red crystals. Crystals suitable for X-ray diffraction were obtained from the reaction mixture.

^1H NMR (400 MHz, DCM- d_2): δ = 7.25 – 7.32 (m, 2 H, H_{19/21}), 7.42 – 7.47 (m, 1 H, H₉), 7.54 – 7.64 (m, 5 H, H₁₄, H_{13/15}, H_{12/16}), 7.73 – 7.76 (m, 1 H, H₂), 7.79 – 7.84 (m, 2 H, H_{18/22}), 8.00 – 8.07 (m, 1 H, H₈), 8.28 – 8.32 (m, 1 H, H₇), 8.34 (d, J = 1.9 Hz, 1 H, H₄), 9.29 – 9.33 (m, 1 H, H₁₀) ppm;

$^{13}\text{C}\{^1\text{H}\}$ NMR (101 MHz, DCM- d_2): δ = 117.1 (d, $^2J_{\text{C-F}}$ = 22.0 Hz, C_{19/21}), 119.3 (d, $^6J_{\text{C-F}}$ = 0.6 Hz, C₄), 123.8 (C₇), 125.1 (d, $^6J_{\text{C-F}}$ = 0.7 Hz, C₂), 126.4 (C₉), 128.9 (C_{12/16} or C_{13/15}), 129.0 (C_{12/16} or C_{13/15}), 129.8 (d, $^3J_{\text{C-F}}$ = 8.7 Hz, C_{18/22}), 130.1 (C₁₄), 133.0 (d, $^4J_{\text{C-F}}$ = 3.3 Hz, C₁₇), 137.8 (C₈), 143.1 (C₁₁), 149.0 (C₃), 153.6 (C₁₀), 157.5 (C₅ or C₆), 157.5 (C₅ or C₆), 163.5 (C₁), 163.7 (d, $^1J_{\text{C-F}}$ = 250.8 Hz, C₂₀), 202.5 ($^1J_{\text{C-W}}$ = 133.2 Hz, CO_{axial}), 210.9 ($^1J_{\text{C-W}}$ = 163.6 Hz, CO_{equatorial}), 217.4 ($^1J_{\text{C-W}}$ = 172.8 Hz, CO_{equatorial}) ppm;

^{19}F NMR (376 MHz, $\text{DCM-}d_2$): $\delta = -110.8$ (tt, $J_{F-H} = 8.6, 5.2$ Hz) ppm;

FT-IR (solid ATR): $\tilde{\nu}(\text{CO})$ 2000, 1872, 1853, 1802, 1783 cm^{-1} .

Crystallographic data: $2 \times (\text{C}_{26}\text{H}_{15}\text{FN}_2\text{O}_4\text{W})$, $\text{C}_2\text{H}_3\text{N}$, $F_w = 1285.53$, $0.21 \times 0.18 \times 0.16$ mm^3 , dark prism, tetragonal, $P4_12_12$, $a = 11.888(1)$, $b = 11.888(1)$, $c = 32.757(5)$ \AA , $V = 4629.4(11)$ \AA^3 , $Z = 4$, $D_x = 1.844$ gcm^{-3} , $\mu = 5.04$ mm^{-1} . 76012 reflections were measured by using a Bruker-AXS smart CCD area detector diffractometer (MoK α radiation, $\lambda = 0.71073$ \AA)¹⁶⁷ up to a resolution of $(\sin\theta/\lambda)_{\text{max}} = 0.72$ \AA^{-1} at a temperature of 100 K. The reflections were corrected for absorption and scaled on the basis of multiple measured reflections by using the SADABS program¹⁶⁷ (0.65–0.75 correction range). 4729 reflections were unique ($R_{\text{int}} = 0.052$). The structures were solved with SHELXS-97¹⁶⁵ by using direct methods and refined with SHELXL-97¹⁶⁵ on F^2 for all reflections. Non-hydrogen atoms were refined by using anisotropic displacement parameters. The positions of the hydrogen atoms were calculated for idealized positions. 330 parameters were refined without restraints. $R_1 = 0.042$ for 4534 reflections with $I > 2\sigma(I)$ and $wR_2 = 0.086$ for 7093 reflections, $S = 1.138$, residual electron density was between -2.13 and 1.40 $\text{e}\text{\AA}^{-3}$. Geometry calculations and checks for higher symmetry were performed with the PLATON program.¹⁶⁶ (Flack x parameter = $0.007(17)$).¹⁶⁸ A .cif data file can be found in the attachments.

2-(2-Pyridyl)-4-(4-trifluoromethylphenyl)-6-phenylpyridine-N,N-tungsten tetracarbonyl (2.7c)

Bipyridine **2.4c** (16 mg, 0.04 mmol), $\text{MeCN-}d_3$ (0.6 mL) and tungsten hexacarbonyl (15 mg, 0.04 mmol) were filled into a Young-NMR-tube. After irradiation with UV light until completion of the reaction recrystallization by slow diffusion of diethyl ether into THF gave the product (25 mg, 0.04 mmol, 87%) as dark red crystals. Crystals suitable for X-ray diffraction were obtained by slow diffusion of diethyl ether into a dichloromethane solution.

^1H NMR (700 MHz, $\text{DCM-}d_2$): $\delta = 7.46$ (ddd, $J = 7.5, 5.5, 1.2$ Hz, 1 H, H_9), 7.55 – 7.60 (m, 3 H, $\text{H}_{13/15}$, H_{14}), 7.60 – 7.63 (m, 2 H, $\text{H}_{12/16}$), 7.79 (d, $J = 1.9$ Hz, 1 H, H_2), 7.85 (d, $J = 8.2$ Hz, 2 H, $\text{H}_{19/21}$), 7.93 (d, $J = 8.1$ Hz, 2 H, $\text{H}_{18/22}$), 8.04 (ddd, $J = 8.2, 7.6, 1.6$ Hz, 1 H, H_8), 8.31 (d, $J = 8.3$ Hz, 1 H, H_7), 8.37 (d, $J = 1.8$ Hz, 1 H, H_4), 9.33 (ddd, $J = 5.5, 1.5, 0.8$ Hz, 1 H, H_{10}) ppm;

^{19}F NMR (376 MHz, $\text{DCM-}d_2$): $\delta = -63.0$ (s) ppm;

$^{13}\text{C}\{^1\text{H}\}$ NMR (176 MHz, $\text{DCM-}d_2$): $\delta = 119.6$ (C_4), 123.9 (C_7), 124.5 (q, $^1J_{C-F} = 271.3$ Hz, CF_3), 125.5 (C_2), 126.6 (C_9), 127.0 (q, $^3J_{C-F} = 3.8$ Hz, $\text{C}_{19/21}$), 128.3 ($\text{C}_{18/22}$), 128.9 ($\text{C}_{12/16}$), 129.1 ($\text{C}_{13/15}$), 130.2 (C_{14}), 132.4 (q, $^2J_{C-F} = 32.7$ Hz, C_{20}), 137.8 (C_8), 140.6 (C_{17}), 143.0 (C_{11}), 148.5 (C_3), 153.7 (C_{10}), 157.3 (C_5 or C_6), 157.8 (C_5 or C_6), 165.2 (C_1), 202.4 ($^1J_{C-W} = 133.3$ Hz, CO_{axial}), 210.8 ($^1J_{C-W} = 163.7$ Hz, $\text{CO}_{\text{equatorial}}$), 217.4 ($^1J_{C-W} = 172.0$ Hz, $\text{CO}_{\text{equatorial}}$) ppm;

FT-IR (solid ATR): $\tilde{\nu}(\text{CO})$ 1997, 1887, 1877, 1867, 1848, 1805 cm^{-1} .

Crystallographic data: $\text{C}_{27}\text{H}_{15}\text{F}_3\text{N}_2\text{O}_4\text{W}$, $F_w = 672.25$, $0.42 \times 0.20 \times 0.07 \text{ mm}^3$, colourless block, monoclinic, $P2_1/c$, $a = 14.5198(7)$, $b = 17.2400(9)$, $c = 19.1014(10) \text{ \AA}$, $\beta = 99.3220(14)^\circ$, $V = 4718.3(4) \text{ \AA}^3$, $Z = 8$, $D_x = 1.893 \text{ g cm}^{-3}$; $\mu = 4.96 \text{ mm}^{-1}$. 78726 reflections were measured by using a D8 Venture, Bruker Photon CMOS Detector (MoK α radiation, $\lambda = 0.71073 \text{ \AA}$) up to a resolution of $(\sin\theta/\lambda)_{\text{max}} = 0.72 \text{ \AA}^{-1}$ at a temperature of 100 K.¹⁶⁷ The reflections were corrected for absorption and scaled on the basis of multiple measured reflections by using the SADABS program¹⁶⁷ (0.34–0.75 correction range). 13202 reflections were unique ($R_{\text{int}} = 0.037$). The structures were solved with SHELXS-2013¹⁶⁵ by using direct methods and refined with SHELXL-2013¹⁶⁵ on F^2 for all reflections. Non-hydrogen atoms were refined by using anisotropic displacement parameters. The positions of the hydrogen atoms were calculated for idealized positions. 667 parameter were refined without restraints. $R_1 = 0.019$ for 13202 reflections with $I > 2\sigma(I)$ and $wR_2 = 0.044$ for 14451 reflections, $S = 1.049$, residual electron density was between -1.49 and 0.84 e \AA^{-3} . Geometry calculations and checks for higher symmetry were performed with the PLATON program.¹⁶⁶ A .cif data file can be found in the attachments.

2-(2-Pyridyl)-4-(4-methoxyphenyl)-6-phenylpyridine-N,N-tungsten tetracarbonyl (2.7d)

Bipyridine **2.4d** (15 mg, 0.04 mmol), MeCN- d_3 (0.6 mL) and tungsten hexacarbonyl (16 mg, 0.05 mmol) were filled into a Young-NMR-tube. After irradiation with UV light until completion of the reaction recrystallization by slow evaporation of THF gave the product (17 mg, 0.03 mmol, 60%) as dark red crystals. Crystals suitable for X-ray diffraction were obtained from slow evaporation of a tetrahydrofuran solution.

^1H NMR (400 MHz, THF- d_8): $\delta = 3.87$ (s, 3 H, OMe), 7.10 (m_s, 2 H, H_{19/21}), 7.45 – 7.54 (m, 4 H, H₁₄, H_{13/15}, H₉), 7.57 – 7.62 (m, 2 H, H_{12/16}), 7.90 (m_s, 1 H, H₂), 7.98 (m_s, 2H, H_{18/22}), 8.09 (ddd, $J = 8.2, 7.5, 1.7 \text{ Hz}$, 1 H, H₈), 8.64 – 8.68 (m, 1 H, H₇), 8.70 (d, $J = 1.9 \text{ Hz}$, 1 H, H₄), 9.32 (ddd, $J = 5.5, 1.6, 0.8 \text{ Hz}$, 1 H, H₁₀) ppm;

$^{13}\text{C}\{^1\text{H}\}$ NMR (101 MHz, THF- d_8): $\delta = 55.7$ (OMe), 115.6 (C_{19/21}), 119.2 (C₄), 124.4 (C₂), 124.7 (C₇), 126.7 (C₉), 129.1 (C₁₇), 129.2 (C_{12/16} or C_{13/15}), 129.3 (C_{12/16} or C_{13/15}), 129.6 (C_{18/22}), 130.2 (C₁₄), 138.1 (C₈), 143.9 (C₁₁), 149.8 (C₃), 153.8 (C₁₀), 158.1 (C₅ or C₆), 158.5 (C₅ or C₆), 162.9 (C₂₀), 165.2 (C₁), 203.1 ($^1J_{\text{C-W}} = 133.1 \text{ Hz}$, CO_{axial}), 210.4 ($^1J_{\text{C-W}} = 162.4 \text{ Hz}$, CO_{equatorial}), 217.0 (CO_{equatorial}) ppm;

FT-IR (solid ATR): $\tilde{\nu}(\text{CO})$ 2015, 1971, 1891, 1857 cm^{-1} .

Crystallographic data: $\text{C}_{27}\text{H}_{18}\text{N}_2\text{O}_5\text{W}$, $F_w = 634.27$, $0.37 \times 0.22 \times 0.14 \text{ mm}^3$, red block, monoclinic, $P2_1/n$, $a = 8.1178(16)$, $b = 16.843(3)$, $c = 16.736(3) \text{ \AA}$, $\beta = 90.90(3)^\circ$, $V = 2288.0(7) \text{ \AA}^3$, $Z = 4$, $D_x = 1.841 \text{ g cm}^{-3}$, $\mu = 5.09 \text{ mm}^{-1}$. 11284 reflections were measured by

using a Stoe IPDS 2T diffractometer with a rotating anode (MoK α radiation, $\lambda = 0.71073 \text{ \AA}$) up to a resolution of $(\sin\theta/\lambda)_{\max} = 0.60 \text{ \AA}^{-1}$ at a temperature of 220 K. The reflections were corrected for absorption and scaled on the basis of multiple measured reflections by using the X-Red program (0.31–0.53 correction range).¹⁶⁴ 3231 reflections were unique ($R_{\text{int}} = 0.043$). The structures were solved with SHELXS-97¹⁶⁵ by using direct methods and refined with SHELXL-97¹⁶⁵ on F^2 for all reflections. Non-hydrogen atoms were refined by using anisotropic displacement parameters. The positions of the hydrogen atoms were calculated for idealized positions. 317 parameters were refined without restraints. $R_1 = 0.044$ for 3231 reflections with $I > 2\sigma(I)$ and $wR_2 = 0.104$ for 4005 reflections, $S = 1.175$, residual electron density was between -1.61 and 2.82 e\AA^{-3} . Geometry calculations and checks for higher symmetry were performed with the PLATON program.¹⁶⁶ A .cif data file can be found in the attachments.

2-(2-Pyridyl)-4-(4-methylthiophenyl)-6-phenylpyridine-N,N-tungsten tetracarbonyl (2.7e)

Bipyridine **2.4e** (20 mg, 0.06 mmol), THF- d_8 (0.6 mL) and tungsten hexacarbonyl (20 mg, 0.06 mmol) were filled into a Young-NMR-tube. After irradiation with UV light until completion of the reaction recrystallization from acetonitrile gave the product (8 mg, 0.01 mmol, 22%) as dark red crystals. Crystals suitable for X-ray diffraction were obtained from a acetonitrile solution.

^1H NMR (400 MHz, DCM- d_2): $\delta = 2.56$ (s, 3 H, SMe), 7.39 – 7.46 (m, 3 H, H_{19/21}, H₉), 7.54 – 7.62 (m, 5 H, H_{12/16}, H_{13/15}, H₁₄), 7.72 – 7.77 (m, 3 H, H_{18/22}, H₂), 8.02 (ddd, $J = 8.1, 7.5, 1.6$ Hz, 1 H, H₈), 8.30 (m_s, 1 H, H₇), 8.36 (d, $J = 1.8$ Hz, 1 H, H₄), 9.30 (ddd, $J = 5.6, 1.6, 0.8$ Hz, 1 H, H₁₀) ppm;

$^{13}\text{C}\{^1\text{H}\}$ NMR (176 MHz, THF- d_8): $\delta = 15.5$ (SMe), 118.9 (C₄), 123.8 (C₇), 124.7 (C₂), 126.4 (C₉), 127.0 (C_{19/21}), 127.9 (C_{18/22}), 128.9 (C_{13/15}), 129.0 (C_{12/16}), 130.0 (C₁₄), 132.7 (C₁₇), 137.8 (C₈), 143.2 (C₂₀ or C₁₁), 143.2 (C₁₁ or C₂₀), 149.3 (C₃), 153.6 (C₁₀), 157.5 (C₅ or C₆), 157.6 (C₅ or C₆), 164.9 (C₁), 202.5 (d, $J_{\text{C-W}} = 132.9$ Hz, CO_{axial}), 211.0 (CO_{equatorial}), 217.4 (CO_{equatorial}) ppm;

FT-IR (solid ATR): $\tilde{\nu}(\text{CO})$ 1999, 1934, 1865, 1823 cm^{-1} .

Crystallographic data: C₂₇H₁₈N₂O₄SW, $F_w = 650.34$, $0.30 \times 0.25 \times 0.20 \text{ mm}^3$, red cube, monoclinic, $P2_1/n$, $a = 7.8635(6)$, $b = 16.7687(9)$, $c = 18.1335(12) \text{ \AA}$, $\beta = 98.182(6)^\circ$, $V = 2366.8(3) \text{ \AA}^3$, $Z = 4$, $D_x = 1.825 \text{ gcm}^{-3}$, $\mu = 5.01 \text{ mm}^{-1}$. 18073 reflections were measured by using a Stoe IPDS 2T diffractometer with a rotating anode (MoK α radiation, $\lambda = 0.71073 \text{ \AA}$) up to a resolution of $(\sin\theta/\lambda)_{\max} = 0.69 \text{ \AA}^{-1}$ at a temperature of 200 K. The reflections were corrected for absorption and scaled on the basis of multiple measured reflections by using the X-Red program (0.35–0.45 correction range).¹⁶⁴ 4616 reflections were unique ($R_{\text{int}} =$

0.050). The structures were solved with SHELXS-97¹⁶⁵ by using direct methods and refined with SHELXL-97¹⁶⁵ on F^2 for all reflections. Non-hydrogen atoms were refined by using anisotropic displacement parameters. The positions of the hydrogen atoms were calculated for idealized positions. 318 parameters were refined without restraints. $R_1 = 0.034$ for 4616 reflections with $I > 2\sigma(I)$ and $wR_2 = 0.078$ for 6352 reflections, $S = 0.944$, residual electron density was between -1.10 and $1.37 \text{ e}\text{\AA}^{-3}$. Geometry calculations and checks for higher symmetry were performed with the PLATON program.¹⁶⁶ A .cif data file can be found in the attachments.

2-(2-Pyridyl)-4-phenyl-6-(4-fluorophenyl)pyridine-N,N-tungsten tetracarbonyl (2.7f)

Bipyridine **2.4f** (41 mg, 0.13 mmol), THF- d_8 (0.6 mL) and tungsten hexacarbonyl (46 mg, 0.13 mmol) were filled into a Young-NMR-tube. After irradiation with UV light until completion of the reaction recrystallization by slow evaporation of THF gave the product (28 mg, 0.05 mmol, 36%) as dark red crystals. Crystals suitable for X-ray diffraction were obtained from slow evaporation of tetrahydrofuran.

^1H NMR (400 MHz, DCM- d_2): $\delta = 7.26$ (m, 2 H, H_{13/15}), 7.45 (ddd, $J = 7.5, 5.5, 1.2$ Hz, 1 H, H₉), 7.55 – 7.63 (m, 5 H, H_{19/21}, H₂₀, H_{13/15}), 7.76 – 7.84 (m, 3 H, H₂, H_{18/22}), 8.03 (ddd, $J = 7.9, 7.9, 1.7$ Hz, 1 H, H₈), 8.31 (d, $J = 8.2$ Hz, 1 H, H₇), 8.39 (d, $J = 1.9$ Hz, 1 H, H₄), 9.29 – 9.33 (m, 1 H, H₁₀) ppm;

$^{13}\text{C}\{^1\text{H}\}$ NMR (101 MHz, DCM- d_2): $\delta = 116.0$ (d, $^2J_{\text{C-F}} = 22.1$ Hz, C_{13/15}), 119.7 (C₄), 123.8 (C₇), 125.2 (C₂), 126.5 (C₉), 127.7 (C_{18/22}), 130.1 (C_{19/21}), 130.9 (d, $^3J_{\text{C-F}} = 8.7$ Hz, C_{12/16}), 131.0 (C₂₀), 136.7 (C₁₇), 137.9 (C₈), 139.5 (d, $^4J_{\text{C-F}} = 3.4$ Hz, C₁₁), 150.2 (C₃), 153.6 (C₁₀), 157.5 (C₅), 157.5 (C₆), 163.8 (C₁), 164.2 (d, $^1J_{\text{C-F}} = 248.2$ Hz, C₁₄), 202.4 ($^1J_{\text{C-W}} = 133.1$ Hz, CO_{axial}), 211.1 (CO_{equatorial}), 217.3 (CO_{equatorial}) ppm;

^{19}F NMR (376 MHz, DCM- d_2): $\delta = -112.5$ (tt, $J = 8.7, 5.4$ Hz) ppm;

FT-IR (solid ATR): $\tilde{\nu}(\text{CO})$ 2002, 1882, 1851, 1819 cm^{-1} .

Crystallographic data: C₂₆H₁₅FN₂O₄W, $F_w = 622.24$, $0.55 \times 0.15 \times 0.04 \text{ mm}^3$, red platelet, triclinic, $P\bar{1}$, $a = 7.611(2)$, $b = 13.016(4)$, $c = 13.175(4) \text{ \AA}$, $\alpha = 79.773(6)^\circ$, $\beta = 73.331(6)$, $\gamma = 83.135(6)^\circ$, $V = 1227.2(6) \text{ \AA}^3$, $Z = 2$, $D_x = 1.684 \text{ gcm}^{-3}$, $\mu = 4.75 \text{ mm}^{-1}$. 15071 reflections were measured by using a Bruker-AXS smart CCD area detector diffractometer (MoK α radiation, $\lambda = 0.71073 \text{ \AA}$)¹⁶⁷ up to a resolution of $(\sin\theta/\lambda)_{\text{max}} = 0.72 \text{ \AA}^{-1}$ at a temperature of 100 K. The reflections were corrected for absorption and scaled on the basis of multiple measured reflections by using the SADABS program¹⁶⁷ (0.49–0.75 correction range). 6419 reflections were unique ($R_{\text{int}} = 0.018$). The structures were solved with SHELXS-2013¹⁶⁵ by using direct methods and refined with SHELXL-2013 on F^2 for all reflections. Non-hydrogen atoms were refined by using anisotropic displacement parameters. The positions of the hydrogen atoms

were calculated for idealized positions. 307 parameter were refined without restraints. $R_1 = 0.018$ for 6419 reflections with $I > 2\sigma(I)$ and $wR_2 = 0.046$ for 6890 reflections, $S = 1.062$, residual electron density was between -0.77 and $1.29 \text{ e}\text{\AA}^{-3}$. Geometry calculations and checks for higher symmetry were performed with the PLATON program.¹⁶⁶ A .cif data file can be found in the attachments.

SQUEEZE RESULTS (APPEND TO CIF)¹⁶⁹

Note: Data are Listed for all Voids in the P1 Unit Cell i.e. Centre of Gravity, Solvent Accessible Volume, Recovered number of Electrons in the Void and Details about the Squeezed Material.

loop_

```
_platon_squeeze_void_nr
_platon_squeeze_void_average_x
_platon_squeeze_void_average_y
_platon_squeeze_void_average_z
_platon_squeeze_void_volume
_platon_squeeze_void_count_electrons
_platon_squeeze_void_content
  1    -0.039      0.000      0.000      184      37 ''
_platon_squeeze_details
```

The general procedure (based on a preliminary implementation of the technique) has been described in more detail in literature.¹⁷⁰

2-(2-Pyridyl)-4-phenyl-6-(4-methoxyphenyl)pyridine-N,N-tungsten tetracarbonyl (2.7g)

Bipyridine **2.4g** (20 mg, 0.06 mmol), THF- d_8 (0.6 mL) and tungsten hexacarbonyl (24 mg, 0.07 mmol) were filled into a Young-NMR-tube. After irradiation with UV light until completion of the reaction recrystallization by slow diffusion of diethyl ether into THF gave the product (15 mg, 0.02 mmol, 40%) as dark red crystals. Crystals suitable for X-ray diffraction were obtained by slow diffusion of diethyl ether into a dichloromethane solution.

^1H NMR (400 MHz, DCM- d_2): $\delta = 3.90$ (s, 3 H, OMe), 7.08 (m_s, 2 H, H_{13/15}), 7.43 (ddd, $J = 7.6, 5.5, 1.3$ Hz, 1 H, H₉), 7.52 – 7.61 (m, 5 H, H_{13/15}, H_{19/21}, H₂₀), 7.78 – 7.83 (m, 3 H, H₂, H_{18/22}), 8.02 (ddd, $J = 8.3, 7.5, 1.6$ Hz, 1 H, H₈), 8.26 – 8.30 (m, 1 H, H₇), 8.35 (d, $J = 1.9$ Hz, 1 H, H₄), 9.31 (ddd, $J = 5.5, 1.6, 0.8$ Hz, 1 H, H₁₀) ppm; $^{13}\text{C}\{^1\text{H}\}$ NMR (101 MHz, DCM- d_2): $\delta = 56.1$ (OMe), 114.4 (C_{13/15}), 119.3 (C₄), 123.8 (C₇), 125.3 (C₂), 126.3 (C₉), 127.7 (C_{18/22}), 130.1 (C_{12/16} or C_{19/21}), 130.3 (C_{19/21} or C_{12/16}), 130.8 (C₂₀), 136.0 (C₁₁), 136.9 (C₁₇), 137.7 (C₈), 150.0 (C₃), 153.6 (C₁₀), 157.4 (C₅ or C₆), 157.8 (C₅ or C₆), 161.5 (C₁₄), 164.8 (C₁), 202.7

($^1J_{C-W}$ = 133.2 Hz, CO_{axial}), 211.1 (CO_{equatorial}), 217.4 (CO_{equatorial}) ppm; FT-IR (solid ATR): $\tilde{\nu}(\text{CO})$ 1989, 1867, 1853, 1817 cm⁻¹.

Crystallographic data: C₂₇H₁₈N₂O₅W, F_w = 634.27, 0.42 0.29×0.05 mm³, red plate, monoclinic, $P2_1/c$, a = 8.3701(5), b = 16.0053(7), c = 17.5299(11) Å, β = 92.967(5)°, V = 2345.3(2) Å³, Z = 4, D_x = 1.796 gcm⁻³, μ = 4.97 mm⁻¹. 22039 reflections were measured by using a Stoe IPDS 2T diffractometer with a rotating anode (MoK α radiation, λ = 0.71073 Å) up to a resolution of $(\sin\theta/\lambda)_{\text{max}}$ = 0.69 Å⁻¹ at a temperature of 200 K. The reflections were corrected for absorption and scaled on the basis of multiple measured reflections by using the X-Red program (0.17–0.59 correction range).¹⁶⁴ 4837 reflections were unique (R_{int} = 0.044). The structures were solved with SHELXS-97¹⁶⁵ by using direct methods and refined with SHELXL-97 on F^2 for all reflections. Non-hydrogen atoms were refined by using anisotropic displacement parameters. The positions of the hydrogen atoms were calculated for idealized positions. 318 parameters were refined without restraints. R_1 = 0.026 for 4837 reflections with $I > 2\sigma(I)$ and wR_2 = 0.063 for 6186 reflections, S = 0.934, residual electron density was between -0.95 and 0.82 eÅ⁻³. Geometry calculations and checks for higher symmetry were performed with the PLATON program.¹⁶⁶ A .cif data file can be found in the attachments.

2-(2-Pyridyl)-4-phenyl-6-(4-methylthiophenyl)pyridine-N,N-tungsten tetracarbonyl (2.7h)

Bipyridine **2.4h** (20 mg, 0.06 mmol), THF-*d*8 (0.6 mL) and tungsten hexacarbonyl (20 mg, 0.06 mmol) were filled into a Young-NMR-tube. After irradiation with UV light until completion of the reaction recrystallization by slow diffusion of diethyl ether into THF gave the product (3 mg, 0.005 mmol, 8%) as dark red crystals. Crystals suitable for X-ray diffraction were obtained by slow diffusion of diethyl ether into a dichloromethane solution.

^1H NMR (700 MHz, DCM-*d*₂): δ = 2.57 (s, 3 H, SMe), 7.42 – 7.45 (m, 3 H, H₉, H_{13/15}), 7.54 (m_s, 2 H, H_{12/16}), 7.55 – 7.60 (m, 3 H, H₂₀, H_{19/21}), 7.78 (d, J = 1.9 Hz, 1 H, H₄), 7.79 – 7.82 (m, 2 H, H_{18/22}), 8.02 (ddd, J = 8.2, 7.6, 1.6 Hz, 1 H, H₈), 8.29 (d, J = 8.2 Hz, 1 H, H₇), 8.37 (d, J = 1.8 Hz, 1 H, H₂), 8.31 (ddd, J = 5.5, 1.5, 0.8 Hz, 1 H, H₁₀) ppm;

$^{13}\text{C}\{^1\text{H}\}$ NMR (176 MHz, DCM-*d*₂): δ = 16.2 (SMe), 119.5 (C₂), 123.8 (C₇), 125.2 (C₄), 126.4 (C₉), 126.7 (C_{12/16}), 127.7 (C_{18/22}), 129.2 (C_{13/15}), 130.1 (C_{19/21}), 130.9 (C₂₀), 136.9 (C₁₇), 137.8 (C₈), 139.8 (C₁₁), 141.4 (C₁₄), 150.1 (C₃), 153.6 (C₁₀), 157.5 (C₆), 157.6 (C₁), 164.4 (C₅), 202.5 (d, J_{C-W} = 133.3 Hz, CO_{axial}), 211.1 (d, J_{C-W} = 164.0 Hz, CO_{equatorial}), 217.3 ($^1J_{C-W}$ = 172.3 Hz, CO_{equatorial}) ppm;

FT-IR (solid ATR): $\tilde{\nu}(\text{CO})$ 1991, 1873, 1850, 1816 cm⁻¹.

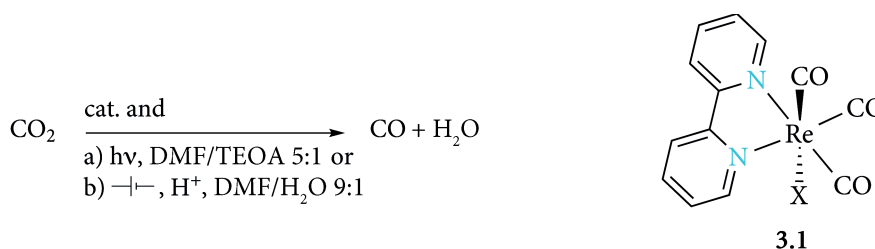
Crystallographic data: $C_{27}H_{18}FN_2O_4SW$, $F_w = 650.34$, $0.14 \times 0.11 \times 0.09$ mm³, red block, monoclinic, $P2_1/c$, $a = 8.4430(17)$, $b = 16.193(3)$, $c = 17.514(4)$ Å, $\beta = 92.85(3)^\circ$, $V = 2391.5(9)$ Å³, $Z = 4$, $D_x = 1.806$ gcm⁻³, $\mu = 4.96$ mm⁻¹. 17632 reflections were measured by using a Stoe IPDS 2T diffractometer with a rotating anode (MoK α radiation, $\lambda = 0.71073$ Å) up to a resolution of $(\sin\theta/\lambda)_{\max} = 0.69$ Å⁻¹ at a temperature of 220 K. The reflections were corrected for absorption and scaled on the basis of multiple measured reflections by using the X-Red program (0.58–0.77 correction range).¹⁶⁴ 2551 reflections were unique ($R_{\text{int}} = 0.090$). The structures were solved with SHELXS-97¹⁶⁵ by using direct methods and refined with SHELXL-97¹⁶⁵ on F^2 for all reflections. Non-hydrogen atoms were refined by using anisotropic displacement parameters. The positions of the hydrogen atoms were calculated for idealized positions. 308 parameters were refined without restraints. $R_1 = 0.041$ for 2551 reflections with $I > 2\sigma(I)$ and $wR_2 = 0.081$ for 6431 reflections, $S = 0.730$, residual electron density was between -3.67 and 1.22 eÅ⁻³. Geometry calculations and checks for higher symmetry were performed with the PLATON program.¹⁶⁶ A .cif data file can be found in the attachments.

**3 Pyridylphosphinine- and Bipyridine-
Based Rhenium(I) Complexes –
Synthesis, Characterisation and Reactivity**

3.1 Introduction

The vastly increasing energy demand and heavy reliance on fossil fuels as energy source of our society over the last three centuries gave rise to number of environmental and societal problems. Seen worldwide, combustion of hydrocarbons into carbon dioxide and water is still the main source of energy and will even gain further importance in the near future. Moreover, chemical industry is in large parts build on petroleum as raw material. However, nowadays the carbon cycle is not a closed one. Only about half of the yearly carbon dioxide emissions are taken up and returned into the cycle by ecosystems. Even though carbon dioxide consequently will be one of the most abundant carbon sources in the future and contrary to nature where carbon dioxide fixation through photosynthesis is the basic reaction for the production of organic matter, there are currently very few economically sensible processes to use carbon dioxide in large scale chemical synthesis due to its inertness. At the moment, carbon dioxide just accumulates with increasing rate in the atmosphere as well as in the oceans and is viewed as one of the main causes of severe environmental problems such as ocean acidification and anthropogenic global warming.^{106,171-174} Therefore, it is no wonder, research interest in methods to make carbon dioxide usable as C₁ carbon source for industrial products and fine chemicals is still unbroken after several decades of intense efforts in various fields such as electrochemistry, homogeneous and heterogeneous catalysis or polymer science.¹⁷⁴⁻¹⁸⁰

One major development was the discovery of the photo- or electrocatalytic reduction of CO₂ with bipyridine-based rhenium(I) carbonyl complexes as catalysts by Lehn *et al.* in 1983 (Scheme 3-1).^{74,181,182} [(bipy)Re(CO)₃X]-type catalyst are able to reduce CO₂ with very high selectivity towards CO with only water as a byproduct.



Scheme 3-1: Photo- (a) and electrocatalytic reduction of CO₂ with catalysts of the type [(bipy)Re(CO)₃X] (X = Cl, Br) (3.1).

With this interesting application in mind, the synthesis and study of [(L)Re(CO)₃X]-type compounds seems worthwhile. While the catalytic activity of bipyridine-rhenium(I) complexes has been known for over 30 years now and much research has been done on them, there are still many directions to explore. So far a focus has been put on the introduction of substituents into the backbone of the bipyridine ligand to adjust the properties for better performance in catalysis.¹⁸³⁻¹⁸⁵ The metal centre has been looked at only recently with the intent of exchanging the expensive and rare rhenium to more cost-effective metals such as manganese or tungsten and some research also went into the variation of ligand X.^{74,186-190} However, the effects of employing a P,N hybrid ligand and replacing a pyridine moiety with a phosphinine have not been considered, yet (Figure 3-1).

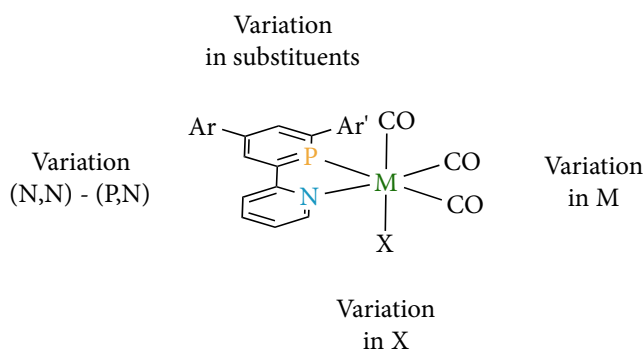
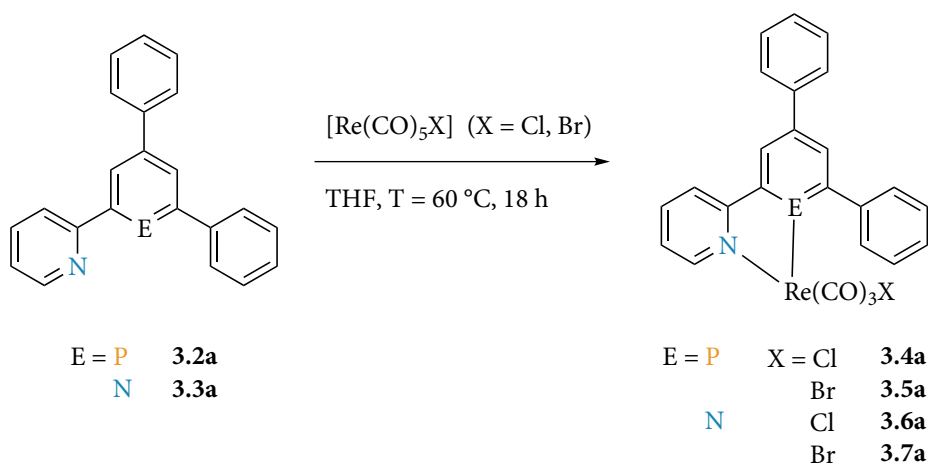


Figure 3-1: Possible aspects of research for rhenium(I) carbonyl complexes in CO₂ reduction catalysis.

With the experience of an in-depth study of electronically and structurally similar tungsten(0) carbonyl compounds, the synthesis and subsequent comparison of pyridylphosphinine analogues to the bipyridine-based rhenium(I) complex **3.1** seemed desirable considering the interesting possibility of application.

Such a P,N-rhenium(I) carbonyl complex has been synthesised by Müller before. Heating of [Re(CO)₅X] (X = Cl, Br) in a solution of 2-(2-pyridyl)-4,6-diphenylphosphinine (**3.2a**) in THF gave the desired compounds **3.4a** (X = Cl) and **3.5a** (X = Br) in quantitative yields (Scheme 3-2).¹⁹¹ For a direct comparison not only with the well studied bipyridine-based complex **3.1** but also with one containing a pyridine ligand bearing the same substitution pattern, 2-(2-pyridyl)-4,6-diphenylpyridine (**3.3a**) was complexed with rhenium(I) carbonyl precursors to give derivatives **3.6a** (X = Cl) and **3.7a** (X = Br) (Scheme 3-2).¹⁹¹



Scheme 3-2: Synthesis of rhenium(I) carbonyl complexes from pyridylphosphinine **3.2a** and bipyridine **3.3a**.

Molecular structures in the crystal of the rhenium(I) bromide **3.5a** as well as of the related bipyridine complex **3.7a** were derived (Figure 3-2).¹⁹¹ Even though only one molecule is shown here, the packing reveals both enantiomers in the crystal for these two complexes.

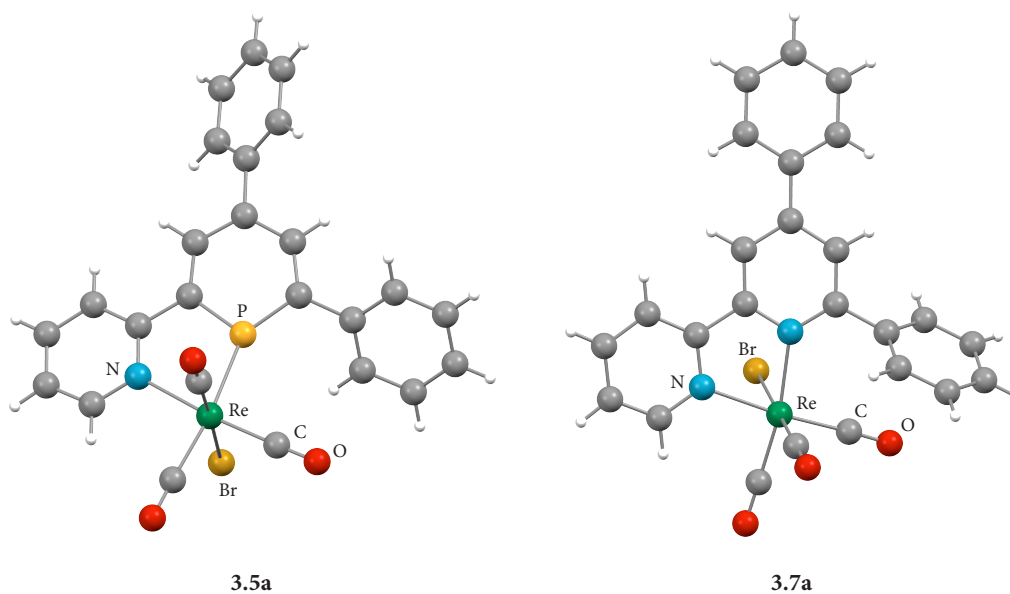
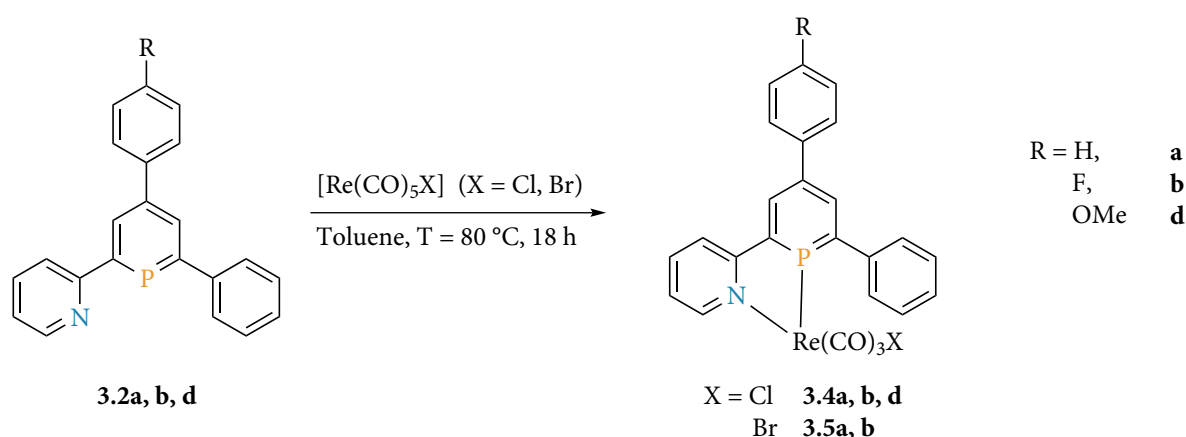


Figure 3-2: Molecular structures in the crystal of pyridylphosphinine-rhenium(I) complex **3.5a** and the equivalent bipyridine compound **3.7a**.¹⁹¹

With these results unpublished and no similar pyridylphosphinine-rhenium(I) species known in literature, coordination compounds **3.4a-3.7a** were to be synthesised again and subsequently fully characterised. Before the final goal of applying these complexes as novel catalysts in CO₂ reduction reactions, the general reactivity of pyridylphosphinine-rhenium(I) complexes is to be evaluated.

3.2 Results for the Synthesis of Pyridylphosphinine- and Bipyridine-Rhenium(I) Complexes

[(P,N)Re(CO)₃X]-type complexes can easily be synthesised through heating a [Re(CO)₅X] (X = Cl, Br) precursor in a solution of pyridylphosphinine ligand. While the reaction proceeds faster in DCM or THF, toluene was chosen for repeated synthesis since it simplifies workup. Already during synthesis, pyridylphosphinine-rhenium(I) complexes proved to be very water sensitive. Workup should therefore be entirely conducted inside a dry box and only freshly dried solvents should be used. DCM, benzene and toluene are to be favoured over THF and acetonitrile which usually have a higher water content and NMR spectra of [(P,N)Re(CO)₃X]-type complexes in these solvents often showed resonances of decomposition products even if used directly after distillation inside a dry box. Additionally, the desired [(P,N)Re(CO)₃X] compounds are significantly less soluble in toluene compared to DCM or THF, allowing workup be reduced to a simple filtration of the reaction mixture inside a dry box followed by drying of the product on vacuum. To allow monitoring of the reaction *via* NMR spectroscopy and minimise possible exposure to air, the coordination of [Re(CO)₅X] (X = Cl, Br) with pyridylphosphinine ligands was done in a J. Young NMR tube in toluene at T = 80 °C over night (Scheme 3-3). The products were isolated as brightly yellow, crystalline solids.



Scheme 3-3: Complexation reaction of rhenium(I) pentacarbonyl precursors with pyridylphosphinine ligands.

Since pyridylphosphinine complexes of the type [(P,N)Re(CO)₃X] (X = Cl, Br) turned out to be very sensitive towards water, not the whole set of differently substituted ligands was used but a first focus was put on the evaluation of **3.4a** and **3.5a**. Rhenium(I) chloride and

bromide compounds were also synthesised of the fluorine-bearing ligand **3.2b**. Methoxy-substituted phosphinine **3.2d** was used to react with rhenium(I) pentacarbonyl chloride only.

Interestingly, the difference in chemical shift in the $^{31}\text{P}\{^1\text{H}\}$ NMR spectra of the free ligand and the resulting rhenium (I) complex is very small; exemplarily shown here in THF for fluorine substituted pyridylphosphinine **3.2b** at $\delta = 186.7$ ppm and the respective rhenium(I) chloride complex **3.4b** at $\delta = 188.1$ ppm (Figure 3-3). Depending on solvent, ligand, rhenium precursor and accuracy of the NMR measurement, no change or barely any change can be seen during the reaction process in the $^{31}\text{P}\{^1\text{H}\}$ NMR spectra. If necessary, monitoring of the reaction is, however, possible through shift differences in the ^1H NMR spectra. In addition to this observation, the complexation of the rhenium(I) carbonyl centre with pyridylphosphinine ligands proceeds without appearance of a resonance belonging to an intermediary monocoordinated complex as was seen for the closely related tungsten(0) hexacarbonyl (Compare Figure 2-1 and Figure 3-3).

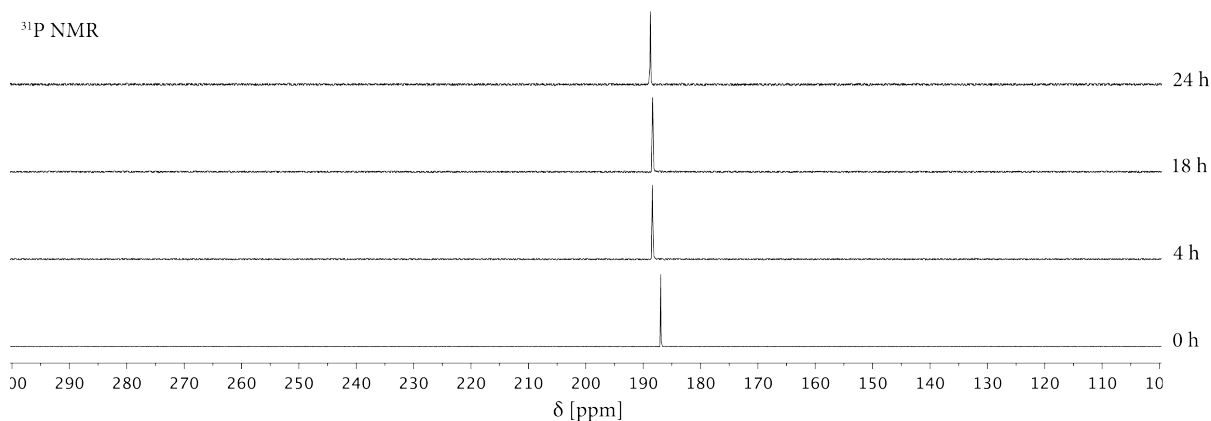
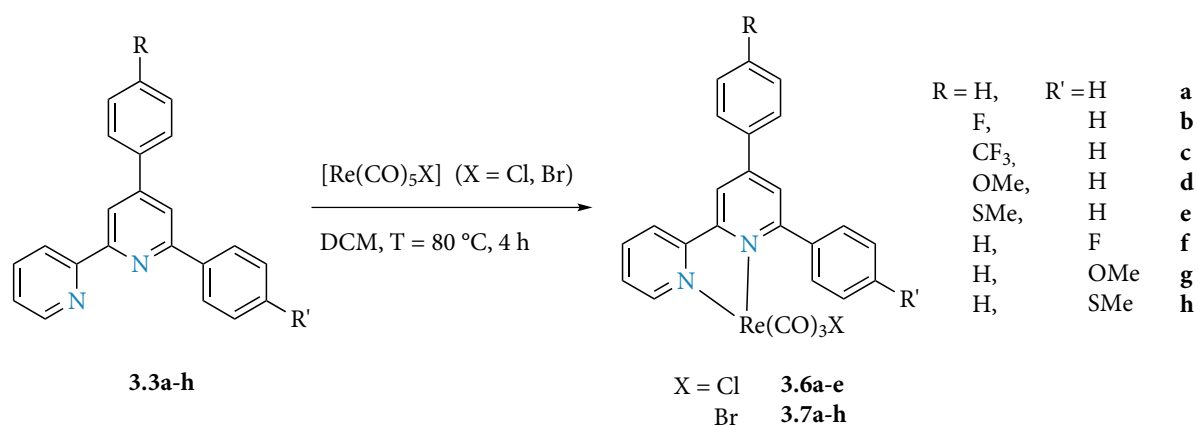


Figure 3-3: Reaction monitoring *via* $^{31}\text{P}\{^1\text{H}\}$ NMR spectroscopy for the complexation of $[\text{Re}(\text{CO})_5\text{Cl}]$ with fluorine substituted pyridylphosphinine **3.2b** in THF.

For the synthesis of $[(\text{N},\text{N})\text{Re}(\text{CO})_3\text{X}]$ -type complexes, a number of only slightly varied synthetic procedures can be found in literature.^{192,193} Here, bipyridine ligands **3.3a-h** were dissolved in DCM and added to $[\text{Re}(\text{CO})_5\text{X}]$ ($\text{X} = \text{Cl}, \text{Br}$) in a J. Young NMR tube. Heating to $T = 80$ °C, yellow crystals of bipyridine-rhenium(I) complex started to form after only a few minutes. Analogous to the procedure for pyridylphosphinine complexes above, the products **3.6a-e** and **3.7a-h** can be easily filtered off from the reaction mixture and dried in vacuum to give bright yellow, crystalline solids (Scheme 3-4).



Scheme 3-4: Complexation reaction of rhenium(I) pentacarbonyl precursors with bipyridine ligands.

Compared to pyridylphosphinine compounds **3.4a, b, d** and **3.5a, b** that are relatively well soluble in DCM and THF, all bipyridine complexes are hardly soluble in DCM, THF, benzene, acetone, acetonitrile or methanol. A reasonable amount of substance for recording NMR spectra can, however, be dissolved in DMSO. On the other hand, DMSO also proved to be a good solvent for crystallisation since **3.6a-e** and **3.7a-h** usually start to crystallise quickly from these NMR solutions. Additionally and contrary to phosphinine complexes **3.4a, b, d** and **3.5a, b**, these bipyridine compounds are stable towards air and moisture and can be heated in DMSO until boiling temperature ($T = 189\text{ }^{\circ}\text{C}$)²¹ without showing any signs of decomposition.

3.3 General Characterisation of Rhenium(I) Complexes

Many observations made for tungsten complexes in terms of the comparison between ligand properties of pyridylphosphinines and bipyridines as well as in the evaluation of substituent effects on these compounds are supported by data derived for rhenium(I) complexes of the type $[(L_2)Re(CO)_3X]$ ($L_2 = P,N$ or N,N , $X = Cl$ or Br). The IR stretching bands of the carbonyl ligands are again used to gain insight into the electronic situation in those complexes. Molecular structures in the crystal prove connectivity and allow the discussion of structural differences. In the context of a possible application of the obtained rhenium(I) complexes as catalysts in CO_2 reduction reactions, the study of their redox behaviour *via* cyclic voltammetry experiments is important and should be looked at in detail. Additionally, temperature dependent NMR spectra were recorded to investigate reasons for very broad resonances observed in the 1H NMR spectra of bipyridine compounds.

IR Spectroscopy

As described in the discussion of tungsten(0) compounds, carbonyl stretching bands in IR spectra are commonly used for the comparison of electronic ligand properties. Strongly donating ligands lead to electron rich metal centres which then, in turn, transfer more electron density into the antibonding π^* -orbital of the carbonyl moiety leading to a weakening of the C=O bond. This can be observed through a shift of the CO stretching bands towards lower wavenumbers and *vice versa* for more electron poor metal centres.¹⁶⁰ From the analysis of IR spectra, only the net-donation can be evaluated because no differentiation between σ -donation, π -donation and π -acceptance is possible.¹²⁶

The metal precursor $[\text{Re}(\text{CO})_5\text{Cl}]$ shows IR bands at $\tilde{\nu} = 2155, 2046, 1983 \text{ cm}^{-1}$.¹⁹⁴ The substitution of two strongly π -accepting carbonyl ligands with the good π -acceptor but also moderately σ -donating phosphinines shifts these carbonyl stretching bands significantly towards smaller wavenumbers ($\tilde{\nu} = 2046, 1992, 1945 \text{ cm}^{-1}$) for the only reported phosphinine rhenium(I) complex *cis*- $[(\text{L})_2\text{Re}(\text{CO})_3\text{Cl}]$ (L = 2-chlorophosphinine).¹⁹⁵ Not surprisingly, the exchange of phosphinine ligands by the σ -donating pyridine rings increases the shift even further. The pyridylphosphinine rhenium(I) complexes **3.4a** and **3.5a** exhibit carbonyl stretching bands at $\tilde{\nu} = 2029, 1948, 1937, 1905$ (sh), 1880 cm^{-1} and $\tilde{\nu} = 2026, 1935, 1899 \text{ cm}^{-1}$, respectively while the bipyridine-based compounds **3.6a** and **3.7a** show bands at $\tilde{\nu} = 2017, 1938, 1907, 1864 \text{ cm}^{-1}$ and $\tilde{\nu} = 2018, 1940, 1911, 1867 \text{ cm}^{-1}$ (Table 3-1). These values for $[(\text{N},\text{N})\text{Re}(\text{CO})_3\text{X}]$ -type compounds **3.6a** and **3.7a** are very close to what is measured for the well researched complex $[(\text{bipy})\text{Re}(\text{CO})_3\text{Cl}]$ (**3.1**, Table 3-1).

	3.4a R = H, X = Cl	3.5a R = H, X = Br	3.6a R = H, X = Cl	3.7a R = H, X = Br	3.1 $[(\text{bipy})\text{Re}(\text{CO})_3\text{Cl}]$
$\tilde{\nu}(\text{CO}) [\text{cm}^{-1}]$	2029	2026	2017	2018	2014
	1948		1938	1940	1971
	1937	1935 (sh)	1907	1911	1889
	1905 (sh)				
	1880	1899	1864	1867	1859

Table 3-1: Carbonyl stretching bands in solid state FT-IR spectra of $[(\text{P},\text{N})\text{Re}(\text{CO})_3\text{X}]$ -type complexes **3.4a** and **3.5a** in comparison with $[(\text{N},\text{N})\text{Re}(\text{CO})_3\text{X}]$ -type complexes **3.6a**, **3.7a** and **3.1**.

Due to the high sensitivity of $[(\text{P},\text{N})\text{Re}(\text{CO})_3\text{X}]$ -type compounds towards nucleophiles, substituent effects were only investigated for bipyridine-rhenium(I) complexes. While for the related tungsten(0) species substituents had a far larger influence on pyridylphosphinine

than on bipyridine complexes, some influence especially of the fluorine and methylthio groups could still be detected in the IR spectra (Chapter 2.4). [(N,N)Re(CO)₃X]-type compounds, on the other hand, do not show any changes in carbonyl stretching bands with varying substituents (Table 3-2). Interestingly enough, also the X-group does not influence the C-O stretching bands since no difference is visible in values of rhenium(I) chloride or bromide complexes (Table 3-1, Table 3-2).

	3.6b R = F X = Cl	3.7b R = F X = Br	3.6d R = OMe X = Cl	3.7d R = OMe X = Br	3.6e R = SMe X = Cl	3.7e R = SMe X = Br	3.7f R' = F X = Br	3.7g R' = OMe X = Br
$\tilde{\nu}(\text{CO})$ [cm ⁻¹]	2014 1914 1871	2017 1914 1874	2014 1912 1859 1842 (sh)	2016 1914 1864	2016 1913 1862	2015 1914 1866	2017 1893 (sh) 1866	2014 1916 1868

Table 3-2: Carbonyl stretching bands in solid state FT-IR spectra of differently substituted [(N,N)Re(CO)₃X]-type complexes **3.6a-e** and **3.7a-h**.

Molecular Structures in the Crystal

It was possible to characterise complexes **3.6a, b, d-g** and **3.7b, e, h** by means of X-ray crystallography (Figure 3-2, Figure 3-4, Figure 3-5, Figure 3-6). Since molecular structures in the solid state are known already for the rhenium(I) bromide complexes **3.5a** and **3.7a**,¹⁹¹ they can be put into context now for comparison between pyridylphosphinine- and bipyridine-based compounds but also between differently substituted complexes.

As expected from the employed method of synthesis *via* heating, all molecular structures in the crystal show the *fac*-isomers (*fac* in relation to the three carbonyl ligands) with both enantiomeric forms of the rhenium(I) halide complexes. For [(bipy)Re(CO)₃Cl] (**3.1**) the transformation into the *mer*-conformation by irradiation with UV light under a CO atmosphere has been reported.¹⁹⁶ Analogous to observations made for tungsten complexes (Chapter 2.4), rhenium(I) compounds **3.5a, 3.6a, b, d-g** and **3.7b, e, h** show a distorted octahedral arrangement of the ligands around the metal centre (Figure 3-2, Figure 3-4, Figure 3-5, Figure 3-6). The rhenium(I) atom is placed in the ideal coordination axis of the pyridyl moiety but slightly shifted from the perfect position on the axis of the phosphinine ring which is necessary due to the rigid geometry of these ligands and easier facilitated by the larger, more diffuse and less directional lone pair of the phosphorus atom than the one of the

nitrogen atom. Hence, bipyridine ligands compensate with an elongation of the central N1-Re1 bond to 2.215-2.238 Å compared to N2-Re1 with 2.156-2.174 Å. In comparison the P1-Re1 bond of phosphinine complex **3.5a** is longer with 2.3654(5) Å which in turn also increases the N2-Re1 bond length to 2.2420(15) Å (Table 3-3).

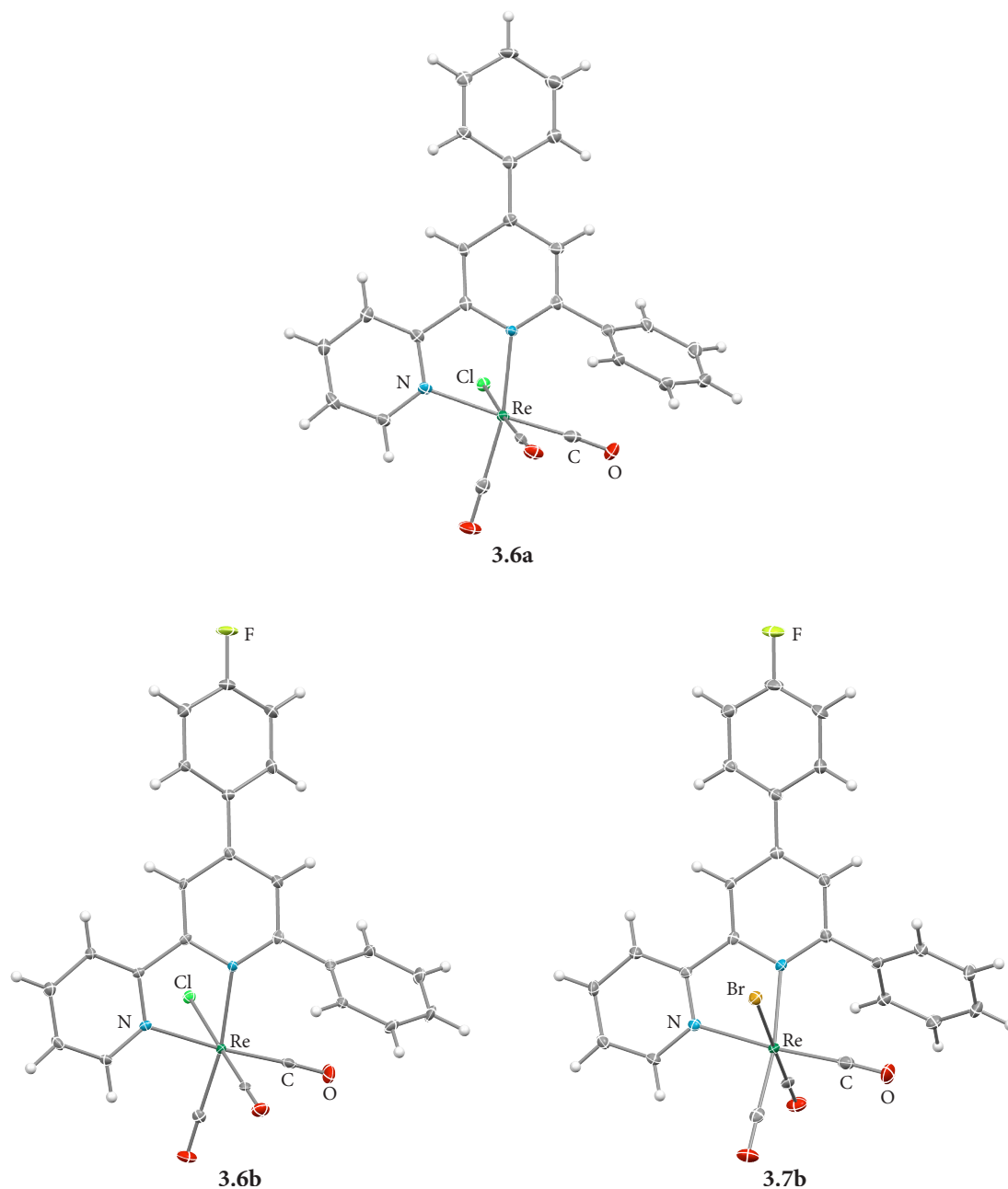


Figure 3-4: Molecular structures in the crystal of bipyridine rhenium(I) carbonyl complex **3.6a, b** and **3.7b**. Displacement ellipsoids are shown at the 50% probability level. Solvent molecules are omitted for clarity. Crystal contained both enantiomers of which only one is displayed here. The structure of **3.6a** displays two molecules in the asymmetric unit of which only one is shown.

In both cases, the ligand-metal bonds in the pyridylphosphinine and bipyridine complexes are shorter for a rhenium(I) than with a tungsten(0) centre (P1-W1: 2.447-2.464 Å, N2-W1:

2.296-2.310 for [(P,N)W(CO)₄]-type complexes and N1-W1: 2.276-2.291 Å, N2-W1: 2.221-2.252 Å for [(N,N)W(CO)₄]-type complexes (Table 2-7 and Table 2-8)). This phenomenon can be attributed to the smaller size of a rhenium(I) atom which is further enhanced by the higher oxidation state compared to tungsten(0). Consequently, the shorter distance between ligand and metal centres in rhenium(I) complexes leads to a slightly wider P-Re-N or N-Re-N angle (75.57° and 74.2-75.3°, respectively) compared to the one observed in tungsten(0) compounds (73.8-74.1° and 71.9-72.6°, respectively).

Bond length (Å), angle (°) or torsion angle (°)	3.5a ¹⁹¹ R = H X = Br	3.6a R = H X = Cl	3.7a ¹⁹¹ R = H X = Br
P1-Re1 / N1-Re1	2.3654(5)	2.210(3) / 2.208(3)	2.220(2)
N2-Re1	2.242(2)	2.162(3) / 2.164(3)	2.167(2)
P1-C1 / N1-C1	1.717(2)	1.360(4) / 1.360(4)	1.357(3)
P1-C5 / N1-C5	1.719(2)	1.363(4) / 1.367(4)	1.361(2)
C1-C2	1.394(3)	1.391(5) / 1.393(5)	1.394(3)
C2-C3	1.399(3)	1.391(5) / 1.396(5)	1.391(3)
C3-C4	1.401(3)	1.408(4) / 1.404(4)	1.398(3)
C4-C5	1.388(3)	1.386(5) / 1.392(5)	1.390(3)
C1-C11	1.481(3)	1.493(5) / 1.487(5)	1.484(3)
C3-C17	1.486(3)	1.479(5) / 1.476(5)	1.492(3)
C5-C6	1.475(3)	1.479(4) / 1.477(5)	1.481(3)
Re1-X	2.6188(2)	2.487(1) / 2.498(1)	2.6277(2)
Re1-C24	1.955(2)	1.928(4) / 1.930(4)	1.904(2)
Re1-C25 (ax.)	1.913(2)	1.907(5) / 1.904(5)	1.908(2)
Re1-C26	1.925(2)	1.910(4) / 1.917(4)	1.935(2)
C24-O2	1.140(3)	1.150(5) / 1.152(5)	1.154(3)
C25-O3 (ax.)	1.139(3)	1.152(6) / 1.149(6)	1.147(3)
C26-O4	1.146(3)	1.149(5) / 1.150(5)	1.153(3)
C1-P1-C5 / C1-N1-C5	106.32(9)	117.6(3) / 117.2(3)	117.3(2)
C6-N2-C10	117.3(2)	118.6(3) / 118.7(3)	118.4(2)
P1-Re1-N2 / N1-Re1-N2	75.57(4)	74.7(1) / 74.5(1)	74.83(6)
P1-C1-C11-C12 / N1-C1-C11-C12	40.9(3)	-60.3(5) / 59.3(5)	-59.7(3)
C2-C3-C17-C22	-44.9(3)	18.0(6) / -10.3(6)	-10.2(3)
P1-C5-C6-N2 / N1-C5-C6-N2	9.5(2)	-3.7(5) / 4.7(5)	-6.6(3)

Table 3-3: Selected bond length (Å), angles (°) and torsion angles (°) for rhenium(I) carbonyl complexes. Compound **3.6a** crystallised with two independent molecules in the asymmetric unit. Numbering of atoms is consistent throughout this work and explained in **Figure 3-15**.

The P-C bonds of 1.717(2) Å and 1.719(2) Å, as well as the C-C bonds of 1.388–1.401 Å of the phosphinine ring in **3.5a** are in the expected range as are N-C and C-C bond length as well as the C1-N1-C5 angle of the central pyridine moiety in **3.6a** and **3.7a** with 1.357-1.367 Å, 1.391-1.408 Å and 117.2-117.6°, respectively.^{11,12} Upon coordination a widening of

the C-P-C angle from approximately 100° in uncomplexed phosphinine¹² to 104.0-104.8° when coordinated to tungsten(0) in **2.6b**, **f** and **g** (Table 2-7) and 106.3° in rhenium(I) complex **3.5a** can be observed (Table 3-3). As explained before, the C-P-C angle can be used as an indicator for the kinetic stability against nucleophilic attack of phosphinine complexes since a wider angle shows disruption of aromaticity in the phosphinine ring caused by the lone pair requiring a higher p-character for coordination.⁹⁹ Coordination compounds with C-P-C angles below 106° are usually stable towards water and alcohols as was confirmed here for the pyridylphosphinine tungsten(0) complexes.²⁰ Pyridylphosphinine-rhenium(I) complexes on the other hand were observed to react quickly with water and indeed **3.5a** shows an C-P-C angle of 106.3°.

With 1.475-1.493 Å (Table 3-3) the three interring distances are in the area of biphenyl (1.487 Å)²¹ and shortened compared to normal C-C single bonds (1.54 Å)²¹ which shows the delocalisation of the π electron system over the entire ligand. Torsion angles between the rings show a slight twisting between the two heterocycles, observed already in tungsten(0) complexes of the same ligands.⁹⁹ Additionally, a strong rotation of the 6-phenyl ring out of the central plane can be noticed which is due to shorter metal-ligand bonds and resulting steric hindrance of one carbonyl group more pronounced for bipyridine compounds **3.6a** and **3.7a** (40.9° for [(P,N)Re(CO)₃Br]-type complex **3.5a** vs. 59.3-60.3° for [(N,N)Re(CO)₃X]-type compounds **3.6a** and **3.7a**). Again this is analogous to observations made for the respective tungsten(0) compounds.

As is expected from their van-der-Waals radii, the Re-Cl bond of 2.487-2.498 Å is shorter than the Re-Br bond with 2.618-2.628 Å. Looking closer at the carbonyl ligands, no real trend can be detected neither for the Re-C (1.904-1.935 Å) nor the C-O (1.139-1.154 Å) bond length. Differences in the *trans*-effect of bromido, chlorido or pyridine ligands are not visible. Only the Re-C bond in *trans*-position to a phosphinine moiety is slightly elongated with 1.955 Å in the molecular structure of complex **3.5a**.

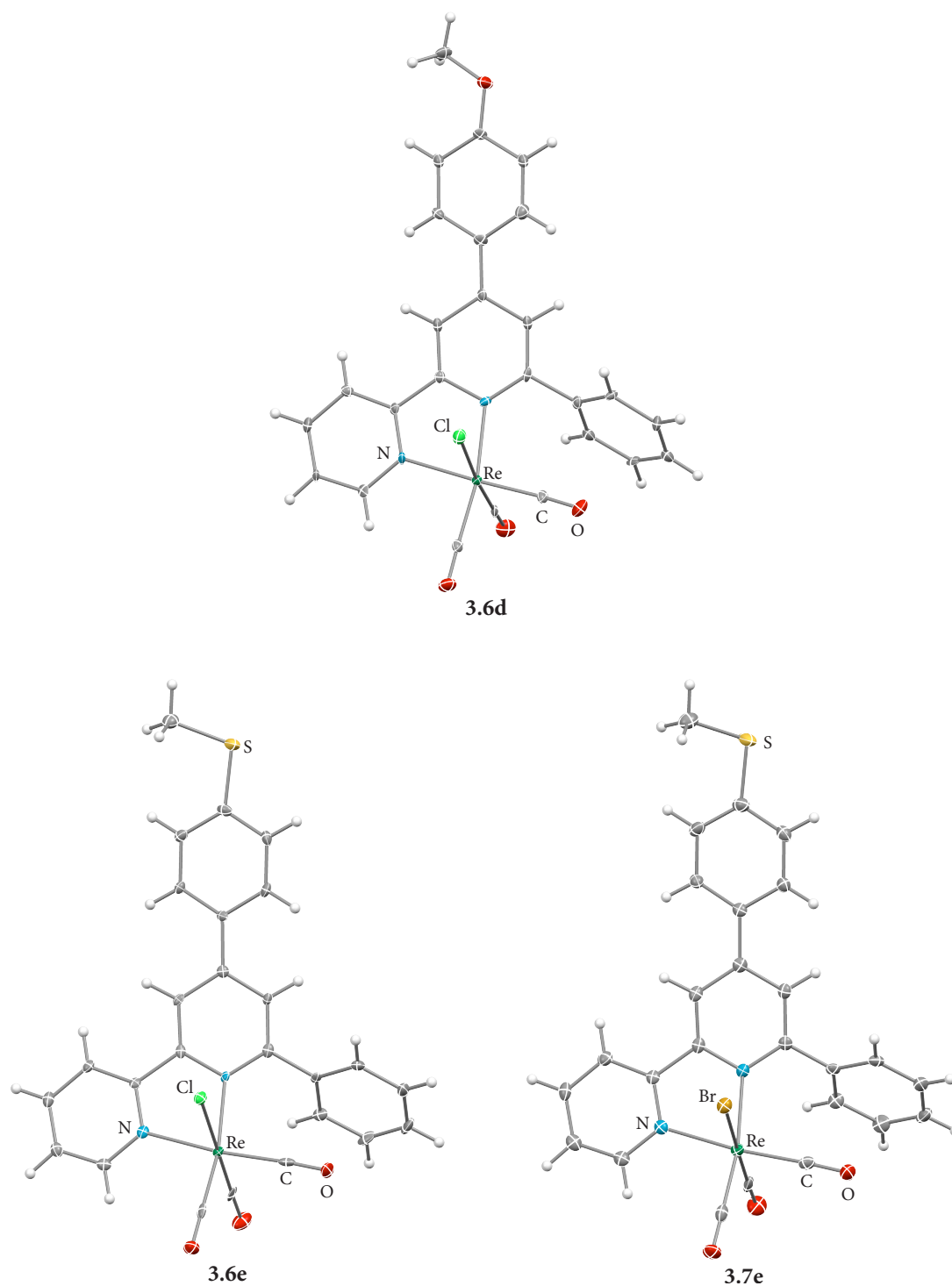


Figure 3-5: Molecular structures in the crystal of bipyridine rhenium(I) carbonyl complexes **3.6d**, **e** and **3.7e**. Displacement ellipsoids are shown at the 50% probability level. All crystals contained both enantiomers of which only one is displayed here.

Looking at the influence of substituents in the bipyridine ligand on the molecular structure of [(N,N)Re(CO)₃X]-type complexes, the arrangement of methoxy and methylthio groups in plane with the phenyl ring they are attached to is observed again here and can be attributed to an interaction of one lone pair of oxygen or sulphur with the delocalised π -system. Metal

ligand bonds are 2.215-2.238 Å and 2.156-2.174 Å long for N1-Re1 and N2-Re2, respectively without showing any substituent effect. The Re-Cl bond length is 2.476-2.493 Å which is elongated for the Re-Br bond to 2.603-2.628 Å. Concerning the carbonyl ligands, the Re-C bond length is 1.897-1.920 Å if located in *trans*-position to N1 and slightly longer with 1.918-1.940 Å if positioned *trans* to N2 (Table 3-4).

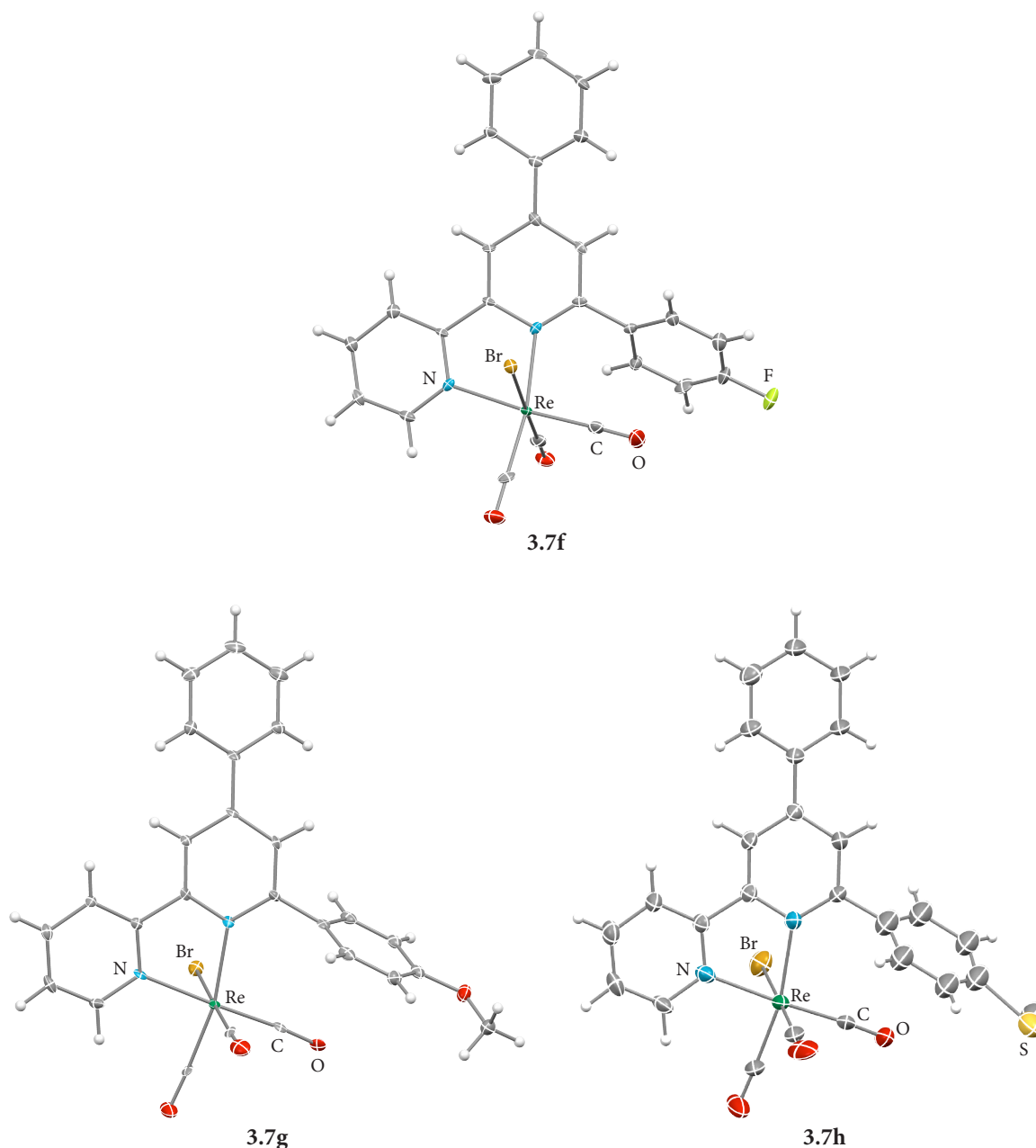


Figure 3-6: Molecular structures in the crystal of bipyridine rhenium(I) carbonyl complexes **3.7f**, **g** and **h**. Displacement ellipsoids are shown at the 50% probability level. Solvent molecules are omitted for clarity.

All crystals contained both enantiomers of which only one is displayed here. For compound **3.7h** the 6-phenyl ring is disordered and only one conformation is shown.

Bond length (Å), angle (°) or torsion angle (°)	3.6b	3.7b	3.6d	3.6e	3.7e	3.7f	3.7g	3.7h
	R = F X = Cl	R = F X = Br	R = OMe X = Cl	R = SMe X = Cl	R = SMe X = Br	R' = F X = Br	R' = OMe X = Br	R' = SMe X = Br
N1-Re1	2.216(3)	2.216(2)	2.238(9)	2.215(3)	2.219(4)	2.224(6)	2.222(5)	2.219(5)
N2-Re1	2.170(3)	2.171(2)	2.174(9)	2.168(3)	2.162(4)	2.160(4)	2.156(5)	2.164(7)
N1-C1	1.357(5)	1.358(3)	1.32(1)	1.356(4)	1.356(6)	1.323(8)	1.371(8)	1.356(9)
N1-C5	1.368(4)	1.370(3)	1.38(2)	1.363(5)	1.365(5)	1.401(7)	1.353(8)	1.367(8)
C1-C2	1.396(5)	1.397(4)	1.39(2)	1.383(5)	1.393(7)	1.403(8)	1.384(8)	1.38(1)
C2-C3	1.392(5)	1.391(4)	1.41(2)	1.389(5)	1.398(5)	1.391(8)	1.383(9)	1.398(9)
C3-C4	1.400(4)	1.398(3)	1.40(2)	1.401(5)	1.399(7)	1.396(8)	1.404(8)	1.384(9)
C4-C5	1.388(5)	1.385(4)	1.39(2)	1.380(5)	1.378(7)	1.383(8)	1.387(8)	1.38(1)
C1-C11	1.480(5)	1.481(3)	1.51(2)	1.475(5)	1.472(5)	1.497(8)	1.494(9)	1.49(1)
C3-C17	1.476(5)	1.490(4)	1.47(2)	1.477(5)	1.477(7)	1.487(8)	1.487(8)	1.48(1)
C5-C6	1.471(5)	1.477(3)	1.47(2)	1.475(4)	1.479(6)	1.449(8)	1.485(8)	1.461(9)
Re1-X	2.4934(9)	2.6288(4)	2.476(3)	2.4842(9)	2.6209(5)	2.6222(6)	2.6169(8)	2.603(1)
Re1-C24	1.919(4)	1.915(3)	1.92(1)	1.905(4)	1.914(5)	1.909(7)	1.902(7)	1.897(8)
Re1-C25 (ax.)	1.899(4)	1.900(3)	1.96(1)	1.909(3)	1.938(5)	1.917(6)	1.986(7)	2.003(9)
Re1-C26	1.937(3)	1.936(3)	1.94(1)	1.934(4)	1.931(4)	1.927(7)	1.925(7)	1.918(8)
C24-O2	1.153(5)	1.154(4)	1.13(1)	1.157(4)	1.153(6)	1.148(9)	1.160(9)	1.15(1)
C25-O3 (ax.)	1.158(5)	1.153(4)	1.08(2)	1.139(4)	1.107(6)	1.144(7)	1.029(9)	0.97(1)
C26-O4	1.146(5)	1.151(4)	1.16(2)	1.146(4)	1.148(5)	1.150(8)	1.155(8)	1.16(1)
C1-N1-C5	117.3(3)	117.5(2)	118(1)	117.8(3)	117.4(4)	118.9(5)	117.2(5)	116.7(6)
C6-N2-C10	119.4(3)	118.9(2)	119(1)	118.9(3)	118.2(4)	118.7(5)	117.4(5)	119.3(6)
N1-Re1-N2	74.3(1)	74.46(8)	74.5(4)	74.3(1)	74.5(1)	75.3(2)	74.2(2)	74.9(2)
N1-C1-C11-C12	-53.0(5)	-52.8(3)	61(2)	54.6(4)	55.0(6)	53.9(8)	-74.4(8)	-
C2-C3-C17-C18	22.3(5)	-21.6(4)	-21(2)	-23.0(5)	-21.8(7)	-20.1(8)	12.4(9)	9(1)
N1-C5-C6-N2	-11.0(5)	11.8(3)	10(2)	12.9(4)	12.8(6)	10.3(7)	-6.4(8)	-5.0(9)

Table 3-4: Selected bond length (Å), angles (°) and torsion angles (°) for substituted bipyridine rhenium(I) carbonyl complexes. Numbering of atoms is consistent throughout this work and explained in **Figure 3-15**.

Rotation Barrier of the 6-Phenyl Ring

Evaluating the ^1H NMR spectra of bipyridine rhenium(I) carbonyl complexes **3.6** and **3.7**, broad resonances in the area of around $\delta = 7.5\text{-}7.8$ ppm can be noticed immediately (Figure 3-7). Depending on the overlap with other signals, the integrals add up to five protons which can be assigned to the 6-phenyl ring of the bipyridine using 2D NMR spectroscopy.

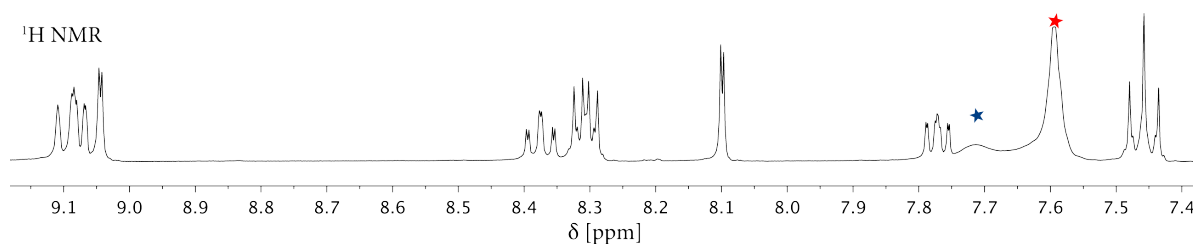


Figure 3-7: ^1H NMR spectrum of fluorine substituted bipyridine rhenium(I) complex **3.7b** in $\text{DMSO-}d_6$.

Depending on the solvent, the ^{13}C NMR spectra of these bipyridine complexes show 16 or 17 resonances for the ligand instead of the expected 18. Additionally, one or two broad resonances in the baseline can be detected in the area of $\delta = 128\text{-}131$ ppm where the missing resonances are anticipated (Figure 3-8). Again, these signals can be assigned to usually equivalent carbon atoms $\text{C}_{12}/\text{C}_{16}$ and $\text{C}_{13}/\text{C}_{15}$ of the 6-phenyl ring of the bipyridine (For numbering of atoms see Figure 2-23).

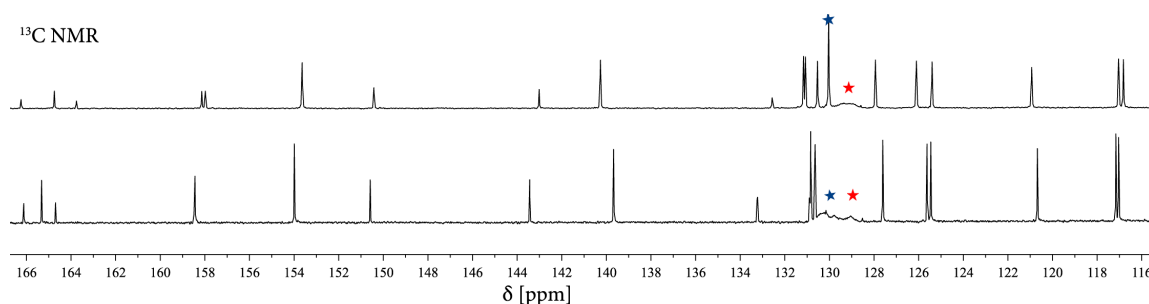


Figure 3-8: ^{13}C NMR spectra of fluorine substituted bipyridine rhenium(I) bromide complex **3.7b** in $\text{DMSO-}d_6$ (top) and $\text{THF-}d_8$ (bottom). One or two expected resonances are often not observed or appear very broad (blue, red).

In contrast to the respective tungsten(0) carbonyl complexes **2.6a-h** showing signs of steric hindrance in the solid state structures but not in solution, rotation of the 6-phenyl ring (Figure 3-9) in bipyridine-rhenium(I) carbonyl compounds **3.6a-e** and **3.7a-h** is apparently slow on the NMR timescale leading to the observed broad signals of the 6-phenyl ring atoms in the ^1H and ^{13}C NMR spectra (Figure 2-2 vs. Figure 3-7).

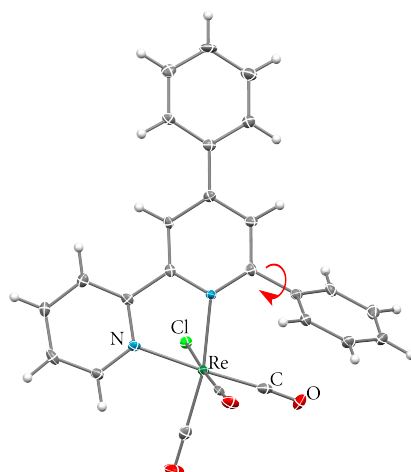


Figure 3-9: Hindered rotation around the 6-phenyl ring due to steric demand of a carbonyl ligand exemplarily shown for **3.6a**.

Therefore temperature dependent NMR experiments allow the evaluation of some kinetic data. Heating the sample in the NMR spectrometer leads to faster rotation of the phenyl

rings making protons H₁₂/H₁₆ and H₁₃/H₁₅ and carbons C₁₂/C₁₆ and C₁₃/C₁₅ indistinguishable on the timescale of a NMR experiment. Cooling down the sample, on the other hand, the rotation of the 6-phenyl ring is hindered causing these four protons and four carbons to give one separate resonance each (Figure 3-10 and Figure 3-11).

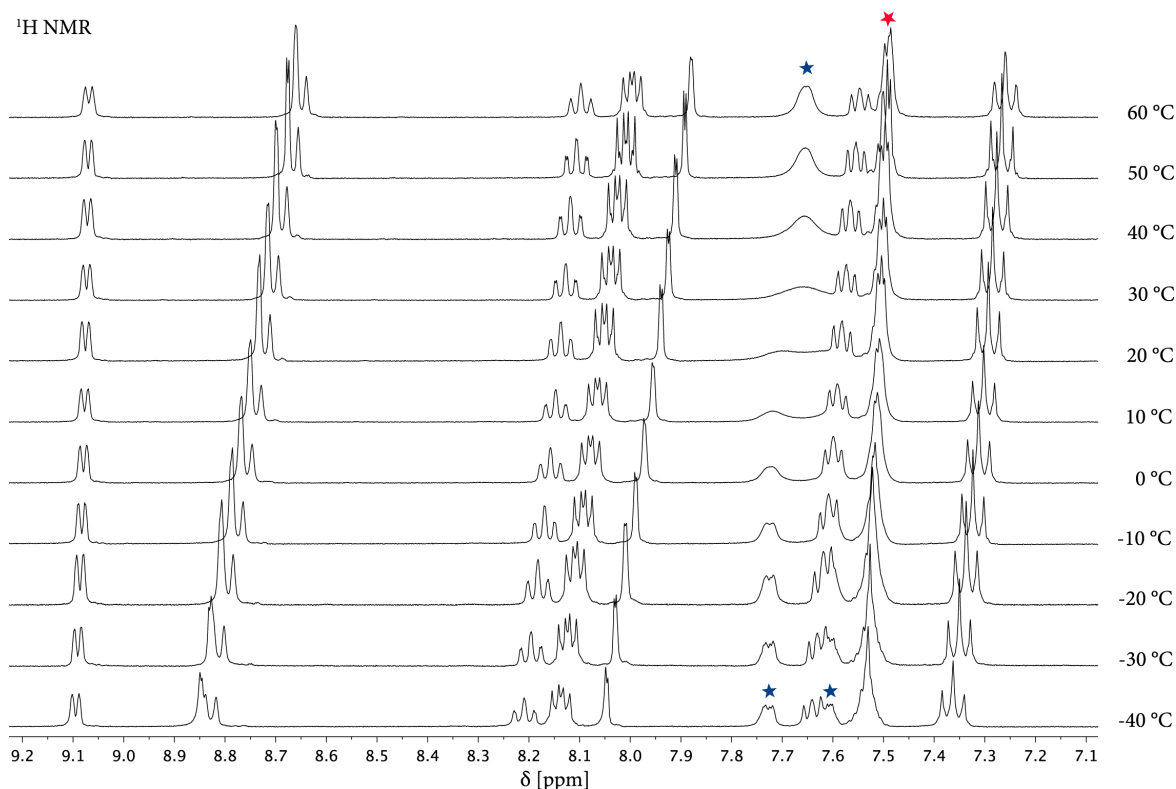


Figure 3-10: Temperature dependent ¹H NMR experiments in THF-*d*₈ of fluorine substituted [N,N-Re(CO)₃X]-type complex **3.7b**. Spectra were measured in steps of 5 °C but not all spectra are shown for better clarity. Protons of the 6-phenyl ring are marked (blue, red).

Temperature dependent NMR experiments allow the calculation of some kinetic data for the rotation of this phenyl ring. If temperature effects on shift values are neglected, the rate constant for the rotation at the temperature of coalescence is only dependent on the shift difference at low temperature (Equation 3-1).¹⁹⁷

$$k_{T_c} = \frac{\pi}{\sqrt{2}} |\nu_1 - \nu_2| \quad \text{Equation 3-1}$$

k – rate constant, T_c – coalescence temperature, ν – chemical shift

Combination of equation 3-1 for the rate constant at coalescence temperature with the Eyring equation, gives the Gibbs energy or in this case specifically the rotation barrier (Equation 3-2).¹⁹⁷

$$\Delta G^\ddagger = RT_c \ln \frac{RT_c \sqrt{2}}{\pi N_A h |v_1 - v_2|} \quad \text{Equation 3-2}$$

ΔG^\ddagger - Gibbs energy, R – gas constant, N_A – Avogadro constant, h – Planck constant

In the temperature dependent ^1H NMR spectra of the fluorine substituted complex $[(\text{N,N})\text{Re}(\text{CO})_3\text{X}]$ (**3.7b**) in $\text{THF-}d_8$, only one of the expected two sets of proton pairs was observed to split into two resonances at low temperature (Figure 3-10, marked blue). From this set a Gibbs energy of $\Delta G^\ddagger = 60.3$ kJ/mol and a rate constant of $k_{Tc} = 104.4$ s $^{-1}$ at the coalescence temperature was calculated for rotation of the 6-phenyl ring (Table 3-5). The second pair of protons (Figure 3-10, marked red) does not give identifiable resonances in this temperature range, also due to overlapping signals.

The ^{13}C NMR spectra on the other hand, show two distinguishable sets of resonances for carbon atoms $\text{C}_{12}/\text{C}_{16}$ and $\text{C}_{13}/\text{C}_{15}$ (Figure 3-11). Caused by low solubility of these bipyridine-rhenium(I) compounds in THF, the signal to noise ratio is not as good as is desired, thereby increasing the error of the coalescence temperature. Aside from DMSO with a melting point of only $T = 19$ °C, no better suited solvent was found.²¹ The Gibbs energies calculated from these two sets of carbon resonances are $\Delta G^\ddagger = 59.8$ and 59.6 kJ/mol, respectively, which are very well in line with the value derived from the ^1H NMR spectra (Table 3-5).

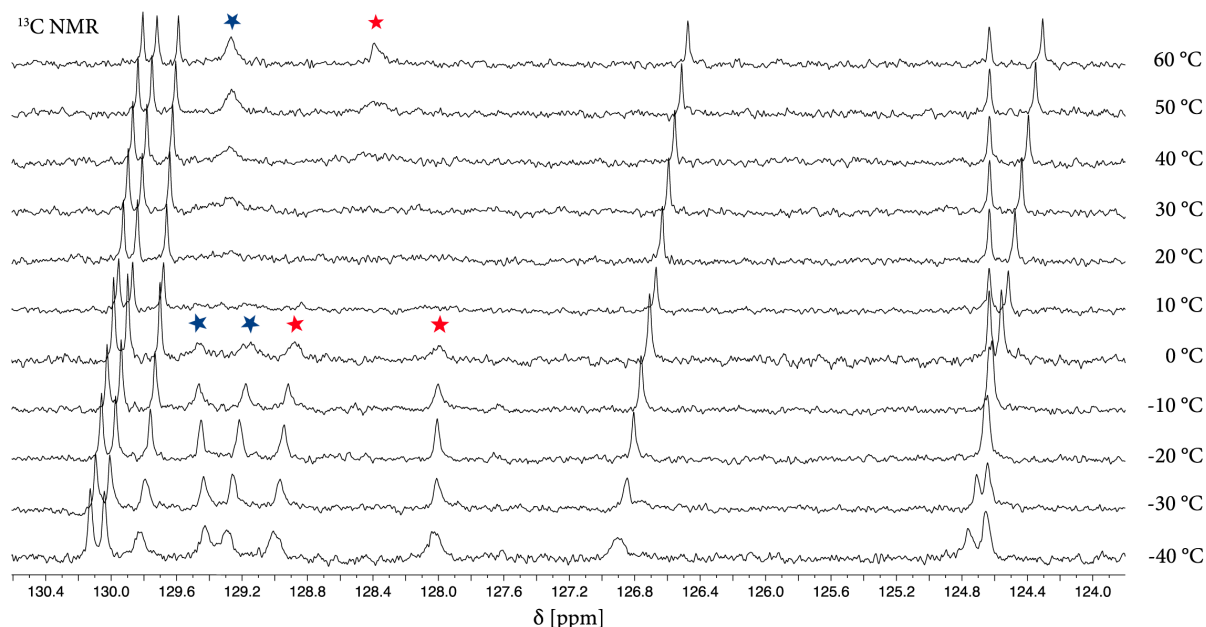


Figure 3-11: Temperature dependent ^{13}C NMR experiments in $\text{THF-}d_8$ of fluorine substituted $[(\text{N,N})\text{Re}(\text{CO})_3\text{X}]$ -type complex **3.7b**. Spectra were measured in steps of 5 °C but not all spectra are shown for better clarity. Carbons $\text{C}_{12}/\text{C}_{16}$ and $\text{C}_{13}/\text{C}_{15}$ are marked (blue, red).

The temperature dependent NMR experiments were repeated for a number of bipyridine-rhenium(I) complexes substituted on the 6-phenyl ring in order to determine a possible influence of substituents on the rotation barrier. The crucial carbon-carbon bond connecting the 6-phenyl ring with the central pyridine moiety is significantly shortened compared to a C-C single bond in all molecular structures presented here which is indicative for conjugation of the π -electron system over both rings. As was shown in detail in chapter 2, methoxy and methylthio groups participate in this π -electron system with the lone pair at the heteroatom. Testing this influence in connection with the hindered rotation of the 6-phenyl ring turned out to be difficult since the low solubility of these compounds severely limited the quality of derived NMR data especially at low temperatures. Rhenium(I) chloride derivatives **3.6** are less soluble than the respective bromide compounds and were discarded early on for this experiment. Methylthio substituted complex **3.7h** precipitated almost completely from THF at low temperature so no exploitable data was obtained. Only, unsubstituted derivative **3.7a** and **3.7g** bearing a methoxy group on the 6-phenyl ring gave satisfying NMR spectra (See Appendix Figure 6-7 and Figure 6-8). The signal to noise ratio, however, is very low which significantly increases errors in determining the coalescence temperature. Additionally, temperature effects on the chemical shifts can be seen clearly making shift differences harder to determine.

NMR	3.7a R = H		3.7b R = F			3.7g R' = OMe	
	¹³ C ★	¹³ C ★	¹ H ★	¹³ C ★	¹³ C ★	¹³ C ★	¹³ C ★
T _c [°C]	20	15	20	10	25	15	5
$\Delta\nu$ [Hz]	95	30	47	23.5	95	86	14
ΔG^\ddagger [kJ/mol]	58.6	60.3	60.3	59.8	59.6	57.8	59.9
k _{Tc} [s ⁻¹]	211.0	66.6	104.4	52.2	211.0	191.0	31.1

Table 3-5: Kinetic Data derived from temperature dependent NMR experiments with [N,N-Re(CO)₃X]-type complexes.

For unsubstituted bipyridine-rhenium(I) complex **3.7a** the rotation barrier was calculated as $\Delta G^\ddagger = 58.6$ and 60.3 kJ/mol and values derived for methoxy derivative **3.7g** are $\Delta G^\ddagger = 57.8$ and 59.9 kJ/mol (Table 3-5). No additional data were obtained by ¹H NMR spectroscopy for those two compounds **3.7a** and **3.7g** due to overlapping signals. The Gibbs energy values shows no determinable influence of the methoxy group; at least none that is larger than the error margin. However, overall the calculations match very well and the rotation barrier in these [(N,N)Re(CO)₃X]-type complexes **3.7** can be assumed with confidence at $\Delta G^\ddagger =$

59.5 kJ/mol. NMR studies with hindered rotation in metal complexes have been reported before.^{198–200} Any comparison is, however, difficult and not appropriate since ligand systems and coordination conditions are entirely different.

This hindrance of rotation in the 6-phenyl ring is not observed for pyridylphosphinine-based complexes. The NMR spectra of compounds **3.4a** and **3.5a** do not show any broad resonances and only one signal each is seen for H_{12/16} and H_{13/15} or C_{12/16} and C_{13/15}. In conclusion the rotation of the 6-phenyl ring is fast on the NMR timescale for complexes of the type [(P,N)Re(CO)₃X]. The longer ligand-metal (P1-Re1: 2.3654(5) Å, N2-Re1: 2.240(2) Å for **3.5a**, Table 3-3) and P-C bond distances (P1-C1: 1.717(2) Å, P1-C5: 1.719(2) Å for **3.5a**, Table 3-3) compared to bipyridine-based compounds (N1-Re1: 2.220(2) Å, N2-Re1: 2.167(2) Å and N1-C1: 1.357(3), N1-C5: 1.361(2) Å for **3.7a**, Table 3-3) obviously diminish the steric hindrance by the carbonyl ligand significantly by moving the 6-phenyl ring further away from the metal fragment.

3.4 Reactivity of [(P,N)Re(CO)₃X] Complexes Towards Water

As mentioned before, the high sensitivity of [(P,N)Re(CO)₃X]-type complexes towards water was obvious already during the synthesis therefore taking a closer look on this reactivity is important for the consideration of future applications. In principle the reactivity of pyridylphosphinine complexes with water or alcohols is known and described in literature for several examples as mentioned in the introduction chapter 1.7 (Pyridylphosphinines as P,N-Hybrid Ligands).^{84,101,103} Via X-ray diffraction and NMR experiments, regio- and diastereoselective addition of water to the external P=C double bond was shown for coordination compounds of pyridylphosphinine ligand **3.2a**. Selectivity for attack of the external P=C double bond can be attributed to the electron withdrawing nature of the nitrogen atom decreasing the nucleophilicity of the C5 carbon of the internal P=C double bond.¹⁰³ In case of palladium and platinum complexes, the *syn* products were formed exclusively.¹⁰³ For rhodium and iridium complexes, on the other hand, selective reaction towards the *anti* products was proven (Figure 3-12).¹⁰¹ Until now, no reason for the opposite selectivity could be given.

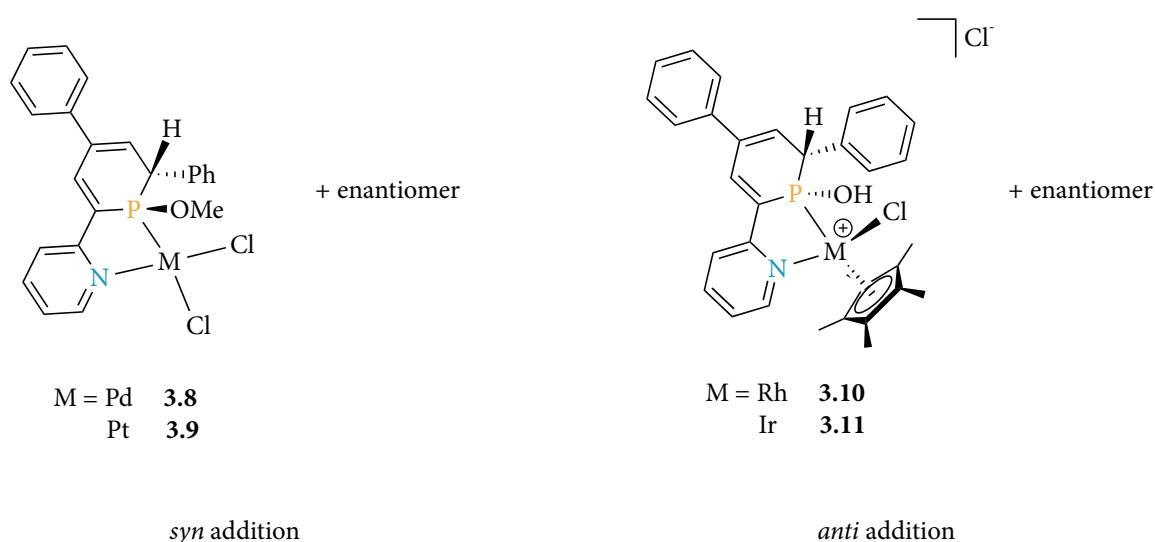
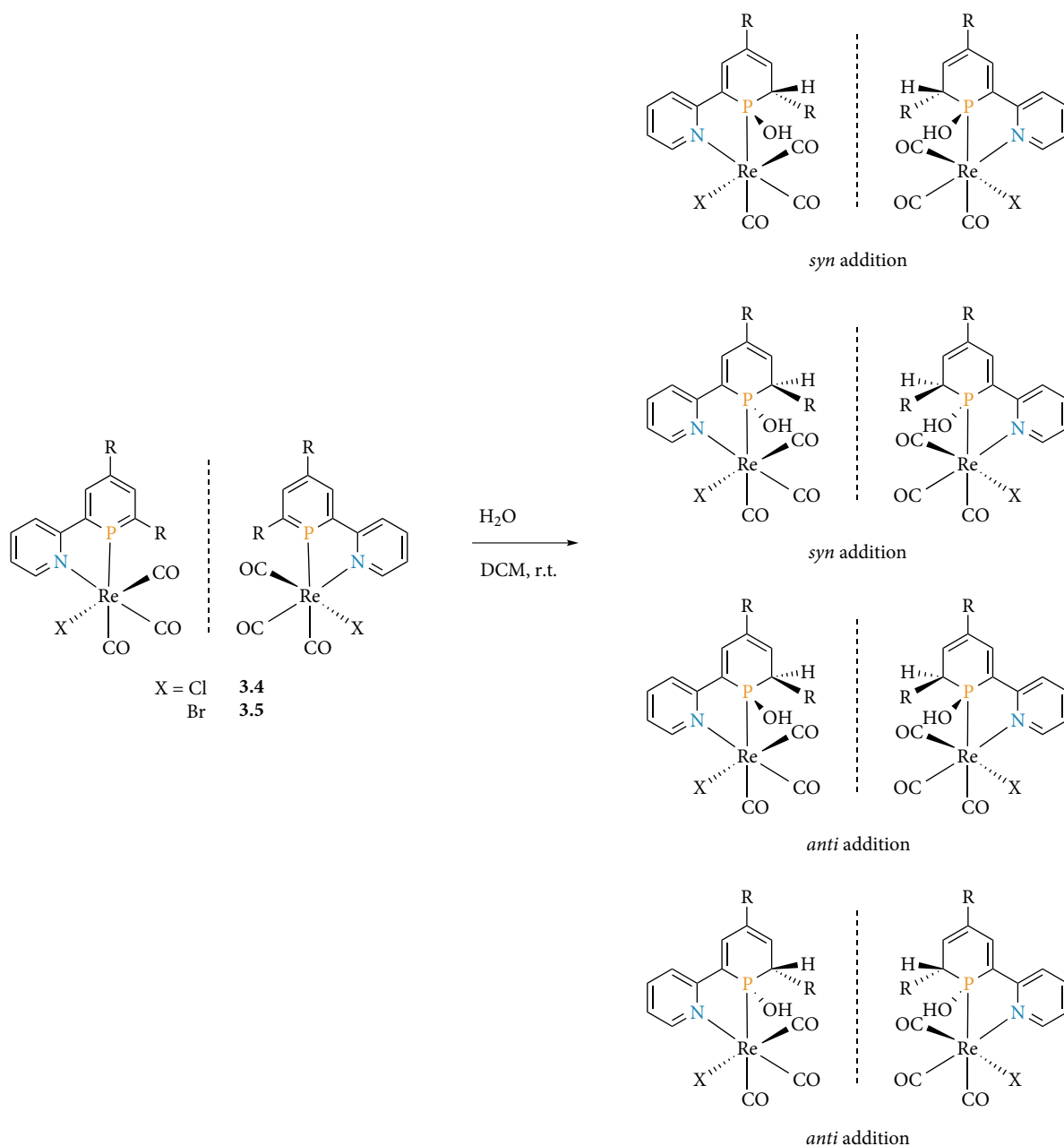


Figure 3-12: Water addition products for complexes of pyridylphosphinine **3.2a**.

If reaction of the internal P=C double bond is excluded due to a lower nucleophilic character of the C5 carbon, addition of water to rhenium(I) compounds could happen on the *re* or *si* face of the external P=C double bond in *syn* or *anti* fashion. Additionally, the reaction already starts from a racemic mixture of enantiomeric complexes since the rhenium(I) atom is a stereocentre. Therefore, a total of eight possible products in four pairs of enantiomers have to be considered (Scheme 3-5).

In the $^{31}\text{P}\{^1\text{H}\}$ NMR spectra, the formation of four new resonances at $\delta = 72.9, 81.2, 95.2$ and 107.2 ppm in a ratio of 1:40:9:49 can indeed be observed after the addition of degassed water to a solution of [P,N-Re(CO)₃Br]-type complex **3.5a** in DCM-*d*₂ (Figure 3-13). Similarly four new signals appeared in the reactions of **3.4a** and fluorine substituted derivatives **3.4b** and **3.5b**. Even though integration of the resonances in the $^{31}\text{P}\{^1\text{H}\}$ NMR spectra is biased by the nuclear Overhauser effect (NOE), the close structural relation of measured compounds should allow the use of signal ratios here for an overall picture of their behaviour in this reaction. Considering that the reaction conditions do not give any reason for enantioselectivity, the formation of all eight possible products can be assumed. Contrary to the observations made for pyridylphosphinine complexes **3.8-3.11**, the addition of water to the P=C double bond in rhenium(I) carbonyl complexes of pyridylphosphinine ligands is therefore not selective towards either *syn* or *anti* addition. The reason for this remains unknown up to this point.



Scheme 3-5: Possible products from the reaction of a $[\text{P,N-Re}(\text{CO})_3\text{X}]$ -type complex with water.

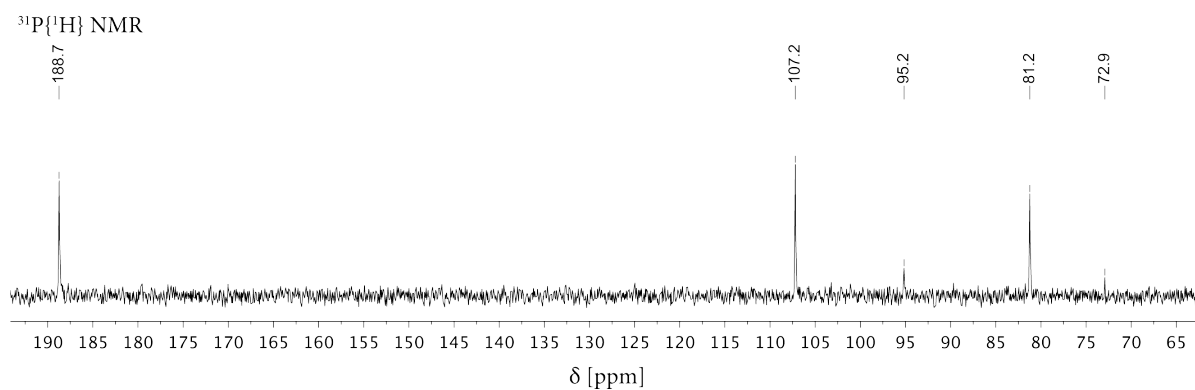
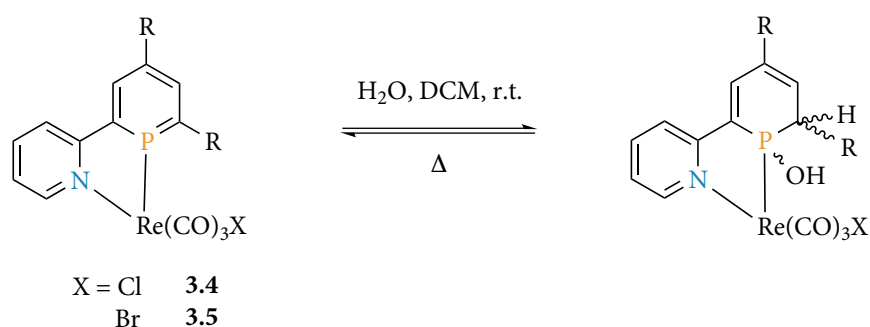


Figure 3-13: ^{31}P NMR spectrum in DCM-d_2 of $[(\text{P,N})\text{Re}(\text{CO})_3\text{Br}]$ -type complex **3.5a** approximately 10 min after the addition of a drop of degassed water.

Additionally, the water addition reaction is slow at room temperature in DCM even though these [(P,N)Re(CO)₃X]-type complexes were found to be very prone to react even with minimal amounts of water left in dry solvents for example. After approximately 10 min at room temperature, the starting material is still the major resonance and even after one hour some starting complex is still present (Figure 3-14). Also the ratio between the four pairs of enantiomers has changed to 0:57:14:29 after one hour at room temperature, hence the water addition can be assumed to be an equilibrium reaction (Scheme 3-6). Therefore the influence of temperature on the reaction was tested (Figure 3-14).



Scheme 3-6: Equilibrium reaction of [(P,N)Re(CO)₃X]-type complexes with water.

After addition of degassed water to a sample of [(P,N)Re(CO)₃X]-type complex **3.5a** in DCM-*d*₂ in a J. Young NMR tube, an hour was waited at room temperature. Then the reaction mixture was heated to $T = 80\text{ }^{\circ}\text{C}$ and ³¹P{¹H} NMR spectra were measured in regular time intervals. At higher temperatures two resonances at $\delta = 72.9$ and 107.2 ppm vanished immediately (Figure 3-14). These two can be considered as the kinetic products. While heating to $T = 80\text{ }^{\circ}\text{C}$, the equilibrium can also shift back to left side. After seven hours the resonances of starting complex and water addition products reached a ratio of 55:45. Cooling down the sample to room temperature leads again to the formation of the water addition products. The two thermodynamic products at $\delta = 81.2$ and 95.2 ppm are detected exclusively after one hour at room temperature. The cycle can be repeated a second time with the same results. Heating to higher temperatures shifts the equilibrium even further to the side of the starting material. After seven hours at $T = 100\text{ }^{\circ}\text{C}$ a ratio of 75:25 of complex **3.5a** to its water addition products is reached. Cooling down to room temperature with the reformation of the water addition products concludes the second cycle.

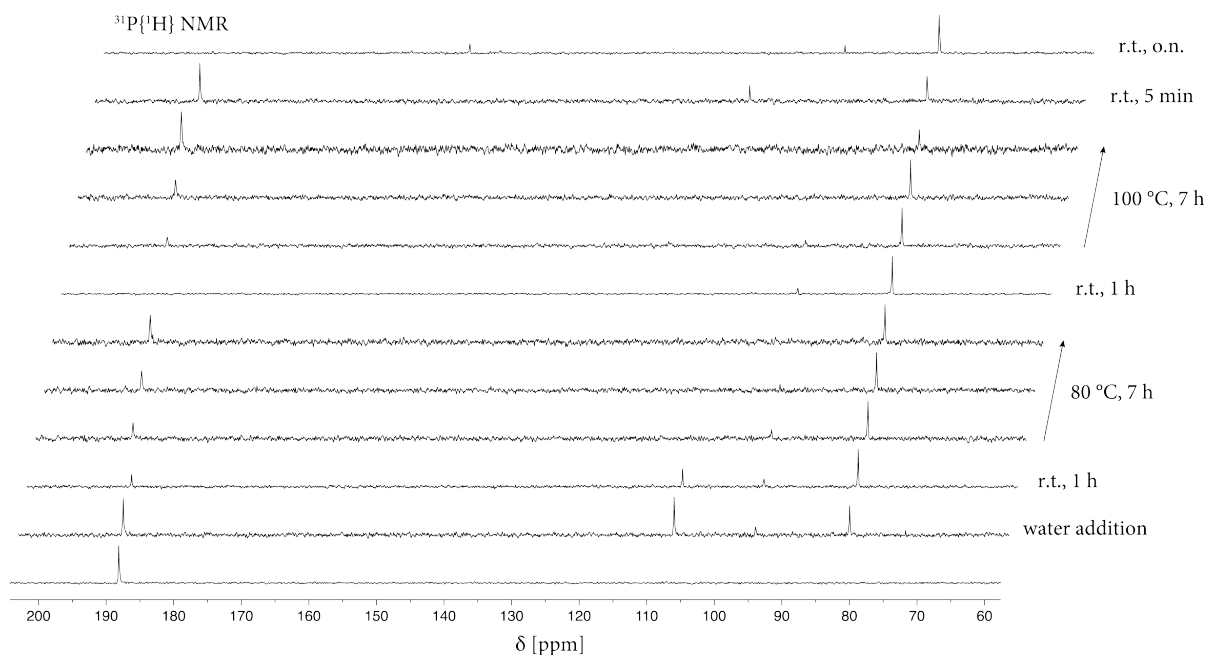


Figure 3-14: Time and temperature dependent ^{31}P NMR experiments of $[(\text{P},\text{N})\text{Re}(\text{CO})_3\text{Br}]$ -complex **3.5a** with water in DCM.

These time and temperature dependent NMR experiments show an unselective but rather unusual reversible water addition reaction to $[(\text{P},\text{N})\text{Re}(\text{CO})_3\text{X}]$ -type complexes that can be reversed and then repeated in cycles of heating and cooling down. However, the number of repetitions is limited. Already after two cycles the appearance of a new signal can be detected at $\delta = 150.0$ ppm. Leaving the reaction mixture at room temperature for several days, a multitude of resonances for unidentified decomposition products around $\delta = 135$ - 155 ppm have appeared in the $^{31}\text{P}\{^1\text{H}\}$ NMR spectra.

^1H NMR spectroscopy shows several characteristic doublet of doublet resonances between $\delta = 4.00$ and 7.00 ppm for the added proton and the proton in α -position to it. These values match well with literature values of rhodium ($\delta = 4.78$ (dd, $^3J_{\text{H-H}} = 2.8$, $^2J_{\text{H-P}} = 12.0$ Hz) and 6.53 ppm (dd, $^3J_{\text{H-H}} = 2.4$, $^3J_{\text{H-P}} = 8.0$ Hz)) and iridium ($\delta = 4.61$ (dd, $^3J_{\text{H-H}} = 2.8$, $^2J_{\text{H-P}} = 12.4$ Hz) and 6.66 ppm (brd, $^3J_{\text{H-P}} = 9.6$ Hz)) compounds **3.10** and **3.11**.¹⁰¹ An exact interpretation of ^1H NMR spectra, however, is not possible due to the number of compounds in the reaction mixture.

Crystallisation of at least one of the water addition products to allow assignment of the four resonances in ^{31}P NMR to the four pairs of enantiomers was tried but, unfortunately, remained unsuccessful. Considering a number of nine kinetically unstable molecules in equilibrium with each other in the solution for crystallisation, this is not surprising.

However, the lack of crystallographic and ^1H NMR data prohibits determination of major and minor or kinetic and thermodynamic products in this equilibrium reaction up to this point.

3.5 Experimental Data

General Remarks

Experiments performed under an inert argon atmosphere were carried out using modified Schlenk techniques or in a MBraun dry box. All common chemicals were commercially available and purchased from Aldrich Chemical Co., ABCR, Alfa Aesar, Acros as well as Eurisol and were used as received. Dry or deoxygenated solvents were prepared using standard techniques or used from a MBraun MB SBS-800 solvent purification system. Tetrahydrofuran and diethyl ether were distilled under argon over potassium/benzophenone and sodium/benzophenone, respectively.

The ^1H , $^{13}\text{C}\{^1\text{H}\}$, ^{19}F and $^{31}\text{P}\{^1\text{H}\}$ NMR spectra were recorded on a JEOL EXZ400 (400 MHz) or a JEOL ECX400 (400 MHz) FT spectrometer and chemical shifts are reported relative to the residual resonance of the deuterated solvents. The mass characterizations have been performed on an Agilent 6210 ESI-TOF instrument by Agilent Technologies with standard settings of 5 L/min, 4 kV and 15 psi for ESI-TOF. All other parameters have been optimized for each substance. IR spectra were measured on a Nicolet iS10 FTIR-ATR spectrometer by Thermo Scientific.

The numbering of atoms is continuous in NMR spectra and molecular structures in the crystal as well as through the complete synthetic pathway (Figure 3-15). Hydrogen atoms bear the same number as the carbon they are attached to.

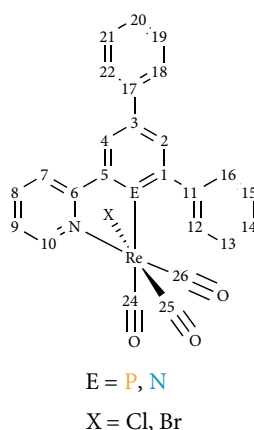


Figure 3-15: Numbering of atoms.

Synthetic Procedures

P,N-Rhenium(I) Carbonyl Complexes

In a dry box, phosphinine (**3a-d**, 0.1 mmol) dissolved in dry toluene (0.5 mL) was added to pentacarbonyl rhenium(I) halide (0.1 mmol) in a Young-NMR-tube. After heating to $T = 80\text{ }^{\circ}\text{C}$ over night, the bright yellow precipitate was filtered off and washed with a very small amount of toluene ($\approx 0.2\text{ mL}$) inside a dry box. Drying under vacuum gave the products as yellow solids.

2-(2-Pyridyl)-4,6-diphenylphosphinine-P,N-rhenium(I) tricarbonyl chloride (**3.4a**)

Pyridylphosphinine **3.2a** (15 mg, 0.046 mmol) and $[\text{Re}(\text{CO})_5\text{Cl}]$ (17 mg, 0.047 mmol) gave the product (21 mg, 0.034 mmol, 74%) as yellow crystals.

^1H NMR (401 MHz, CD_2Cl_2): $\delta = 7.42$ (ddt, $J = 7.1, 5.7, 1.3\text{ Hz}$, 1 H), 7.46 - 7.66 (m, 6 H), 7.67 - 7.74 (m, 2 H), 7.83 - 7.91 (m, 2 H), 8.05 - 8.12 (m, 1 H), 8.30 - 8.36 (m, 1 H), 8.44 (dd, $J = 19.6, 1.4\text{ Hz}$, 1 H), 8.66 (dd, $J = 15.6, 1.5\text{ Hz}$, 1 H), 9.21 - 9.27 (m, 1 H) ppm;

$^{13}\text{C}\{^1\text{H}\}$ NMR (101 MHz, CD_2Cl_2): $\delta = 121.2$ (d, $J_{\text{C-P}} = 12.7\text{ Hz}$), 126.8 (d, $J_{\text{C-P}} = 3.3\text{ Hz}$), 128.3 (d, $J_{\text{C-P}} = 2.5\text{ Hz}$), 129.0 (d, $J_{\text{C-P}} = 11.2\text{ Hz}$), 129.3, 129.9, 130.0, 130.1, 132.9 (d, $J_{\text{C-P}} = 13.7\text{ Hz}$), 138.5 (d, $J = 12.3\text{ Hz}$), 138.9 (d, $J = 15.0\text{ Hz}$), 140.3, 141.6 (d, $J = 4.7\text{ Hz}$), 143.3 (d, $J = 24.1\text{ Hz}$), 158.2 (d, $J_{\text{C-P}} = 2.9\text{ Hz}$), 158.6 (d, $J_{\text{C-P}} = 23.0\text{ Hz}$), 159.3 (d, $J_{\text{C-P}} = 21.3\text{ Hz}$), 159.7 (d, $J_{\text{C-P}} = 16.0\text{ Hz}$), 185.7 (d, $J_{\text{C-P}} = 11.6\text{ Hz}$), 193.5 (d, $J_{\text{C-P}} = 52.4\text{ Hz}$), 194.0 (d, $J_{\text{C-P}} = 32.1\text{ Hz}$) ppm;

$^{31}\text{P}\{^1\text{H}\}$ NMR (162 MHz, CD_2Cl_2): $\delta = 189.6$ ppm;

FT-IR (solid ATR): $\tilde{\nu}(\text{CO})$ 2029, 1947, 1937, 1905 (sh), 1880 cm^{-1} .

2-(2-Pyridyl)-4,6-diphenylphosphinine-P,N-rhenium(I) tricarbonyl bromide (**3.5a**)

Pyridylphosphinine **3.2a** (16 mg, 0.049 mmol) and $[\text{Re}(\text{CO})_5\text{Cl}]$ (19 mg, 0.047 mmol) gave the product (21 mg, 0.032 mmol, 68%) as yellow crystals.

^1H NMR (401 MHz, CD_2Cl_2): $\delta = 7.40$ (ddt, $J = 7.3, 5.8, 1.3\text{ Hz}$, 1 H), 7.46 - 7.65 (m, 6H), 7.66 - 7.74 (m, 2 H), 7.83 - 7.91 (m, 2 H), 8.04 - 8.12 (m, 1 H), 8.29 - 8.36 (m, 1 H), 8.45 (dd, $J = 19.9, 1.4\text{ Hz}$, 1 H), 8.66 (dd, $J = 15.7, 1.4\text{ Hz}$, 1 H), 9.23 - 9.27 (m, 1 H) ppm;

$^{13}\text{C}\{^1\text{H}\}$ NMR (101 MHz, CD_2Cl_2): $\delta = 121.3$ (d, $J_{\text{C-P}} = 12.7\text{ Hz}$), 126.6 (d, $J_{\text{C-P}} = 3.6\text{ Hz}$), 128.3 (d, $J_{\text{C-P}} = 2.9\text{ Hz}$), 129.1 (d, $J_{\text{C-P}} = 11.1\text{ Hz}$), 129.2, 129.9, 129.9 (d, $J = 2.0\text{ Hz}$), 130.1, 132.8 (d,

$J_{C-P} = 13.7$ Hz), 138.5 (d, $J = 12.2$ Hz), 138.8 (d, $J = 14.9$ Hz), 140.2, 141.5 (d, $J = 5.0$ Hz), 143.2 (d, $J = 24.1$ Hz), 158.1 (d, $J_{C-P} = 2.9$ Hz), 158.3 (d, $J_{C-P} = 3.2$ Hz), 158.5 (d, $J_{C-P} = 22.5$ Hz), 159.8 (d, $J_{C-P} = 15.9$ Hz), 185.2 (d, $J_{C-P} = 11.5$ Hz), 192.9 (d, $J_{C-P} = 40.9$ Hz), 193.4 (d, $J_{C-P} = 40.5$ Hz) ppm;

$^{31}\text{P}\{^1\text{H}\}$ NMR (162 MHz, CD_2Cl_2): $\delta = 188.1$ ppm;

ESI-TOF (m/z): 669.9649 (calc.: 669.9552 g/mol) $[\text{M} - \text{CO} + \text{Na}]^+$, 613.9751 (calc.: 613.9659 g/mol) $[\text{M} - 3 \text{CO} + \text{Na}]^+$, 568.0624 (calc.: 568.0476 g/mol) $[\text{M} - \text{CO} - \text{Br}]^+$;

FT-IR (solid ATR): $\tilde{\nu}(\text{CO})$ 2026, 1935 (sh), 1899 cm^{-1} .

2-(2-Pyridyl)-4-(4-fluorophenyl)-6-phenylphosphinine-P,N-rhenium(I) tricarbonyl chloride (3.4b)

^1H NMR (401 MHz, CD_2Cl_2): $\delta = 7.25$ (m, 2 H, $\text{H}_{19/21}$), 7.37 - 7.41 (m, 1 H, H_9), 7.54 - 7.58 (m, 1 H, H_{14}), 7.58 - 7.64 (m, 2 H, $\text{H}_{13/15}$), 7.64 - 7.70 (m, 2 H, $\text{H}_{18/22}$), 7.81 - 7.91 (m, 2 H, $\text{H}_{12/16}$), 8.01 - 8.12 (m, 1 H, H_8), 8.28 - 8.37 (m, 1 H, H_7), 8.38 (dd, $J = 19.8, 1.4$ Hz, 1 H, H_2 or H_4), 8.60 (dd, $J = 15.7, 1.4$ Hz, 1 H, H_2 or H_4), 9.20 - 9.29 (m, 1 H, H_{10}) ppm;

^{19}F NMR (376 MHz, CD_2Cl_2): $\delta = -113.7$ (m_s) ppm;

$^{31}\text{P}\{^1\text{H}\}$ NMR (162 MHz, CD_2Cl_2): $\delta = 188.1$ ppm.

2-(2-Pyridyl)-4-(4-fluorophenyl)-6-phenylphosphinine-P,N-rhenium(I) tricarbonyl bromide (3.5b)

^1H NMR (400 MHz, CD_2Cl_2): $\delta = 7.22$ (m_s , 2 H, $\text{H}_{19/21}$), 7.34 - 7.39 (m, 1 H, H_9), 7.52 - 7.68 (m, 5 H, H_{14} , $\text{H}_{13/15}$, $\text{H}_{18/22}$), 7.81 - 7.85 (m, 2 H, $\text{H}_{12/16}$), 7.98 - 8.04 (m, 1 H, H_8), 8.29 - 8.32 (m, 1 H, H_7), 8.33 (dd, $^3J_{H-P} = 19.7$, $^4J_{H-H} = 1.4$ Hz, 1 H, H_2 or H_4), 8.53 (dd, $^3J_{H-P} = 15.7$, $^4J_{H-H} = 1.4$ Hz, 1 H, H_2 or H_4), 9.20 (ddd, $J = 5.7, 1.7, 0.8$ Hz, 1 H, H_{10}) ppm;

$^{13}\text{C}\{^1\text{H}\}$ NMR (101 MHz, CD_2Cl_2): $\delta = 116.8$ (d, $J_{C-F} = 21.8$ Hz, $\text{C}_{19/21}$), 121.4 (d, $J_{C-P} = 12.7$ Hz, C_7), 126.7 (d, $J_{C-P} = 3.5$ Hz, C_9), 129.1 (d, $J_{C-P} = 11.1$ Hz, $\text{C}_{12/16}$), 130.0 (d, $J_{C-P} = 2.1$ Hz, C_{14}), 130.1 ($\text{C}_{13/15}$), 130.2 (dd, $J_{C-F} = 8.4$ Hz, $J_{C-P} = 2.0$ Hz, $\text{C}_{18/22}$), 132.6 (d, $J_{C-P} = 13.7$ Hz, C_2 or C_4), 137.7 (dd, $J_{C-P} = 5.1$ Hz, $J_{C-F} = 3.3$ Hz, C_{17}), 138.3 (d, $J_{C-P} = 12.2$ Hz, C_2 or C_4), 138.8 (d, $J_{C-P} = 15.0$ Hz, C_{11}), 140.2 (C_8), 142.1 (d, $J_{C-P} = 24.3$ Hz, C_3), 158.3 (d, $J_{C-P} = 23.9$ Hz, C_1), 158.3 (d, $J_{C-P} = 3.2$ Hz, C_{10}), 158.6 (d, $J_{C-P} = 22.4$ Hz, C_5), 159.8 (d, $J_{C-P} = 16.2$ Hz, C_6), 163.8 (d, $J_{C-F} = 247.6$ Hz, C_{20}), 185.2 (d, $J_{C-P} = 11.5$ Hz, CO), 192.9 (d, $J_{C-P} = 37.0$ Hz, CO), 193.4 (d, $J_{C-P} = 43.7$ Hz, CO) ppm;

^{19}F NMR (376 MHz, CD_2Cl_2): $\delta = -113.7$ (m_s) ppm;

$^{31}\text{P}\{^1\text{H}\}$ NMR (162 MHz, CD_2Cl_2): $\delta = 189.9$ ppm.

2-(2-Pyridyl)-4-(4-methoxyphenyl)-6-phenylphosphinine-P,N-rhenium(I) tricarbonyl chloride (3.4d)

^1H NMR (400 MHz, CD_2Cl_2): δ = 3.87 (s, 3 H, MeO), 7.06 (m, 2 H, $\text{H}_{19/21}$), 7.35 - 7.40 (m, 1 H, H_9), 7.52 - 7.65 (m, 5 H, H_{14} , $\text{H}_{13/15}$, $\text{H}_{18/22}$), 7.81 - 7.86 (m, 2 H, $\text{H}_{12/16}$), 8.00 - 8.06 (m, 1 H, H_8), 8.29 - 8.33 (m, 1 H, H_7), 8.37 (dd, $^3J_{\text{H-P}} = 19.8$, $^4J_{\text{H-H}} = 1.4$ Hz, 1 H, H_2), 8.58 (dd, $^3J_{\text{H-P}} = 15.5$ Hz, $^4J_{\text{H-H}} = 1.4$ Hz, 1 H, H_4), 9.21 (ddd, $J = 5.6, 1.7, 0.7$ Hz, 1 H, H_{10}) ppm;

$^{13}\text{C}\{^1\text{H}\}$ NMR (101 MHz, CD_2Cl_2): δ = 56.0 (MeO), 115.3 ($\text{C}_{19/21}$), 121.3 (d, $J_{\text{C-P}} = 12.6$ Hz, C_7), 126.7 (d, $J_{\text{C-P}} = 3.4$ Hz, C_9), 129.0 (d, $J_{\text{C-P}} = 11.2$ Hz, $\text{C}_{12/16}$), 129.5 (d, $J_{\text{C-P}} = 2.8$ Hz, $\text{C}_{18/22}$), 129.9 (d, $J_{\text{C-P}} = 2.0$ Hz, C_{14}), 130.1 ($\text{C}_{13/15}$), 132.4 (d, $J_{\text{C-P}} = 13.7$ Hz, C_4), 133.6 (d, $J_{\text{C-P}} = 5.2$ Hz, C_{17}), 137.9 (d, $J_{\text{C-P}} = 12.5$ Hz, C_2), 138.9 (d, $J_{\text{C-P}} = 15.1$ Hz, C_{11}), 140.2 (C_8), 143.0 (d, $J_{\text{C-P}} = 24.1$ Hz, C_3), 158.1 (d, $J_{\text{C-P}} = 3.1$ Hz, C_{10}), 158.5 (d, $J_{\text{C-P}} = 23.0$ Hz, C_1), 159.3 (d, $J_{\text{C-P}} = 21.6$ Hz, C_5), 159.7 (d, $J_{\text{C-P}} = 16.4$ Hz, C_6), 160.9 (C_{20}), 185.8 (d, $J_{\text{C-P}} = 11.3$ Hz, CO), 193.6 (d, $J_{\text{C-P}} = 54.0$ Hz, CO), 194.1 (d, $J_{\text{C-P}} = 29.1$ Hz, CO) ppm;

$^{31}\text{P}\{^1\text{H}\}$ NMR (162 MHz, CD_2Cl_2): δ = 185.9 ppm.

NN,-Rhenium(I) Carbonyl Complexes

Bipyridine (**2.4a-h**, 0.1 mmol) dissolved in DCM (0.5 mL) was added to pentacarbonyl rhenium(I) halide (0.1 mmol) in a NMR-tube. After heating to $T = 40$ °C for $t = 4$ h, the bright yellow precipitate was filtered off and washed with a very small amount of cold DCM (≈ 0.2 mL). Drying under vacuum gave the products as yellow solids.

2-(2-Pyridyl)-4,6-diphenylpyridine-N,N-rhenium(I) tricarbonyl chloride (3.6a)

Bipyridine **3.3a** (36 mg, 0.117 mmol) and $[\text{Re}(\text{CO})_5\text{Cl}]$ (43 mg, 0.119 mmol) gave the product (58 mg, 0.095 mmol, 81%) as yellow crystals. Crystals suitable for X-ray diffraction were obtained from a NMR-solution in $\text{DMSO}-d_6$.

^1H NMR (400 MHz, $\text{DMSO}-d_6$): δ = 7.55 - 7.75 (m, broad, 8 H, $\text{H}_{12/16}$, $\text{H}_{13/15}$, H_{14} , $\text{H}_{19/21}$, H_{20}), 7.75 - 7.81 (m, 1 H, H_9), 8.10 (d, $J = 2.1$ Hz, 1 H, H_2), 8.17 - 8.24 (m, 2 H, $\text{H}_{18/22}$), 8.35 - 8.42 (m, 1 H, H_8), 8.97 (d, $J = 1.8$ Hz, 1 H, H_4), 8.95 - 8.98 (m, 1 H, H_7), 9.02 - 9.05 (m, 1 H, H_{10}) ppm;

$^{13}\text{C}\{^1\text{H}\}$ NMR (101 MHz, $\text{DCM}-d_2$): δ = 120.4 (C_4), 124.9 (C_2), 125.8 (C_7), 127.9 (C_9), 128.2 ($\text{C}_{18/22}$), 129.6 ($\text{C}_{12/16}$ or $\text{C}_{13/15}$), 129.8 ($\text{C}_{19/21}$), 130.4 (C_{14}), 131.3 (C_{20}), 135.2 (C_{17}), 140.4 (C_8), 142.1 (C_{11}), 150.9 (C_3), 153.1 (C_{10}), 156.5 (C_5 or C_6), 157.3 (C_5 or C_6), 163.7 (C_1), 191.6 (CO), 194.0 (CO), 198.0 (CO) ppm;

ESI-TOF (m/z): 653.0046 (calc.: 653.0044 g/mol) [M + K]⁺, 637.0306 (calc.: 637.0305 g/mol) [M + Na]⁺, 579.0727 (calc.: 579.0719 g/mol) [M - Cl]⁺;

FT-IR (solid ATR): $\tilde{\nu}(\text{CO})$ 2017, 1938, 1907, 1864 cm⁻¹.

Crystallographic data: C₂₅H₁₆ClN₂O₃Re, C₂H₆OS, *Fw* = 692.19, 0.40×0.08×0.08 mm³, yellow needle, triclinic, *P* $\bar{1}$, *a* = 13.1175(2), *b* = 14.7724(2), *c* = 15.4793(2) Å, α = 63.659(1)°, β = 73.626(1)°, γ = 73.403(1)°, *V* = 2533.70(7) Å³, *Z* = 4, *D*_x = 1.815 gcm⁻³, μ = 5.02 mm⁻¹. 65116 reflections were measured by using a Bruker D8-Venture Photon area detector (MoK α radiation, λ = 0.71073 Å) up to a resolution of (sin θ / λ)_{max} = 0.63 Å⁻¹ at a temperature of 100 K. The reflections were corrected for absorption and scaled on the basis of multiple measured reflections by using the SADABS program (0.17–0.29 correction range).¹⁶⁷ 9126 reflections were unique (*R*_{int} = 0.040). Using ShelXle, the structures were solved with SHELXS-97 by using direct methods and refined with SHELXL-97 on *F*² for all reflections.^{201,202} Non-hydrogen atoms were refined by using anisotropic displacement parameters. The positions of the hydrogen atoms were calculated for idealized positions. 653 parameters were refined without restraints. *R*₁ = 0.022 for 9126 reflections with *I* > 2 σ (*I*) and *wR*₂ = 0.084 for 10424 reflections, *S* = 0.711, residual electron density was between -1.16 and 1.57 eÅ⁻³. Geometry calculations and checks for higher symmetry were performed with the PLATON program.¹⁶⁶ A .cif data file can be found in the attachments.

2-(2-Pyridyl)-4,6-diphenylpyridine-N,N-rhenium(I) tricarbonyl bromide (3.7a)

Bipyridine **3.2a** (36 mg, 0.117 mmol) and [Re(CO)₅Cl] (48 mg, 0.118 mmol) gave the product (54 mg, 0.082 mmol, 70%) as yellow crystals. The molecular structure in the crystal is known already.¹⁹¹

¹H NMR (400 MHz, DMSO-*d*₆): δ = 7.54 – 7.73 (m, broad, 8 H, H_{12/16}, H_{13/15}, H₁₄, H_{19/21}, H₂₀), 7.73 – 7.78 (m, 1 H, H₉), 8.04 (d, *J* = 1.9 Hz, 1 H, H₂), 8.12 – 8.16 (m, 2 H, H_{18/22}), 8.30 – 8.36 (m, 1 H, H₈), 8.98 (d, *J* = 1.9 Hz, 1 H, H₄), 9.00 – 9.04 (m, 1 H, H₇), 9.04 – 9.07 (m, 1 H, H₁₀) ppm;

¹³C{¹H} NMR (101 MHz, DMSO-*d*₆): δ = 120.4 (C₄), 124.9 (C₂), 125.7 (C₇), 127.8 (C₉), 128.1 (C_{18/22}), 129.4 (C_{12/16} or C_{13/15}), 129.8 (C_{19/21}), 130.3 (C₁₄), 131.3 (C₂₀), 135.1 (C₁₇), 140.3 (C₈), 142.2 (C₁₁), 150.8 (C₃), 153.2 (C₁₀), 157.0 (C₅ or C₆), 157.3 (C₅ or C₆), 163.9 (C₁), 190.9 (CO), 193.5 (CO), 197.7 (CO) ppm;

ESI-TOF (m/z): 680.9794 (calc.: 680.9800 g/mol) [M + Na]⁺, 607.0710 (calc.: 607.0668 g/mol) [M - Br + CO]⁺, 579.0729 (calc.: 579.0719 g/mol) [M - Br]⁺, 551.0776 (calc.: 551.0769 g/mol) [M - Br - CO]⁺, 523.0867 (calc.: 523.0820 g/mol) [M - Br - 2 CO]⁺;

FT-IR (solid ATR): $\tilde{\nu}(\text{CO})$ 2018, 1940, 1911, 1867 cm⁻¹.

2-(2-Pyridyl)-4-(4-fluorophenyl)-6-phenylpyridine-N,N-rhenium(I) tricarbonyl chloride (3.6b)

Bipyridine **3.3b** (32 mg, 0.098 mmol) and $[\text{Re}(\text{CO})_5\text{Cl}]$ (36 mg, 0.100 mmol) gave the product (51 mg, 0.081 mmol, 82%) as yellow crystals. Crystals suitable for X-ray diffraction were obtained from cooling down a DCM solution.

^1H NMR (400 MHz, $\text{DMSO}-d_6$): $\delta = 7.42 - 7.49$ (m, 2 H, $\text{H}_{19/21}$), $7.54 - 7.75$ (m, broad, 5 H, $\text{H}_{12/16}$, $\text{H}_{13/15}$, H_{14}), $7.75 - 7.80$ (m, 1 H, H_9), 8.09 (d, $J = 1.9$ Hz, 1 H, H_2), $8.26 - 7.32$ (m, 2 H, $\text{H}_{18/22}$), $8.33 - 8.41$ (m, 1 H, H_8), 9.02 (d, $J = 1.9$ Hz, 1 H, H_4), $9.04 - 9.10$ (m, 2 H, H_{10} , H_7) ppm;

$^{13}\text{C}\{^1\text{H}\}$ NMR (101 MHz, $\text{DMSO}-d_6$): $\delta = 116.3$ (d, $^2J_{\text{C-F}} = 21.7$ Hz, $\text{C}_{19/21}$), 120.0 (d, C_4), 124.5 (C_2), 125.5 (C_7), 127.5 (C_9), 129.3 ($\text{C}_{12/16}$ or $\text{C}_{13/15}$), 129.9 (C_{14}), 130.5 (d, $^3J_{\text{C-F}} = 8.8$ Hz, $\text{C}_{18/22}$), 131.3 (C_{17}), 139.9 (C_8), 141.7 (C_{11}), 149.3 (C_3), 152.7 (C_{10}), 156.6 (C_5 or C_6), 156.9 (C_5 or C_6), 162.6 (C_1), 163.9 (d, $^1J_{\text{C-F}} = 249.4$ Hz, C_{20}), 191.2 (CO), 193.7 (CO), 197.7 (CO) ppm;

^{19}F NMR (376 MHz, $\text{DMSO}-d$): $\delta = -110.0$ (m_s) ppm;

ESI-TOF (m/z): 670.9937 (calc.: 670.9950 g/mol) $[\text{M} + \text{K}]^+$, 655.0201 (calc.: 655.0210 g/mol) $[\text{M} + \text{Na}]^+$, 625.0592 (calc.: 625.0574 g/mol) $[\text{M} - \text{Cl} + \text{CO}]^+$, 597.0631 (calc.: 597.0624 g/mol) $[\text{M} - \text{Cl}]^+$, 569.0657 (calc.: 569.0675 g/mol) $[\text{M} - \text{Cl} - \text{CO}]^+$, 541.0718 (calc.: 541.0726 g/mol) $[\text{M} - \text{Cl} - 2 \text{CO}]^+$;

FT-IR (solid ATR): $\tilde{\nu}(\text{CO})$ 2014, 1914, 1871, 1852 (sh) cm^{-1} .

Crystallographic data: $\text{C}_{25}\text{H}_{15}\text{FClN}_2\text{O}_3\text{Re}$, CH_2Cl_2 , $F_w = 716.98$, $0.75 \times 0.02 \times 0.02$ mm^3 , yellow needle, monoclinic, $P2_1/c$, $a = 7.4816(4)$, $b = 19.8766(10)$, $c = 17.1967(9)$ \AA , $\beta = 99.301(2)^\circ$, $V = 2523.7(2)$ \AA^3 , $Z = 4$, $D_x = 1.887$ gcm^{-3} , $\mu = 5.17$ mm^{-1} . 97039 reflections were measured by using a Bruker D8-Venture Photon area detector (MoK α radiation, $\lambda = 0.71073$ \AA) up to a resolution of $(\sin\theta/\lambda)_{\text{max}} = 0.63$ \AA^{-1} at a temperature of 100 K. The reflections were corrected for absorption and scaled on the basis of multiple measured reflections by using the SADABS program (0.60–0.75 correction range).¹⁶⁷ 5002 reflections were unique ($R_{\text{int}} = 0.032$). Using Olex,²⁰³ the structures were solved with SHELXS-97 by using direct methods and refined with SHELXL-97 on F^2 for all reflections.²⁰¹ Non-hydrogen atoms were refined by using anisotropic displacement parameters. The positions of the hydrogen atoms were calculated for idealized positions. 330 parameters were refined without restraints. $R_1 = 0.025$ for 5002 reflections with $I > 2\sigma(I)$ and $wR_2 = 0.057$ for 5236 reflections, $S = 1.127$, residual electron density was between -2.37 and 0.62 $\text{e}\text{\AA}^{-3}$. Geometry calculations and checks for higher symmetry were performed with the PLATON program.¹⁶⁶ A .cif data file can be found in the attachments.

2-(2-Pyridyl)-4-(4-fluorophenyl)-6-phenylpyridine-N,N-rhenium(I) tricarbonyl bromide (3.7b)

Bipyridine **3.3b** (33 mg, 0.101 mmol) and [Re(CO)₅Br] (41 mg, 0.1009 mmol) gave the product (46 mg, 0.068 mmol, 67%) as yellow crystals. Crystals suitable for X-ray diffraction were obtained from a reaction mixture in DCM.

¹H NMR (400 MHz, DMSO-*d*₆): δ = 7.42 – 7.49 (m, 2 H, H_{19/21}), 7.55 – 7.75 (m, broad, 5 H, H_{12/16}, H_{13/15}, H₁₄), 7.77 (ddd, *J* = 7.5, 5.5, 1.2 Hz, 1 H, H₉), 8.10 (d, *J* = 1.9 Hz, 1 H, H₂), 8.27 – 7.34 (m, 2 H, H_{18/22}), 8.34 – 8.41 (m, 1 H, H₈), 9.04 (d, *J* = 1.9 Hz, 1 H, H₄), 9.06 – 9.12 (m, 2 H, H₁₀, H₇) ppm;

¹³C{¹H} NMR (101 MHz, DMSO-*d*₆): δ = 116.3 (d, ²*J*_{C-F} = 21.7 Hz, C_{19/21}), 120.1 (d, C₄), 124.5 (C₂), 125.5 (C₇), 127.5 (C₉), 129.2 (C_{12/16} or C_{13/15}), 129.9 (C₁₄), 130.6 (d, ³*J*_{C-F} = 8.8 Hz, C_{18/22}), 131.3 (d, ⁴*J*_{C-F} = 3.0 Hz, C₁₇), 139.9 (C₈), 141.9 (C₁₁), 149.2 (C₃), 152.9 (C₁₀), 156.7 (C₅ or C₆), 156.9 (C₅ or C₆), 163.7 (C₁), 163.9 (d, ¹*J*_{C-F} = 249.5 Hz, C₂₀), 190.6 (CO), 193.7 (CO), 197.4 (CO) ppm;

¹⁹F NMR (376 MHz, DMSO-*d*): δ = -109.9 (tt, ³*J*_{F-H} = 8.8 Hz, ⁴*J*_{F-H} = 5.3 Hz) ppm;

ESI-TOF (*m/z*): 670.9937 (calc.: 670.9950 g/mol) [M + K]⁺, 698.9672 (calc.: 698.9705 g/mol) [M + Na]⁺, 625.0739 (calc.: 625.0574 g/mol) [M - Br + CO]⁺, 597.0660 (calc.: 597.0624 g/mol) [M - Br]⁺, 569.0649 (calc.: 569.0675 g/mol) [M - Br - CO]⁺, 541.0724 (calc.: 541.0726 g/mol) [M - Br - 2 CO]⁺;

FT-IR (solid ATR): $\tilde{\nu}$ (CO) 2017, 1958 (sh), 1914, 1874 cm⁻¹.

Crystallographic data: C₂₅H₁₅FBrN₂O₃Re, CD₂Cl₂, *F*_w = 763.43, 0.35×0.05×0.03 mm³, yellow needle, monoclinic, *P*2₁/*c*, *a* = 7.5465(2), *b* = 20.0061(5), *c* = 17.3842(5) Å, β = 99.904(1)°, *V* = 2585.48(12) Å³, *Z* = 4, *D*_x = 1.961 gcm⁻³, μ = 6.49 mm⁻¹. 20982 reflections were measured by using a Bruker D8-Venture Photon area detector (MoKα radiation, λ = 0.71073 Å) up to a resolution of (sinθ/λ)_{max} = 0.63 Å⁻¹ at a temperature of 100 K. The reflections were corrected for absorption and scaled on the basis of multiple measured reflections by using the SADABS program (0.60–0.75 correction range).¹⁶⁷ 4858 reflections were unique (*R*_{int} = 0.020). Using Olex,²⁰³ the structures were solved with SHELXS-97 by using direct methods and refined with SHELXL-97 on *F*² for all reflections.²⁰¹ Non-hydrogen atoms were refined by using anisotropic displacement parameters. The positions of the hydrogen atoms were calculated for idealized positions. 343 parameters were refined without restraints. *R*₁ = 0.017 for 4858 reflections with *I* > 2σ(*I*) and *wR*₂ = 0.051 for 5265 reflections, *S* = 1.226, residual electron density was between -0.89 and 0.67 eÅ⁻³. Geometry calculations and checks for higher symmetry were performed with the PLATON program.¹⁶⁶ A .cif data file can be found in the attachments.

2-(2-Pyridyl)-4-(4-methoxyphenyl)-6-phenylpyridine-N,N-rhenium(I) tricarbonyl chloride (3.6d)

Bipyridine **3.3d** (25 mg, 0.074 mmol) and $[\text{Re}(\text{CO})_5\text{Cl}]$ (26 mg, 0.072 mmol) gave the product (30 mg, 0.046 mmol, 64%) as yellow crystals. Crystals suitable for X-ray diffraction were obtained from a NMR solution in $\text{DMSO}-d_6$.

^1H NMR (401 MHz, $\text{DMSO}-d_6$): δ = 3.87 (s, 3 H, MeO), 7.10 – 7.18 (m, 2 H, $\text{H}_{19/21}$), 7.54 – 7.74 (m, broad, 5 H, $\text{H}_{12/16}$, $\text{H}_{13/15}$, H_{14}), 7.74 – 7.79 (m, 1 H, H_9), 8.04 (d, J = 1.9 Hz, 1 H, H_2), 8.17 – 8.24 (m, 2 H, $\text{H}_{18/22}$), 8.34 – 8.41 (m, 1 H, H_8), 8.98 (d, J = 2.0 Hz, 1 H, H_4), 9.03 – 9.11 (m, 2 H, H_7 , H_{10}) ppm;

$^{13}\text{C}\{^1\text{H}\}$ NMR (101 MHz, $\text{DMSO}-d_6$): δ = 55.5 (MeO), 114.8 ($\text{C}_{19/21}$), 119.2 (C_4), 123.5 (C_2), 125.4 (C_7), 126.8 (C_{17}), 127.3 (C_9), 129.2 ($\text{C}_{12/16}$ or $\text{C}_{13/15}$), 129.5 ($\text{C}_{18/22}$), 129.8 (C_{14}), 139.8 (C_8), 141.9 (C_{11}), 149.9 (C_3), 152.6 (C_{10}), 156.7 (C_5), 156.7 (C_6), 161.6 (C_{20}), 163.1 (C_1), 191.2 (CO), 193.7 (CO), 197.7 (CO) ppm;

ESI-TOF (m/z): 683.0121 (calc.: 683.0150 g/mol) $[\text{M} + \text{K}]^+$, 667.0386 (calc.: 667.0410 g/mol) $[\text{M} + \text{Na}]^+$, 609.0811 (calc.: 609.0824 g/mol) $[\text{M} - \text{Cl}]^+$, 581.0860 (calc.: 581.0875 g/mol) $[\text{M} - \text{Cl} - \text{CO}]^+$, 553.0953 (calc.: 553.0926 g/mol) $[\text{M} - \text{Cl} - 2 \text{CO}]^+$;

FT-IR (solid ATR): $\tilde{\nu}(\text{CO})$ 2014, 1912, 1859, 1842 (sh) cm^{-1} .

Crystallographic data: $\text{C}_{26}\text{H}_{18}\text{ClN}_2\text{O}_4\text{Re}$, $F_w = 644.08$, $0.37 \times 0.04 \times 0.03 \text{ mm}^3$, yellow needle, monoclinic, $P2_1/n$, $a = 7.2574(2)$, $b = 17.4715(3)$, $c = 17.6204(4) \text{ \AA}$, $\beta = 98.2501(9)^\circ$, $V = 2211.10(9) \text{ \AA}^3$, $Z = 4$, $D_x = 1.935 \text{ g cm}^{-3}$, $\mu = 5.66 \text{ mm}^{-1}$. 26510 reflections were measured by using a Bruker D8-Venture Photon area detector (MoK α radiation, $\lambda = 0.71073 \text{ \AA}$) up to a resolution of $(\sin\theta/\lambda)_{\text{max}} = 0.63 \text{ \AA}^{-1}$ at a temperature of 100 K. The reflections were corrected for absorption and scaled on the basis of multiple measured reflections by using the SADABS program (0.15–0.23 correction range).¹⁶⁷ 4021 reflections were unique ($R_{\text{int}} = 0.053$). Using ShelXle, the structures were solved with SHELXS-97 by using direct methods and refined with SHELXL-97 on F^2 for all reflections.^{201,202} Non-hydrogen atoms were refined by using anisotropic displacement parameters. The positions of the hydrogen atoms were calculated for idealized positions. 248 parameters were refined without restraints. $R_1 = 0.065$ for 4021 reflections with $I > 2\sigma(I)$ and $wR_2 = 0.153$ for 4524 reflections, $S = 1.365$, residual electron density was between -3.65 and 4.39 e \AA^{-3} . Geometry calculations and checks for higher symmetry were performed with the PLATON program.¹⁶⁶ A .cif data file can be found in the attachments.

2-(2-Pyridyl)-4-(4-methoxyphenyl-6-phenylpyridine-N,N-rhenium(I) tricarbonyl bromide (3.7d)

Bipyridine **3.3d** (26 mg, 0.077 mmol) and $[\text{Re}(\text{CO})_5\text{Cl}]$ (31 mg, 0.076 mmol) gave the product (42 mg, 0.061 mmol, 80%) as yellow crystals.

^1H NMR (401 MHz, $\text{DMSO}-d_6$): $\delta = 3.87$ (s, 3 H, MeO), 7.11 – 7.17 (m, 2 H, $\text{H}_{19/21}$), 7.53 – 7.73 (m, broad, 5 H, $\text{H}_{12/16}$, $\text{H}_{13/15}$, H_{14}), 7.76 (d, $J = 7.6, 5.5, 1.2$ Hz, 1 H, H_9), 8.03 (d, $J = 1.9$ Hz, 1 H, H_2), 8.18 – 8.24 (m, 2 H, $\text{H}_{18/22}$), 8.33 – 8.39 (m, 1 H, H_8), 8.99 (d, $J = 2.0$ Hz, 1 H, H_4), 9.04 – 9.11 (m, 2 H, H_7 , H_{10}) ppm;

$^{13}\text{C}\{^1\text{H}\}$ NMR (101 MHz, $\text{DMSO}-d_6$): $\delta = 55.5$ (MeO), 114.7 ($\text{C}_{19/21}$), 119.2 (C_4), 123.5 (C_2), 125.4 (C_7), 126.7 (C_{17}), 127.4 (C_9), 129.1 ($\text{C}_{12/16}$ or $\text{C}_{13/15}$), 129.5 ($\text{C}_{18/22}$), 129.8 (C_{14}), 139.8 (C_8), 142.0 (C_{11}), 149.8 (C_3), 152.8 (C_{10}), 156.8 (C_5), 156.8 (C_6), 161.6 (C_{20}), 163.3 (C_1), 190.7 (CO), 193.2 (CO), 197.7 (CO) ppm;

ESI-TOF (m/z): 710.9882 (calc.: 710.9905 g/mol) $[\text{M} + \text{Na}]^+$, 637.0830 (calc.: 637.0773 g/mol) $[\text{M} - \text{Br} + \text{CO}]^+$, 609.0825 (calc.: 609.0824 g/mol) $[\text{M} - \text{Br}]^+$, 581.0872 (calc.: 581.0875 g/mol) $[\text{M} - \text{Br} - \text{CO}]^+$, 553.0963 (calc.: 553.0926 g/mol) $[\text{M} - \text{Br} - 2 \text{CO}]^+$;

FT-IR (solid ATR): $\tilde{\nu}(\text{CO})$ 2016, 1914, 1864, 1846 (sh) cm^{-1} .

2-(2-Pyridyl)-4-(4-methylthiophenyl-6-phenylpyridine-N,N-rhenium(I) tricarbonyl chloride (3.6e)

Bipyridine **3.3e** (25 mg, 0.071 mmol) and $[\text{Re}(\text{CO})_5\text{Cl}]$ (26 mg, 0.072 mmol) gave the product (37 mg, 0.056 mmol, 79%) as yellow crystals. Crystals suitable for X-ray diffraction were obtained from a NMR solution in $\text{DMSO}-d_6$.

^1H NMR (401 MHz, $\text{DMSO}-d_6$): $\delta = 2.57$ (s, 3 H, MeS), 7.43 – 7.47 (m, 2 H, $\text{H}_{19/21}$), 7.56 – 7.74 (m, broad, 5 H, $\text{H}_{12/16}$, $\text{H}_{13/15}$, H_{14}), 7.77 (ddd, $J = 7.6, 5.5, 1.2$ Hz, 1 H, H_9), 8.08 (d, $J = 1.8$ Hz, 1 H, H_2), 8.15 – 8.20 (m, 2 H, $\text{H}_{18/22}$), 8.35 – 8.41 (m, 1 H, H_8), 9.01 (d, $J = 2.0$ Hz, 1 H, H_4), 9.03 – 9.07 (m, 1 H, H_{10}), 9.07 – 9.11 (m, 1 H, H_7) ppm;

$^{13}\text{C}\{^1\text{H}\}$ NMR (101 MHz, $\text{DMSO}-d_6$): $\delta = 14.1$ (MeS), 119.5 (C_4), 123.8 (C_2), 125.5 (C_7), 125.8 ($\text{C}_{19/21}$), 127.4 (C_9), 128.2 ($\text{C}_{18/22}$), 129.3 ($\text{C}_{12/16}$ or $\text{C}_{13/15}$), 129.9 (C_{14}), 130.7 (C_{17}), 139.9 (C_8), 141.8 (C_{11}), 142.6 (C_{20}), 149.7 (C_3), 152.7 (C_{10}), 156.7 (C_5 or C_6), 156.8 (C_5 or C_6), 163.2 (C_1), 191.2 (CO), 193.7 (CO), 197.8 (CO) ppm;

ESI-TOF (m/z): 698.9947 (calc.: 698.9921 g/mol) $[\text{M} + \text{K}]^+$, 683.0203 (calc.: 683.0182 g/mol) $[\text{M} + \text{Na}]^+$, 669.0509 (calc.: 669.0494 g/mol) $[\text{M} - \text{Cl} + \text{CO}_2]^+$, 653.0568 (calc.: 653.0545 g/mol) $[\text{M} - \text{Cl} + \text{CO}]^+$, 625.0613 (calc.: 625.0596 g/mol) $[\text{M} - \text{Cl}]^+$, 597.0658 (calc.: 597.0647 g/mol) $[\text{M} - \text{Cl} - \text{CO}]^+$, 569.0742 (calc.: 569.0698 g/mol) $[\text{M} - \text{Cl} - 2 \text{CO}]^+$;

FT-IR (solid ATR): $\tilde{\nu}(\text{CO})$ 2016, 1913, 1862 cm^{-1} .

Crystallographic data: $\text{C}_{26}\text{H}_{18}\text{ClN}_2\text{O}_3\text{ReS}$, $F_w = 660.14$, $0.37 \times 0.02 \times 0.02 \text{ mm}^3$, yellow needle, monoclinic, $P2_1/n$, $a = 7.5393(4)$, $b = 17.0203(11)$, $c = 18.0268(13) \text{ \AA}$, $\beta = 96.823(2)^\circ$, $V = 2296.8(2) \text{ \AA}^3$, $Z = 4$, $D_x = 1.909 \text{ g cm}^{-3}$, $\mu = 5.53 \text{ mm}^{-1}$. 45636 reflections were measured by using a Bruker D8-Venture Photon area detector (MoK α radiation, $\lambda = 0.71073 \text{ \AA}$) up to a resolution of $(\sin\theta/\lambda)_{\text{max}} = 0.63 \text{ \AA}^{-1}$ at a temperature of 99 K. The reflections were corrected for absorption and scaled on the basis of multiple measured reflections by using the SADABS program (0.62–0.75 correction range).¹⁶⁷ 3872 reflections were unique ($R_{\text{int}} = 0.079$). Using ShelXle, the structures were solved with SHELXS-97 by using direct methods and refined with SHELXL-97 on F^2 for all reflections.^{201,202} Non-hydrogen atoms were refined by using anisotropic displacement parameters. The positions of the hydrogen atoms were calculated for idealized positions. 308 parameters were refined without restraints. $R_1 = 0.024$ for 3872 reflections with $I > 2\sigma(I)$ and $wR_2 = 0.039$ for 4734 reflections, $S = 1.056$, residual electron density was between -0.71 and 0.71 e \AA^{-3} . Geometry calculations and checks for higher symmetry were performed with the PLATON program.¹⁶⁶ A .cif data file can be found in the attachments.

2-(2-Pyridyl)-4-(4-methylthiophenyl-6-phenylpyridine-N,N-rhenium(I) tricarbonyl bromide (3.7e)

Bipyridine **3.3e** (27 mg, 0.076 mmol) and $[\text{Re}(\text{CO})_5\text{Cl}]$ (31 mg, 0.076 mmol) gave the product (41 mg, 0.058 mmol, 76%) as yellow crystals. Crystals suitable for X-ray diffraction were obtained from a reaction mixture in DCM.

^1H NMR (401 MHz, DMSO- d_6): $\delta = 2.57$ (s, 3 H, MeS), 7.42 – 7.47 (m, 2 H, $\text{H}_{19/21}$), 7.55 – 7.74 (m, broad, 5 H, $\text{H}_{12/16}$, $\text{H}_{13/15}$, H_{14}), 7.77 (ddd, $J = 7.7, 5.6, 1.2 \text{ Hz}$, 1 H, H_9), 8.06 (d, $J = 1.9 \text{ Hz}$, 1 H, H_2), 8.15 – 8.20 (m, 2 H, $\text{H}_{18/22}$), 8.33 – 8.39 (m, 1 H, H_8), 9.02 (d, $J = 2.0 \text{ Hz}$, 1 H, H_4), 9.05 – 9.11 (m, 2 H, H_{10} , H_7) ppm;

$^{13}\text{C}\{^1\text{H}\}$ NMR (101 MHz, DMSO- d_6): $\delta = 14.1$ (MeS), 119.5 (C_4), 123.8 (C_2), 125.4 (C_7), 125.8 ($\text{C}_{19/21}$), 127.4 (C_9), 128.2 ($\text{C}_{18/22}$), 129.1 ($\text{C}_{12/16}$ or $\text{C}_{13/15}$), 129.8 (C_{14}), 130.6 (C_{17}), 139.8 (C_8), 141.9 (C_{11}), 142.6 (C_{20}), 149.6 (C_3), 152.8 (C_{10}), 156.7 (C_5 or C_6), 156.9 (C_5 or C_6), 163.4 (C_1), 190.6 (CO), 193.1 (CO), 197.4 (CO) ppm;

ESI-TOF (m/z): 742.9413 (calc.: 742.9416 g/mol) $[\text{M} + \text{K}]^+$, 726.9657 (calc.: 726.9677 g/mol) $[\text{M} + \text{Na}]^+$, 653.0642 (calc.: 653.0545 g/mol) $[\text{M} - \text{Br} + \text{CO}]^+$, 641.0593 (calc.: 641.0545 g/mol) $[\text{M} - \text{Br} - \text{CO} + \text{CO}_2]^+$, 625.0599 (calc.: 625.0596 g/mol) $[\text{M} - \text{Br}]^+$, 597.0647 (calc.: 597.0647 g/mol) $[\text{M} - \text{Br} - \text{CO}]^+$, 569.0738 (calc.: 569.0698 g/mol) $[\text{M} - \text{Br} - 2 \text{ CO}]^+$;

FT-IR (solid ATR): $\tilde{\nu}(\text{CO})$ 2015, 1914, 1866 cm^{-1} .

Crystallographic data: $C_{26}H_{18}BrN_2O_4ReS$, $F_w = 704.59$, $0.60 \times 0.15 \times 0.14$ mm³, yellow rod, monoclinic, $P2_1/n$, $a = 7.6604(1)$, $b = 16.7822(3)$, $c = 18.3706(3)$ Å, $\beta = 97.1224(6)^\circ$, $V = 2343.47(6)$ Å³, $Z = 4$, $D_x = 1.997$ gcm⁻³, $\mu = 7.01$ mm⁻¹. 31220 reflections were measured by using a Bruker D8-Venture Photon area detector (MoK α radiation, $\lambda = 0.71073$ Å) up to a resolution of $(\sin\theta/\lambda)_{\max} = 0.63$ Å⁻¹ at a temperature of 100 K. The reflections were corrected for absorption and scaled on the basis of multiple measured reflections by using the SADABS program (0.03–0.09 correction range).¹⁶⁷ 4488 reflections were unique ($R_{\text{int}} = 0.031$). Using ShelXle, the structures were solved with SHELXS-97 by using direct methods and refined with SHELXL-97 on F^2 for all reflections.^{201,202} Non-hydrogen atoms were refined by using anisotropic displacement parameters. The positions of the hydrogen atoms were calculated for idealized positions. 308 parameters were refined without restraints. $R_1 = 0.028$ for 4488 reflections with $I > 2\sigma(I)$ and $wR_2 = 0.075$ for 4791 reflections, $S = 1.155$, residual electron density was between -1.80 and 1.54 eÅ⁻³. Geometry calculations and checks for higher symmetry were performed with the PLATON program.¹⁶⁶ A .cif data file can be found in the attachments.

2-(2-Pyridyl)-4-phenyl-6-(4-fluorophenyl)pyridine-N,N-rhenium(I) tricarbonyl (3.7f)

Bipyridine **3.3f** (15 mg, 0.046 mmol) and [Re(CO)₅Cl] (17 mg, 0.042 mmol) gave the product (16 mg, 0.024 mmol, 58%) as yellow crystals. Crystals suitable for X-ray diffraction were obtained from a NMR solution in DMSO-*d*₆.

¹H NMR (400 MHz, DMSO-*d*₆): $\delta = 7.40 - 7.47$ (m, 2 H, H_{13/15}), 7.58 – 7.75 (m, broad, 5 H, H_{18/22}, H₂₀, H_{12/16}), 7.75 – 7.80 (m, 1 H, H₉), 8.10 (d, $J = 1.9$ Hz, 1 H, H₂), 8.17 – 8.21 (m, 2 H, H_{18/22}), 8.34 – 8.39 (m, 1 H, H₈), 9.04 (d, $J = 1.9$ Hz, 1 H, H₄), 9.06 – 9.11 (m, 1 H, H₁₀, H₇) ppm; ¹⁹F NMR (376 MHz, DMSO-*d*₆): $\delta = -111.4$ (m_s) ppm;

¹³C{¹H} NMR (101 MHz, DMSO-*d*₆): $\delta = 120.3$ (C₄), 124.7 (C₂), 125.6 (C₇), 127.6 (C₉), 128.0 (C_{18/22}), 129.4 (C_{19/21}), 131.0 (C₂₀), 131.6 (d, ³ $J_{C-F} = 9.2$ Hz, C_{12/16}), 134.8 (C₁₇), 138.6 (d, ⁴ $J_{C-F} = 3.3$ Hz, C₁₁), 140.0 (C₈), 150.4 (C₃), 152.9 (C₁₀), 156.7 (C₆), 157.0 (C₅), 162.0 (C₁), 163.3 (d, ¹ $J_{C-F} = 247.1$ Hz, C₁₄), 190.4 (CO), 193.5 (CO), 197.3 (CO) ppm;

ESI-TOF (m/z): 714.9385 (calc.: 714.9445 g/mol) [M + K]⁺, 698.9654 (calc.: 698.9705 g/mol) [M + Na]⁺, 597.0596 (calc.: 597.0624 g/mol) [M – Br]⁺, 569.0645 (calc.: 569.0675 g/mol) [M – Br – CO]⁺, 541.0739 (calc.: 541.0726 g/mol) [M – Br – 2 CO]⁺;

FT-IR (solid ATR): $\tilde{\nu}(\text{CO})$ 2017, 1893 (sh), 1866 cm⁻¹.

Crystallographic data: $C_{25}H_{15}BrFN_2O_3Re$, $F_w = 676.50$, $0.42 \times 0.05 \times 0.04$ mm³, yellow needle, triclinic, $P\bar{1}$, $a = 7.4937(2)$, $b = 13.0962(3)$, $c = 13.4017(3)$ Å, $\alpha = 94.4701(7)^\circ$, $\beta = 97.5257(8)^\circ$, $\gamma = 106.2429(8)^\circ$, $V = 1242.75(5)$ Å³, $Z = 2$, $D_x = 1.808$ gcm⁻³, $\mu = 6.53$ mm⁻¹. 20079 reflections were measured by using a Bruker D8-Venture Photon area detector (MoK α radiation, $\lambda = 0.71073$ Å) up to a resolution of $(\sin\theta/\lambda)_{\max} = 0.61$ Å⁻¹ at a temperature of 100 K. The

reflections were corrected for absorption and scaled on the basis of multiple measured reflections by using the SADABS program (0.48–0.75 correction range).¹⁶⁷ 4378 reflections were unique ($R_{\text{int}} = 0.045$). Using ShelXle, the structures were solved with SHELXS-97 by using direct methods and refined with SHELXL-97 on F^2 for all reflections.^{201,202} Non-hydrogen atoms were refined by using anisotropic displacement parameters. The positions of the hydrogen atoms were calculated for idealized positions. 281 parameters were refined without restraints. $R_1 = 0.033$ for 4378 reflections with $I > 2\sigma(I)$ and $wR_2 = 0.079$ for 4693 reflections, $S = 1.140$, residual electron density was between -1.84 and $2.47 \text{ e}\text{\AA}^{-3}$. Geometry calculations and checks for higher symmetry were performed with the PLATON program.¹⁶⁶ A .cif data file can be found in the attachments.

SQUEEZE RESULTS (Version = 50315)¹⁶⁹

Note: Data are Listed for all Voids in the P1 Unit Cell i.e. Centre of Gravity, Solvent Accessible Volume, Recovered number of Electrons in the Void and Details about the Squeezed Material

```

_platon_squeeze_void_nr
_platon_squeeze_void_average_x
_platon_squeeze_void_average_y
_platon_squeeze_void_average_z
_platon_squeeze_void_volume
_platon_squeeze_void_count_electrons
_platon_squeeze_void_content
 1    -0.033    0.000    0.000    186    75    ''
_platon_squeeze_void_probe_radius    1.20
_platon_squeeze_details

```

The general procedure (based on a preliminary implementation of the technique) has been described in more detail in literature.¹⁷⁰

2-(2-Pyridyl)-4-phenyl-6-(4-methoxyphenyl)pyridine-N,N-rhenium(I) tricarbonyl (3.7g)

Bipyridine **3.3g** (12 mg, 0.035 mmol) and $[\text{Re}(\text{CO})_5\text{Cl}]$ (14 mg, 0.034 mmol) gave the product (15 mg, 0.022 mmol, 61%) as yellow crystals. Crystals suitable for X-ray diffraction were obtained from a NMR solution in THF- d_8 .

¹H NMR (401 MHz, DMSO- d_6): $\delta = 3.82$ (s, 3 H, MeO), 7.06 – 7.14 (m, broad, 2 H, H_{13/15}), 7.27 – 7.33 (m, broad, 2 H, H_{12/16}), 7.56 – 7.62 (m, 3 H, H_{19/21}, H₂₀), 7.74 (ddd, $J = 7.5, 5.5, 1.2$ Hz, 1 H, H₉), 8.00 (d, $J = 1.9$ Hz, 1 H, H₂), 8.09 – 8.15 (m, 2 H, H_{18/22}), 8.28 – 8.34 (m, 1 H, H₈), 8.92 (d, $J = 1.9$ Hz, 1 H, H₄), 8.96 – 9.00 (m, 1H, H₇), 9.03 – 9.07 (m, 1 H, H₁₀) ppm;

$^{13}\text{C}\{^1\text{H}\}$ NMR (101 MHz, DMSO- d_6): δ = 55.8 (MeO), 120.1 (C₄), 124.9 (C₂), 125.7 (C₇), 127.7 (C₉), 128.1 (C_{18/22}), 129.8 (C_{19/21}), 131.0 (C_{12/16}), 131.2 (C₂₀), 135.0 (C₁₁ or C₁₇), 135.2 (C₁₁ or C₁₇), 140.2 (C₈), 150.6 (C₃), 153.1 (C₁₀), 157.2 (C₅ or C₆), 157.2 (C₅ or C₆), 161.0 (C₁₄), 163.8 (C₁), 191.1 (CO), 193.6 (CO), 197.7 (CO) ppm;

ESI-TOF (m/z): 726.9624 (calc.: 726.9645 g/mol) [M + K]⁺, 710.9886 (calc.: 710.9905 g/mol) [M + Na]⁺, 609.0827 (calc.: 609.0824 g/mol) [M - Br]⁺, 581.0885 (calc.: 581.0875 g/mol) [M - Br - CO]⁺, 553.0968 (calc.: 553.0926 g/mol) [M - Br - 2 CO]⁺;

FT-IR (solid ATR): $\tilde{\nu}(\text{CO})$ 2017, 1915, 1865 cm⁻¹.

Crystallographic data: C₂₆H₁₈BrN₂O₄Re, *F*_w = 688.53, 0.26×0.13×0.08 mm³, yellow block, monoclinic, *P*2₁/*c*, *a* = 7.9191(8), *b* = 16.4302(16), *c* = 17.6259(17) Å, β = 92.991(4)°, *V* = 2290.2(4) Å³, *Z* = 4, *D*_x = 1.997 gcm⁻³, μ = 7.09 mm⁻¹. 14110 reflections were measured by using a Bruker D8-Venture Photon area detector (MoK α radiation, λ = 0.71073 Å) up to a resolution of $(\sin\theta/\lambda)_{\text{max}}$ = 0.60 Å⁻¹ at a temperature of 102 K. The reflections were corrected for absorption and scaled on the basis of multiple measured reflections by using the SADABS program (0.34–0.75 correction range).¹⁶⁷ 3603 reflections were unique (*R*_{int} = 0.040). Using Olex,²⁰³ the structures were solved with SHELXS-97 by using direct methods and refined with SHELXL-97 on *F*² for all reflections.²⁰¹ Non-hydrogen atoms were refined by using anisotropic displacement parameters. The positions of the hydrogen atoms were calculated for idealized positions. 278 parameters were refined without restraints. *R*₁ = 0.036 for 3603 reflections with *I* > 2σ(*I*) and *wR*₂ = 0.084 for 4140 reflections, *S* = 1.071, residual electron density was between -1.67 and 2.98 eÅ⁻³. Geometry calculations and checks for higher symmetry were performed with the PLATON program.¹⁶⁶ A .cif data file can be found in the attachments.

2-(2-Pyridyl)-4-phenyl-6-(4-methylthiophenyl)pyridine-N,N-rhenium(I) tricarbonyl (3.7h)

Bipyridine **3.3h** (31 mg, 0.087 mmol) and [Re(CO)₅Cl] (34 mg, 0.084 mmol) gave the product (47 mg, 0.067 mmol, 80%) as yellow crystals. Crystals suitable for X-ray diffraction were obtained from a NMR solution in DMSO-*d*₆.

¹H NMR (401 MHz, DMSO-*d*₆): δ = 2.52 (s, 3 H, MeS), 7.39 – 7.47 (m, broad, 2 H, H_{13/15}), 7.55 – 7.64 (m, 5 H, H_{12/16}, H_{19/21}, H₂₀), 7.75 (ddd, *J* = 7.6, 5.6, 1.1 Hz, 1 H, H₉), 8.03 (d, *J* = 1.8 Hz, 1 H, H₂), 8.10 – 8.16 (m, 2 H, H_{18/22}), 8.29 – 8.35 (m, 1 H, H₈), 8.95 (d, *J* = 1.9 Hz, 1 H, H₄), 8.97 – 9.02 (m, 1 H, H₇), 9.03 – 9.07 (m, 1 H, H₁₀) ppm;

$^{13}\text{C}\{^1\text{H}\}$ NMR (101 MHz, DMSO-*d*₆): δ = 15.0 (MeS), 120.4 (C₄), 124.9 (C₂), 125.8 (C₇), 127.9 (C₉), 128.2 (C_{18/22}), 129.8 (C_{19/21}), 130.0 (C_{12/16}), 131.3 (C₂₀), 135.1 (C₁₇), 138.7 (C₁₁), 140.3 (C₈),

141.3 (C₁₄), 150.8 (C₃), 153.2 (C₁₀), 157.1 (C₅ or C₆), 157.4 (C₅ or C₆), 163.5 (C₁), 191.0 (CO), 193.9 (CO), 197.6 (CO) ppm;

ESI-TOF (m/z): 742.9600 (calc.: 742.9416 g/mol) [M + K]⁺, 726.9652 (calc.: 726.9677 g/mol) [M + Na]⁺, 613.0596 (calc.: 613.0596 g/mol) [M - Br - 2 CO + CO₂]⁺, 557.0698 (calc.: 557.0698 g/mol) [M - Br - 3 CO + O]⁺;

Crystallographic data: C₂₆H₁₂BrN₂O₃Re, CH₃S, *F*_w = 701.57, 0.14×0.12×0.05 mm³, yellow prism, monoclinic, *P*2₁/*c*, *a* = 8.0913(1), *b* = 16.3345(3), *c* = 17.9314(7) Å, β = 93.543(1)°, *V* = 2365.42(7) Å³, *Z* = 4, *D*_x = 1.970 gcm⁻³, μ = 6.95 mm⁻¹. 26898 reflections were measured by using a Bruker D8-Venture Photon area detector (MoKα radiation, λ = 0.71073 Å) up to a resolution of (sinθ/λ)_{max} = 0.63 Å⁻¹ at a temperature of 100 K. The reflections were corrected for absorption and scaled on the basis of multiple measured reflections by using the SADABS program (0.43–0.59 correction range).¹⁶⁷ 4149 reflections were unique (*R*_{int} = 0.045). Using ShelXle, the structures were solved with SHELXS-9 by using direct methods and refined with SHELXL-97 on *F*² for all reflections.^{201,202} Non-hydrogen atoms were refined by using anisotropic displacement parameters. The positions of the hydrogen atoms were calculated for idealized positions. 286 parameters were refined without restraints. *R*₁ = 0.043 for 4149 reflections with *I* > 2σ(*I*) and *wR*₂ = 0.107 for 4857 reflections, *S* = 1.031, residual electron density was between -1.43 and 2.42 eÅ⁻³. Geometry calculations and checks for higher symmetry were performed with the PLATON program.¹⁶⁶ A .cif data file can be found in the attachments.

Reactivity of [(P,N)Re(CO)₃X]-type Complexes Towards Water

In a J. Young NMR tube pyridylphosphinine-rhenium(I) complex (0.027 mmol) was dissolved in deuterated DCM (0.45 mL) and degassed water (1 μL, 1 mg, 0.055 mmol, 2 eq.) was added.

Water addition to [(P,N)Re(CO)₃Cl] 3.4a

³¹P{¹H} NMR (162 MHz, CD₂Cl₂): δ = 83.8, 97.6, 109.9 ppm

Water addition to [(P,N)Re(CO)₃Br] 3.5a

³¹P{¹H} NMR (162 MHz, CD₂Cl₂): δ = 72.9, 81.2, 95.2, 107.2 ppm

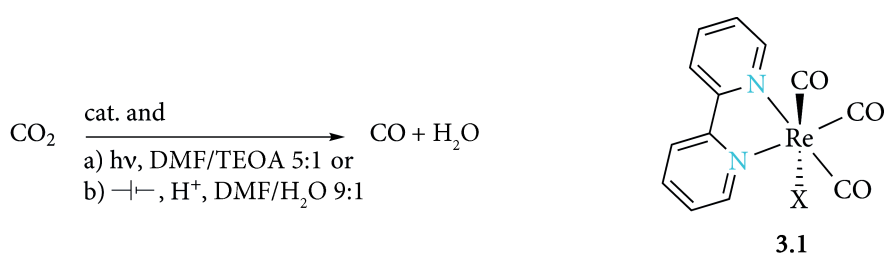
Water addition to [(P,N)Re(CO)₃Br] 3.5b

³¹P{¹H} NMR (162 MHz, CD₂Cl₂): δ = 72.7, 81.2, 95.0, 107.8 ppm

4 Pyridylphosphinines and Bipyridines
– Application as Ligands in Catalysts
for the Reduction of CO₂

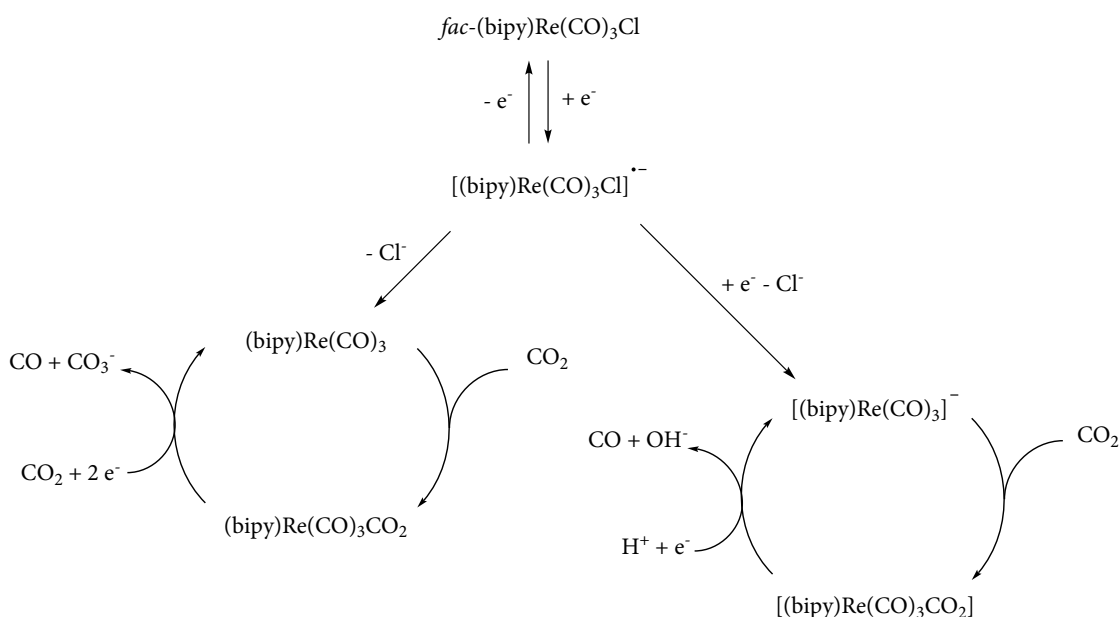
4.1 Introduction

As mentioned in chapter 3.1, the discovery by Lehn *et al.* in 1983 that bipyridine-rhenium(I) complexes are photosensitisers as well as photocatalysts for the reduction of CO₂ was a major step on the way to exploitation of this overabundant gas as a chemical building block.^{74,181,182} Next to the photochemical procedure, also an electrochemical approach was presented by Lehn and coworkers (Scheme 4-1). Interestingly, both methods lead to the production of CO and water with a very high selectivity that is only rarely reached for CO₂ reduction experiments even with newer catalysts.¹⁰⁷



Scheme 4-1: Photo- (a) and electrocatalytic (b) reduction of CO₂ with catalysts of the type [(bipy)Re(CO)₃X] (X = Cl, Br) (**3.1**).

The electrocatalytic reduction of carbon dioxide with [(bipy)Re(CO)₃X]-type coordination compounds is usually done in either dimethylformamide (DMF) or acetonitrile as solvent. According to Mayer *et al.*, these rhenium(I) complexes can reduce CO₂ electrochemically *via* two possible reaction pathways (Scheme 4-2). In a slow 1 e⁻ mechanism CO₂ disproportionates into carbonate and CO. Much faster and therefore more significant is the 2 e⁻ pathway producing carbon monoxide and an oxide anion which is usually captured by protons to form water.²⁰⁴ Providing a proton source by mixing the chosen solvent with water or alcohols such as methanol or phenol is common practice. However, the reaction is known to proceed on small scale without an additional proton source with the catalyst scavenging protons from the solvent or of tetrabutylammonium salts that are generally added as electrolytes. If renewable energy sources are used and considering a much easier scale-up for an electrochemical process, the electrocatalytic reduction of CO₂ is often considered more sustainable and more likely to succeed economically.^{74,106,182}

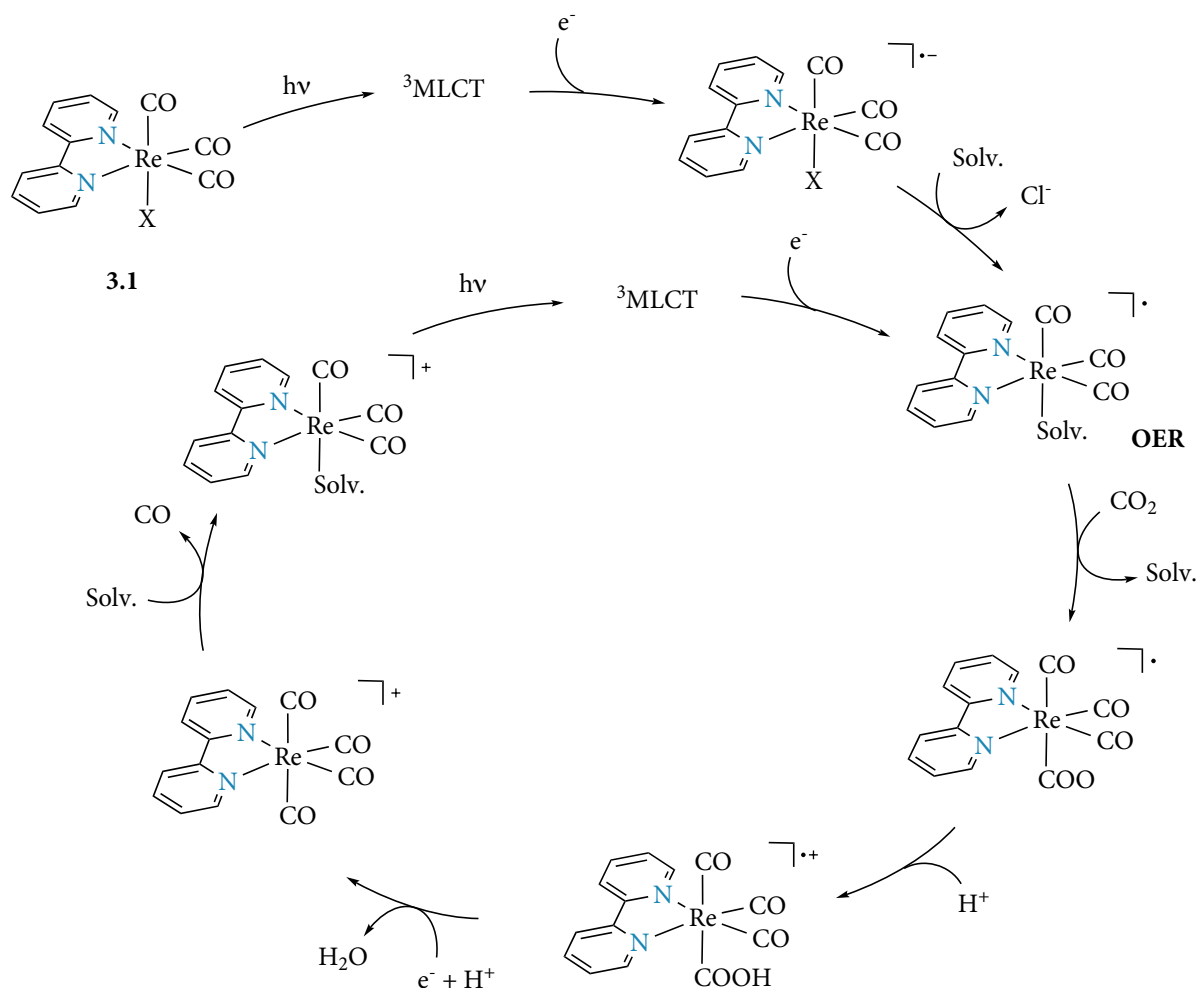


Scheme 4-2: Electrochemical CO₂ reduction *via* a 1 e⁻ (left) or 2 e⁻ (right) pathway proposed by Mayer *et al.*²⁰⁴

On the other hand, the prospect of using sunlight in the photocatalytic reduction of CO₂ for the production of C₁-building blocks as basis for further chemistry, exactly like nature does, has a special appeal to many scientists. The photocatalytically active compounds of the type [(bipy)Re(CO)₃X] (X = Cl, Br) (**3.1**) are brightly yellow, very stable solids with a maximum absorption band at λ = 370 nm. In a CO₂ saturated DMF solution under UV-light radiation, they are able to act as both photosensitisers as well as catalytic species and reduce carbon dioxide to carbon monoxide. Electrons and protons for the photocatalytic reduction process are usually donated by triethanolamine (TEOA), which is commonly added as a sacrificial agent. For an economical process in the future, the CO₂ reduction half reaction needs to be paired with an marketable oxidation half reaction instead of a sacrificial reagent. For example, coupling the CO₂ reduction with water oxidation would lead to artificial photosynthesis. Interestingly enough, these rhenium(I) complexes are still the most selective reduction catalysts up until today with only rarely observed small amounts of hydrogen as a byproduct.^{74,107,181}

Mechanistically, the photocatalytic reduction cycle of CO₂ starts with light excitation of the rhenium complex into its ³MLCT state which undergoes reductive quenching by the sacrificial reagent to form a radical anion. After exchange of a halogen anion with a solvent molecule, a one-electron reduced (OER) species is formed whose stability is considered crucial for a good performance of a catalyst. Electrophilic attack by CO₂ leads to a CO₂-

rhodium adduct which was structurally unknown until Ishitani *et al.* observed a mono-nuclear CO₂ complex recently. Subsequent protonation and uptake of a second electron from either the neutral or deprotonated form of the sacrificial reagent or more likely the OER solvent-coordinated rhodium complex gives the product carbon monoxide and a cationic solvent-coordinated rhodium complex. Excitation through light absorption and reductive quenching closes the cycle with formation of the OER species (Scheme 4-3).^{107,205,206}



Scheme 4-3: Photochemical CO₂ reduction cycle with [(bipy)Re(CO)₃X]-type catalysts.²⁰⁵

Within the context of a comparison between pyridylphosphinine- and bipyridine-based complexes, the report of very good photocatalytic CO₂ reduction results with a [(bipy)Re(CO)₃(P(OEt)₃)]⁺ catalyst by Ishitani *et al.* in 1996 is especially noteworthy.¹⁸⁶ Depending on the light intensity this catalyst reaches quantum yields of $\Phi = 0.38$ which was attributed to the good π -acceptor properties of the phosphite ligand stabilising and therefore elongating the lifetime of the OER species of the CO₂ reduction cycle. Further improvement to a quantum yield of $\Phi = 0.59$ was achieved by combining the standard cationic

$[(\text{bpy})\text{Re}(\text{CO})_3(\text{MeCN})]^+$ -species and its readily available coordination site for CO_2 with $[(4,4'-(\text{MeO})_2\text{bpy})\text{Re}(\text{CO})_3(\text{P}(\text{OEt})_3)]^+$ providing a long-lived OER state with the reduction power to reduce the CO_2 -adduct of the former complex.²⁰⁷ With 2,4,6-triphenylphosphinine having almost the same Tolman electronic parameter than $\text{P}(\text{OMe})_3$ (2079.2 cm^{-1} vs. 2079.5 cm^{-1}), phosphinines were only recently reported as very similar to phosphites in their π -accepting properties by Müller and coworkers.³⁴ Therefore, the idea of employing phosphinine ligands in CO_2 reduction catalysis becomes self-evident. Additionally, the incorporation of π -acceptor abilities into the chelating ligand by using a pyridylphosphinine would avoid the use of an additional ligand such as $\text{P}(\text{OEt})_3$ which is potentially blocking the coordination site of CO_2 .

4.2 Cyclic Voltammetry Experiments

With regards to a possible application of pyridylphosphinine-rhenium(I) complexes as redox active catalysts, the study of their reduction and oxidation behaviour *via* cyclic voltammetry and comparison of results to bipyridine analogues is indispensable. Looking at catalytic CO_2 reduction reactions, a multitude of 2,2'-bipyridine-based rhenium(I) carbonyl catalysts but also other transition metal compounds have been tested in cyclic voltammetry experiments with a special focus on the reduction part.^{183,204,208–211} $[(\text{N,N})\text{Re}(\text{CO})_3\text{X}]$ -type complexes with a bipyridine ligand are known to show a first quasireversible reduction wave at around $E_{1/2} = -1.35 \text{ V}$ vs. SCE which is located on the bipyridine moiety and a second irreversible metal-centred reduction at approximately $E_{pa} = (-1.50)\text{--}(-2.10) \text{ V}$ vs. SCE in acetonitrile under argon.²⁰⁴ If cyclic voltammograms are measured in acetonitrile saturated with CO_2 , a current enhancement at the second reduction wave indicates the catalytic reduction of CO_2 .^{106,183,204}

Very similar to what has been reported for $[(\text{bipy})\text{Re}(\text{CO})_3\text{Cl}]$ (**3.1**), the here investigated $[(\text{N,N})\text{Re}(\text{CO})_3\text{X}]$ -type complexes **3.6a-g** ($\text{X} = \text{Cl}$) and **3.7a-g** ($\text{X} = \text{Br}$) display three reduction waves with the first one at $E_{pa} = (-1.34)\text{--}(-1.40) \text{ V}$ being quasireversible and the other two showing irreversible behaviour (Figure 4-1 for **3.1**, **3.5a**, **3.7a** and **2.6a**, other cyclic voltammograms can be found in the appendix under 6.3). The first reduction is independent from substituent X and does show a very small influence of the substituent groups on the 4-

and 6-phenyl rings which is in agreement with the localisation of the reduction on the bipyridine ligand.²⁰⁴ The complexes bearing an electron withdrawing fluorine atom on the bipyridine moiety are the easiest to reduce at $E_{pa} = -1.34$ V (**3.7f**) and $E_{pa} = -1.35$ V (**3.6b**, **3.7b**). Methoxy substituted compounds **3.6d** and **3.7d**, on the other hand, are slightly harder to reduce at $E_{pa} = -1.40$ V and $E_{pa} = -1.38$ V, respectively (Table 4-1). Interestingly, the stronger donating methylthio group does not show any substituent effect.

The second reduction is assumed to be metal centred and is therefore influenced by the X group.²⁰⁴ Rhenium(I) chloride compounds exhibit the second, irreversible reduction wave at higher potentials of $E_{pa} = (-1.69)$ - (-1.77) V compared to rhenium(I) bromide complexes with the second reduction at $E_{pa} = (-1.61)$ - (-1.69) V. As expected from the localisation on the metal centre, no substituent influence is observed for the second reduction wave.

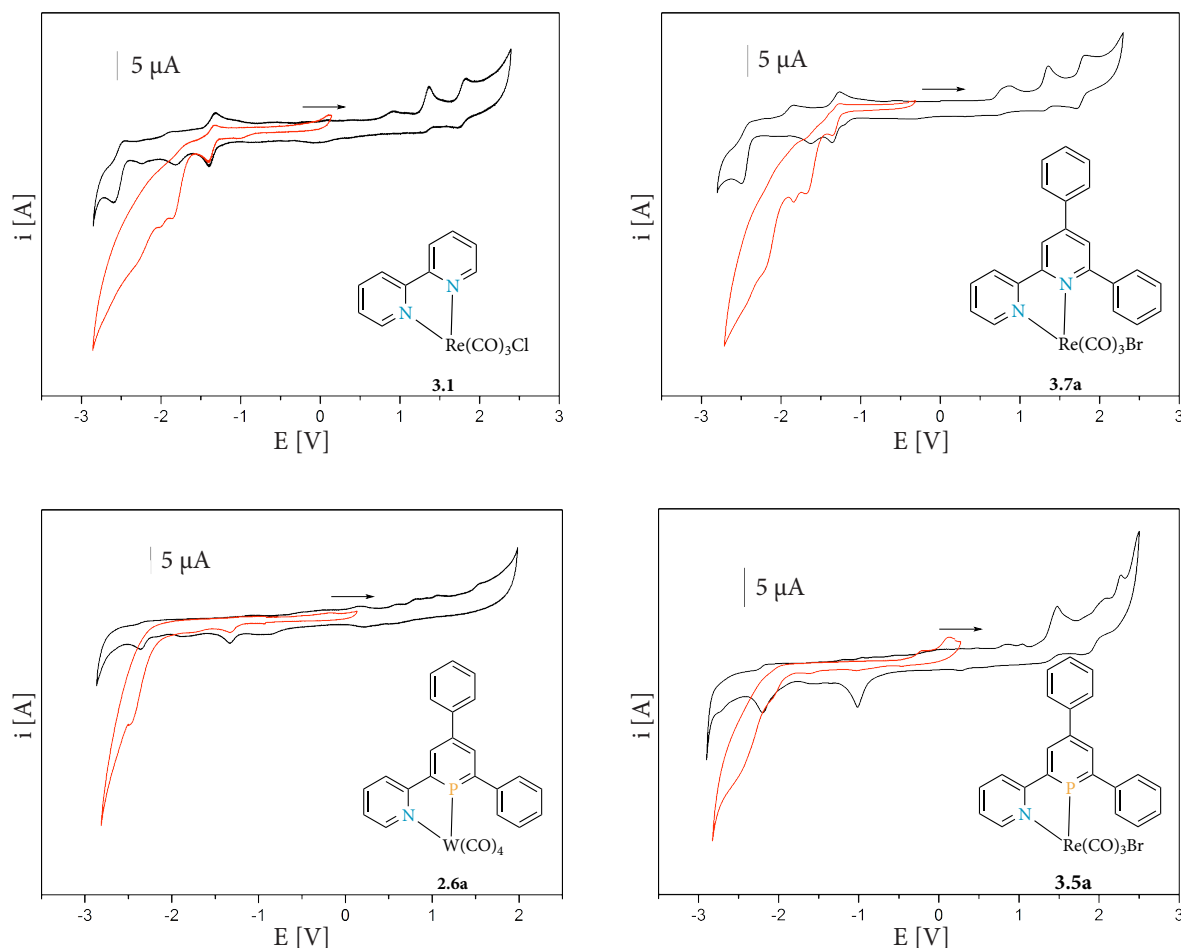


Figure 4-1: Cyclic voltammograms of [(bipy)Re(CO)₃Cl] (**3.1**), [(N,N)Re(CO)₃Br]-type complex **3.7a**, [(P,N)Re(CO)₃Br]-type complex **3.5a** and [(P,N)W(CO)₄]-compound **2.6a** measured 0.5 mM in acetonitrile with 0.1 M TBAPF₆ as electrolyte at 100 mV/s under argon (black) and under CO₂ (red).

A third reduction can be observed in acetonitrile which is usually not reported in literature likely due to its assumed irrelevance for catalytic CO₂ reduction. Hydrogen and fluorine substituted complexes show the third reduction at peak potentials of $E_{pa} = (-2.49)$ - (-2.52) V (**3.6a, b** and **3.7a, b, f**), while electron donating substituents push it to slightly higher potentials of $E_{pa} = (-2.54)$ - (-2.60) V (Table 4-1). Additionally no influence of X is visible leading to the assumption that the third reduction again takes place on the bipyridine ligand. Only methylthio substituted compounds display another irreversible reduction at peak potentials of $E_{pa} = -2.45$ V (**3.6e**) and $E_{pa} = -2.47$ V (**3.7e**) that can obviously be attributed to the substituent.

	Reduction Potentials E_{pa} [V] vs. SCE			
[(bipy)-Re(CO) ₃ Cl]	-1.39 (qr)	-1.82 (ir)		-2.59 (ir)
3.4a (R = H)	-1.07 (ir)	-2.14 (ir)		
3.5a (R = H)	-1.02 (ir)	-2.19 (ir)		-2.74 (ir)
3.6a (R = H)	-1.37 (qr)	-1.74 (ir)		-2.50 (ir)
3.7a (R = H)	-1.36 (qr)	-1.62 (ir)		-2.49 (ir)
3.6b (R = F)	-1.35 (qr)	-1.74 (ir)		-2.52 (ir)
3.7b (R = F)	-1.35 (qr)	-1.61 (ir)		-2.49 (ir)
3.6d (R = OMe)	-1.40 (qr)	-1.77 (ir)		-2.56 (ir)
3.7d (R = OMe)	-1.38 (qr)	-1.63 (ir)		-2.54 (ir)
3.6e (R = SMe)	-1.36 (qr)	-1.69 (ir)	-2.45 (ir)	-2.60 (ir)
3.7e (R = SMe)	-1.36 (qr)	-1.69 (ir)	-2.47 (ir)	-2.60 (ir)
3.7f (R' = F)	-1.34 (qr)	-1.62 (ir)		-2.51 (ir)
3.7g (R' = OMe)	-1.37 (qr)	-1.62 (ir)		-2.59 (ir)
2.6a (R = H)	-1.33 (ir)	-2.36 (ir)		
2.7a (R = H) ²¹²	-1.42 (r)	-2.04 (ir)		

Table 4-1: Reduction potentials of pyridylphosphinine-based rhenium(I) complexes **3.4a** (X = Cl) and **3.5a** (X = Br) as well as bipyridine-rhenium(I) compounds **3.6a-g** (X = Cl) and **3.7a-g** (X = Br) in comparison with 2,2'-bipyridine rhenium(I) tricarbonyl chloride as well as [(P,N)W(CO)₄]-type complex **2.6a** and [(N,N)W(CO)₄]-type complex **2.7a**. Cyclic voltammograms were measured 0.5 mM in acetonitrile with 0.1 M TBAPF₆ as electrolyte and ferrocene as internal standard at 100 mV/s under argon.

Comparing the reduction behaviour of these bipyridine-based compounds **3.6a-e** and **3.7a-g** with pyridylphosphinine-rhenium(I) complexes **3.4a** and **3.5a**, the general observations with three reduction waves are quite similar. Contrary than for bipyridine complexes, the first reduction is irreversible and appears at much a less negative potential of $E_{pa} = -1.07$ V (**3.4a**) and $E_{pa} = -1.02$ V (**3.5a**). Considering the first reduction is localised on the ligand system, this is not surprising when recapitulating the results of presented DFT calculations. The LUMOs of pyridylphosphinines was shown to be considerably lower in energy than the ones of bipyridine which consequently facilitates the ligand-centred reduction of their rhenium(I)

complexes (Chapter 2.4 Figure 2-10). The second reduction, however, is shifted to more negative potential with $E_{pa} = -2.14$ V (**3.4a**) and $E_{pa} = -2.19$ V (**3.5a**). And opposite to bipyridine-based complexes, the chloride compound **3.4a** is slightly easier to reduce twice than the respective bromide **3.5a**. The third reduction is right at the edge of the measurement window of acetonitrile. No value could be determined for **3.4a** but **3.5a** shows an irreversible reduction wave at $E_{pa} = -2.74$ V.

If the measurement solution is saturated with carbon dioxide instead of argon before the experiment, all rhenium(I) complexes with pyridylphosphinine or bipyridine ligands showed a strong current enhancement at the second reduction wave that is commonly used as an indicator for the successful catalytic reduction of CO₂ by the measured complex. Looking at the results of cyclic voltammetry, not only the reduced form of bipyridine-based rhenium(I) complexes but interestingly also the respective pyridylphosphinine compounds are able to take up CO₂ from the solution and transfer electrons to it.

Since recent reports mention bipyridine-tungsten(0) carbonyl complexes as possible option to avoid the expensive and rare metal rhenium, complexes **2.6a** and **2.7a** discussed in chapter 2 were evaluated in the context of CO₂ reduction catalysis as well. The [(L)W(CO)₄] (d⁶) fragment is electronically and also structurally very similar to the [(L)Re(CO)₃X] (d⁶) moiety and showed potential as catalyst of the reduction of CO₂ to CO in first experiments.^{190,212–215} [(N,N)W(CO)₄]-type complex **2.7a** has been described as active catalyst in bulk electrolysis experiments and reduction peak potentials in acetonitrile were stated as $E_{pa} = -1.42$ V and -2.04 V.²¹² Comparing to the respective rhenium(I) compounds **3.6a** and **3.7a**, both reduction waves are significantly shifted to more negative potentials which could be due to the higher oxidation state of the rhenium making the reduction easier. However, this shift necessitates higher overpotentials for electrocatalysis which is an undesirable effect. Just as observed for rhenium(I) complexes, the exchange of the bipyridine to a pyridylphosphinine ligand shifts the first reduction to a less negative potential of $E_{pa} = -1.33$ V which can again be attributed to the LUMO being lower in energy for pyridylphosphinine than bipyridine (Figure 2-10), and the second, metal-based reduction to a more negative potential of $E_{pa} = -2.36$ V (**2.6**, Table 4-1). And analogous to observations for bipyridine complexes, the reduction waves of [(P,N)W(CO)₄]-type complex **2.6a** appear at more

negative potential than the ones of [(P,N)Re(CO)₃X] compounds **2.4a** and **2.5a** which would again require higher overpotential for a potential electrocatalysis.

To conclude the redox behaviour of the rhenium(I) carbonyl complexes with bipyridine or pyridylphosphinine ligands, oxidation potentials should be mentioned in spite of their irrelevance for the CO₂ reduction catalysis experiments (Table 4-2). All compounds including [(bipy)Re(CO)₃Cl] (**3.1**) display a first, irreversible oxidation with a peak potential of $E_{pc} = 1.33$ - 1.48 V. Concluding from the lack of ligand influence, this oxidation happens most likely at the metal centre. An small oxidation wave often observed at less positive potential is only seen in later cycles of the experiment and is therefore attributed to a decomposition product of the oxidation reaction.

	Oxidation Potentials E_{pc} [V] vs. SCE				
[(bipy)-Re(CO) ₃ Cl] 3.1	1.36 (ir)			1.82 (ir)	
3.4a (R = H)	1.37 (ir)	1.50 (ir)		2.22 (ir)	
3.5a (R = H)	1.48 (ir)		2.08 (ir)	2.27 (ir)	
3.6a (R = H)	1.36 (ir)			n. d.	
3.7a (R = H)	1.35 (ir)			1.81 (ir)	
3.6b (R = F)	1.37 (ir)			n. d.	
3.7b (R = F)	1.36 (ir)			n. d.	
3.6d (R = OMe)	1.33 (ir)		1.74 (ir)	1.98 (ir)	
3.7d (R = OMe)	1.34 (ir)		1.76 (ir)	1.96 (ir)	
3.6e (R = SMe)	1.40 (ir)	1.55 (ir)	1.67 (ir)	1.84 (ir)	2.11 (ir)
3.7e (R = SMe)	1.40 (ir)	1.59 (ir)		1.80 (ir)	2.10 (ir)
3.7f (R' = F)	1.38 (ir)			1.83 (ir)	
3.7g (R' = OMe)	1.35 (ir)		1.78 (ir)	2.09 (ir)	

Table 4-2: Oxidation potentials of pyridylphosphinine-based rhenium(I) complexes **3.4a** (X = Cl) and **3.5a** (X = Br) as well as bipyridine-rhenium(I) compounds **3.6a-g** (X = Cl) and **3.7a-g** (X = Br) in comparison with 2,2'-bipyridine rhenium(I) tricarbonyl chloride. Cyclic voltammograms were measured 0.5 mM in acetonitrile with 0.1 M TBAPF₆ as electrolyte and ferrocene as internal standard at 100 mV/s under argon.

A second, irreversible oxidation wave detected for all tested rhenium(I) complexes appears at peak potentials of $E_{pc} = 1.81$ - 2.09 V for bipyridine-based compounds and at more positive potentials of $E_{pc} = 2.22$ V and $E_{pc} = 2.27$ V for pyridylphosphinine complexes **3.4a** and **3.5a**, respectively. This leads to the assumption of the second oxidation being localised at the ligand which is supported by the obvious influence of the methoxy substituent shifting this oxidation wave to more positive potentials through the electron withdrawing abilities of the oxygen atom. The substituents also cause additional irreversible oxidation steps at a peak potential of $E_{pc} = 1.74$ - 1.78 V for a methoxy group and peak potentials of $E_{pc} = 1.55$ - 1.59 V and $E_{pc} = 2.10$ - 2.11 V for the methylthio group. Interestingly, pyridylphosphinine

compounds **3.4a** and **3.5a** display another oxidation at a peak potential of $E_{pc} = 1.50$ V and $E_{pc} = 2.08$ V, respectively. This is difficult to rationalise due to the large difference in potential.

4.3 Photocatalytic Reduction of CO₂

Fascinated by the special ability of [(bipy)Re(CO)₃Cl] (**3.1**) to act as a photosensitiser as well as a reaction site in the photocatalytic reduction of carbon dioxide, the synthesised complexes were applied as possible new catalysts in this reaction. While a multitude of differently substituted bipyridine-based catalysts are known, no [(P,N)Re(CO)₃X]-type complex containing a phosphinine or even any other type of P,N-hybrid ligand was reported in literature so far.^{183,185,206,216} Since no pre-existing photocatalysis cell were available, a new reaction setup including a gas chromatography protocol was developed on the basis of the initial reports by Lehn *et al.*^{74,181} In a next step the synthesised rhenium(I) carbonyl complexes of pyridylphosphinine as well as bipyridine ligands were used in the photocatalytic reduction of CO₂ and the outcome was analysed by means of gas chromatography and ¹³C{¹H} NMR spectroscopy.

Development of a Reaction Setup

Photocatalysis reactions have been carried out with two different methods. Small scale reactions can be used for ¹³C NMR experiments with ¹³C-labeled carbon dioxide which allows a general evaluation if the catalyst is active or not and what kind of side products are produced in the liquid phase. In this case, catalyst, solvent and sacrificial hydrogen donor are filled in a J. Young NMR tube and degassed by the freeze-pump method before carbon dioxide is condensed on the reaction mixture.

For full size photocatalysis experiments, several different reaction vessels were tried and a simple one-neck 25 mL flask equipped with septum and small stirring bar proved to be the best option. With a volume of 10 mL for the reaction solution, enough headspace (30.5 mL) is available to take regular gas samples over several hours in order to monitor the reaction progress *via* gas chromatography without creating too much underpressure. Additionally, the risk of gas leaks is minimised by this simplified reaction vessel. The photocatalysis

reactions were carried out with a mixture of N,N-dimethylformamid (DMF) and triethanolamine (TEOA) in a ratio of 5:1 as solvent and proton/electron donor and a catalyst concentration of 1 mM. In order to simplify a possible reaction of [(P,N)Re(CO)₃X]-type catalysts with the sacrificial hydrogen donor, triethylamine (TEA) and isopropanol were tested as literature known alternatives to TEOA in a NMR tube reaction with [(bipy)Re(CO)₃Cl] (**3.1**) as catalyst which did not lead to CO production.^{177,205,217,218}

The reaction mixture and headspace are saturated with carbon dioxide by bubbling it through the solution for 20 min. Evaporation of DMF or TEOA is negligible due to their high boiling points of 153 °C and 335 °C, respectively.²¹ The vessel is closed and placed under a 300 W sunlight lamp. In the ¹³C NMR experiments with [(bipy)Re(CO)₃Cl] (**3.1**) as catalyst, the effect of a 365 nm cut-off filter was tested which indeed slightly minimised the production of a formate complex [(bipy)Re(CO)₃(HCOO)] (¹³C{¹H} NMR δ = 167 ppm) as side product. Since the filter was too small for full size reactions, all further experiments were carried out without it. However, the positive effect should be kept in mind in case fine tuning of reaction conditions is necessary in the future.

A measurable influence on CO production is observed for the distance between reaction vessel and lamp (Figure 4-2). Not surprisingly the reaction rate is increasing the closer the vessel is placed to the lamp. On the other hand, with a distance of 10 cm the catalyst seems to be deactivated after only 90 min since the production of CO stops at this point. Consequently, an intermediate distance of 20 cm was chosen for all further experiments.

Reaction products were analysed by means of gas chromatography. For the gases CO₂ and CO a calibration curve was made for samples up to 20 μL (Figure 6-14). Additionally, oxygen and nitrogen were monitored qualitatively meaning reactions were discarded due to a gas leak in case significant amounts of nitrogen and oxygen became visible. The measurement of hydrogen is interesting within the evaluation of CO₂ reduction catalysts since the reduction of protons to hydrogen is known to be a competing reaction. Using a thermal conductivity detector small amounts of hydrogen are difficult to observe and even though techniques have been developed with certain mixtures of carrier gases the analysis of hydrogen content in the reaction mixture was beyond the means of available equipment.²¹⁹ Larger amounts of several

per cent hydrogen in the reaction atmosphere should be visible but were never observed in the here presented gas chromatograms.

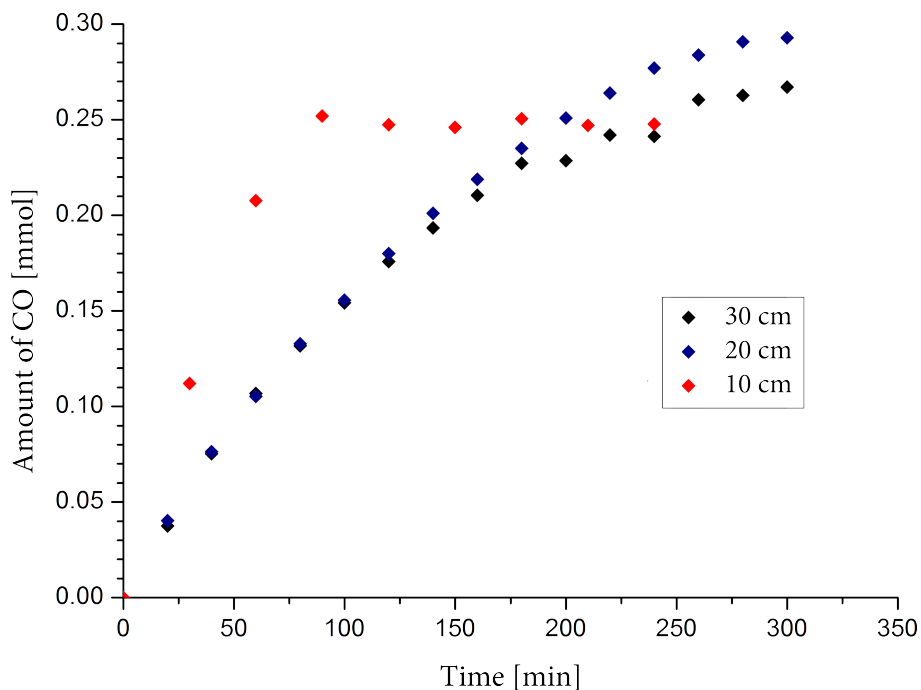


Figure 4-2: Production of CO over time in the photocatalytic reduction of CO₂ with [(bipy)Re(CO)₃Cl] (3.1) as catalyst depending on the distance between reaction vessel and lamp.



Figure 4-3: Simple reaction setup for photocatalytic reduction of CO₂: One-neck flask with stirring bar and septum, gas-tight syringe for headspace samples, magnetic stirrer and 300 W sunlight lamp.

[(N,N)Re(CO)₃X]-type Complexes as Catalysts

The literature known CO₂ reduction catalyst [(bipy)Re(CO)₃Cl] (**3.1**) was employed under described conditions and produced, as expected, carbon monoxide as main product which could be seen leaving the reaction mixture as small bubbles on the stirring bar. The reaction was followed for five hours and was shown to be reproducible. A turnover number (TON) of 36 until complete deactivation was calculated for this catalyst (Figure 4-4). Lehn and coworkers reported values that translate to a comparable TON of 23 after 2 h of photocatalysis.⁷⁴

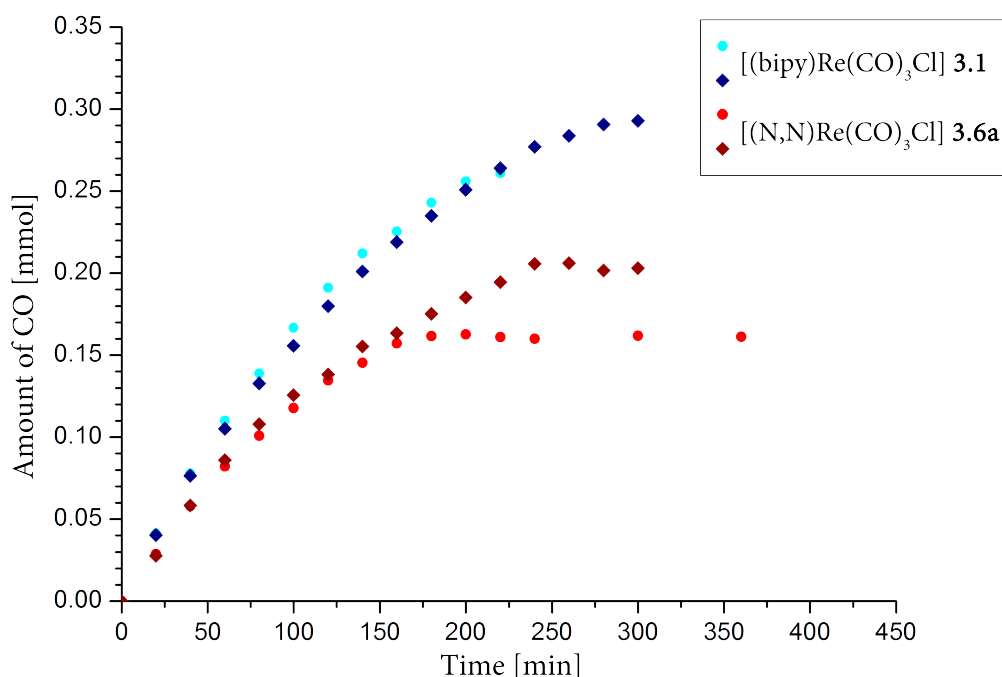


Figure 4-4: Amount of CO measured in the headspace over time during the photocatalytic reduction of CO₂ using [(bipy)Re(CO)₃Cl] (**3.1**) or [(N,N)Re(CO)₃Cl]-type complex **3.6a** as catalyst.

The unsubstituted [(N,N)Re(CO)₃Cl]-type complex **3.6a** was tested in the photocatalytic reduction of CO₂ as well and it proved to be able to produce CO (Figure 4-4). After a reaction time of six hours the evolution of CO stops completely and since the headspace still contains mainly carbon dioxide, the catalyst can be assumed to be entirely deactivated at this point. On average a total amount of 0.18 mmol of carbon monoxide was produced which translates to a TON of 20 until complete deactivation of the catalyst.

The full curves of CO₂ and CO content in the headspace over the reaction mixture over time can be found for both catalysts, **3.1** and **3.6a**, under 6.4 in the appendix (Figure 6-15 for **3.1**, Figure 6-16 for **3.6a**).

Searching for reasons why **3.6a** is a less active catalyst compared to **3.1**, the reaction was repeated in a J. Young NMR tube using ^{13}C -labelled carbon dioxide since gas chromatography showed only CO_2 and CO in the headspace and is not suitable to give information about the liquid phase in this type of reaction (Figure 4-5). Detailed ^{13}C -labelled NMR experiments were reported by Lehn and co-workers for **3.1** which allows the assignment of signals.⁷⁴

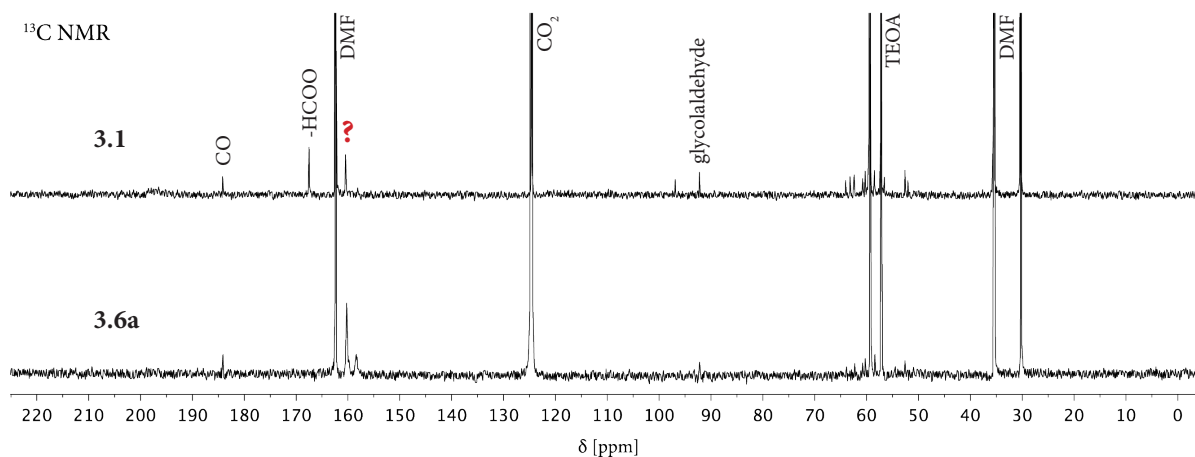


Figure 4-5: ^{13}C NMR spectra of photocatalytic reduction experiments with ^{13}C -labelled CO_2 using $[(\text{bipy})\text{Re}(\text{CO})_3\text{Cl}]$ (**3.1**) or $[(\text{N,N})\text{Re}(\text{CO})_3\text{Cl}]$ -type complex **3.6a** as catalyst.

Besides very intense signals for DMF ($\delta = 31.1, 36.2, 163.2$ ppm) and TEOA ($\delta = 58.0, 60.2$ ppm), leftover dissolved CO_2 and the product CO are visible with chemical shifts of $\delta = 125.3$ and 184.9 ppm, respectively. The latter does only give a signal of small intensity due to its very low solubility in DMF. The sacrificial electron and proton donor TEOA is oxidised during the reaction process to form glycolaldehyde ($\delta = 63.1, 93.0$ ppm) and iminodiethanol ($\delta = 53.4, 59.2$ ppm) as well as other unidentified species. Interestingly, only **3.1** but not **3.6a** shows the formation of a formate complex of the type $[(\text{bipy})\text{Re}(\text{CO})_3(\text{HCOO})]$ with a chemical shift of $\delta = 168.3$ ppm which is considered to be a side product and not a reaction intermediate.⁷⁴ In several NMR experiments of $[(\text{N,N})\text{Re}(\text{CO})_3\text{X}]$ -type catalysts formate complexes were never detected which, in theory, should make these compounds more efficient catalysts. One more signal was observed with a chemical shift of $\delta = 161.2$ ppm. Lehn *et al.* report the formation of a CO_2 adduct to iminodiethanol under CO_2 pressure which was referenced with chemical shifts of $\delta = 59.7$ and 162.4 ppm. An expected third resonance was not observed under photocatalytic reaction conditions and in obtained NMR spectra no clear decision can be made about the presence of a matching signal around

$\delta = 59.7$ ppm due to overlap with TEOA and its oxidised forms. Kubiak and coworkers, on the other hand, reported on the detection of complex $[(4,4'\text{-}t\text{Bu-bipy})\text{Re}(\text{CO})_3(\text{COOH})]$ as an intermediate in the catalytic cycle. The chemical shift is given as $\delta = 161.6$ ppm which was however, measured in THF- d_8 .²⁰⁶ The resonance with a chemical shift of $\delta = 161.2$ ppm was observed for **3.1** as well as **3.6a**, it appears to be slightly more intense for the latter. Therefore the only reasonable explanation for **3.6a** being the less active catalyst at this point is a more stable $[(\text{N,N})\text{Re}(\text{CO})_3(\text{COOH})]$ -type intermediate which slows down the release of CO.

$[(\text{P,N})\text{Re}(\text{CO})_3\text{X}]$ - and $[(\text{P,N})\text{W}(\text{CO})_4]$ -type Complexes as Catalysts

Following the procedure for bipyridine-based catalysts but keeping inert conditions, pyridyl-phosphinine-rhenium(I) complex **3.4a** was added under argon to a mixture of DMF/TEOA (5:1). The solution and headspace was saturated with CO₂ and the reaction vessel was placed under a 300 W sunlight lamp for five hours. The headspace was analysed *via* gas chromatography regularly. Unfortunately, no traces of carbon monoxide were detected.

Considering the observed high reactivity of $[(\text{P,N})\text{Re}(\text{CO})_3\text{X}]$ -type complexes with water, a reaction of **3.4a** with TEOA in the reaction mixture can be assumed as likely. The addition of water to the P-C double bond was shown to be neither regio- nor stereoselective and gave therefore four pairs of enantiomers as products (Chapter 3.4 Reactivity of $[(\text{P,N})\text{Re}(\text{CO})_3\text{X}]$ Complexes Towards Water). An analogous reaction with TEOA which provides not one but three reactive alcohol groups complicates the outcome even more. Cyclic voltammetry experiments under CO₂ to determine the ability to still react as catalytic site after an addition reaction to the P-C double bond have therefore been carried out with water instead of TEOA. Contrary to cyclic voltammograms of **3.4a** and **3.5a** under inert conditions, no significant current enhancement indicating a possible catalytic reduction of CO₂ is visible after the addition of a drop of water to the measurement solution (Figure 4-6). These observations lead to the conclusion that $[(\text{P,N})\text{Re}(\text{CO})_3\text{X}]$ -type complexes react with TEOA towards a multitude of products which are not able to behave as a catalytic site for the reduction of CO₂ anymore. Substitution of TEOA with a different sacrificial hydrogen donor does not improve chances for a functioning catalytic cycle since water is produced as a side product in the reduction of CO₂ to CO which would again add to the P-C double bond and deactivate the catalyst. Running photocatalysis experiments at higher temperatures with

[(P,N)Re(CO)₃X]-type catalysts could be considered in the future. The water addition reaction to these compounds is reversible with temperature and NMR spectra showed 75% of the complex in its original state in the presence of water at a temperature of T = 100 °C. However, decomposition of the complexes was observed already after two cycles of heating up and subsequently cooling down.

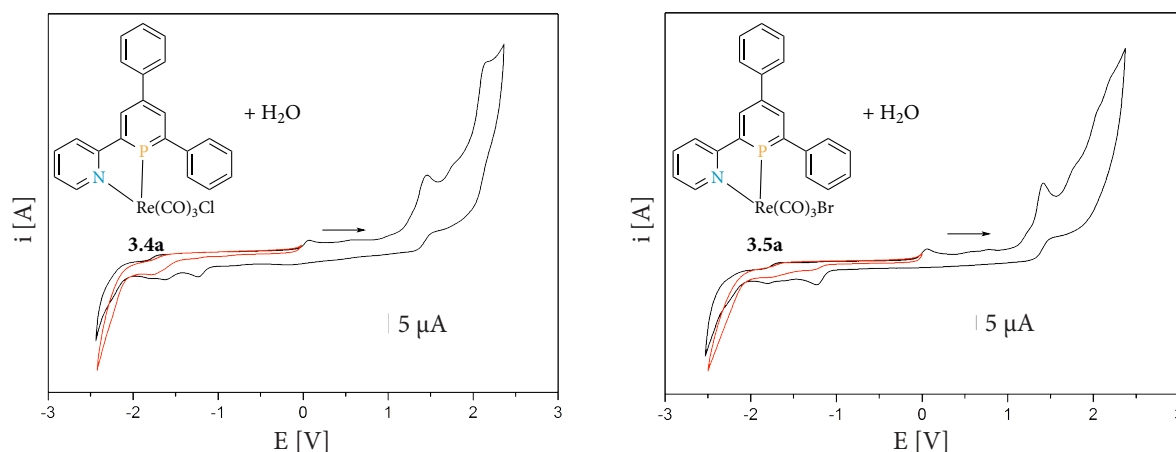


Figure 4-6: Cyclic voltammograms of [(P,N)Re(CO)₃X]-type complexes **3.4a** and **3.5a** measured 0.5 mM in acetonitrile with a drop of degassed water and 0.1 M TBAPF₆ as electrolyte at 100 mV/s under argon (black) and under CO₂ (red).

As mentioned earlier (Chapter 3.3 Cyclic Voltammetry Experiments) there has been a discussion in recent years to substitute the expensive and rare rhenium centre by the cheaper, more abundant tungsten in CO₂ reduction catalysts.^{190,212–215} [(N,N)W(CO)₄]-type complex **2.7a** has already been described as active catalyst in bulk electrolysis experiments and the respective [(P,N)W(CO)₄]-type compound **2.6a** showed a significant current enhancement in cyclic voltammetry experiments under CO₂ atmosphere thereby proving its ability to react with carbon dioxide (Figure 4-1).²¹² In addition, **2.6a** unlike rhenium(I) analogues **3.4a** and **3.5a**, does not immediately react with water. Therefore photocatalysis experiments were repeated with pyridylphosphinine tungsten(0) complex **2.6a**. However, gas chromatograms did not show any traces of carbon monoxide in the headspace over the reaction.

[(P,N)W(CO)₄]-type compounds show a different absorption behaviour than rhenium(I) carbonyl complexes which can already be seen from their colours in solid state or solution. While the latter are brightly yellow, pyridylphosphinine but also bipyridine carbonyl complexes of tungsten(0) are dark red. Absorption spectra of **2.6a** and **2.7a** are reported in

several different solvents and show maximum absorption in the area of 450-550 nm.^{99,100} [(N,N)Re(CO)₃Cl]-type complexes are known to have absorption bands below 400 nm such as 365 nm for [(bipy)Re(CO)₃Cl] (**3.1**).¹⁸³ Most likely, [(P,N)W(CO)₄]-type complex **2.6a** is therefore not able to act as photosensitiser in the photocatalytic reduction of CO₂.

[(bipy)Re(CO)₃Cl] (**3.1**) and related compounds are able to act as both photosensitiser and catalytic site. However, experiments have been reported to separate these two tasks in order to adjust both metal centres to its specific task separately.¹⁷⁷ Ishitani *et al.* studied supramolecular compounds bearing a [Ru(4,4'-Me₂bipy)₃]²⁺ (**4.1**) moiety as photosensitiser connected *via* a linker to [(bipy)Re(CO)₃Cl] as catalytic site. The added ruthenium complex requires the use of a second sacrificial reductant which usually is 1-benzyl-1,4-dihydronicotinamide (BNAH).²²⁰⁻²²² Besides this intramolecular cooperation between ruthenium and rhenium, an intermolecular system of [Ru(4,4'-Me-bipy)₃]²⁺ (**3.8**) and *fac*-[(bipy)Mn(CO)₃Br] has been reported as active in the photocatalytic reduction of CO₂.²²³ While these type of manganese(I) carbonyl complexes are known to function as catalytic sites in bulk electrolysis of carbon dioxide, they have not been mentioned as active in photocatalysis experiments before, similar to [(N,N)W(CO)₄]-type complex **2.7a**.

Therefore pyridylphosphinine tungsten(0) complex **2.6a** has been tried in combination with [Ru(4,4'-Me-bipy)₃]²⁺ (**3.8**) as photosensitiser in the photocatalytic reduction of CO₂ but again no production of carbon monoxide was observed. However, this experiment has to be considered as a first attempt. Photosensitisers need to be carefully matched to the catalytic species in order to guarantee efficient energy transfer from one to the other otherwise no reaction can take place. In this case the system is additionally dependent on a reducing agent for the ruthenium(II) as well as one for the rhenium(I) centre which results in a difficult mixture of intertwining reactions.^{177,223} Tuning of the reaction conditions could in the future very well lead to a successful pyridylphosphinine-based catalytic system.

4.4 Experimental Data

General Remarks

Experiments performed under an inert argon atmosphere were carried out using modified Schlenk techniques or in a MBraun dry box. All common chemicals were commercially available and purchased from Aldrich Chemical Co., ABCR, Alfa Aesar, Acros as well as Eurisol and were used as received. Tris(4,4'-dimethyl-2,2'-bipyridine)-N,N-ruthenium(II) hexafluorophosphate (**4.1**) was synthesised according to literature and [(bipy)Re(CO)₃Cl] (**3.1**) was made like all other [(N,N)Re(CO)₃X]-type complexes (see 3.5 Experimental Data).²²⁴ Triethanolamine was bought from Acros in 99+% quality and stored over molecular sieve (3 Å) under argon. Dry acetonitrile was used from a MBraun MB SBS-800 solvent purification system and dry DMF was bought and stored over molecular sieve (3 Å).

The ¹H, ¹³C{¹H}, ¹⁹F and ³¹P{¹H} NMR spectra were recorded on a JEOL EXZ400 (400 MHz) or a JEOL ECX400 (400 MHz) FT spectrometer and chemical shifts are reported relative to the residual resonance of the deuterated solvents.

Cyclic Voltammetry Experiments

Cyclic voltammograms were measured at room temperature with substance (0.5 mM) in acetonitrile (10 mL) and 0.1 M TBAPF₆ added as electrolyte at 100 mV/s under argon or carbon dioxide. Ferrocene was employed as internal standard. An Autolab PGSTAT302N potentiostat by Metrohm was used in combination with a in-house made, gas-tight glass cell equipped with a glassy carbon disk working electrode by Metrohm, a platinum wire as counter electrode and a leak free Ag/AgCl reference electrode LF-2 by Innovative Instruments, Inc.

Catalytic CO₂ Reduction Experiments

General procedure – lab scale

In a 25-mL one-neck flask (total volume: 40.5 mL) equipped with a septum and stirring bar, catalyst (1 mM) was dissolved in 10 mL of a 5:1 mixture of dry DMF/TEOA. For catalysts containing pyridylphosphinine ligands mixing of reactants and solvents was done under argon. Carbon dioxide was bubbled through the reaction solution for 20 min. Then the flask was placed under an Osram Ultra-Vitalux 300 W sunlight lamp in a distance of 20 cm. The solution was stirred and gas bubbles were observed rising up from the stirring bar in case of a functioning reaction setup. Using a gas-tight syringe, samples (20 µL) were taken from the headspace which were analysed by gas chromatography which was carried out with a GC-2010 Plus machine by Shimadzu. Injection was done by hand at T = 110 °C. Helium was used as carrier gas with a flow rate of 40 mL/min and a purge flow of 3 mL/min. A Restek ShinCarbon ST 80/100 packed column was used heating from T = 40 °C to 250 °C with a heating rate of 20 °C/min. The thermal conductivity detector measured at T = 260 °C with a current of 80 mA. Samples were measured every 20 min. If significant amounts of air (nitrogen, oxygen) became visible in the gas chromatograms the experiment was discarded due to leakage of the septum. Otherwise catalysis experiments were run for five hours.

General procedure - NMR scale

Catalyst was put into a pressure-tight J. Young NMR tube and DMF/TEOA (10:1, 0.2 mL) was added. After degassing with the freeze-pump method, ¹³C-labeled carbon dioxide (1 bar) was condensed onto the mixture which was warmed up to room temperature and placed under an Osram Ultra-Vitalux 300 W sunlight lamp for four hours before ¹³C NMR spectra were measured.

Catalyst [(bipy)Re(CO)₃Cl] (3.1)

time [min]	Experiment 1		Experiment 2	
	Amount CO ₂ [mmol]	Amount CO [mmol]	Amount CO ₂ [mmol]	Amount CO [mmol]
0	1.327	0	1.310	0
20	1.260	0.041	1.235	0.040
40	1.208	0.078	1.220	0.076
60	1.185	0.110	1.176	0.105
80	1.162	0.139	1.151	0.133
100	1.139	0.167	1.111	0.156
120	1.096	0.191	1.115	0.180
140	1.083	0.212	1.088	0.201
160	1.054	0.225	1.064	0.219
180	1.044	0.243	1.040	0.235
200	1.039	0.256	1.023	0.251
220	1.008	0.261	1.011	0.264
240			1.005	0.277
260			0.992	0.284
280			0.988	0.291
300			0.979	0.293

Table 4-3: Gas chromatography results for the photocatalytic reduction experiments with **3.1** as catalyst. Gas amounts refer to the entire headspace of 30.5 mL. Graphic representations in **Figure 4-4** and **Figure 6-15**.

Catalyst [(N,N)Re(CO)₃Cl] (3.5a)

time [min]	Experiment 1		Experiment 2	
	Amount CO ₂ [mmol]	Amount CO [mmol]	Amount CO ₂ [mmol]	Amount CO [mmol]
0	1.317	0	1.312	0
20	1.269	0.029	1.285	0.028
40	1.241	0.058	1.238	0.058
60	1.225	0.082	1.231	0.086
80	1.139	0.101	1.207	0.108
100	1.173	0.118	1.192	0.126
120	1.157	0.135	1.145	0.138
140	1.136	0.145	1.164	0.155
160	1.134	0.157	1.136	0.163
180	1.118	0.162	1.124	0.175
200	1.121	0.163	1.123	0.185
220	1.124	0.161	1.115	0.195
240	1.110	0.160	1.106	0.206
260			1.103	0.206
280			1.083	0.202
300	1.127	0.162	1.094	0.203
360	1.114	0.161		

Table 4-4: Gas chromatography results for the photocatalytic reduction experiments with **3.5a** as catalyst. Gas amounts refer to the entire headspace of 30.5 mL. Graphic representations in **Figure 4-4** and **Figure 6-16**.

Catalyst [(P,N)Re(CO)₃Cl] (3.4a)

No formation of carbon monoxide was observed within five hours.

Catalyst [(P,N)W(CO)₄] (2.6a)

No formation of carbon monoxide was observed within five hours.

Catalyst [(P,N)W(CO)₄] (2.6a) / [(4,4'-Me₂bipy)₃Ru](PF₆)₂ (4.1)

The reaction has been conducted as described in the general procedure but additionally to [(P,N)W(CO)₄] (**2.6a**, 1 mM) [(4,4'-Me₂bipy)₃Ru](PF₆)₂ (**4.1**, 1 mM) and 1-benzyl-1,4-dihydronicotinamide (BNAH, 0.1 M) as a reductant was added to the reaction solution. After placement of the reaction under the sunlight lamp, no formation of carbon monoxide was observed within five hours.

5 Conclusions and Outlook

Starting from the fact that 2,2'-bipyridines are very well established and often successfully applied in various fields of chemistry, a research project about the comparison of properties between 2,2'-bipyridine-based compounds with their higher phosphorus homologues, 2-pyridylphosphinines, was of great interest. Only the recently developed synthetic route for 2-(2'-Pyridyl)-4,6-diphenylphosphinine (**5.3a**, Scheme 5-1) by the group of Müller gave an easy access to a stable derivative of this class of P,N-hybrid heterocycles for the first time. With its modular approach, targeting of specific substitution patterns was then within reach. Therefore, a special focus was put on the investigation of substituent effects on phosphinines, which have never been evaluated before, and the differences in impact of substituents on pyridylphosphinines and bipyridines (Figure 5-1).

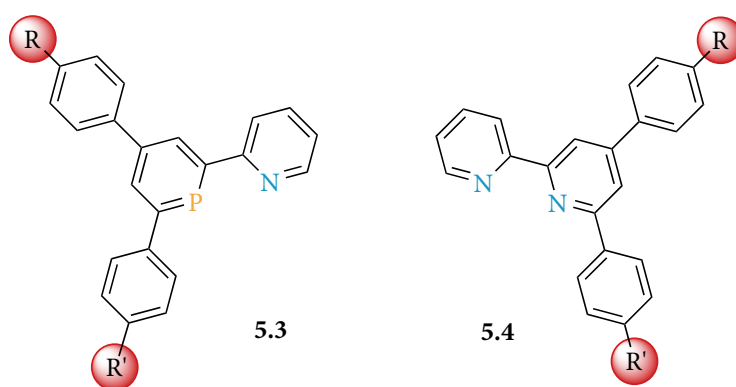
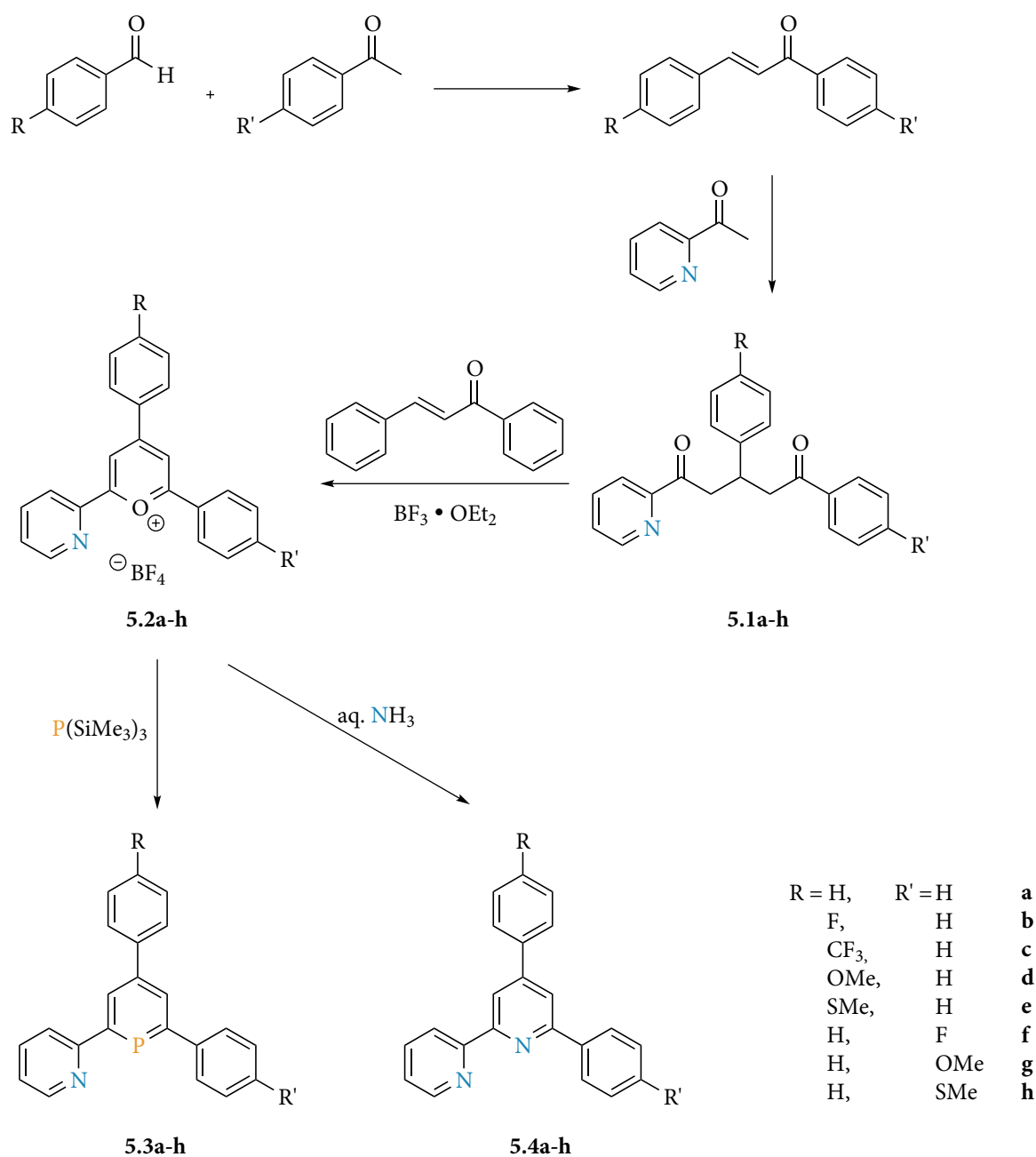


Figure 5-1: Targeting the comparison of substituent effects on pyridylphosphinines and bipyridines.

Thus the scope of the synthetic route towards 2-(2'-Pyridyl)-4,6-diphenylphosphinine (**5.3a**) was broadened to allow introduction of a variety of different substituting groups (R and R' in Scheme 5-1). To achieve a spectrum from electron withdrawing to electron donating properties, fluorine, trifluoromethyl, methoxy and methylthio groups were chosen. Introducing them in *para*-position of the 4- or the 6-phenyl ring of the molecule allowed an evaluation of not only the effect of certain substituents but also the impact of its position in the backbone of the molecule.

The starting materials of the synthetic route, functionalised benzaldehydes and acetophenones, are cheap and easily available with a wide selection of substituents. In a base-catalysed aldol condensation, they formed the respective chalcones which can be reacted with 2-acetylpyridine towards diketones **5.1a-h**. Using *trans*-chalcone as hydrogen acceptor, diketones **5.1a-h** were transformed into pyrylium salts **5.2a-h** with boron trifluoride etherate. Depending on the used nucleophile, pyrylium salts formed pyridylphosphinines

5.3a-h in an O⁺/P-exchange reaction with tris(trimethylsilyl)phosphane or 2,2'-bipyridines **5.4a-h** through O⁺/N-exchange with aqueous ammonia (Scheme 5-1).

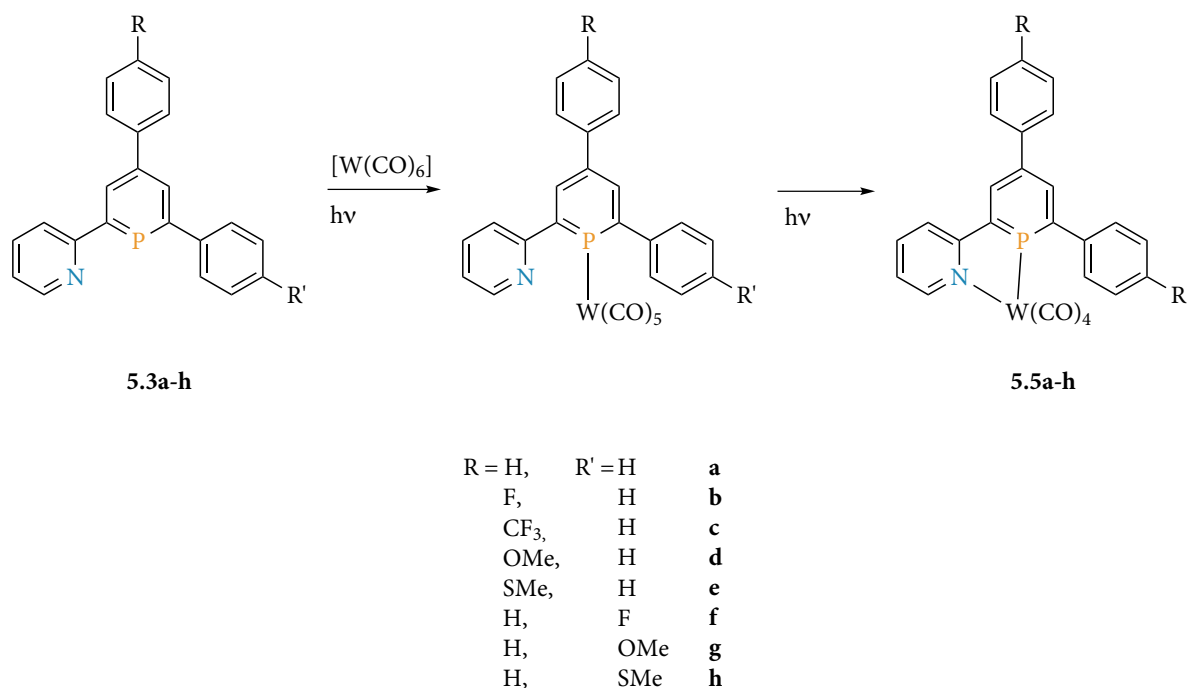


Scheme 5-1: Synthetic pathway to differently substituted 2-pyridylphosphinines **5.3a-h** and their 2,2'-bipyridine-based analogues **5.4a-h**.

While the introduction of substituents did lower the yield in comparison to the unsubstituted compound **5.3a**, the reaction conditions were successfully adjusted to allow isolation in pure form and full characterisation of the differently substituted pyridylphosphinines **5.3a-h**. Additionally, the versatility of pyrylium salts as precursors in the synthesis of heterocycles was taken advantage of and the corresponding bipyridines **5.4a-h** bearing the

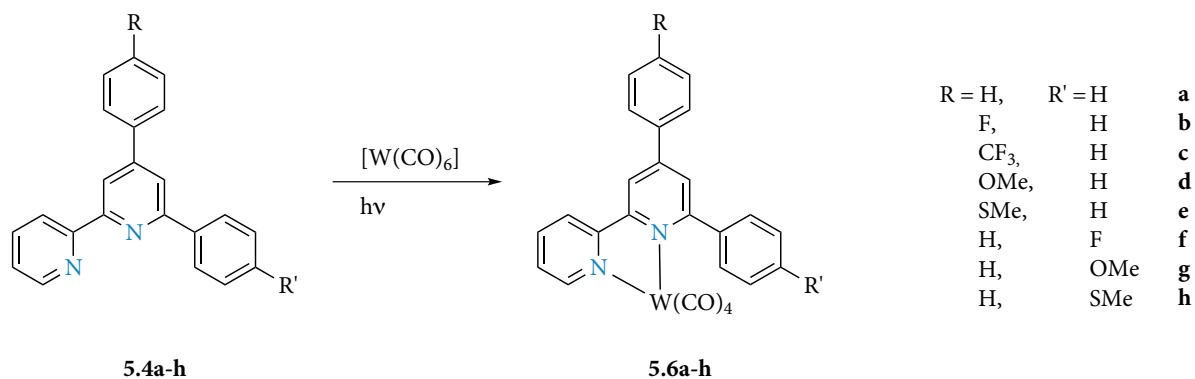
same substitution pattern were obtained through the same synthetic route in good yields as well.

Tungsten(0) carbonyl complexes **5.5a-h** were synthesised of pyridylphosphinines **5.3a-h** in order to exploit the carbonyl stretching bands in the IR spectra for insight into the impact of substituents on electronic ligand properties (Scheme 5-2). Using a photochemical approach which is facilitated by the stability of pyridylphosphinines **5.3a-h** towards UV light radiation, [(P,N)W(CO)₄]-type complexes **5.5a-h** were obtained as dark red solids that are stable towards air and moisture for several hours or even days. The ³¹P NMR spectra of the reaction mixture over time revealed an intermediate, a monocoordinated complex of the type [(κ-P,N)W(CO)₅] which could not be isolated since it spontaneously loses carbon monoxide to form the final chelated product **5.5a-h** (Scheme 5-2). All differently substituted [(P,N)W(CO)₄]-type compounds **5.5a-h** were isolated in pure form and fully characterised.



Scheme 5-2: Synthesis of pyridylphosphinine-based tungsten(0) carbonyl complexes **5.5a-h**.

The same approach of irradiating a mixture of ligand and [W(CO)₆] in THF with UV light also allowed the synthesis of the corresponding bipyridine-based tungsten(0) complexes **5.6a-h** (Scheme 5-3). Again these compounds were isolated in pure form as dark red solids and could be fully characterised.



Scheme 5-3: Synthesis of bipyridine-based complexes **5.6a-h** of the type [(N,N)W(CO)₄].

The study of substituent effects was carried out on three different levels, on pyrylium salts **5.2a-h**, pyridylphosphinines **5.3a-h** and bipyridines **5.4a-h** as well as on their tungsten(0) carbonyl complexes **5.5a-h** and **5.6a-h**, using a variety of different methods. X-ray diffraction was used to gain insight into the molecular structures of the molecules in the solid state and revealed significant differences between pyridylphosphinine- and bipyridine-based complexes **5.5a-h** and **5.6a-h** (Figure 5-2). For the evaluation of substituent effects however, this method was not sensitive enough.

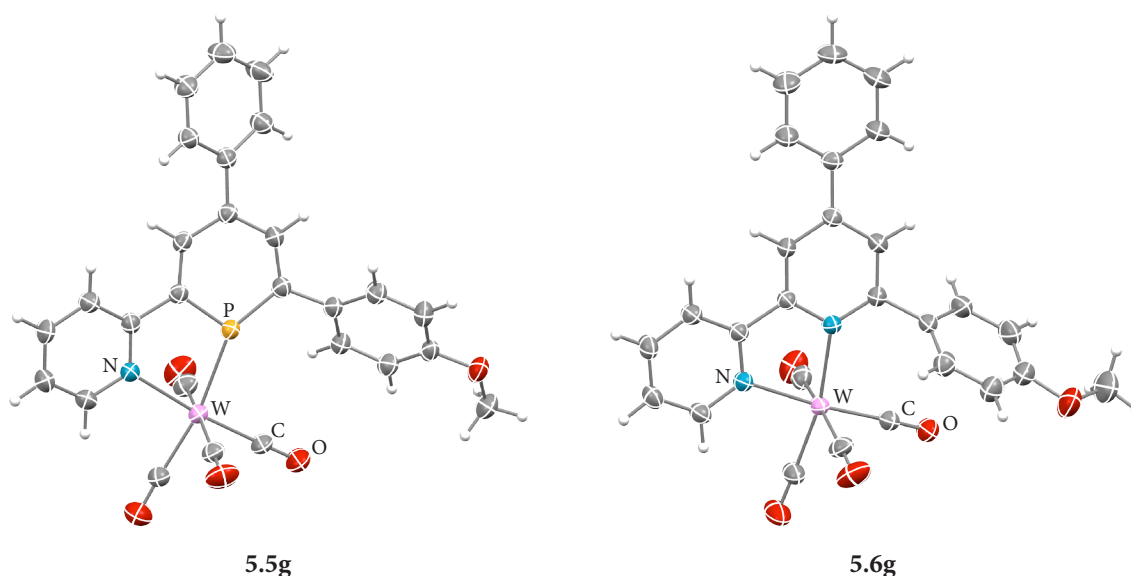


Figure 5-2: Molecular structures in the crystal of tungsten(0) complexes **5.5g** and **5.6g**.

Pyrylium salts are known to be strongly coloured and often highly fluorescent compounds. Therefore UV-Vis and fluorescence spectroscopy were used to determine changes in their properties with the variation of substituents. First effects were already visible looking at the isolated compounds in the solid state which varied in colour from bright yellow (**5.2a-c**, **f**: R or R' = H, F, CF₃) to orange (**5.2d**, **g**: R or R' = OMe) and even dark red to violet (**5.2e**, **h**: R

or $R' = \text{SMe}$). Consequently, electron withdrawing groups did not exhibit a significant impact in the UV-Vis spectra. Methoxy and methylthio substituents, however, caused a strong red-shift of the longest wavelength absorption band, which can be attributed to their ability to transfer electron density to the π -system. As expected from their stronger electron donating properties, the band of pyrylium salts **5.2e** and **h** bearing a methylthio group is more red-shifted than the ones of methoxy substituted derivatives **5.2d** and **g**.

Looking at fluorescence spectra of pyrylium salts **5.2a-h**, a range of colours with strong differences in intensity of the emission was detected (Figure 5-3). Explaining the connection of a specific substituent with the observed photoluminescence properties of the respective pyrylium salt proved to be not straightforward. However, using a model of viewing 2,4,6-triarylpyrylium salts as two-dimensional chromophore systems originally established for triphenylmethane dyes, a conclusive reasoning for the obtained observations was possible and clear guidelines on how to use substituents for colour tuning the photoluminescence of pyrylium salts were presented. While the colour of emission can be modified with substituents on the 6-phenyl ring from blue (**5.2f**: $R' = \text{F}$) to yellow (**5.2g**: $R' = \text{OMe}$) to red (**5.2h**: $R' = \text{SMe}$), the emission intensity can be influenced with electron donating groups on the 4-phenyl ring. If a future application demands it, combination of both effects could be an interesting strategy to obtain pyrylium salts with tuneable light emission of good intensity.

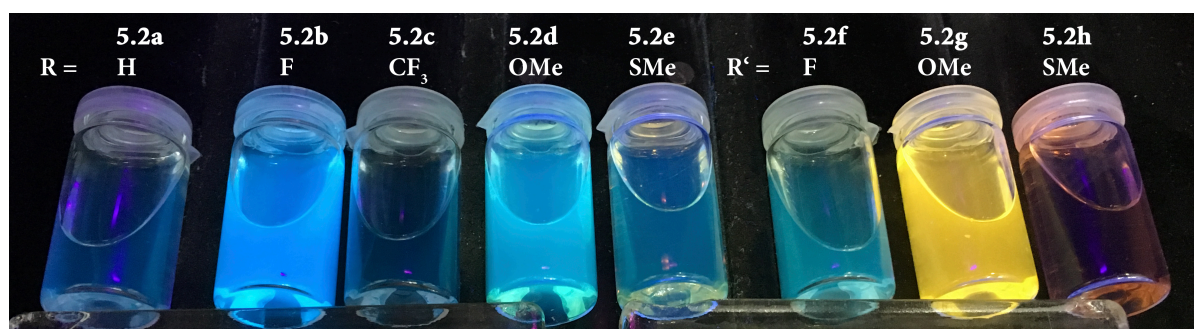


Figure 5-3: Solutions of pyrylium salts **5.2a-h** under UV light showing their varying photoluminescence properties.

Furthermore, the electronic properties of differently substituted pyridylphosphinines **5.3a-h** and bipyridines **5.4a-h** were evaluated by comparison of their frontier orbitals, which were calculated at the B3LYP/6-311+G(d,p) level of DFT theory. The general classification of pyridines as good σ -donors and phosphinines as good π -acceptors but significantly weaker

σ -donors is reflected in the shape and energy levels of the frontier orbitals of the here evaluated P,N-hybrid and N,N compounds (Figure 5-4).

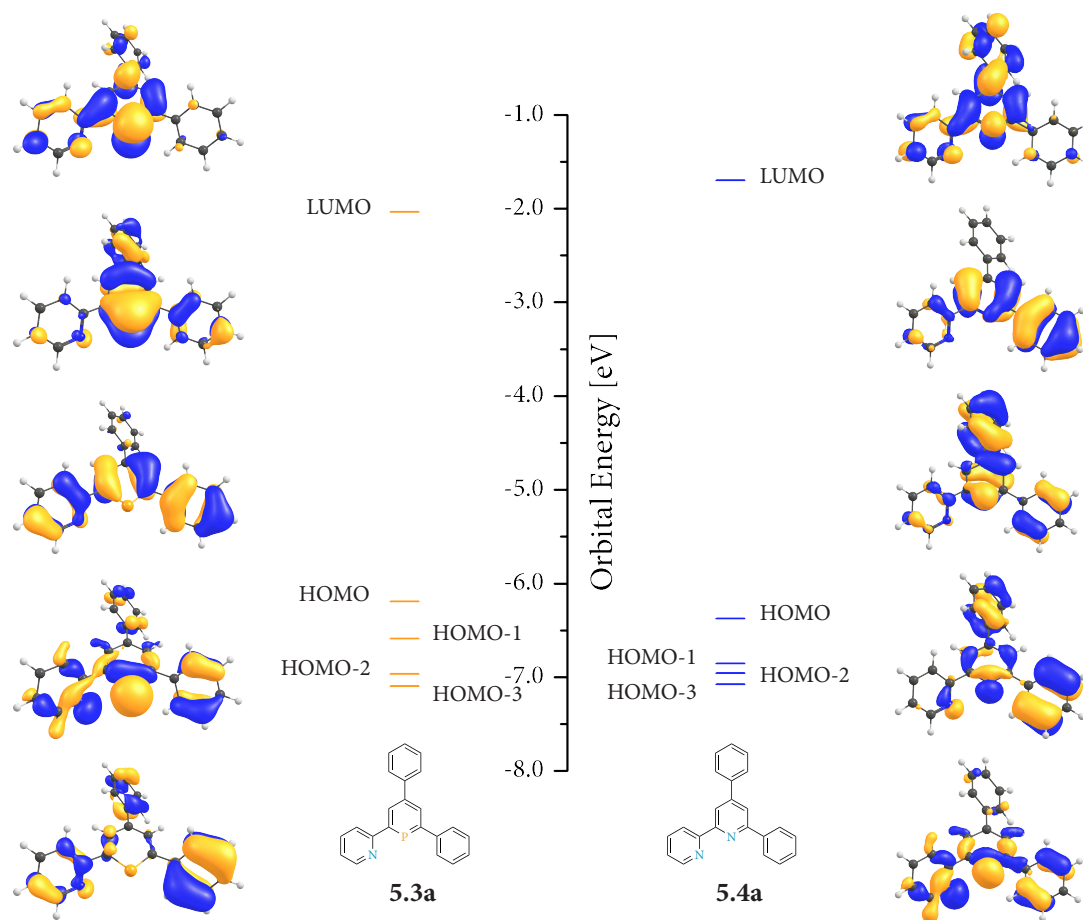


Figure 5-4: Molecular orbital scheme of the frontier orbitals of pyridylphosphinine **5.3a** and bipyridine **5.4a**.

While the lone pairs (HOMO-2, HOMO-3) are similar in energy, the one at the phosphorus atom in pyridylphosphinines is more diffuse, larger and less directional than the ones of bipyridine; it is of higher s -character making σ -donation less efficient. HOMO and LUMO are of π -symmetry. For pyridylphosphinines, they have high coefficients on the phosphorus atom. The contribution by the nitrogen atom in bipyridines is, however, much less pronounced. Additionally, the LUMO is lower and the HOMO higher in energy for pyridylphosphinines compared to the corresponding bipyridine. Hence, the P,N-hybrid compounds exhibit the expected good π -acceptor properties but also do have the potential for π -donation abilities, which has never been investigated before. And indeed with the introduction of substituents able to donate electrons to the π -system (**5.3d, e, g, h**: R or R' = OMe, SMe), the π -shaped HOMO of pyridylphosphinines is raised significantly in energy which has visible ramifications on their experimental properties. Electron-withdrawing

groups (**5.3b, c, f**: R or R' = F, CF₃), on the other hand, slightly lower the energy levels of all frontier orbitals thereby decreasing σ - and π -donor properties and enhancing the π -acceptor character. Considering solely the results from calculated frontier orbitals, the introduction of substituents has a very clear effect on the properties of pyridylphosphinines and bipyridines and the type of impact is similar for both. A systematic tuning of properties using different substituents in the backbone is therefore possible.

For the experimental confirmation of substituent effects on electronic properties of pyridylphosphinines and bipyridines, the carbonyl stretching frequencies in the IR spectra of their tungsten(0) carbonyl complexes **5.5a-h** and **5.6a-h** were measured and compared. Generally, carbonyl stretching bands of pyridylphosphinine complexes appear at higher wavenumbers than of the respective bipyridine compounds, which corresponds to their weaker σ -donating and stronger π -accepting properties. Confirming the results of the DFT calculations, electron withdrawing substituents on the pyridylphosphinine (**5.5b, c, f**: R or R' = F, CF₃) shift the carbonyl stretching bands to slightly higher wavenumbers in line with a weaker donating and stronger accepting ligand. Interestingly, the electron donating groups cause an even stronger shift to higher wavenumbers (**5.5d, e, h** and **5.6d, e, g, h**: R or R' = OMe, SMe) which seems counterintuitive at first but can be explained by a repulsion of the energetically high lying and potentially π -donating HOMO and a filled d-orbital of the electron rich tungsten(0) metal centre (Figure 5-5).

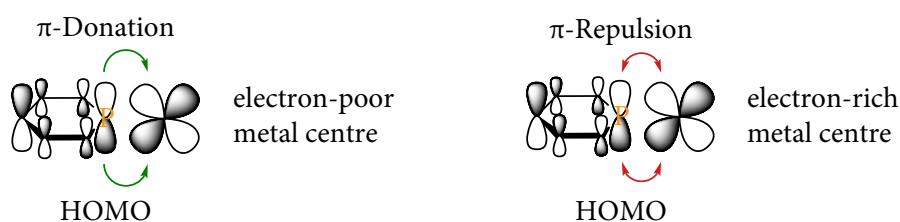


Figure 5-5: Two possible forms of interaction for the HOMO of a phosphinine with a metal centre.

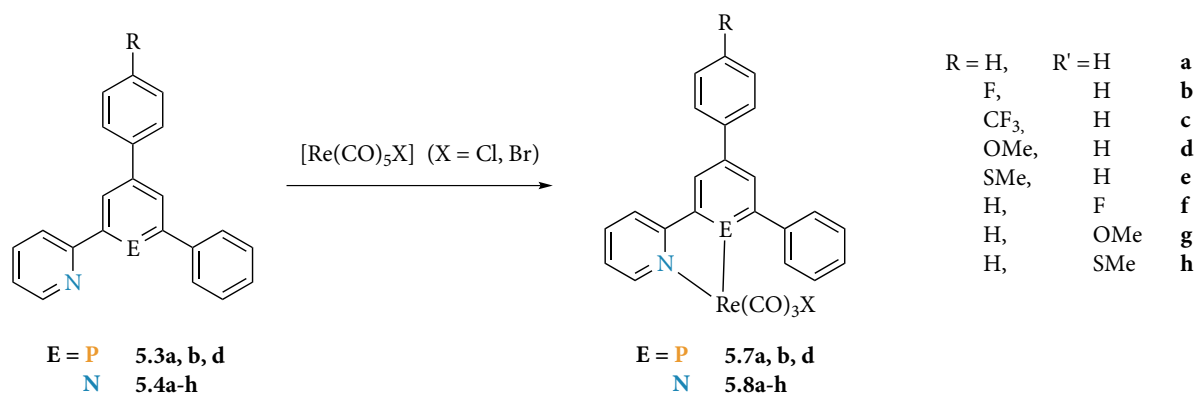
This has to be considered the first time, π -donating properties have been experimentally shown to have a significant impact on the coordination properties of phosphinines. And while this behaviour has here been deliberately enhanced by substituents, the π -donor character of the HOMO should be taken into account for the evaluation of phosphinines from now on. Additionally, displaying a HOMO and a LUMO with the same shape and orientation, phosphinines are unique compared to conventional π -donor ligands like

sulphide, thiocyanate or halides where π -donating and π -accepting orbitals are orthogonal to each other. The implications for the coordination properties of pyridylphosphinines were shown here with the HOMO causing a repulsion of the ligand from the metal centre instead of strengthening the metal-ligand bond through π -donation (Figure 5-5).

Bipyridine-based tungsten(0) complexes generally exhibit the same trends. Electron withdrawing substituents weaken the donor abilities and strengthen the acceptor properties (**5.6b, c, f**: R or R' = F, CF₃). On the other hand, electron donating groups raise the π -shaped HOMO in energy which again causes weakening of the metal-ligand bond through repulsion with a filled d-orbital of the tungsten centre. This effect, however, is less pronounced for bipyridine ligands since the coefficient on the central nitrogen atom is much smaller compared to pyridylphosphinines (**5.6d, e**: R or R' = OMe, SMe). Additionally, the metal-ligand bond is shorter in [(N,N)W(CO)₄]-type complexes which causes the 6-phenyl ring to rotate out of the central pyridine plane to avoid steric hindrance with the metal carbonyl fragment thereby effectively disrupting conjugation of the π -system. Hence, methoxy and methylthio groups on the 6-phenyl ring do not show any electronic effect on the complex (**5.6g, h**: R or R' = OMe, SMe). Compared to [(P,N)W(CO)₄]-type complexes, the systematic manipulation of the electronic situation is therefore more difficult for bipyridine-based compounds.

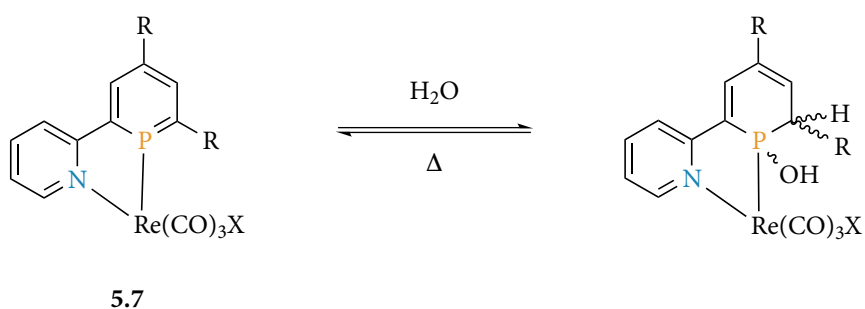
Looking for a possible application and subsequent comparison of pyridylphosphinine-based coordination compounds in a field where so far only bipyridine ligands were exploited, [(L)Re(CO)₃X]-type complexes (X = Cl, Br, **5.7**: L = P,N or **5.8**: L = N,N) were synthesised and characterised (Scheme 5-4). Bipyridine-rhenium(I) carbonyl compounds are able to catalyse both the photo- and electrocatalytic reduction of CO₂ selectively towards CO which is a desirable process from an environmental and economical point of view.

To further support results from the investigation of tungsten(0) complexes, substituent effects were again investigated using IR spectroscopy and X-ray diffraction. Temperature dependent NMR spectra were measured to analyse the hindered rotation of the 6-phenyl ring in [(N,N)Re(CO)₃X]-type complexes **5.8** and to calculate kinetic data for this rotation. Pyridylphosphinine-based rhenium(I) compounds did not show this phenomenon due to structural differences between the phosphinine heterocycle and the pyridine ring.



Scheme 5-4: Synthesis of rhenium(I) carbonyl complexes with pyridylphosphinine and bipyridine ligands.

Pyridylphosphinine-based rhenium(I) carbonyl compounds **5.7** are sensitive towards nucleophiles and the reaction with water was studied in detail. An unselective *syn*- and *anti*-addition of water to the external P=C double bond was observed leading to a mixture of eight stereoisomers in four pairs of enantiomers (Scheme 5-5). Interestingly enough, this water addition is an equilibrium reaction and its temperature-dependent reversibility was shown in a ³¹P NMR study. Bipyridine-based rhenium(I) complexes **5.8** on the other hand are stable towards attack of nucleophiles.



Scheme 5-5: Reversible but unselective addition of water to the external P=C double bond of [(P,N)Re(CO)₃X]-type complexes.

Working towards the application of rhenium(I) complexes as redox active catalysts in CO₂ reduction reaction, the redox behaviour of coordination compounds **5.7** and **5.8** was investigated *via* cyclic voltammetry experiments. Similar to what is known for bipyridine-based rhenium(I) carbonyl complexes, a first reduction located on the ligand and a second metal-centred reduction wave was observed. In line with the energetically low lying LUMO of pyridylphosphinines, the first reduction takes place at much less negative potentials for complexes of the type [(P,N)Re(CO)₃X] (**5.7**) compared to the respective bipyridine compounds **5.8**. However, the second reduction wave is shifted to more negative potentials

lead to the detection of CO as a product. However, these experiments should be viewed as very first attempts for the application of pyridylphosphinine-based catalysts in the photocatalytic reduction of CO₂ to CO. Since [(P,N)Re(CO)₃X]-type compounds **5.7** react with nucleophiles, the addition of water or the sacrificial agent triethanolamine most likely leads to deactivation of the catalysts. However, this addition reaction was shown to be reversible with temperature. Therefore conducting photocatalysis experiments at higher temperatures would be a viable option for future experiments. Alternatively, the two tasks of a photocatalyst, as a photosensitiser and as the reactive site, could be separated into two compounds working together, which has been reported in literature only for a few examples. The [(P,N)W(CO)₄]-type complex **5.5a** could be used as reactive site since it displayed a strong current enhancement under CO₂ atmosphere in cyclic voltammetry experiments. For this approach to succeed, a suitable photosensitiser with enough reduction power to reduce **5.5a** twice needs to be found. However, also switching to an electrochemical setup has to be considered (Scheme 5-6b). The complex of the type [(P,N)W(CO)₄] (**5.5a**) should be applied in the electrochemical reduction of CO₂ which was already successfully reported for the bipyridine analogue **5.6a**. Not suitable as a photosensitiser but showing reactivity towards CO₂ in cyclic voltammograms, the water stable compound **5.5a** shows promise as an electrocatalyst.

In summary, an in-depth investigation of electronic properties has been presented for an interesting new class of P,N-hybrid compounds, the 2-pyridylphosphinines. Direct comparison with the analogous 2,2'-bipyridines lead to the discovery of similarities but also exploitable differences between those compounds. The introduction of substituents into the backbone of pyridylphosphinines was shown to be a viable method of systematically tuning their electronic properties as adjustment for future applications. Using electron donating groups, an unprecedented, experimental proof of the π -donating HOMO having a significant influence on the ligand properties of phosphinines has been presented. Moreover, first steps towards the application of pyridylphosphinines in homogeneous catalysis were described and showed promising results for future investigations.

6 Appendix

6.1 Frontier Orbitals of Ligands

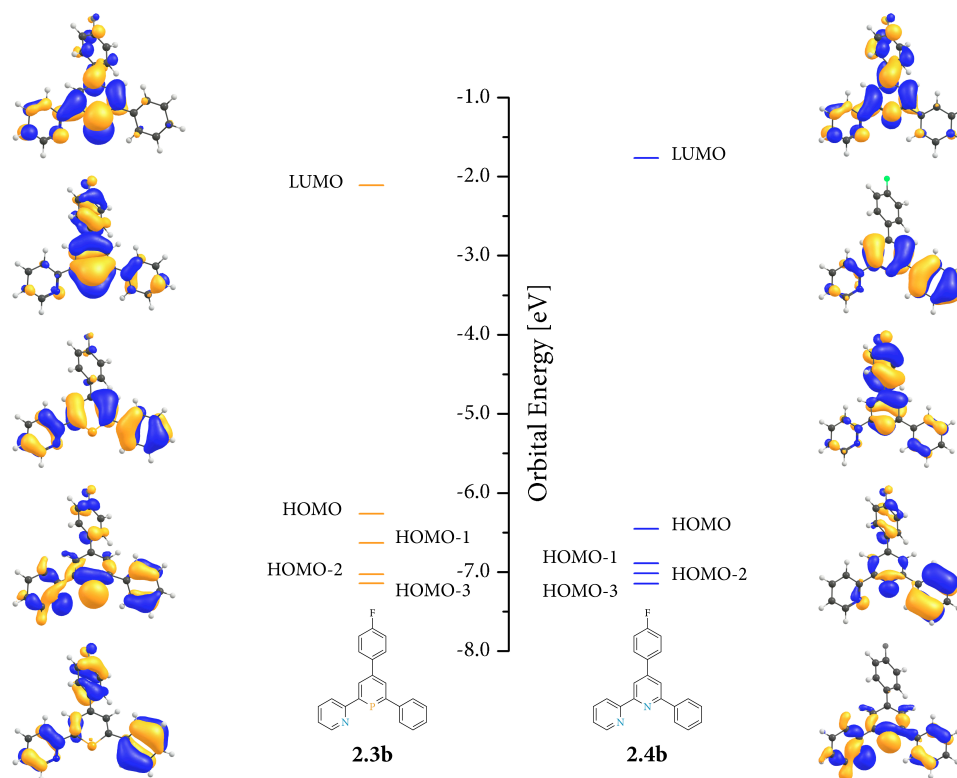


Figure 6-1: Frontier orbitals of the unsubstituted ligands 2.3b and 2.4b.

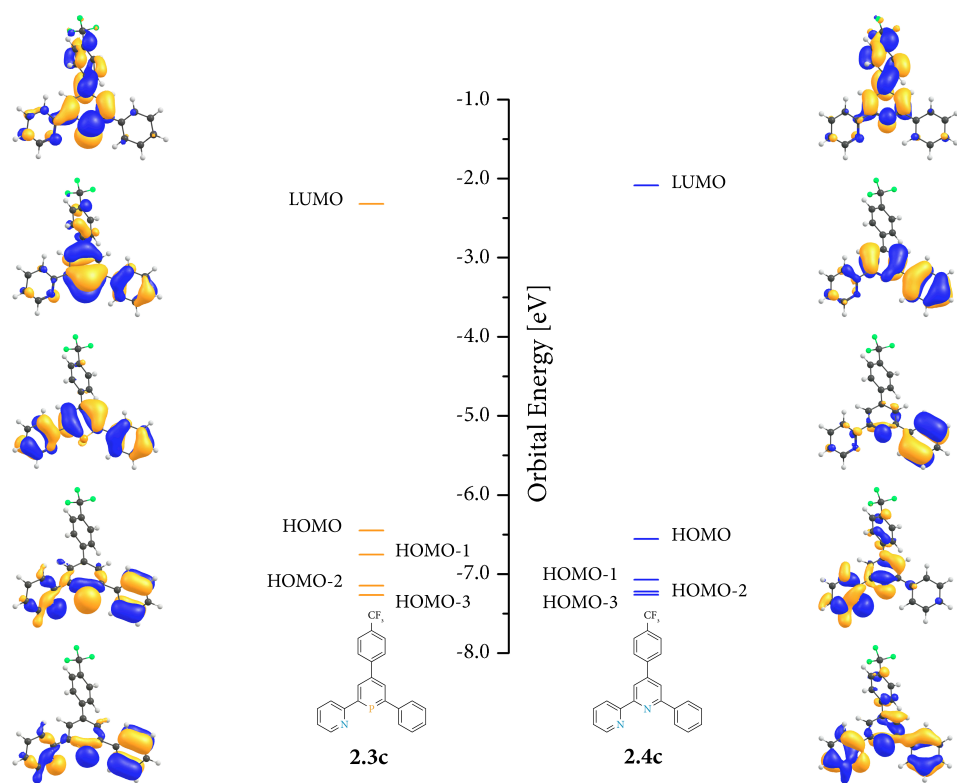


Figure 6-2: Frontier orbitals of the unsubstituted ligands 2.3c and 2.4c.

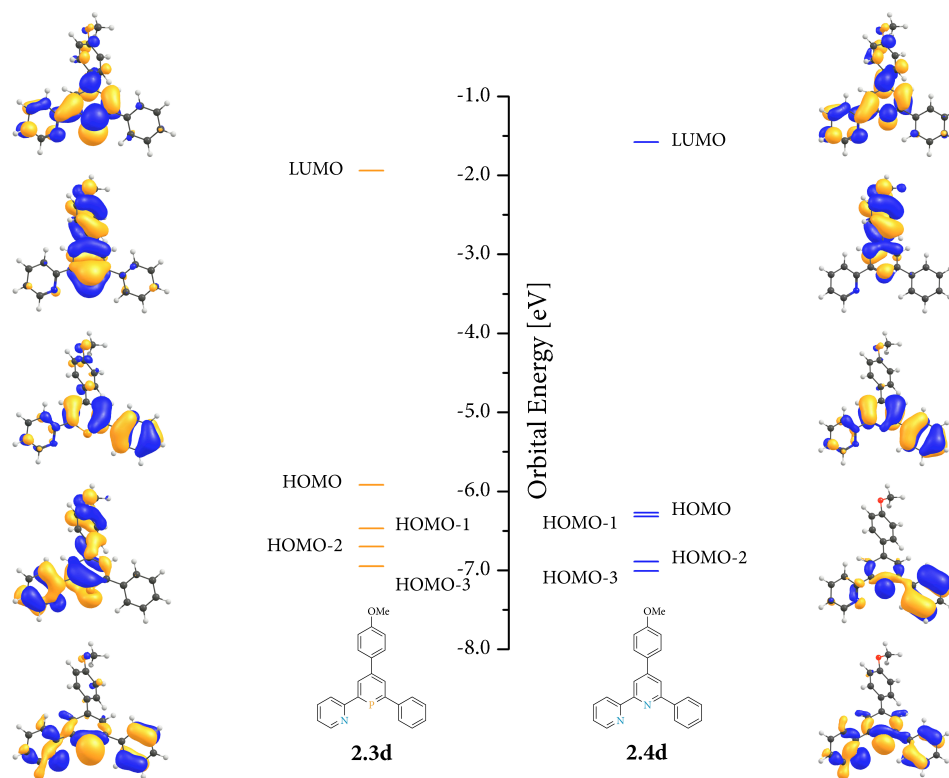


Figure 6-3: Frontier orbitals of the unsubstituted ligands **2.3d** and **2.4d**.

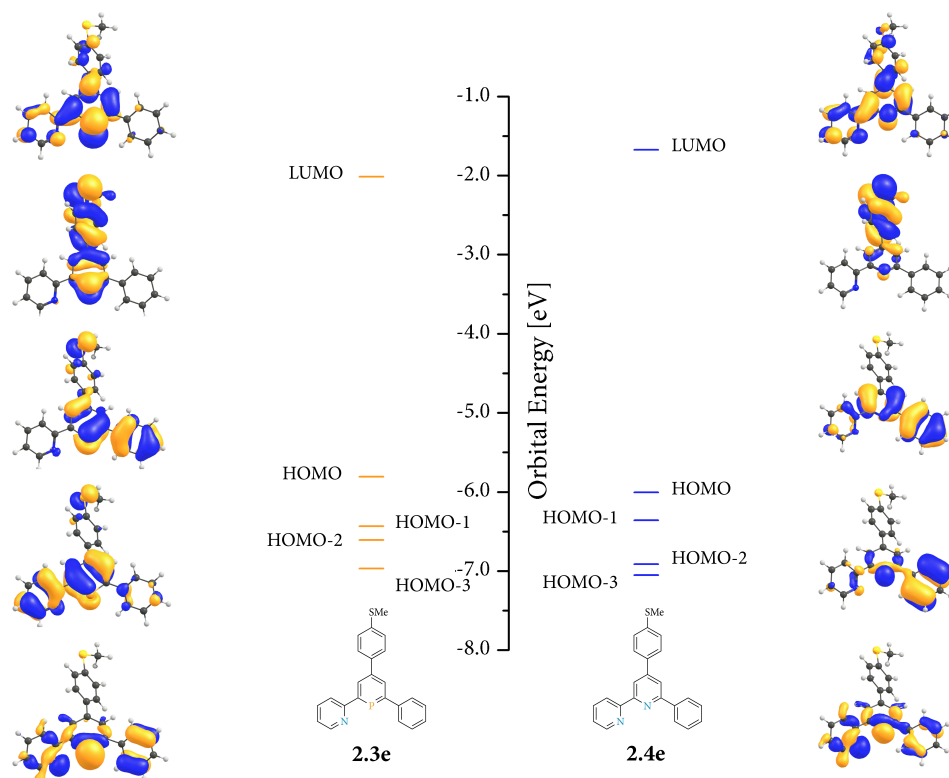


Figure 6-4: Frontier orbitals of the unsubstituted ligands **2.3e** and **2.4e**.

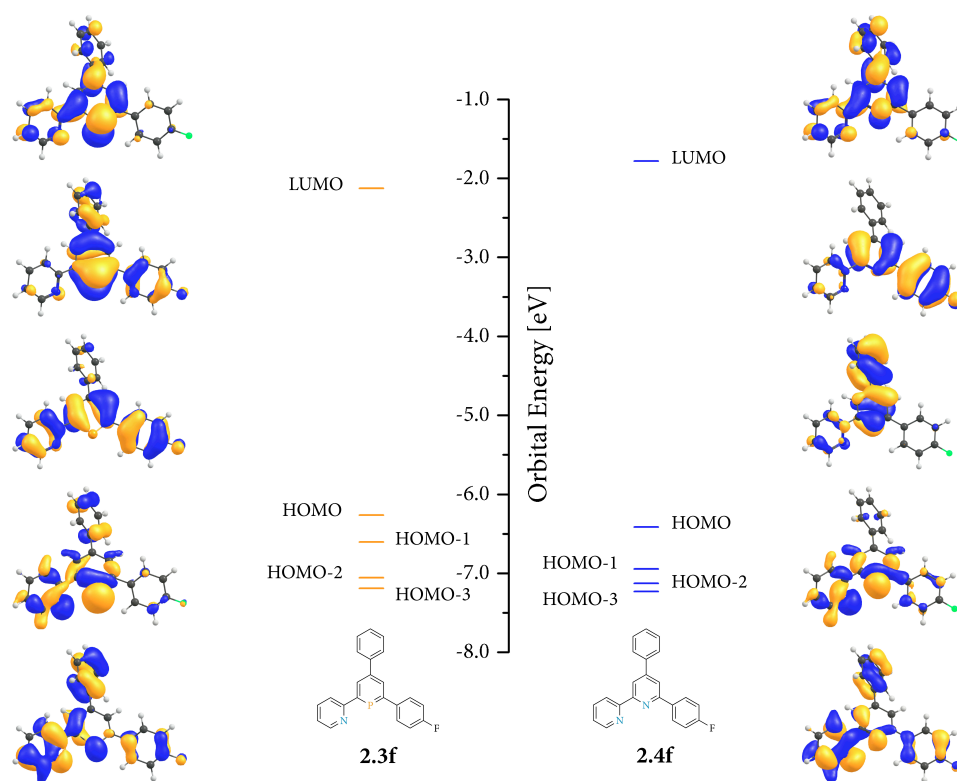


Figure 6-5: Frontier orbitals of the unsubstituted ligands 2.3f and 2.4f.

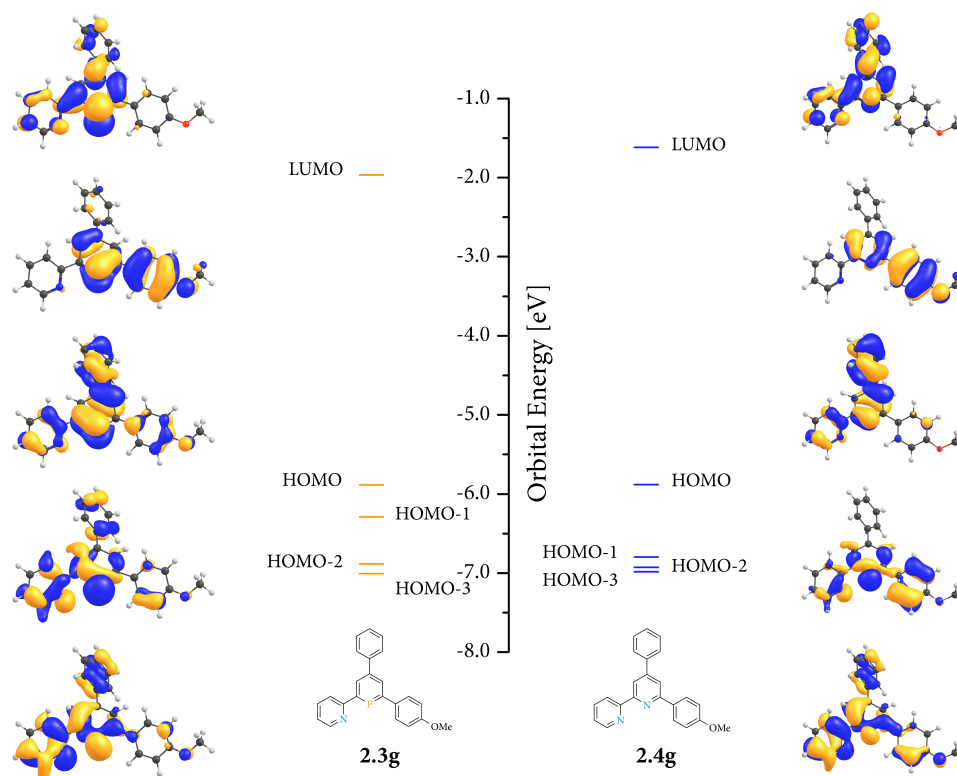


Figure 6-6: Frontier orbitals of the unsubstituted ligands 2.3g and 2.4g.

6.2 Temperature Dependent NMR Experiments

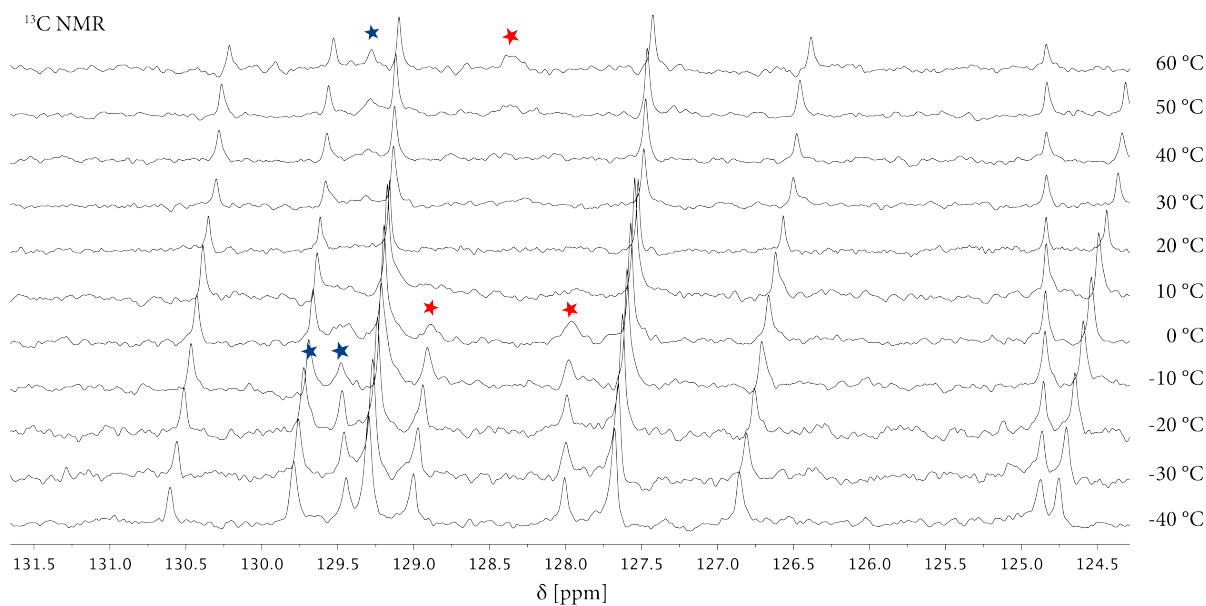


Figure 6-7: Temperature dependent ¹³C NMR experiments in THF-*d*₈ of [N,N-Re(CO)₃X]-type complex **3.7a**. Spectra were measured in steps of 5 °C but not all spectra are shown for better clarity.

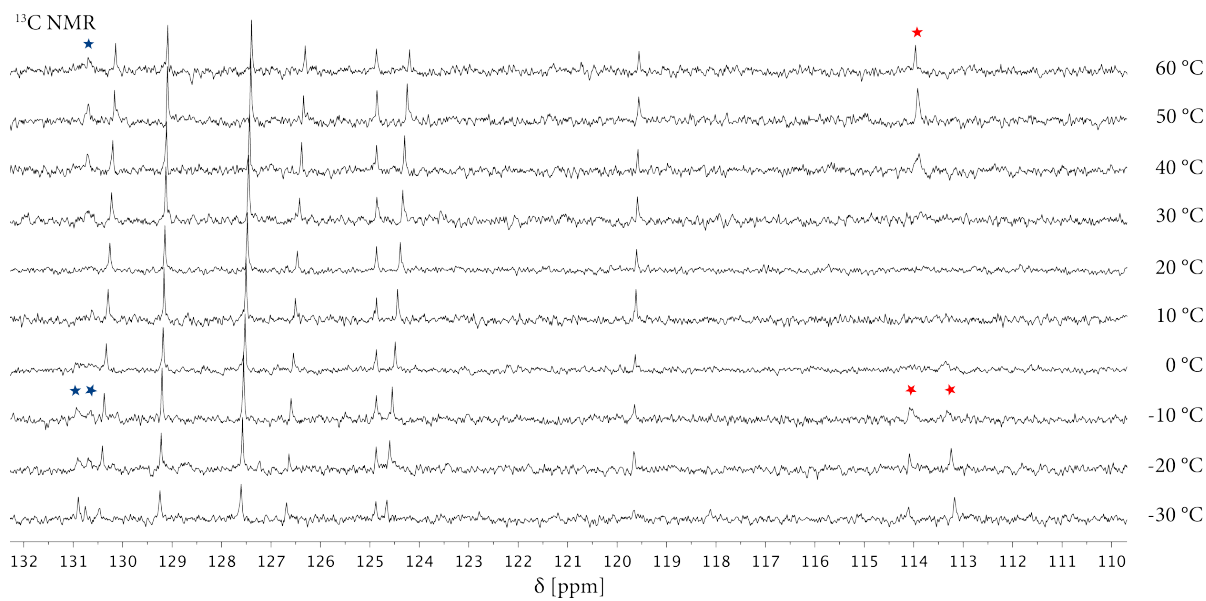


Figure 6-8: Temperature dependent ¹³C NMR experiments in THF-*d*₈ of methoxy substituted [N,N-Re(CO)₃X]-type complex **3.7d**. Spectra were measured in steps of 5 °C but not all spectra are shown for better clarity.

6.3 Cyclic Voltammograms of Rhenium(I) Complexes

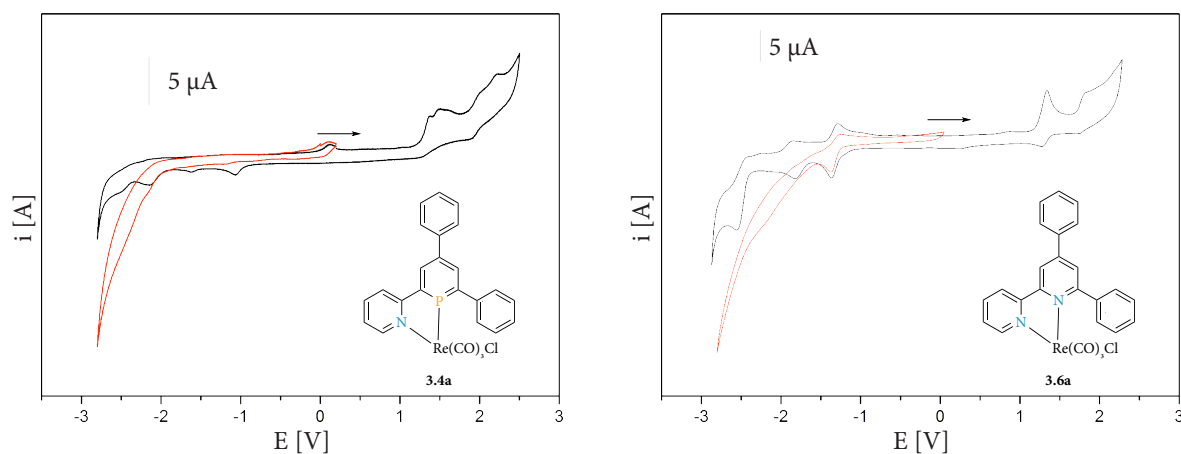


Figure 6-9: Cyclic voltammograms of [P,N-Re(CO)₃Cl]-type complex **3.4a** and [N,N-Re(CO)₃Cl]-type complex **3.6a** measured 0.5 mM in acetonitrile with 0.1 M TBAPF₆ as electrolyte at 50 mV/s (**3.4a**) or 100 mV/s (**3.6a**) under argon (black) and under CO₂ (red).

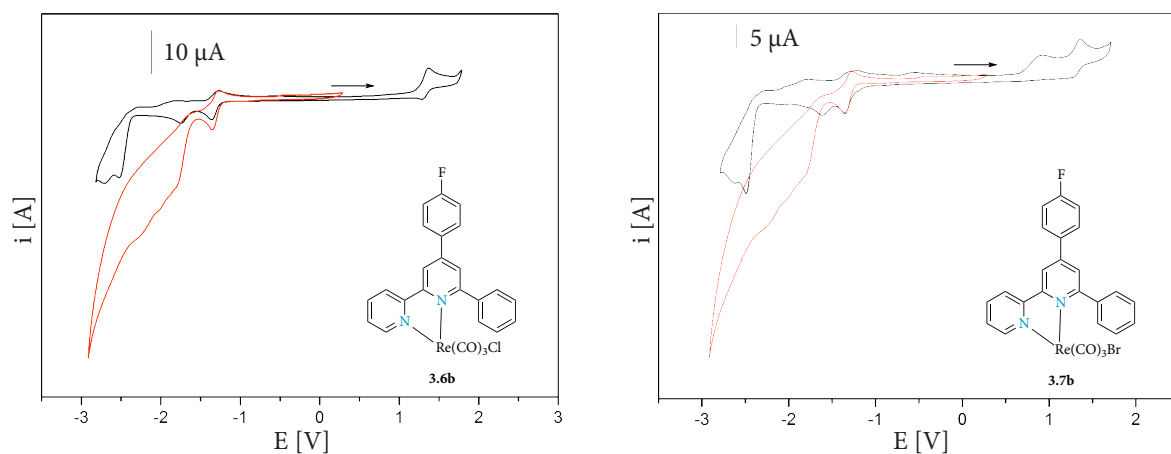


Figure 6-10: Cyclic voltammograms of [N,N-Re(CO)₃Cl]-type complexes **3.6b** and **3.7b** measured 0.5 mM in acetonitrile with 0.1 M TBAPF₆ as electrolyte at 100 mV/s under argon (black) and under CO₂ (red).

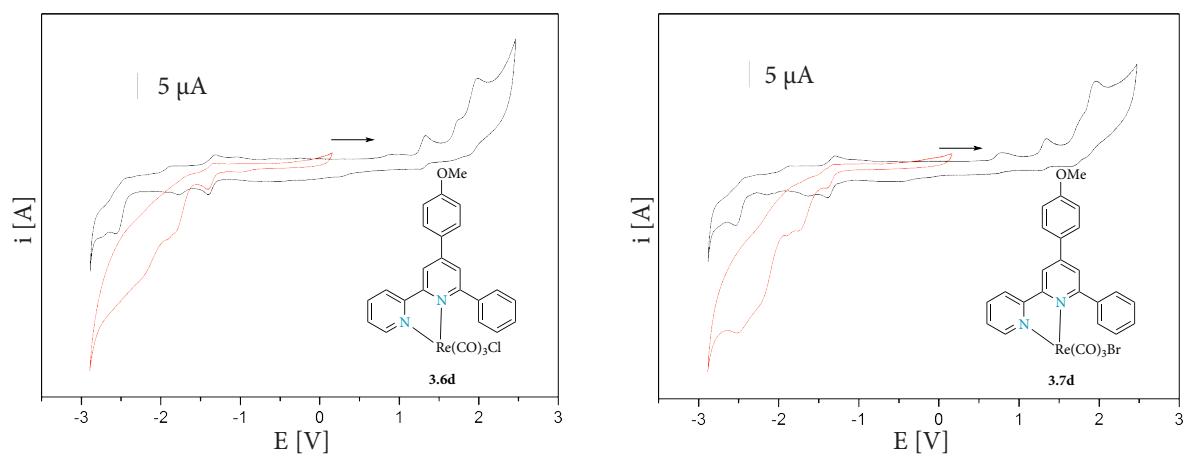


Figure 6-11: Cyclic voltammograms of [N,N-Re(CO)₃Cl]-type complexes **3.6d** and **3.7d** measured 0.5 mM in acetonitrile with 0.1 M TBAPF₆ as electrolyte at 100 mV/s under argon (black) and under CO₂ (red).

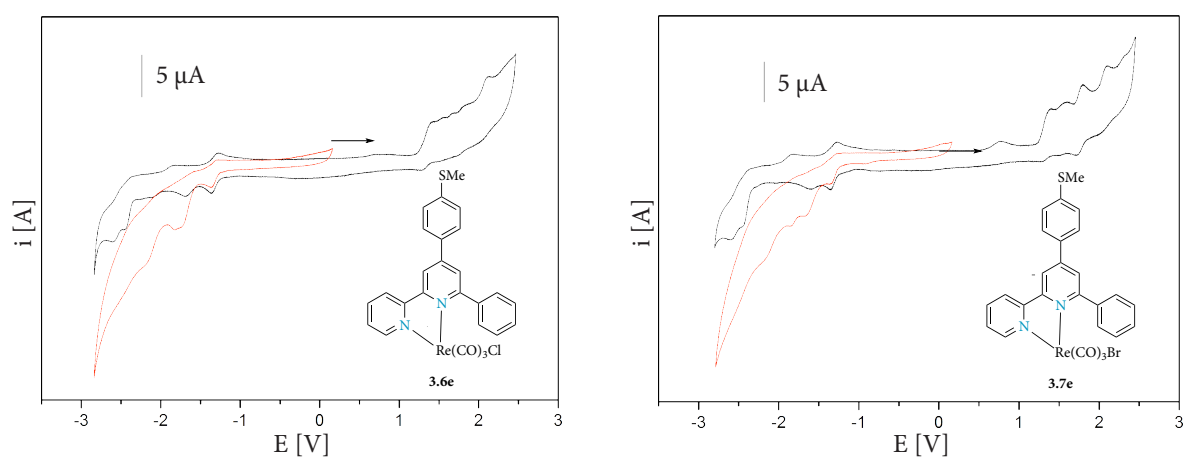


Figure 6-12: Cyclic voltammograms of [N,N-Re(CO)₃Cl]-type complexes **3.6e** and **3.7e** measured 0.5 mM in acetonitrile with 0.1 M TBAPF₆ as electrolyte at 100 mV/s under argon (black) and under CO₂ (red).

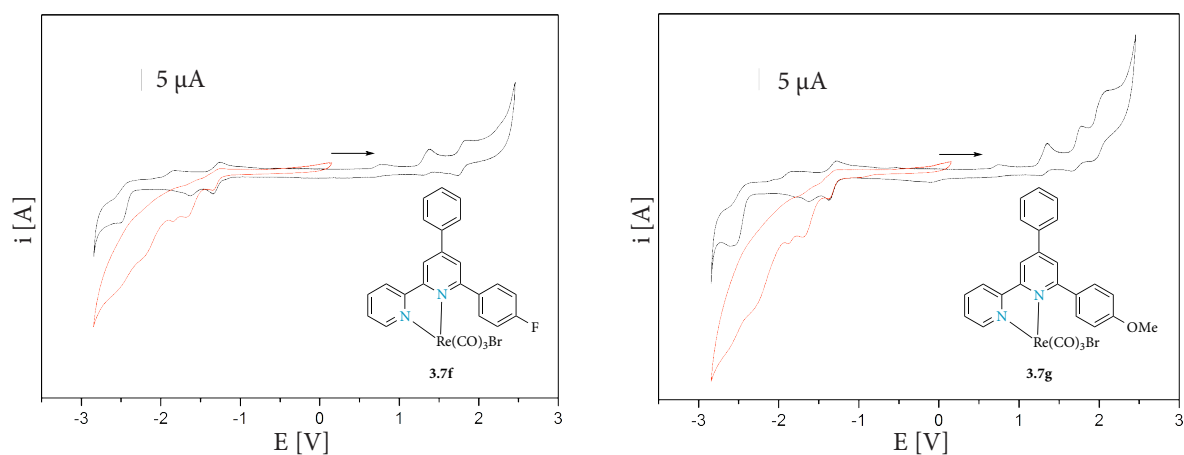


Figure 6-13: Cyclic voltammograms of [N,N-Re(CO)₃Cl]-type complexes **3.7f** and **3.7g** measured 0.5 mM in acetonitrile with 0.1 M TBAPF₆ as electrolyte at 100 mV/s under argon (black) and under CO₂ (red).

6.4 Photocatalytic Reduction of CO₂

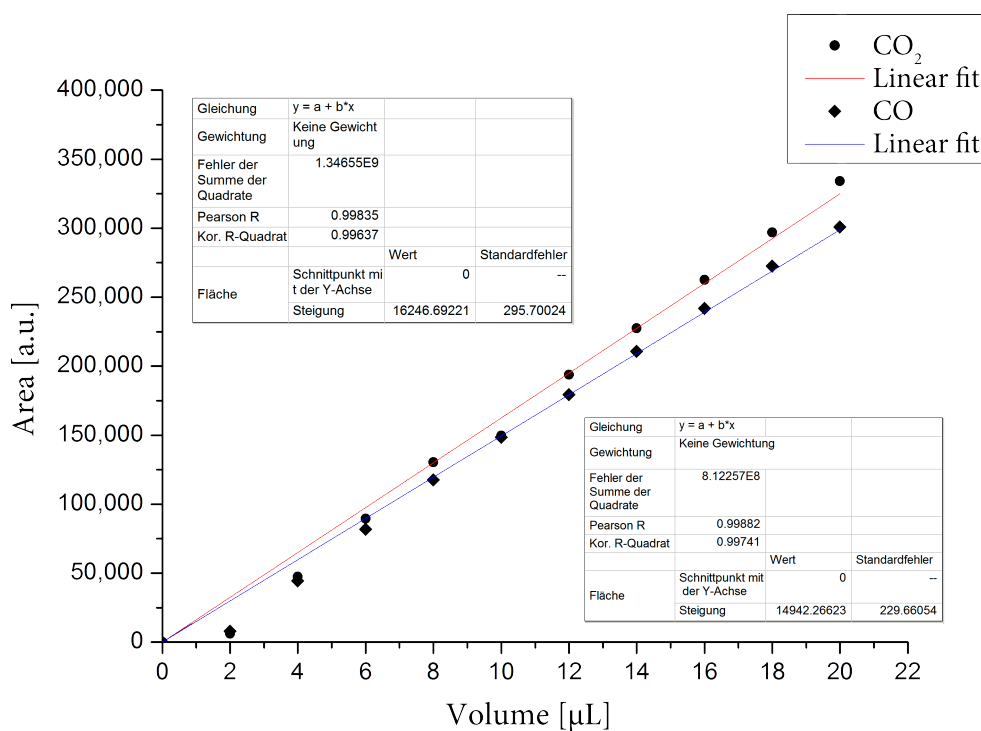


Figure 6-14: Calibration curve for gases CO₂ and CO for gas chromatography analysis.

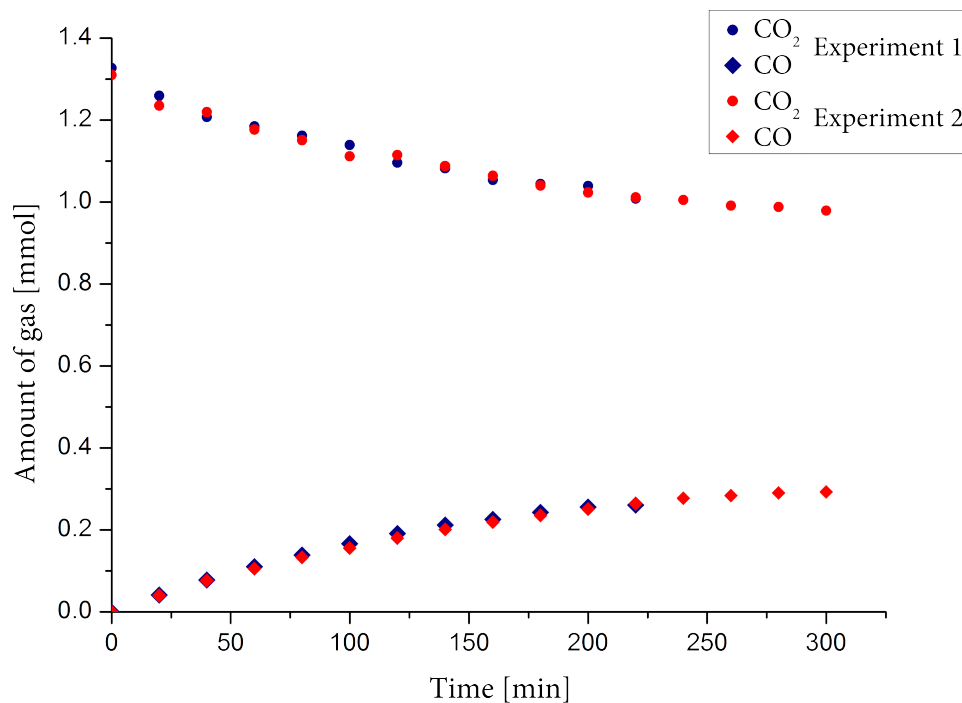


Figure 6-15: Monitoring *via* gas chromatography of the headspace content over time during a photocatalytic reduction of CO₂ using [(bipy)Re(CO)₃Cl] (3.1) as catalyst.

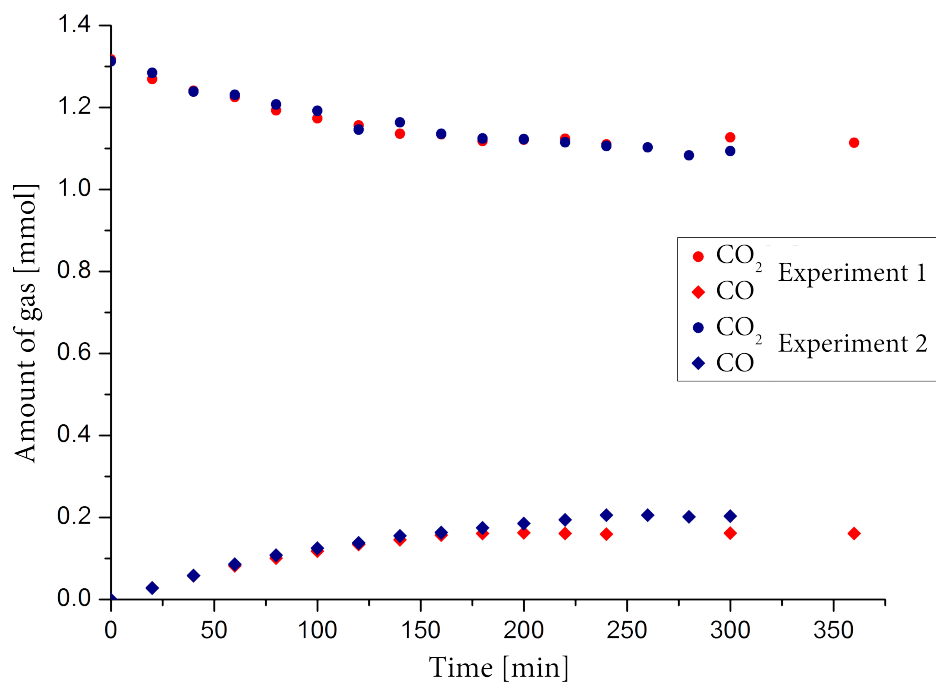


Figure 6-16: Monitoring *via* gas chromatography of the headspace content over time during a photocatalytic reduction of CO₂ using [(N,N)Re(CO)₃Cl]-type complex **3.6a** as catalyst.

6.5 Table of Abbreviations

Ar	Aryl
ax	Axial
BNAH	1-Benzyl-1,4- dihydronicotinamide
bpy	Bipyridine
COD	1,5-Cyclooctadiene
Cp	Cyclopentadienyl
Cp*	Pentamethylcyclopentadienyl
CV	Cyclic voltammetry
δ	Chemical shift
d	Doublet
DCM	Dichloromethane
DFT	Density functional theory
DMF	N,N-Dimethylformamide
DMSO	Dimethyl sulfoxide
E°	Standard electrode potential
$E_{1/2}$	Half wave potential
E_{pa}	Anodic peak potential
E_{pc}	Cathodic peak potential
Ed	Editor
Et	Ethyl

Fc	Ferrocene
Fc ⁺	Ferrocenium
<i>h</i>	Planck constant
HOMO	Highest Occupied Molecular Orbital
Hz	Hertz
IR	Infrared
ir	Irreversible
IUPAC	International Union of Pure and Applied Chemistry
<i>J</i>	Coupling Constant
λ	Wave length / Valency
LUMO	Lowest Unoccupied Molecular Orbital
m	multiplet
<i>m-</i>	Meta
mbar	Millibar
Me	Methyl
MeCN	Acetonitrile
MHz	Megahertz
MLCT	Metal-to-ligand charge-transfer
MO	Molecular Orbital
NBD	Norbornadiene
NIPHOS	2-(2'-Pyridyl)-4,5-dimethylphosphinine
NMR	Nuclear Magnetic Resonance

NOE	Nuclear Overhauser effect
Ortep	Oak Ridge Thermal Ellipsoid Plot
p _a	Anodic potential
P _c	Cathodic potential
Ph	Phenyl
ppm	Parts per million
Py	Pyridine
qr	Quasireversible
quin	Quintet
R	Gas constant
r.t.	Room temperature
s	Singlet
SCE	Saturated calomel electrode
t	Triplet
TBAPF ₆	Tetrabutylammonium hexafluorophosphate
TEA	Triethylamine
TEOA	Triethanolamine
THF	Tetrahydrofuran
TICT	Twisted intramolecular charge transfer
TMS	Trimethylsilyl
TOF	Turnover frequency
TON	Turnover number

UV	Ultra violet
ν	Stretching modes
$\tilde{\nu}$	Wave number

6.6 Literature References

- (1) T. Anderson, *Ann. Chem. Pharm.* **1851**, 80 (1), 44.
- (2) G. Märkl, *Angew. Chem.* **1966**, 78 (18–19), 907.
- (3) A. J. Ashe, *J. Am. Chem. Soc.* **1971**, 93 (13), 3293.
- (4) P. Le Floch, In *Phosphorus-Carbon Heterocyclic Chemistry*, F. Mathey (Ed.), Elsevier: Oxford, **2001**, 485–533.
- (5) C. Müller, L. E. E. Broeckx, I. de Krom, J. J. M. Weemers, *Eur. J. Inorg. Chem.* **2013**, 2013 (2), 187.
- (6) J. C. J. Bart, J. J. Daly, *Angew. Chem.* **1968**, 80 (20), 843.
- (7) C. Müller, M. Lutz, A. L. Spek, D. Vogt, *J. Chem. Crystallogr.* **2006**, 36 (12), 869.
- (8) W. Fischer, E. Hellner, A. Chatzidakis, K. Dimroth, *Tetrahedron Lett.* **1968**, 9 (59), 6227.
- (9) J. C. J. Bart, *Angew. Chem. Int. Ed. Engl.* **1968**, 7 (9), 730.
- (10) E. G. Cox, J. A. S. Smith, *Nature* **1954**, 173 (4393), 75.
- (11) D. Mootz, *J. Chem. Phys.* **1981**, 75 (3), 1517.
- (12) C. Müller, In *Phosphorus(III) Ligands in Homogeneous Catalysis: Design and Synthesis*, P. C. J. Kamer, P. W. N. M. van Leeuwen (Eds.), John Wiley & Sons, Ltd.: Chichester, UK, **2012**, 287–307.
- (13) K. K. Baldridge, M. S. Gordon, *J. Am. Chem. Soc.* **1988**, 110 (13), 4204.
- (14) L. Nyulaszi, T. Veszpremi, J. Reffy, B. Burkhardt, M. Regitz, *J. Am. Chem. Soc.* **1992**, 114 (23), 9080.
- (15) G. Frison, A. Sevin, N. Avarvari, F. Mathey, P. Le Floch, *J. Org. Chem.* **1999**, 64 (15), 5524.
- (16) J. A. Chamizo, J. Morgado, P. Sosa, *Organometallics* **1993**, 12 (12), 5005.
- (17) C. A. Tolman, *Chem. Rev.* **1977**, 77 (3), 313.
- (18) A. Poater, B. Cosenza, A. Correa, S. Giudice, F. Ragone, V. Scarano, L. Cavallo, *Eur. J. Inorg. Chem.* **2009**, 2009 (13), 1759.
- (19) H. Clavier, S. P. Nolan, *Chem. Commun.* **2010**, 46 (6), 841.
- (20) M. Bruce, *Synthesis of Novel Ligands Based on 2-(2'-Pyridyl)-4,6-diphenylphosphinine: Coordination Chemistry and Reactivity*, Freie Universität Berlin, **2016**.

- (21) D. R. Lide, G. Baysinger, L. I. Berger (Eds.), *CRC Handbook of Chemistry and Physics*, 87th ed., Taylor and Francis: Boca Raton, FL, **2007**.
- (22) C. Batich, E. Heilbronner, V. Hornung, A. J. Ashe, D. T. Clark, U. T. Cogley, D. Kilcast, I. Scanlan, *J. Am. Chem. Soc.* **1973**, 95 (3), 928.
- (23) N. Mezailles, F. Mathey, P. Le Floch, In *Progress in Inorganic Chemistry*, K. D. Karlin (Ed.), John Wiley & Sons, Inc.: Hoboken, **2001** Vol. 49, 455–550.
- (24) N.-N. Pham-Tran, G. Bouchoux, D. Delaere, M. T. Nguyen, *J. Phys. Chem. A* **2005**, 109 (12), 2957.
- (25) C. Elschenbroich, *Organometallicchemie*, 6th ed., C. Elschenbroich, F. Hensel, H. Hopf (Eds.), B. G. Teubner Verlag: Wiesbaden, **2008**.
- (26) A. Loibl, I. de Krom, E. A. Pidko, M. Weber, J. Wiecko, C. Müller, *Chem. Commun.* **2014**, 50 (64), 8842.
- (27) F. Mathey, P. Le Floch, *Sci. Synth.* **2005**, 15, 1097.
- (28) W. Rösch, M. Regitz, *Z. Naturforsch. B* **1986**, 41b, 931.
- (29) U. Amena, M. Regitz, H. Klugeb, *Chem. Ber.* **1990**, 123 (4), 935.
- (30) M. H. Habicht, F. Wossidlo, M. Weber, C. Müller, *Chem. Eur. J.* **2016**, 22 (36), 12877.
- (31) X. Chen, S. Alidori, F. F. Puschmann, G. Santiso-Quinones, Z. Benkő, Z. Li, G. Becker, H.-F. Grützmacher, H. Grützmacher, *Angew. Chem. Int. Ed.* **2014**, 53 (6), 1641.
- (32) M. H. Habicht, *Neue Syntheserouten zu funktionalisierten Phosphabenzolen*, Freie Universität Berlin, **2013**.
- (33) M. Rigo, J. A. W. Sklorz, N. Hatje, F. Noack, M. Weber, J. Wiecko, C. Müller, *Dalton Trans.* **2016**, 45 (5), 2218.
- (34) M. Rigo, *Phosphinines as platforms for the design of new phosphorus-based ligands*, Freie Universität Berlin, **2017**.
- (35) B. Breit, R. Winde, T. Mackewitz, R. Paciello, K. Harms, *Chem. Eur. J.* **2001**, 7 (14), 3106.
- (36) G. Märkl, F. Lieb, A. Merz, *Angew. Chem. Int. Ed. Engl.* **1967**, 6 (5), 458.
- (37) C. Müller, D. Wasserberg, J. J. M. Weemers, E. A. Pidko, S. Hoffmann, M. Lutz, A. L. Spek, S. C. J. Meskers, R. A. J. Janssen, R. A. Van Santen, D. Vogt, *Chem. Eur. J.* **2007**, 13 (16), 4548.
- (38) C. Müller, E. A. Pidko, A. J. P. M. Staring, M. Lutz, A. L. Spek, R. A. Van Santen, D. Vogt, *Chem. Eur. J.* **2008**, 14 (16), 4899.
- (39) C. Müller, Z. Freixa, M. Lutz, A. L. Spek, D. Vogt, P. W. N. M. Van Leeuwen, *Organometallics* **2008**, 27 (5), 834.

- (40) J. J. M. Weemers, W. N. P. van der Graaff, E. A. Pidko, M. Lutz, C. Müller, *Chem. Eur. J.* **2013**, *19* (27), 8991.
- (41) J. A. Joule, K. Mills, *Heterocyclic Chemistry*, 5. ed., Wiley: Chichester, **2010**.
- (42) C. Elschenbroich, M. Nowotny, A. Behrendt, W. Massa, S. Wocadlo, *Angew. Chem.* **1992**, *104* (10), 1388.
- (43) N. Mézailles, P. Rosa, L. Ricard, F. Mathey, P. Le Floch, *Organometallics* **2000**, *19* (16), 2941.
- (44) C. Elschenbroich, M. Nowotny, B. Metz, W. Massa, J. Graulich, K. Biehler, W. Sauer, *Angew. Chem. Int. Ed. Engl.* **1991**, *30* (5), 547.
- (45) P. L. Arnold, F. G. N. Cloke, K. Khan, P. Scott, *J. Organomet. Chem.* **1997**, *528* (1–2), 77.
- (46) C. Müller, D. Vogt, In *Phosphorus Compounds*, M. Peruzzini, L. Gonsalvi (Eds.), Springer Netherlands: Dordrecht, **2011**, 151–181.
- (47) M. Doux, L. Ricard, F. Mathey, P. Le Floch, N. Mézailles, *Eur. J. Inorg. Chem.* **2003**, *2003* (4), 687.
- (48) F. Nief, C. Charrier, F. Mathey, M. Simalty, *J. Organomet. Chem.* **1980**, *187* (2), 277.
- (49) Y. Mao, K. M. H. Lim, Y. Li, R. Ganguly, F. Mathey, *Organometallics* **2013**, *32* (12), 3562.
- (50) F. Knoch, F. Kremer, U. Schmidt, U. Zenneck, P. Le Floch, F. Mathey, *Organometallics* **1996**, *15* (12), 2713.
- (51) P. Le Floch, F. Knoch, F. Kremer, F. Mathey, J. Scholz, W. Scholz, K.-H. Thiele, U. Zenneck, *Eur. J. Inorg. Chem.* **1998**, *1998* (1), 119.
- (52) B. Breit, *Chem. Commun.* **1996**, *17*, 2071.
- (53) B. Breit, R. Winde, K. Harms, *J. Chem. Soc. Perkin Trans. 1* **1997**, *4* (18), 2681.
- (54) B. Breit, *J. Mol. Catal. A Chem.* **1999**, *143* (1–3), 143.
- (55) E. F. DiMauro, M. C. Kozlowski, *J. Chem. Soc. Perkin Trans. 1* **2002**, No. 3, 439.
- (56) M. T. Reetz, G. Mehler, *Tetrahedron Lett.* **2003**, *44* (24), 4593.
- (57) C. Müller, L. G. López, H. Kooijman, A. L. Spek, D. Vogt, *Tetrahedron Lett.* **2006**, *47* (12), 2017.
- (58) E. Neumann, *Transition Metal Complexes with P,N-Ligands and Silylenes: Synthesis and Catalytic Studies*, Universität Basel, **2006**.
- (59) C. Müller, D. Vogt, *Dalton Trans.* **2007**, 9226 (47), 5505.
- (60) Y. Miyake, E. Isomura, M. Iyoda, *Chem. Lett.* **2006**, *35* (8), 836.

- (61) J. R. Bell, A. Franken, C. M. Garner, *Tetrahedron* **2009**, 65 (45), 9368.
- (62) M. Reetz, H. Guo, *Synlett* **2006**, 2006 (13), 2127.
- (63) L. E. E. Broeckx, A. Bucci, C. Zuccaccia, M. Lutz, A. Macchioni, C. Müller, *Organometallics* **2015**, 34 (12), 2943.
- (64) L. E. E. Broeckx, *Cyclometalation of Phosphinines via C-H Activation: Towards Functional Coordination Compounds*, Technische Universiteit Eindhoven, **2013**.
- (65) M. Rigo, L. Hettmanczyk, F. J. L. Heutz, S. Hohloch, M. Lutz, B. Sarkar, C. Müller, *Dalton Trans.* **2017**, 46 (1), 86.
- (66) D. W. Thompson, A. Ito, T. J. Meyer, *Pure Appl. Chem.* **2013**, 85 (7), 1257.
- (67) A. Adeloye, P. Ajibade, *Molecules* **2014**, 19 (8), 12421.
- (68) F. Puntoriero, S. Serroni, F. Nastasi, S. Campagna, In *Electrochemistry of Functional Supramolecular Systems*, John Wiley & Sons, Inc.: Hoboken, NJ, USA, **2010**, 121–143.
- (69) F. Teplý, *Collect. Czechoslov. Chem. Commun.* **2011**, 76 (7), 859.
- (70) Q. Yang, J. Lalevéé, J. Poly, *Macromolecules* **2016**, 49 (20), 7653.
- (71) M. Durandetti, J. Maddaluno, In *Encyclopedia of Reagents for Organic Synthesis*, John Wiley & Sons, Ltd: Chichester, UK, **2014**, Vol. 1, 1–3.
- (72) W.-P. Wu, Y.-J. Xu, S.-W. Chang, J. Deng, Y. Fu, *ChemCatChem* **2016**, 8 (21), 3375.
- (73) T. A. Matias, A. P. Mangoni, S. H. Toma, F. N. Rein, R. C. Rocha, H. E. Toma, K. Araki, *Eur. J. Inorg. Chem.* **2016**, 2016 (36), 5547.
- (74) J. Hawecker, J. M. Lehn, R. Ziessel, *Helv. Chim. Acta* **1986**, 69 (8), 1990.
- (75) C. Kaes, A. Katz, M. W. Hosseini, *Chem. Rev.* **2000**, 100 (10), 3553.
- (76) P. Ceroni, M. Venturi, In *Electrochemistry of Functional Supramolecular Systems*, John Wiley & Sons, Inc.: Hoboken, NJ, USA, **2010**, 145–184.
- (77) K. Manna, T. Zhang, F. X. Greene, W. Lin, *J. Am. Chem. Soc.* **2015**, 137 (7), 2665.
- (78) R. Tatikonda, K. Bertula, N. Nonappa, S. Hietala, K. Rissanen, M. Haukka, *Dalton Trans.* **2017**, 46 (9), 2793.
- (79) R. G. Pearson, *J. Am. Chem. Soc.* **1963**, 85 (22), 3533.
- (80) A. Campos-Carrasco, E. A. Pidko, A. M. Masdeu-Bultó, M. Lutz, A. L. Spek, D. Vogt, C. Müller, *New J. Chem.* **2010**, 34 (8), 1547.
- (81) J.-M. Alcaraz, A. Breque, F. Mathey, *Tetrahedron Lett.* **1982**, 23 (15), 1565.
- (82) A. Breque, C. C. Santini, F. Mathey, J. Fischer, A. Mitschler, *Inorg. Chem.* **1984**, 23 (22), 3463.

- (83) B. Schmid, L. M. Venanzi, T. Gerfin, V. Gramlich, F. Mathey, *Inorg. Chem.* **1992**, *31* (24), 5117.
- (84) B. Schmid, L. M. Venanzi, A. Albinati, F. Mathey, *Inorg. Chem.* **1991**, *30* (25), 4693.
- (85) D. Carmichael, P. Le Floch, F. Mathey, *Phosphorus Sulfur Silicon Relat. Elem.* **1993**, *77* (1–4), 255.
- (86) P. Le Floch, S. Mansuy, L. Ricard, F. Mathey, A. Jutand, C. Amatore, *Organometallics* **1996**, *15* (15), 3267.
- (87) K. H. Al-Obaidi, R. D. Gillard, L. A. P. Kane-Maguire, P. A. Williams, *Transit. Met. Chem.* **1977**, *2* (1), 64.
- (88) P. Le Floch, D. Carmichael, L. Ricard, F. Mathey, *J. Am. Chem. Soc.* **1993**, *115* (23), 10665.
- (89) G. Märkl, F. Lieb, A. Merz, *Angew. Chem.* **1967**, *79* (1), 59.
- (90) M. Bruce, G. Meissner, M. Weber, J. Wiecko, C. Müller, *Eur. J. Inorg. Chem.* **2014**, *2014* (10), 1719.
- (91) K. Dimroth, *Top. Curr. Chem.* **1973**, *38*, 1.
- (92) A. Moores, T. Cantat, L. Ricard, N. Mézailles, P. Le Floch, *New J. Chem.* **2007**, *31* (8), 1493.
- (93) G. Pfeifer, P. Ribagnac, X.-F. Le Goff, J. Wiecko, N. Mézailles, C. Müller, *Eur. J. Inorg. Chem.* **2015**, *2015* (2), 240.
- (94) G. Märkl, F. Lieb, *Angew. Chem. Int. Ed. Engl.* **1968**, *7* (9), 733.
- (95) G. Märkl, F. Lieb, C. Martin, *Tetrahedron Lett.* **1971**, *12* (17), 1249.
- (96) C. Wallis, P. G. Edwards, M. Hanton, P. D. Newman, A. Stasch, C. Jones, R. P. Tooze, *Dalton Trans.* **2009**, *12*, 2170.
- (97) B. Breit, E. Fuchs, *Chem. Commun.* **2004**, *6*, 694.
- (98) I. de Krom, E. a. Pidko, M. Lutz, C. Müller, *Chem. Eur. J.* **2013**, *19* (23), 7523.
- (99) I. de Krom, M. Lutz, C. Müller, *Dalton Trans.* **2015**, *44* (22), 10304.
- (100) I. M. J. de Krom, *2-(2'-Pyridyl)-4,6-diphenylphosphinine: Synthesis, characterization, and reactivity of novel transition metal complexes based on aromatic phosphorus heterocycles*, Technische Univeriteit Eindhoven, **2015**.
- (101) I. de Krom, L. E. E. Broeckx, M. Lutz, C. Müller, *Chem. Eur. J.* **2013**, *19* (11), 3676.
- (102) C. Müller, J. A. W. Sklorz, I. de Krom, A. Loibl, M. Habicht, M. Bruce, G. Pfeifer, J. Wiecko, *Chem. Lett.* **2014**, *43* (9), 1390.
- (103) A. Campos-Carrasco, L. E. E. Broeckx, J. J. M. Weemers, E. a. Pidko, M. Lutz, A. M. Masdeu-Bultó, D. Vogt, C. Müller, *Chem. Eur. J.* **2011**, *17* (8), 2510.

- (104) A. Fürstner, P. W. Davies, *Angew. Chem. Int. Ed.* **2007**, 46 (19), 3410.
- (105) H. Teller, M. Corbet, L. Mantilli, G. Gopakumar, R. Goddard, W. Thiel, A. Fürstner, *J. Am. Chem. Soc.* **2012**, 134 (37), 15331.
- (106) K. Grice, C. P. Kubiak, *Adv. Inorg. Chem.* **2014**, 66, 163.
- (107) R. Reithmeier, C. Bruckmeier, B. Rieger, *Catalysts* **2012**, 2 (4), 544.
- (108) P. A. Mabrouk, M. S. Wrighton, *Inorg. Chem.* **1986**, 25 (4), 526.
- (109) D. Guillaumont, H. Bazin, J.-M. Benech, M. Boyer, G. Mathis, *ChemPhysChem* **2007**, 8 (3), 480.
- (110) Y. Ohsawa, M. H. Whangbo, K. W. Hanck, M. K. DeArmond, *Inorg. Chem.* **1984**, 23 (21), 3426.
- (111) Y. Himeda, N. Onozawa-Komatsuzaki, S. Miyazawa, H. Sugihara, T. Hirose, K. Kasuga, *Chem. Eur. J.* **2008**, 14 (35), 11076.
- (112) T. Ishiyama, J. Takagi, J. F. Hartwig, N. Miyaura, *Angew. Chem. Int. Ed.* **2002**, 41 (16), 3056.
- (113) D. Hong, M. Murakami, Y. Yamada, S. Fukuzumi, *Energy Environ. Sci.* **2012**, 5 (2), 5708.
- (114) G. Frenking, N. Fröhlich, *Chem. Rev.* **2000**, 100 (2), 717.
- (115) C. J. Ballhausen, *Introduction to Ligand Field Theory*, McGraw-Hill: New York, **1962**.
- (116) M. J. S. Dewar, *Bull. Soc. Chim. Fr.* **1951**, 18, C71.
- (117) J. Chatt, L. A. Duncanson, *J. Chem. Soc.* **1953**, 2939.
- (118) J. Chatt, L. A. Duncanson, L. M. Venanzi, *J. Chem. Soc.* **1955**, 4456.
- (119) D. Mingos, P. Michael, *J. Organomet. Chem.* **2001**, 635 (1-2), 1.
- (120) C. A. Tolman, *J. Am. Chem. Soc.* **1970**, 92 (10), 2953.
- (121) O. Köhl, *Coord. Chem. Rev.* **2005**, 249 (5-6), 693.
- (122) A. Chianese, X. Li, M. Janzen, J. Faller, R. Crabtree, *Organometallics* **2003**, 22 (c), 1663.
- (123) D. R. Anton, R. H. Crabtree, *Organometallics* **1983**, 2 (5), 621.
- (124) F. A. Cotton, W. T. Edwards, F. C. Rauch, M. A. Graham, R. N. Perutz, J. J. Turner, *J. Coord. Chem.* **1973**, 2 (4), 247.
- (125) K. Verlinden, H. Buhl, W. Frank, C. Ganter, *Eur. J. Inorg. Chem.* **2015**, 2015 (14), 2416.

- (126) O. Back, M. Henry-Ellinger, C. D. Martin, D. Martin, G. Bertrand, *Angew. Chem. Int. Ed.* **2013**, 52 (10), 2939.
- (127) S. Halbert, C. Copéret, C. Raynaud, O. Eisenstein, *J. Am. Chem. Soc.* **2016**, 138 (7), 2261.
- (128) R. R. Rodrigues, C. L. Dorsey, C. A. Arceneaux, T. W. Hudnall, *Chem. Commun.* **2014**, 50 (2), 162.
- (129) A. B. P. Lever, *Inorg. Chem.* **1990**, 29 (6), 1271.
- (130) N. Xamonaki, A. Asimakopoulos, A. Balafas, M. Dasenaki, I. Choinopoulos, S. Coco, E. Simandiras, S. Koinis, *Inorg. Chem.* **2016**, 55 (10), 4771.
- (131) A. C. Hillier, W. J. Sommer, B. S. Yong, J. L. Petersen, L. Cavallo, S. P. Nolan, *Organometallics* **2003**, 22 (21), 4322.
- (132) M. Vogler, *Entwicklung funktionalisierter Phosphinine zur Darstellung heterobimetallischer Koordinationsverbindungen*, Freie Universität Berlin, **2013**.
- (133) A. Loibl, *Pyridylfunktionalisierte Phosphinine und Pyridine: Design, Synthese und Koordinationschemie*, Freie Universität Berlin, **2013**.
- (134) B. S. Holla, M. Mahalinga, M. Ashok, P. Karegoudar, *Phosphorus Sulfur Silicon Relat. Elem.* **2006**, 181 (6), 1427.
- (135) J.-L. Mao, X.-K. Ran, J.-Z. Tian, B. Jiao, H.-L. Zhou, L. Chen, Z.-G. Wang, *Bioorg. Med. Chem. Lett.* **2011**, 21 (5), 1549.
- (136) A. Stroba, F. Schaeffer, V. Hindie, L. Lopez-Garcia, I. Adrian, W. Fröhner, R. W. Hartmann, R. M. Biondi, M. Engel, *J. Med. Chem.* **2009**, 52 (15), 4683.
- (137) M. Cabrera, M. Simoens, G. Falchi, M. L. Lavaggi, O. E. Piro, E. E. Castellano, A. Vidal, A. Azqueta, A. Monge, A. L. de Ceráin, G. Sagrera, G. Seoane, H. Cerecetto, M. González, *Bioorg. Med. Chem.* **2007**, 15 (10), 3356.
- (138) P.-C. Lv, J. Sun, Y. Luo, Y. Yang, H.-L. Zhu, *Bioorg. Med. Chem. Lett.* **2010**, 20 (15), 4657.
- (139) M. N. Patel, B. S. Bhatt, P. A. Dosi, *Z. Anorg. Allg. Chemie* **2012**, 638 (1), 152.
- (140) Z. He, D. Dobrovolsky, P. Trinchera, A. K. Yudin, *Org. Lett.* **2013**, 15 (2), 334.
- (141) M. I. J. Polson, F. Scandola, P. J. Steel, *Acta Crystallogr. E* **2008**, 64 (1), o279.
- (142) J. Santamaría, C. Valdés, *Mod. Heterocycl. Chem.* **2011**, 3, 1631.
- (143) B. Branchi, M. Bietti, G. Ercolani, M. A. Izquierdo, M. A. Miranda, L. Stella, *J. Org. Chem.* **2004**, 69 (25), 8874.
- (144) M. A. Miranda, H. Garcia, *Chem. Rev.* **1994**, 94 (4), 1063.

- (145) F. Delgado-Vargas, O. Paredes-Lopez, *Natural Colorants for Food and Nutraceutical Uses*, CRC Press: Boca Raton, FL, USA, **2002**.
- (146) M. Fakis, J. Polyzos, G. Tsigaridas, J. Parthenios, A. Fragos, V. Giannetas, P. Persephonis, J. Mikroyannidis, *Chem. Phys. Lett.* **2000**, 323 (1–2), 111.
- (147) A. J. Perkowski, W. You, D. A. Nicewicz, *J. Am. Chem. Soc.* **2015**, 137 (24), 7580.
- (148) S. M. Yarmoluk, A. M. Kostenko, I. Y. Dubey, *Bioorg. Med. Chem. Lett.* **2000**, 10 (19), 2201.
- (149) S. Gavriilyuk, S. Polyutov, P. C. Jha, Z. Rinkevicius, H. Ågren, F. Gel'mukhanov, *J. Phys. Chem. A* **2007**, 111 (47), 11961.
- (150) L. Yang, J. Ye, Y. Gao, D. Deng, W. Gong, Y. Lin, G. Ning, *Tetrahedron Lett.* **2013**, 54 (23), 2967.
- (151) Yi Chen, Shi-Kang Wu, *J. Photochem. Photobiol. A* **1997**, 102 (2–3), 203.
- (152) D. Markovitsi, C. Jallabert, H. Strzelecka, M. Veber, *J. Chem. Soc. Faraday Trans.* **1990**, 86 (16), 2819.
- (153) D. Markovitsi, H. Sigal, C. Ecoffet, P. Millié, F. Charra, C. Fiorini, J.-M. Nunzi, H. Strzelecka, M. Veber, C. Jallabert, *Chem. Phys.* **1994**, 182 (1), 69.
- (154) C. Ecoffet, D. Markovitsi, C. Jallabert, H. Strzelecka, M. Veber, *J. Chem. Soc. Faraday Trans.* **1992**, 88 (20), 3007.
- (155) J. R. Wilt, G. A. Reynolds, J. A. Van Allan, *Tetrahedron* **1973**, 29 (6), 795.
- (156) G. Haucke, P. Czerney, F. Cebulla, *Ber. Bunsenges. Phys. Chem.* **1992**, 96 (7), 880.
- (157) J. Ye, X. Zhang, D. Deng, G. Ning, T. Liu, M. Zhuang, L. Yang, W. Gong, Y. Lin, *RSC Adv.* **2013**, 3 (22), 8232.
- (158) S. Parret, F. Morlet-Savary, J.-P. Fouassier, K. Inomata, T. Matsumoto, F. Heisel, *Bull. Chem. Soc. Jpn.* **1995**, 68 (10), 2791.
- (159) R. S. Rowland, R. Taylor, **1996**, 3654 (95), 7384.
- (160) C. E. Housecroft, E. C. Constable, *An Introduction to Organic, Inorganic and Physical Chemistry*, 4th ed., Pearson Education Limited: Harlow, UK, **2010**.
- (161) M. H. B. Stiddard, *J. Chem. Soc.* **1962**, 4712.
- (162) P. D. E. Niecke, H. Westermann, *Synthesis* **1988**, 4, 330.
- (163) M. J. Frisch, G. W. Trucks, H. B. Schlegel, G. E. Scuseria, M. A. Robb, J. R. Cheeseman, G. Scalmani, V. Barone, B. Mennucci, G. A. Petersson, H. Nakatsuji, M. Caricato, X. Li, H. P. Hratchian, A. F. Izmaylov, J. Bloino, G. Zheng, J. L. Sonnenberg, M. Hada, M. Ehara, K. Toyota, R. Fukuda, J. Hasegawa, M. Ishida, T. Nakajima, Y. Honda, O. Kitao, H. Nakai, T. Vreven, J. Montgomery, J. A., J. E. Peralta, F. Ogliaro, M. Bearpark, J. J. Heyd, E. Brothers, K. N. Kudin, V. N. Staroverov, R. Kobayashi, J.

- Normand, K. Raghavachari, A. Rendell, J. C. Burant, S. S. Iyengar, J. Tomasi, M. Cossi, N. Rega, J. M. Millam, M. Klene, J. E. Knox, J. B. Cross, V. Bakken, C. Adamo, J. Jaramillo, R. Gomperts, R. E. Stratmann, O. Yazyev, A. J. Austin, R. Cammi, C. Pomelli, J. W. Ochterski, R. L. Martin, K. Morokuma, V. G. Zakrzewski, P. Voth, G. A.; Salvador, J. J. Dannenberg, S. Dapprich, A. D. Daniels, Ö. Farkas, J. B. Foresman, J. V. Ortiz, J. Cioslowski, D. J. Fox, Gaussian Inc.: Wallingford, CT, USA, **2009**.
- (164) P. Coppens, *Crystallographic Computing*, F. R. Ahmed, S. R. Hall, C. P. Huber, (Eds.), Scandinavian University Press: Copenhagen, DK, **1970**.
- (165) G. M. Sheldrick, *Acta Crystallogr. A* **2008**, 64 (1), 112.
- (166) A. L. Spek, *Acta Crystallogr. D* **2009**, 65 (2), 148.
- (167) Bruker, Bruker AXS Inc.: Madison, WI, USA, **2010**.
- (168) H. D. Flack, *Acta Crystallogr. A* **1983**, 39 (6), 876.
- (169) A. L. Spek, *Acta Crystallogr. C* **2015**, 71, 9.
- (170) P. van der Sluis, A. L. Spek, *Acta Crystallogr. A* **1990**, 46 (3), 194.
- (171) IPCC, *Climate Change 2013 – The Physical Science Basis*, T. F. Stocker, D. Qin, G.-K. Plattner, M. M. B. Tignor, S. K. Allen, J. Boschung, A. Nauels, Y. Xia, V. Bex, P. M. Midgley (Eds.), Cambridge University Press: New York, NY, USA, **2014**.
- (172) R. A. Feely, C. L. Sabine, K. Lee, W. Berelson, J. Kleypas, V. J. Fabry, F. J. Millero, *Science* **2004**, 305 (5682), 362.
- (173) H. Andruleit, H. G. Babies, S. Fleig, S. Ladage, J. Meßner, M. Pein, D. Rebscher, M. Schauer, S. Schmidt, G. von Goerne, *Energiestudie 2016 - Reserven, Ressourcen und Verfügbarkeit von Energierohstoffen*, Bundesanstalt für Geowissenschaften und Rohstoffe: Hannover, DE, **2016**.
- (174) M. Cokoja, C. Bruckmeier, B. Rieger, W. A. Herrmann, F. E. Kühn, *Angew. Chem. Int. Ed.* **2011**, 50 (37), 8510.
- (175) N. Yang, S. R. Waldvogel, X. Jiang, *ACS Appl. Mater. Interfaces* **2016**, 8 (42), 28357.
- (176) C. D. Windle, R. N. Perutz, *Coord. Chem. Rev.* **2012**, 256 (21–22), 2562.
- (177) B. Kumar, M. Llorente, J. Froehlich, T. Dang, A. Sathrum, C. P. Kubiak, *Annu. Rev. Phys. Chem.* **2012**, 63 (1), 541.
- (178) K. Ramseyer, C. Rasmussen, *Carbon and Climate - Frontiers of Climate Science: A Breathing Planet, Off Balance*, NASA Jet Propulsion Laboratory: Pasadena, CA, USA, **2015**.
- (179) W. Wang, S. Wang, X. Ma, J. Gong, *Chem. Soc. Rev.* **2011**, 40 (7), 3703.
- (180) S. Kraus, B. Rieger, In *Carbon Dioxide and Organometallics*, X.-B. Lu (Ed.), Springer International Publishing: Cham, CH, **2016**, 199–223.

- (181) J. Hawecker, J.-M. Lehn, R. Ziessel, *J. Chem. Soc., Chem. Commun.* **1983**, 9, 536.
- (182) J. Hawecker, J.-M. Lehn, R. Ziessel, *J. Chem. Soc., Chem. Commun.* **1984**, 6, 328.
- (183) E. Portenkirchner, S. Schlager, D. Apaydin, K. Oppelt, M. Himmelsbach, D. a. M. Egbe, H. Neugebauer, G. Knör, T. Yoshida, N. S. Sariciftci, *Electrocatalysis* **2014**, 6 (2), 185.
- (184) M. D. Sampson, C. P. Kubiak, *J. Am. Chem. Soc.* **2016**, 138 (4), 1386.
- (185) Y. Ono, J. Nakamura, M. Hayashi, K. I. Takahashi, *Am. J. Appl. Chem.* **2014**, 2 (5), 74.
- (186) H. Hori, F. P. A. Johnson, K. Koike, O. Ishitani, T. Ibusuki, *J. Photochem. Photobiol. A* **1996**, 96 (1–3), 171.
- (187) H. Hori, F. P. A. Johnson, K. Koike, K. Takeuchi, T. Ibusuki, O. Ishitani, *Dalton Trans.* **1997**, 3 (6), 1019.
- (188) J. M. Smieja, M. D. Sampson, K. A. Grice, E. E. Benson, J. D. Froehlich, C. P. Kubiak, *Inorg. Chem.* **2013**, 52 (5), 2484.
- (189) M. Bourrez, F. Molton, S. Chardon-Noblat, A. Deronzier, *Angew. Chem. Int. Ed.* **2011**, 50 (42), 9903.
- (190) M. L. Clark, K. A. Grice, C. E. Moore, A. L. Rheingold, C. P. Kubiak, *Chem. Sci.* **2014**, 5 (5), 1894.
- (191) C. Müller, *unpublished results*.
- (192) M. Wrighton, D. L. Morse, *J. Am. Chem. Soc.* **1974**, 96 (4), 998.
- (193) L. A. Worl, R. Duesing, P. Chen, L. Della Ciana, T. J. Meyer, *Dalton Trans.* **1991**, S, 849.
- (194) S. Bucknor, F. A. Cotton, L. R. Falvello, A. H. Reid, C. D. Schmulbach, *Inorg. Chem.* **1986**, 25 (7), 1021.
- (195) M. Hollering, R. O. Reithmeier, S. Meister, E. Herdtweck, F. E. Kühn, B. Rieger, *RSC Adv.* **2016**, 6 (17), 14134.
- (196) S. Sato, T. Morimoto, O. Ishitani, *Inorg. Chem.* **2007**, 46 (22), 9051.
- (197) M. Hesse, H. Meier, B. Zeeh, *Spektroskopische Methoden in der organischen Chemie*, 7. ed., Georg Thieme Verlag: Stuttgart, **2005**.
- (198) S. S. Eaton, G. R. Eaton, *J. Am. Chem. Soc.* **1975**, 97 (13), 3660.
- (199) L. Baradello, S. Lo Schiavo, F. Nicolò, S. Lanza, G. Alibrandi, G. Tresoldi, *Eur. J. Inorg. Chem.* **2004**, 2004 (16), 3358.
- (200) L. E. Harrington, J. F. Britten, D. W. Hughes, A. D. Bain, J.-Y. Thépot, M. J. McGlinchey, *J. Organomet. Chem.* **2002**, 656 (1–2), 243.
- (201) G. M. Sheldrick, *Acta Crystallogr. C* **2015**, 71 (1), 3.

- (202) C. B. Hübschle, G. M. Sheldrick, B. Dittrich, *J. Appl. Crystallogr.* **2011**, *44* (6), 1281.
- (203) O. V. Dolomanov, L. J. Bourhis, R. J. Gildea, J. A. K. Howard, H. Puschmann, *J. Appl. Crystallogr.* **2009**, *42* (2), 339.
- (204) B. P. Sullivan, C. M. Bolinger, D. Conrad, W. J. Vining, T. J. Meyer, *J. Chem. Soc., Chem. Commun.* **1985**, 985 (20), 1414.
- (205) Y. Kou, Y. Nabetani, D. Masui, T. Shimada, S. Takagi, H. Tachibana, H. Inoue, *J. Am. Chem. Soc.* **2014**, *136* (16), 6021.
- (206) M. D. Sampson, J. D. Froehlich, J. M. Smieja, E. E. Benson, I. D. Sharp, C. P. Kubiak, *Energy Environ. Sci.* **2013**, *6* (12), 3748.
- (207) H. Takeda, K. Koike, H. Inoue, O. Ishitani, *J. Am. Chem. Soc.* **2008**, *130* (6), 2023.
- (208) C. Costentin, M. Robert, J.-M. Savéant, *Chem. Soc. Rev.* **2013**, *42* (6), 2423.
- (209) C. Costentin, G. Passard, M. Robert, J.-M. Savéant, *Proc. Natl. Acad. Sci.* **2014**, *111* (42), 14990.
- (210) C. J. Stanton, C. W. Machan, J. E. Vandezande, T. Jin, G. F. Majetich, H. F. Schaefer, C. P. Kubiak, G. Li, J. Agarwal, *Inorg. Chem.* **2016**, *55* (6), 3136.
- (211) K. A. Grice, N. X. Gu, M. D. Sampson, C. P. Kubiak, *Dalton Trans.* **2013**, *42* (23), 8498.
- (212) F. Franco, C. Cometto, F. Sordello, C. Minero, L. Nencini, J. Fiedler, R. Gobetto, C. Nervi, *ChemElectroChem* **2015**, *2* (9), 1372.
- (213) K. A. Grice, C. Saucedo, *Inorg. Chem.* **2016**, *55* (12), 6240.
- (214) U. Jayarathne, P. Chandrasekaran, H. Jacobsen, J. T. Mague, J. P. Donahue, *Dalton Trans.* **2010**, *39* (40), 9662.
- (215) D. Sieh, D. C. Lacy, J. C. Peters, C. P. Kubiak, *Chem. Eur. J.* **2015**, *21* (23), 8497.
- (216) F. W. M. Vanhelmont, M. V Rajasekharan, H. U. Güdel, S. C. Capelli, J. Hauser, H.-B. Bürgi, *Dalton Trans.* **1998**, *4* (17), 2893.
- (217) U. Pal, S. Ghosh, D. Chatterjee, *Transit. Met. Chem.* **2012**, *37* (1), 93.
- (218) H. Hori, K. Koike, Y. Suzuki, M. Ishizuka, J. Tanaka, K. Takeuchi, Y. Sasaki, *J. Mol. Catal. A Chem.* **2002**, *179* (1–2), 1.
- (219) A. Toonen, R. van Loon, *Hydrogen Detection with a TCD using Mixed Carrier Gas on the Agilent Micro GC*, Middelburg, NL, **2013**.
- (220) B. Gholamkhash, H. Mametsuka, K. Koike, T. Tanabe, M. Furue, O. Ishitani, *Inorg. Chem.* **2005**, *44* (7), 2326.
- (221) K. Koike, S. Naito, S. Sato, Y. Tamaki, O. Ishitani, *J. Photochem. Photobiol. A* **2009**, *207* (1), 109.

- (222) Z.-Y. Bian, S.-M. Chi, L. Li, W. Fu, *Dalton Trans.* **2010**, 39 (34), 7884.
- (223) H. Takeda, H. Koizumi, K. Okamoto, O. Ishitani, *Chem. Commun.* **2014**, 50 (12), 1491.
- (224) Y. Hong, C. B. Gorman, *J. Org. Chem.* **2003**, 68 (23), 9019.